University of Alberta

Data-based Harmonic Source Identification

by

Hooman Erfanian Mazin

A thesis submitted to the Faculty of Graduate Studies and Research
in partial fulfillment of the requirements for the degree of

Doctor of Philosophy

in

Power Engineering and Power Electronics

Department of Electrical and Computer Engineering

Fall 2012

Edmonton, Alberta

Abstract

Harmonic distortion is one of the main power quality problems for power system utilities. Nowadays, there are many harmonic-generating loads in a given distribution or sub-transmission system. Developing methods and techniques to quantify the harmonic contributions of the customers and the utility system, especially when a harmonic problem occurs in a system, is highly important for power quality management. After identifying the major harmonic-producing customers, utility companies can negotiate with them to reduce their generated harmonic contents by either installing filters or using other harmonic mitigation approaches. However, the first step is to identify the major harmonic-producing loads and quantify their impact.

In the past, this problem was approached from a single-point perspective. The single-point problem is a classic harmonic determination problem. However, the previous methods are circuit-based and classified as invasive methods. The thesis proposes a new non-invasive data-based method. The harmonic impact of a load is calculated by just measuring its voltage and current at the Point of Common Coupling (PCC). The challenge here is data selection. Not all the measured voltage and current sets are suitable for the analysis. The method is verified and characterized by extensive simulation studies. By using field measurement data, the effectiveness of the method is verified.

While the single-point approach is still very important and worthwhile, another type of harmonic-source-detection problem has emerged, primarily because an increasing number of loads now contain some harmonic sources. In this multi-point problem, the goal is to quantify harmonic impacts of the potential suspicious loads in the network on a reported harmonic problem. It must be determined if these loads are causing the problem and, if so, which load is producing the most significant impact. The multi-point problem has never been studied by other researchers. This thesis proposes two new data-based methods for the multi-point problem. For these methods, the harmonic currents of the suspicious customers and the harmonic voltage at the point of the reported problem

should be monitored. By using statistical inference, the harmonic impacts of the loads are estimated directly from the measurement. The idea is to correlate the gradual change of a load to the gradual change of the problem. One of the main challenges of this correlation analysis is the data selection. The thesis proposes and studies different data selection algorithms. The methods are verified and characterized through extensive simulation and field measurement studies.

Acknowledgment

I am grateful to all who helped me to complete this thesis. First and foremost, I would like to thank my wife Sorour for her understanding and love during the past few years. She has lost a lot due to my research abroad. I owe my deepest gratitude to my beloved wife. Without her encouragement, support and love, this dissertation would have never been completed. She always stood by me through the good times and bad. This thesis is dedicated to her. I am forever indebted to my parents for all their endless patience, encouragement and love for my entire life. They raised me with a love of science and supported me in all my pursuits.

The expert guidance, advice, and support from my supervisor, Dr. Wilsun Xu, made its completion possible. In the thousands of hours he devoted to my education and research, he showed me how to think like a researcher as well as formulate, test, express, and defend my ideas in a clear and concise manner. His passion for research is respected and will never be forgotten. I also give special thanks to my co-supervisor, Dr. Biao Huang for his constructive feedback in our technical discussions, especially on Least Square and Partial Least Square methods.

It is a pleasure to thank my colleagues in the Power Disturbance and Signaling Research Laboratory. I would like to thank all of them specially Dr. Ali Arefifar, Enrique Nino, Iraj Rahimi, Hesam Yazdanpanahi, Pooya Bagheri, and Jin Hui for their cooperation and valuable discussions

This thesis was supported by NSERC and Alberta Power Industry Consortium with generous grants, the University of Alberta with the Provost Doctoral Entrance Scholarships, my supervisor and the ECE department with several terms of R.A. and T.A., and the GSA with a PD travel grant. This collection of financial sources made my student life a lot more pleasant, and is highly appreciated.

Table of Content

List of Tables

List of Figures

Chapter 1

Introduction

Harmonic distortion is one of the main power quality problems for power system utilities. Nowadays, there are many harmonic-generating loads in a given distribution or sub-transmission system. Developing methods and techniques to quantify the harmonic contributions of the customers and the utility system, especially when a harmonic problem occurs in a system, is highly important for power quality management. This thesis focuses mainly on developing techniques and algorithms for data-based harmonic source identification problems.

This introductory chapter starts with a brief overview of harmonic distortions in power systems. It includes the fundamentals of power system harmonics, harmonic-generating loads, and harmonic measurement in the power systems. Next, the harmonic source identification problems are explained and classified. Finally, the scope, objectives and brief outline of the thesis are presented.

1.1 Harmonics in Power system

Harmonics are sinusoidal components of a periodic waveform with a frequency that is an integral multiple of the fundamental power frequency [1]. When harmonics are combined with the fundamental frequency component, waveform distortions are caused. Harmonic distortion has been a significant power quality issue for utility companies due to the growth of power electronic technology, which converts the old bulky power system loads into small-sized power electronic loads. These commonly used electronic devices generate more harmonic distortions and are also more sensitive to the harmonic distortions than the previous devices [2].

Harmonic distortions have significant adverse effects on both power system components and customers' electronic devices. Harmonics degrade the insulation of electric components and cause electrical plant components to malfunction. In addition, they can also increase losses and cause pulsating torques and noise in rotating machines and additional heat and losses in transformers [3]. In this regard, IEEE Std. 519 [3], IEC 1000-3 [4] and other similar standards impose limitations on the harmonic level in power systems.

1.1.1 Fundamentals of Power System Harmonics

Harmonics are a mathematical way to describe a steady-state non-sinusoidal waveform [5]. A periodic waveform described by a function of *f(t)* with period T seconds and fundamental frequency of $f_0=1/T$ can be expressed by a Fourier series:

$$f(t) = c_0 + \sum_{h=1}^{\infty} c_k \cos(2\pi h f_0 t + \phi_h), \tag{1-1}$$

where $c_k \angle \phi_h = \frac{1}{T} \int_{-\frac{T}{2}}^{\frac{T}{2}} f(t) e^{-j2\pi h f_0 t} dt$.

The Fourier series decomposes the original waveforms into a series of sinusoidal components with different frequencies. The component of f_0 is called the fundamental component, and the hf_0 component is called the h-th harmonic of the periodic function. As an example, Figure 1-1 shows the distorted harmonic current of a typical DC power supply load, and Figure 1-2 presents the harmonic spectrum of this waveform.

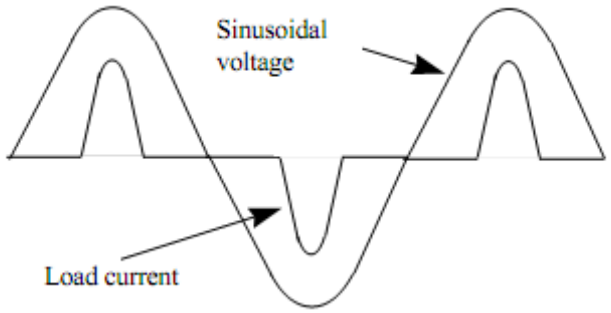

Figure 1-1: Distorted harmonic current of a typical DC power supply load

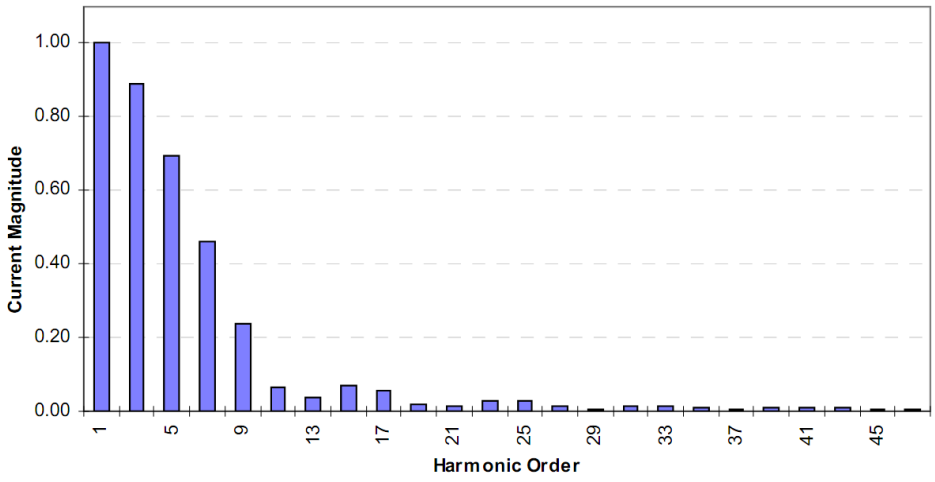

Figure 1-2: Harmonic spectrum of a typical DC power supply load

1.1.2 Harmonic generating loads

The two main types of harmonic generating-loads are power electronic loads and non-linear loads. Power electronic devices generate harmonic distortion due to their waveform-switching operations. Power electronic loads can also be further divided into three-phase and single-phase loads. VFD and DC drive are examples of three-phase power electronic loads. The second type produces harmonics due to a nonlinear voltage-and-current relationship. Examples of the second type are arc furnaces and saturated transformers. Figure 1-3 presents a summary of the harmonic-generating loads, organized according to this classification.

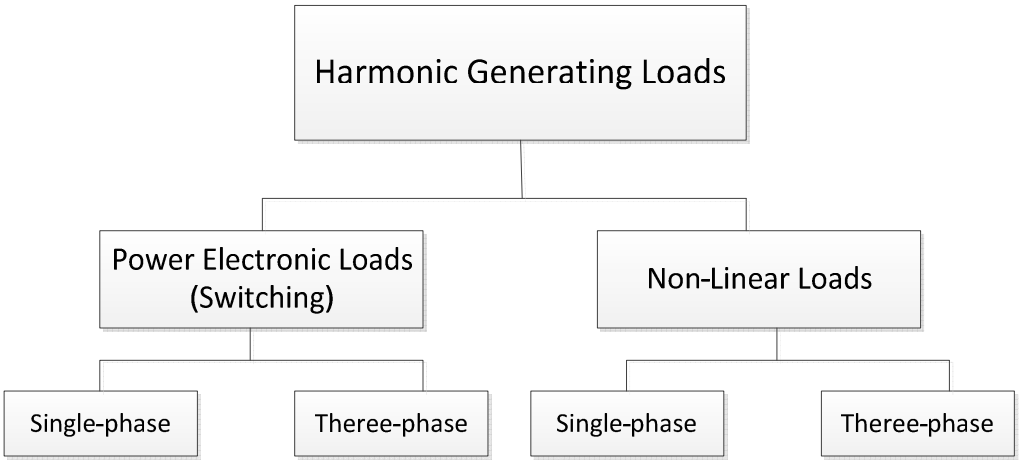

Figure 1-3: Classification of harmonic generating loads

1.2 Harmonic identification problem

The identification of harmonic sources is highly important for power quality management, especially when a harmonic problem occurs in a system. After identifying the major harmonic-producing customers, utility companies can negotiate with them to reduce their generated harmonic contents by either installing filters or using other harmonic mitigation approaches. The first step is to identify the major harmonic-producing loads and quantify their impact. The harmonic identification problem can be classified into two categories: single-point and multi-point problems.

In the past, this problem was approached from a single-point perspective. In this approach, the harmonic impact of a customer on its Point of Common Coupling (PCC) was studied. By using this approach, a customer can be charged based on the amount of harmonic pollution that injects to the system. However, the existing methods are mostly circuit-based and require man-made disturbances (such as capacitor switching) for the identification process.

While this approach is still very important and worthwhile, another type of harmonic-source-identification problem has emerged primarily because an increasing number of loads now contain some harmonic sources. In this multi-point problem, the goal is to quantify the harmonic impacts of the suspicious loads in the network on a reported harmonic problem. It must be determined if these loads are causing the problem and, if so, which load is producing the most significant impact. This problem has been never studied by other researchers. In 2004, a local industry approached the University of Alberta to solve a complex harmonic problem. This request led to the formation of the multi-point harmonic source identification problem.

1.3 Thesis scope and outline

The scope of this thesis is to research data-based methods for both types of harmonic source identification problems. This objective has been approached according to the following strategy:

- establishing a technically sound formulation of the problem by considering the practical constraints of existing power quality instruments;
- defining a special index to quantify the impact of harmonic-producing loads for the harmonic source identification problem;
- developing practical methods to solve the problems;
- verifying and characterizing the methods by using simulation studies and field test studies;
- implementing the methods in a software package and providing a technical tutorial on the project results to facilitate technology transfer.

The thesis is organized as follows: Chapter 2 formulizes the problems and presents a literature review of previous works. Chapter 3 proposes a new index for the quantification of the harmonic load impact. The proposed single-point method is presented in Chapter 4. The multi-point problem is investigated in Chapter 5, and two data-based methods are proposed to solve this problem. The proposed methods are verified by using simulation studies and characterized through sensitivity studies in Chapter 6. Finally, the conclusion and references are presented in Chapters 7 and 8, respectively.

Chapter 2

Problem Definition and Literature Review

In this chapter, both the single- and multi-point harmonic source identification problems are defined. The problem definitions start by introducing the single-point problem. The problem definition is followed by a literature review. Next, the multi-point harmonic source identification problem is presented. This problem has been never studied by other researchers. In 2004, a local industry approached the University of Alberta to solve a complex harmonic problem. This request led to the formation of the multi-point harmonic source identification problem. In this chapter, the problem is defined by providing a historical overview of the problem and by explaining the first intuitive solution.

2.1 Single-Point Harmonic Source Identification Problem

The single-point harmonic source identification problem is a classic scheme for harmonic source detection study. The schematic diagram of this approach is shown in Figure 2-1. From the PCC, the power network is divided into two parts: the utility- and the customer-side. The problem to solve is to determine if the studied customer (load) is causing the harmonic problem at the PCC. A qualitative Yes or No answer is useful, but not sufficient. Harmonic distortions are usually caused by both the utility and the customer sides. For example, a customer may contribute 37% of the harmonic distortions at the PCC, and the remaining 63% was caused by the utility system. This quantitative answer can be used to charge customers based on their contributions to the harmonic distortion problem.

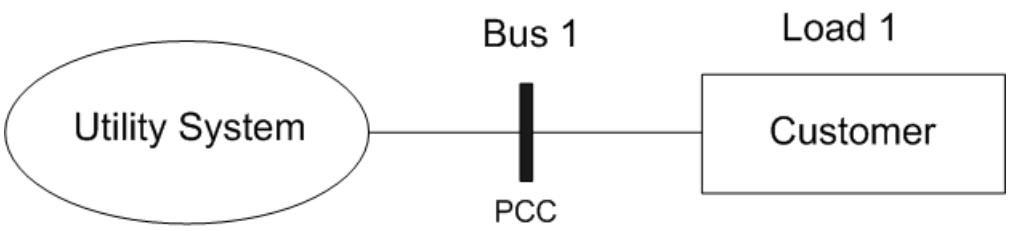

Figure 2-1: Schematic diagram of Single-Point Problem

The literature review reveals that five major methods have been proposed to solve this problem. Some are not quantitative and are suitable only for a qualitative analysis of the problem. Some methods are model-based, while others are data-based. These methods are reviewed and discussed below.

2.1.1 Direction of harmonic active power

The active power direction method is the earliest proposed method to quantify the harmonic contribution of a load [6]-[7]. This method is more qualitative than quantitative. The basic idea is based on the simple fact that linear loads do not generate harmonic active power. The active power generation is recognized as a sign of non-linear behavior and the load is identified as a harmonic source. The method is apparently sound and has been used in industry as a tool for many years [8]-[10]. However, reference [11] showed that if both the utility and customer sides contain harmonic sources, the direction of the harmonic active power is not a reliable sign for identifying the major contributor. The main reason for the problem is that the direction of the active power flow is affected mainly by the relative phase angle between the two harmonic sources (I_C and I_U) and not the magnitudes.

2.1.2 Direction of harmonic reactive power

Power engineers commonly know that the phase angles affect mainly the flow of the active power while the magnitudes affect mainly the flow of the reactive power. In this regard, [11] suggested that the reactive power could be a better indicator than the active power for harmonic source identification. This suggestion was expanded in other works [12]-[15] suggesting the use of other non-active harmonic power indices such as Fryze's

reactive power and Quadrature Reactive Power [16], instead of the simple reactive harmonic power. Like the harmonic active power method, this method is also more qualitative than quantitative. So, it shows only which side is the main contributor, but does not separate the contribution of each. The main theoretical drawback of the method is its lack of rigorous theoretical support. The method has been verified by only a limited number of computer simulation studies, and a theoretical study has found that the characteristics of the utility impedance (X/R) can affects the reliability of reactive power-direction methods [11].

2.1.3 Non-Conforming current

This method is based on the separation of the PCC current into its conforming and non-conforming components [17]. The conforming current has the same wave-shape as that of the voltage. The rest is named the non-conforming current and is used to quantify the harmonic distortion caused by the load. The method provides an overall index for all the harmonics and inter-harmonics of the waveform rather than a separate index for each harmonic order. The results are also highly dependent on the voltage waveform. This method has not been well accepted by other researchers.

2.1.4 Superposition method

The superposition method [18] is the most well-known method for quantifying of customer and utility harmonic contributions. Unlike the previous methods, this method is quantitative. In this method, both the utility and the customer sides should be first modeled by their equivalent circuits. The most commonly used model for harmonic study is the Norton equivalent circuit model [2] as shown in Figure 2-2. The Harmonic Modeling and Simulation Taskforce of the IEEE [19]-[20] explains that for harmonic studies, any component of the power system can be modeled by using a harmonic impedance, a harmonic source, or a combination of both.

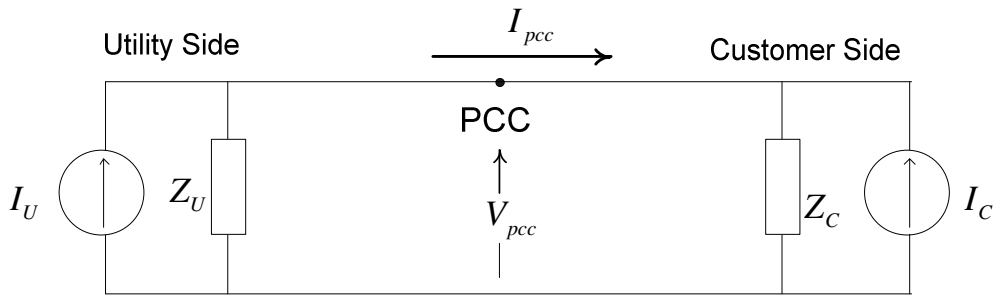

Figure 2-2: Harmonic equivalent circuit of single-point scheme

The key idea of the superposition method is to consider linear loads as innocent parties in the harmonic distortion problem. The harmonic sources within the utility- and customer-sides are considered as the main source of the harmonic distortion problem, and the harmonic contributions should be calculated based on the interaction of these harmonic sources. It is assumed that the customer and utility impedances (Z_c and Z_u) are known accurately. This method is explained by using the equivalent circuit shown in Figure 2-3.

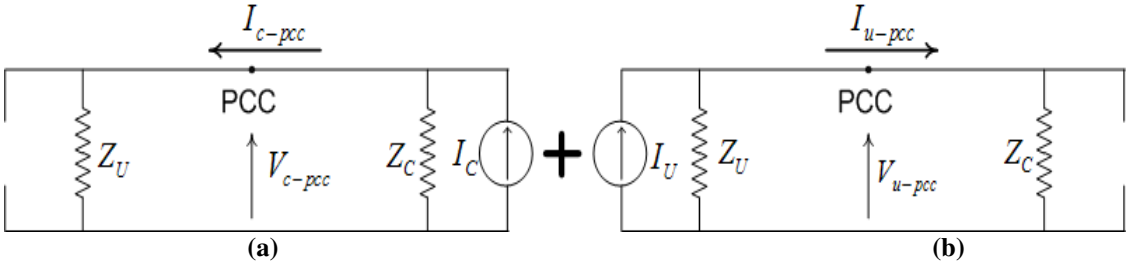

Figure 2-3: Applying the superposition principle to the equivalent circuit at PCC
(a) Customer-side contribution (b) Utility-side contribution

According to the principle of superposition, any branch current or node voltage is the summation of the individual contribution of all the sources in a network. In this regard, V_{pcc} and I_{pcc} can be expressed as follows:

$$\begin{cases} V_{pcc} = V_{u-pcc} + V_{c-pcc} \\ I_{pcc} = I_{u-pcc} - I_{c-pcc}, \end{cases} \tag{2-1}$$

where $V_{u\text{-}pcc}$ and $I_{u\text{-}pcc}$ are the voltage and current that can be measured at the PCC if only the utility-side current source is active. Similarly, $V_{c\text{-}pcc}$ and $I_{c\text{-}pcc}$ are the measured

voltage and current when only the customer-side current source is active. $V_{u\text{-}pcc}$ and $V_{c\text{-}pcc}$ represent the contributions of the utility and the customer to the PCC voltage and can be calculated as follows:

$$\begin{cases} V_{u-pcc} = \dfrac{Z_u Z_c}{Z_u + Z_c} I_u \\ V_{c-pcc} = \dfrac{Z_u Z_c}{Z_u + Z_c} I_c . \end{cases} \tag{2-2}$$

However, $V_{u\text{-}pcc}$ and $V_{c\text{-}pcc}$ are phasors, and, as a result, the utility contribution cannot be directly compared with the customer contribution. $V_{u\text{-}f}$ and $V_{c\text{-}f}$ are the projections of the $V_{u\text{-}pcc}$ and $V_{c\text{-}pcc}$ in the direction of the PCC voltage as shown in Figure 2-4.

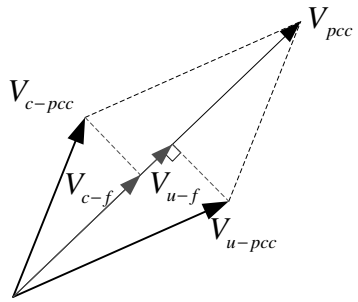

Figure 2-4: Scalar superposition indices

The projections are in the same direction as V_{pcc}; as a result, $|V_{pcc}|$ is the algebraic summation of the two components, one due to $V_{u\text{-}pcc}$ and the other due to $V_{c\text{-}pcc}$:

$$\left|V_{pcc}\right| = \left|V_{u-f}\right| + \left|V_{c-f}\right| . \tag{2-3}$$

The projection components can be calculated as follows:

$$\begin{cases} \left|V_{u-f}\right| = \left|V_{u-pcc}\right| \cos\left(\angle V_{u-pcc} - \angle V_{pcc}\right) \\ \left|V_{c-f}\right| = \left|V_{c-pcc}\right| \cos\left(\angle V_{c-pcc} - \angle V_{pcc}\right). \end{cases} \tag{2-4}$$

These components can be used as one possible index to characterize the contribution levels of the customers as well as the utility. The percentage that $|V_{u\text{-}f}|$ contributes in $|V_{pcc}|$ is defined as the contribution of the utility side to the PCC voltage. The same applies to the customer side. The harmonic contribution index (HC index) can be defined as follows:

$$\begin{cases} HC_{pcc}^{u} = \dfrac{|V_{u-f}|}{|V_{pcc}|} \times 100\% = \dfrac{|V_{u-pcc}|}{|V_{pcc}|} \cos\left(\angle V_{u-pcc} - \angle V_{pcc}\right) \times 100\% \\ HC_{pcc}^{c} = \dfrac{|V_{c-f}|}{|V_{pcc}|} \times 100\% = \dfrac{|V_{c-pcc}|}{|V_{pcc}|} \cos\left(\angle V_{c-pcc} - \angle V_{pcc}\right) \times 100\% \end{cases} \tag{2-5}$$

Needless to say, the sum of the contributions of both sides is 100 percent. A contribution can be positive or negative. If the contribution of both sides is positive, the customer and utility harmonics add up to form $|V_{pcc}|$. If the contributions have opposite signs, the negative one has the effect of reducing the harmonic voltage at the PCC.

2.1.5 Correlation methods

Correlation methods is a general name for a broad type of data-based methods that use correlation of measured parameters (such as the harmonic voltages and currents) to quantify harmonic contribution of loads. For example, [21] proposes a correlation method described as a simplified approach. In this method, the correlation of the harmonic voltage and the apparent power is analyzed to find the harmonic impact of the studied load. Figure 2-5 shows a graphical presentation of the correlation for a sample case. The harmonic distortion level can be roughly calculated by using the difference between the harmonic voltages corresponding to the maximum and zero power of the considered load. However, this method can give acceptable results in practice only when the considered load brings a significant contribution to the PCC.

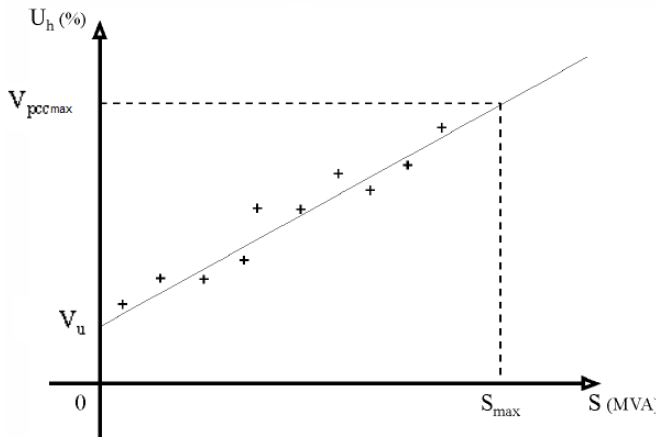

Figure 2-5: Correlation of harmonic voltages and apparent power[21]

In another work, [22] studied the linear correlation characteristics among the harmonic current and voltage of a load in different situations to identify the harmonic sources. Generally, when the network background disturbance level was rather stable (e.g., during the night), a good correlation was observed between the harmonic voltage and current. For example, Figure 2-6 shows a strong correlation between the 5^{th} order harmonic current and the voltage in a measured industrial load. Applying a linear regression to the data led to an analytical representation of the load and also gave an estimation of the background harmonic level (obtained as the extrapolation for $I_h = 0$). However, when the network background disturbance level varied greatly, a weaker correlation degree was found. Although the correlation methods are based on engineering common sense, the main drawback of these methods is their lack of rigorous theoretical support.

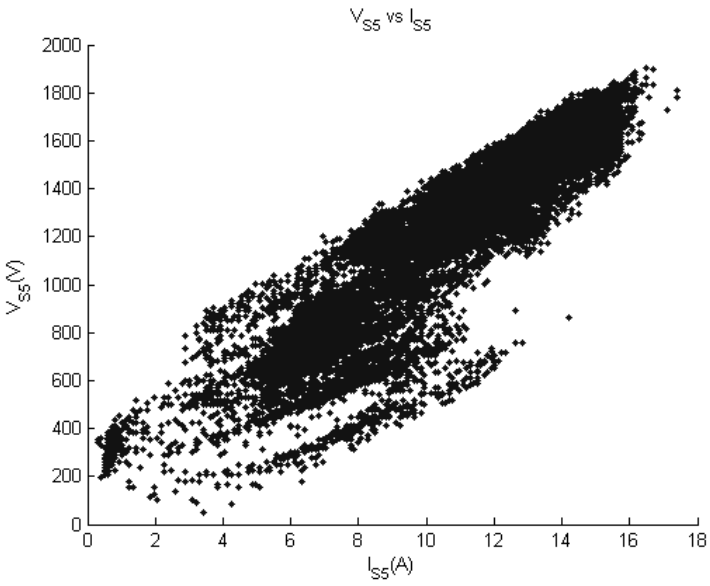

Figure 2-6: Harmonic voltage versus harmonic current in a measured industrial load

2.1.6 Summary and discussion of single-point methods

Table 2-1 presents a classification of the aforementioned single-point methods. The first three methods (the direction of Active/Reactive power methods and non-conforming current method) are data-based qualitative methods. These qualitative methods can identify only which side contributes more to the harmonic problem. Because of their qualitative nature, their applications in harmonic source identification are limited. The superposition and correlation methods are quantitative and can identify the contribution of each party. The methods can also be divided into data-based and model-based methods.

Table 2-1: Classification of Single-point harmonic identification methods

	Qualitative	**Quantitative**
Data-based	1- Direction of Active power 2- Direction of Reactive power 3- Non-Conforming current	5- Correlation method
Model-based		4- Superposition Method

The superposition method is a model-based method. In this method, it is assumed that the customer and utility impedances (Z_c and Z_u) are known accurately. Then the

harmonic contribution of the customer and the utility can be evaluated by using the equivalent circuit. However, the estimation of the impedances is not a trivial task and usually requires the generation of man-made disturbances [23]-[26]. In addition, the nature of customer-side harmonic impedance is still vague and not fully understood by researchers. For example, [27] found that the harmonic impedance of residential customers showed capacitive characteristics in the studied cases. However, no reasonable explanation is available to explain why this capacitive characteristic exists. The procedure for evaluating the harmonic contribution in the model-based method is shown in Figure 2-7.

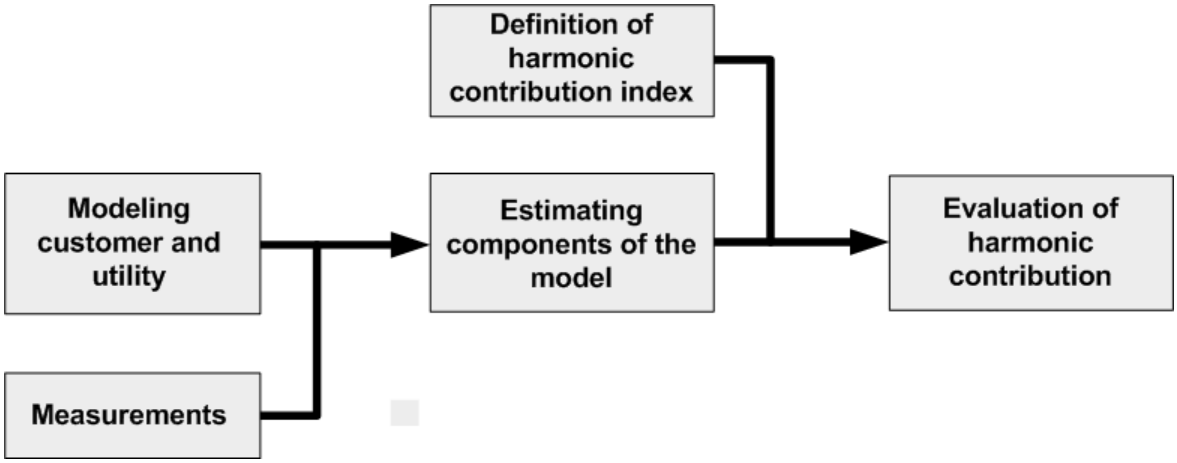

Figure 2-7: Procedure for harmonic contribution evaluation in the model-based method

In contrast, data-based methods try to evaluate harmonic contributions without constructing any model. This type of method tries to quantify the harmonic impact of each side by establishing a cause-and-effect relationship directly from the measured data. The procedure for evaluating the harmonic impacts of the loads in the data-based methods is shown in Figure 2-8. The main advantage is that the utility and customer impedances are not required. The main drawback is the lack of rigorous theoretical support.

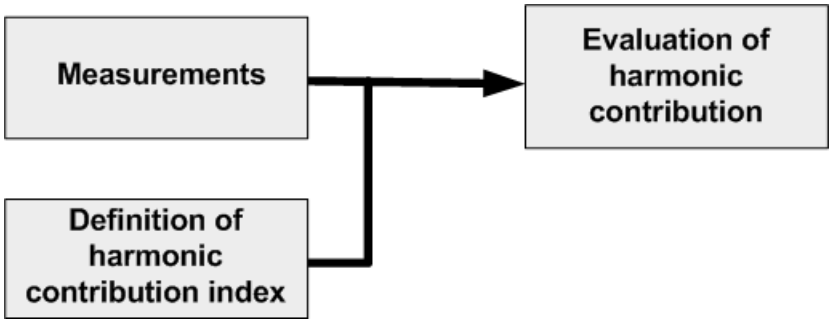

Figure 2-8: Procedure of harmonic contribution evaluation in the data-based method

2.2 Multi-Point problem

The multi-point problem has never been studied by other researchers in the published literature. In 2004, a local utility company approached the University of Alberta, asking it to solve a complex harmonic problem. This request led to the formation of the multi-point harmonic source identification problem. A harmonic distortion problem was found in a local distribution network in southern Alberta, Canada. A simplified presentation of the local distribution network is shown in Figure 2-9. Three major loads were identified as potential harmonic-causing loads (loads A, B and C). The exact impedance of the network was unknown by the utility company. The main goal was to find the problematic loads and quantify their impacts on the harmonic distortions problem. This real problem led to the formation of a new class of harmonic source identification problem.

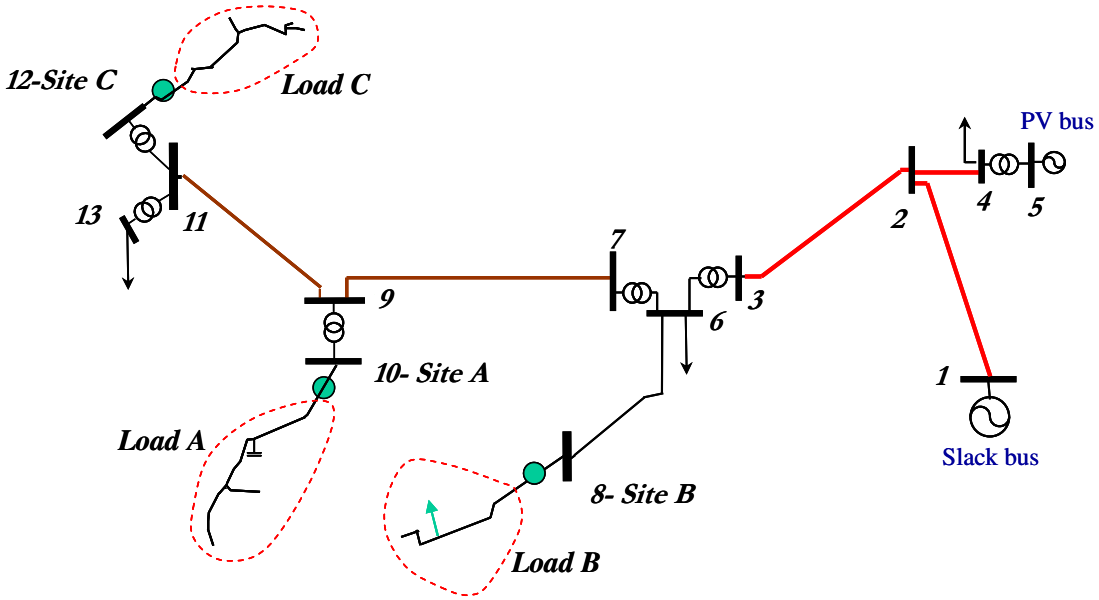

Figure 2-9: Simplified presentation of a local distribution network

2.2.1 Problem definition

The multi-point harmonic source identification problem can be illustrated by using the example shown in Figure 2-10. A harmonic problem is reported in bus *X* of a power distribution or transmission system. This bus is identified as the observation point. The system is known to contain, for example, three major harmonic-producing customers, *A*, *B* and *C*. These loads are identified as the suspicious loads. The problem to solve is to determine if these three suspicious loads are the cause of the problem. The harmonic voltages at point X are used as the quantitative indictor of the reported problem. Clearly, the contribution of each suspicious load to this indicator should be quantified. A qualitative Yes or No answer is not sufficient in this case since all the suspicious loads are likely to contribute to the voltage distortions at point X. One of the goals of this thesis is to research and develop a technically sound and practically useful method for utility companies to quantify and estimate the contributions of the major harmonic-producing customers to the reported problem.

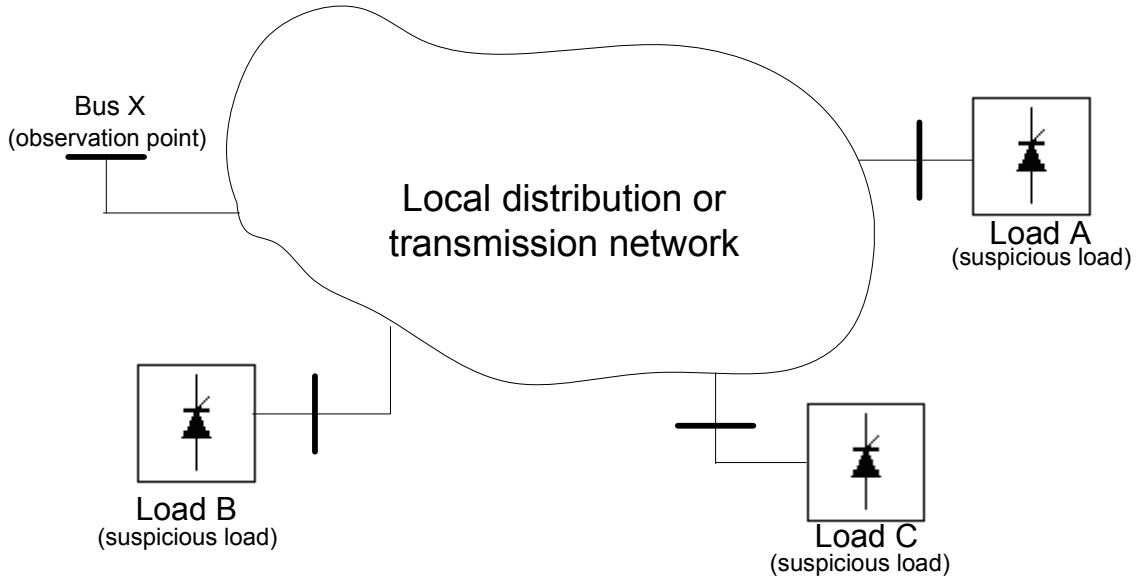

Figure 2-10: A typical power distribution or transmission system

2.2.2 Statistical Correlation method

The statistical correlation method is the first method proposed in this thesis. This method extends the correlation concept previously suggested for the single-point

harmonic identification problem. Although this method does not have rigorous theoretical support, the method is intuitively sound and easy to understand. The results were presented at the PES General Meeting in 2009 [27].

This method suggests taking synchronous harmonic measurements of the loads. Data were recorded with the resolution of one sample per second. In the measurement, a DAQ pad and a laptop with appropriate probes were utilized as one measurement set. The measurement had the following specifications:

- Data recording resolutions of one sample per second
- The sampling period of 6 cycles per sample
- The sampling rate of 256 samples per cycle.

It was found that synchronizing the laptops provides enough synchronization for 24 hours, so the laptops were synchronized daily. The measured datasets can be correlated to determine if a relationship exists between them. As an example, Figure 2-11 shows the correlation between the 5th harmonic voltage and current at the point of common coupling of customer A. This figure reveals that the harmonic voltage at Site A is strongly influenced by its harmonic current. The harmonic voltage and current exhibit an almost linear relationship. By using linear regression, the relation can be stated as follows:

$$\mathbf{V_{5Site\ A}(\%) = 0.5743\ I_{5Site\ A}(\%) + 3.549\ .} \qquad \mathbf{(2\text{-}6)}$$

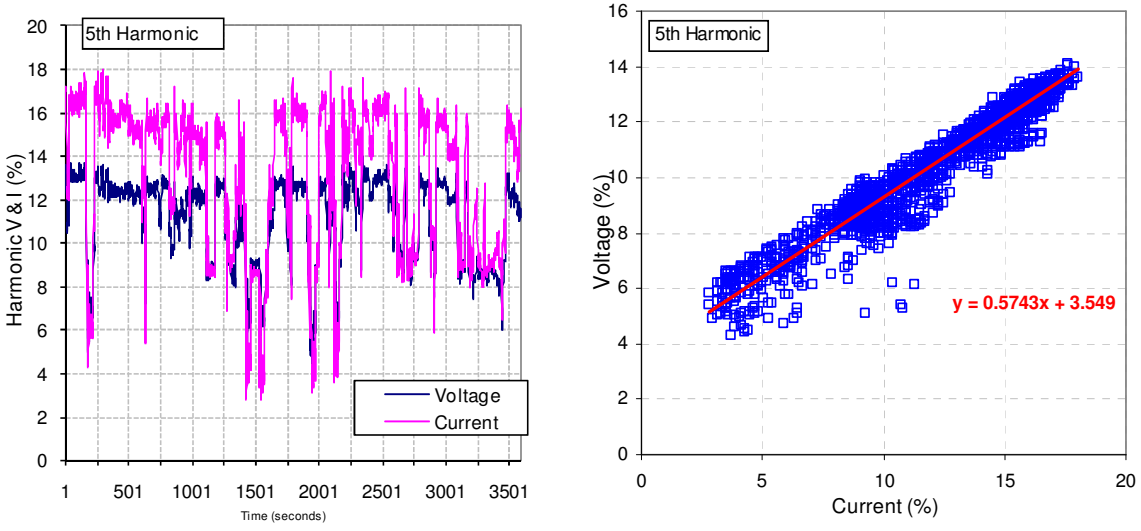

(a) Harmonic voltage and current trend (b) Correlation of harmonic voltage and current trend

Figure 2-11: Self-Correlation characteristics of the 5th harmonic current and voltage of site A

The equation suggests that a 1% increase in the PCC current distortion increases the voltage distortion by 0.57%. As well, if no harmonic current occurred at the PCC of Site A (I_5=0), the harmonic voltage at that location would be 3.549%. This voltage is the background harmonic voltage that would exist if the load of Site A did not absorb or inject harmonic currents. Thus, the background voltage distortion is about 3.549%.

As an example, the mutual impacts of load A on other sites are analyzed. Figure 2-12 shows the mutual-correlation characteristics of the 5th harmonic current of site A and the harmonic voltages at sites B and C. This figure reveals that the current of Site A has a significant impact on the voltage distortions at Sites B and C. The data are selected so that only load A varies. The impact of each load can be quantified by using the linear regression equations derived from the data.

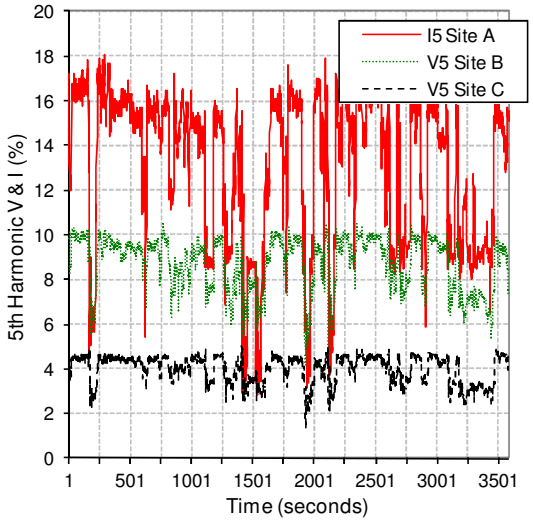

(a) variations of harmonic current of site A and harmonic voltages at sites B and C with time

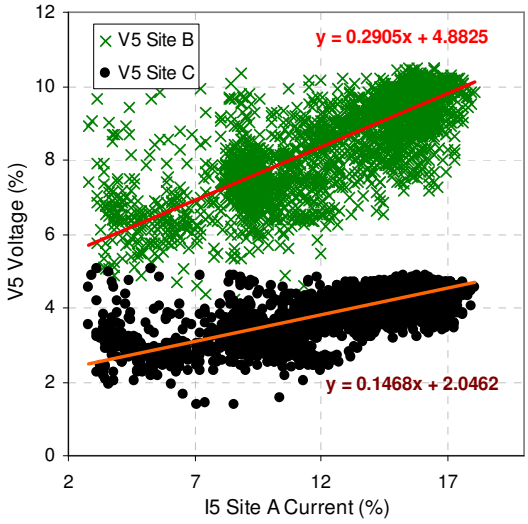

(b) correlation between harmonic current and voltages

Figure 2-12: Mutual-Correlation characteristics of the 5th harmonic current of site A and harmonic voltages at sites B and C

2.3 Summary

In this chapter, the harmonic source identification problems were defined, and the existing methods were reviewed. Two classes of methods were identified: model-based and data-based methods. Model-based methods' need detailed information of the internal

circuit of both the utility system and the customers, which makes these methods impractical in most real applications. In contrast, data-based methods are based solely on measurement data and do not need any information about the system. This feature makes them very practical. However, the existing data-based methods do not have strong theoretical support. The aim of this thesis is to develop theoretically sound and practical data-based methods for both single- and multi-point problems. In the next chapter, a unified index will be proposed for both single- and multi-point harmonic source identification problems to quantify the harmonic impact of the loads. The proposed single-point and multi-point methods to estimate this index by using data-based analysis will be presented in Chapters 4 and 5, respectively.

Chapter 3

Quantification of Harmonic Load Impact

In the previous chapter, the single-point and multi-point harmonic source identification problems were introduced. By reviewing the existing identification methods, it was found that the superposition and correlation methods are the only quantitative methods. The data-based correlation method has practical applications, but suffers from its lack of theoretical support. In contrast, the superposition method has strong theoretical support but is model-based, so it has limited practical applications. In this chapter, the superposition method and its corresponding harmonic contribution index (HC index) are discussed in detail to reveal limitations of this index. Its main limitation can be observed in dealing with linear loads, especially from capacitors. It will be shown that the harmonic contribution index's descriptions of the behavior of linear loads are misleading. To overcome this limitation, a new quantification method and index will be introduced in this chapter.

3.1 Limitation of HC Index

The harmonic contribution index was introduced in Section 2.1.4. The discussion suggested that linear loads should be considered as innocent parties in the harmonic contribution process, and that harmonic contributions should be calculated based on the interaction of the harmonic sources within the utility and customer. In this regard, when a linear load (Z_c) is connected to the utility system as shown in Figure 3-1, the contributions of the utility and customer to the PCC voltage can be calculated by using equation **(2-2)** as follows:

$$\begin{cases} V_{u-pcc} = \dfrac{Z_u Z_c}{Z_u + Z_c} I_u \\ V_{c-pcc} = \dfrac{Z_u Z_c}{Z_u + Z_c} I_c = \dfrac{Z_u Z_c}{Z_u + Z_c} \times 0 = 0 \end{cases} \tag{3-1}$$

As the customer does not contain a harmonic source (I_c), its contribution component ($V_{c\text{-}pcc}$) is zero. By considering that in this case, V_{pcc}=$V_{u\text{-}pcc}$, and by using equation **(2-5)**, the harmonic contribution index of each party is calculated as follows:

$$\begin{cases} HC^{u}_{pcc} = \dfrac{\left|V_{u-pcc}\right|}{\left|V_{pcc}\right|} \cos\left(\angle V_{u-pcc} - \angle V_{pcc}\right) \times 100\% = 100\% \\ HC^{c}_{pcc} = \dfrac{\left|V_{c-pcc}\right|}{\left|V_{pcc}\right|} \cos\left(\angle V_{c-pcc} - \angle V_{pcc}\right) \times 100\% = 0\% \end{cases} \tag{3-2}.$$

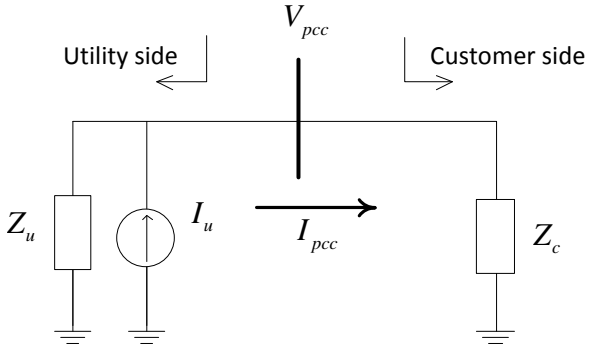

Figure 3-1: Harmonic equivalent system when customer is a linear load

The HC index suggests that harmonic contribution of the customer is zero. However, it can be shown by case studies that the customer affects the harmonic voltage distortions. The variation of the customer impedance can cause the variation of the harmonic voltage distortion. As a sample case, the following parameters are assumed for the system:

$$\begin{cases} Z_u = 0.5829 + 11.36\text{j} \\ I_u = \left(-0.183 + 0.339\text{j}\right) \times 10^{-3} \\ Z_c = 50 + 100\,j \end{cases}$$

From the variation of Z_c, it can be seen that V_{pcc} varies. Figure 3-2 shows that V_{pcc} is increased by the increase of Z_c. At the same time, increasing Z_c causes the decrease of

I_{pcc}. As Figure 3-3 shows, V_{pcc} and I_{pcc} are negatively correlated in this case. Thus, based on this observation, one can state that the customer current has a negative incremental impact on the voltage distortion. As the customer current increases, the voltage distortion decreases. In this regard, if the customer draws more harmonic current, this process helps the utility system by reducing the voltage distortion, thereby having a negative (reducing) harmonic impact on the voltage distortion.

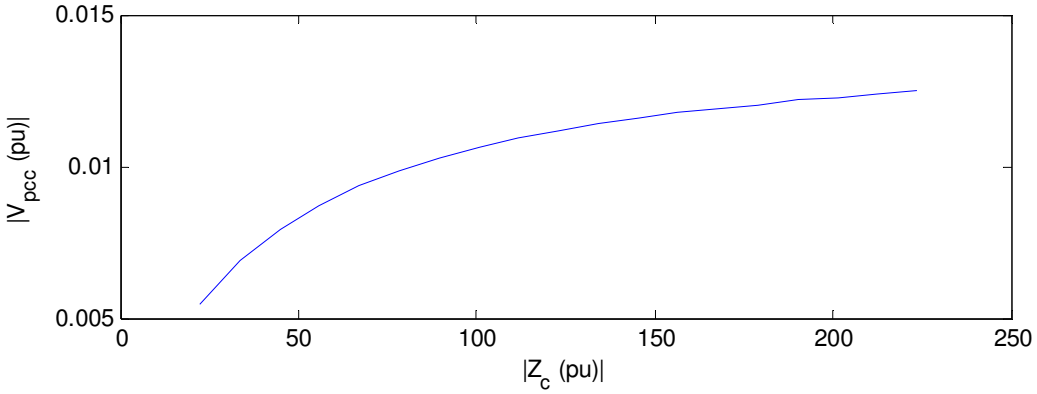

Figure 3-2: Variation of V_{pcc} by changing Z_c (inductive load)

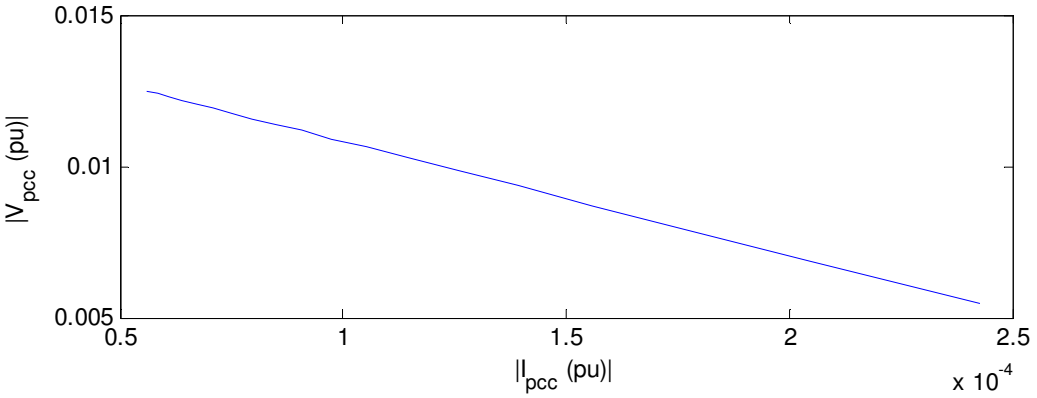

Figure 3-3: Correlation of V_{pcc} and I_{pcc} for linear load (inductive load)

As another example, Zc is replaced by -100j, which represents a capacitor on the customer side. Figure 3-4 shows that the variation of Z_c affects V_{pcc}. In contrast to the previous case, a positive correlation exists between V_{pcc} and I_{pcc}, as Figure 3-5 reveals. If the customer draws more current, the harmonic voltage distortion will increase. In this case, the customer has a positive (increasing) harmonic impact.

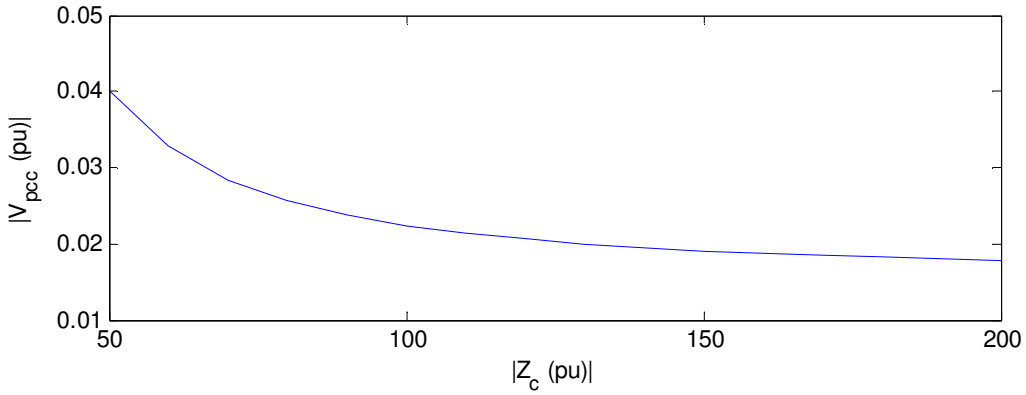

Figure 3-4: Variation of V_{pcc} by changing Z_c (capacitive load)

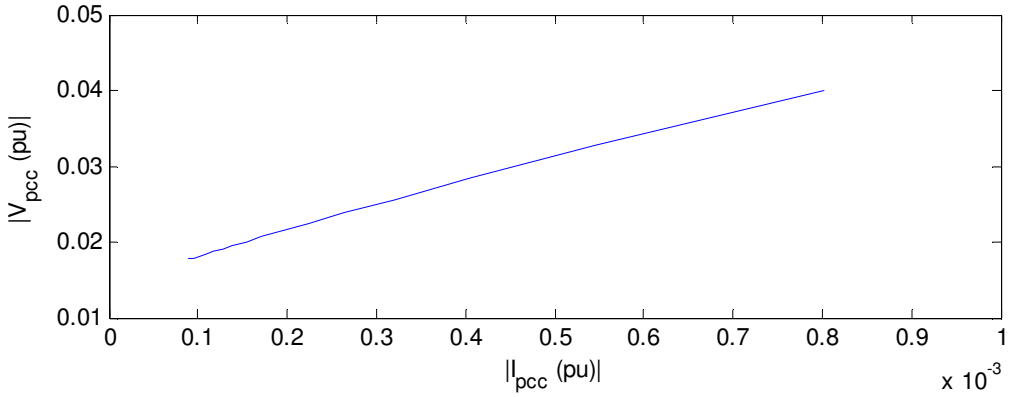

Figure 3-5: Correlation of V_{pcc} and I_{pcc} for linear load (capacitive load)

The simple studied cases showed that linear loads impact on the voltage distortions and should be responsible for a harmonic distortion problem. The HC index does not show this responsibility, so a new index is needed for this purpose. In the next sections, the HC index is first further analyzed, and a new index is proposed.

3.2 Analysis of HC index

In the previous section, the HC index was studied for linear loads. In this section, the HC index will be further studied for harmonic loads, and it will be shown that this index presents the incremental harmonic impact of the loads. Figure 3-6 shows an equivalent harmonic system for the case of a harmonic load on the customer side. In the first study case, the following parameters are assumed as the base case:

$$\begin{cases} Z_u = 0.5829 + 11.36\text{j} \\ I_u = \left(-0.183 + 0.339\text{j}\right) \times 10^{-3} \\ I_c = 0.4 \angle 270^\circ \times 10^{-3} \end{cases}$$

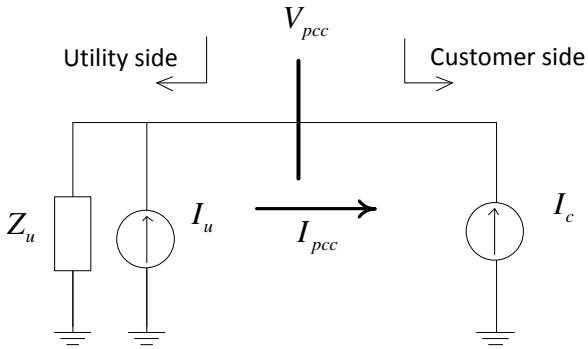

Figure 3-6: Harmonic equivalent system for a case of harmonic load in customer side

By using the superposition method and equation **(2-2)**, $V_{u\text{-}pcc}$, $V_{c\text{-}pcc}$ and V_{pcc} are calculated as follows:

$$\begin{cases} V_{u-pcc} = 0.0146 \angle -169^\circ \\ V_{c-pcc} = 0.0151 \angle -18^\circ \\ V_{pcc} = 0.0073 \angle -89^\circ \end{cases}$$

Figure 3-7 shows that the phasor diagram of the superposition voltage components. $V_{u\text{-}f}$ and $V_{c\text{-}f}$ can be achieved by projecting the $V_{u\text{-}pcc}$ and $V_{c\text{-}pcc}$ in the direction of the PCC voltage. The harmonic contributions of the customer and utility can be achieved by using equation **(2-5)**. The contribution of the utility system and customer are 65% and 35%, respectively. As Figure 3-7 reveals, the customer side and utility side voltages add up to construct V_{pcc}.

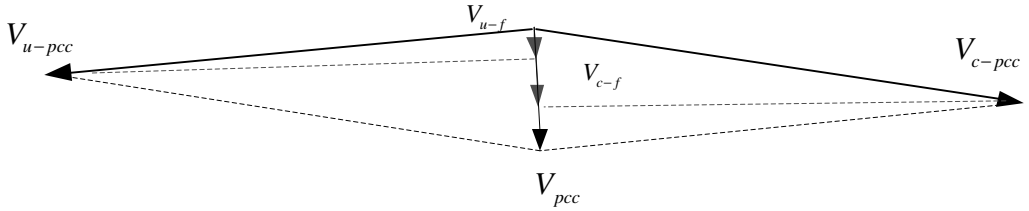

Figure 3-7: Phasor diagram of superposition voltage components for the base case

To determine how the variation of I_c affects the voltage of the PCC, the magnitude of I_c ($|I_c|$) is varied from 0 to 2×10^{-3} pu. Figure 3-8 shows how V_{ppc} is changed by the variation of I_c.

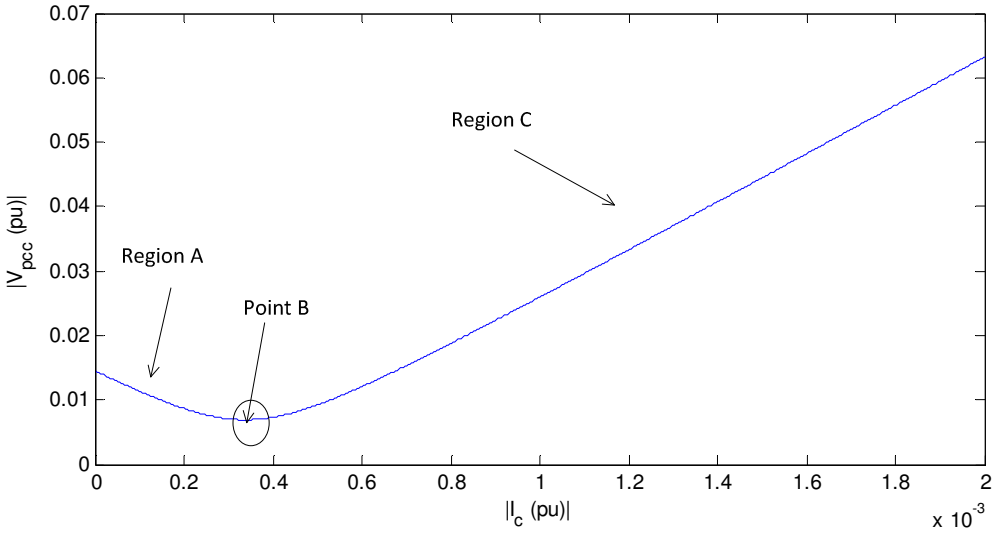

Figure 3-8: Impact of variation of I_c on V_{pcc}

Three regions can be identified in this graph. In region C, increasing I_c causes the voltage to increase. *Ic* was in this region in the studied base case. In region A, increasing I_c causes the voltage to decrease. Assume $I_c = 0.2\angle 270^\circ \times 10^{-3}$. The phasor diagram of the superposition components is presented in Figure 3-9. The customer partially cancels out the voltage produced by the utility and causes the voltage to decrease. The harmonic contribution index for the customer and the utility system are -53% and 153%, respectively.

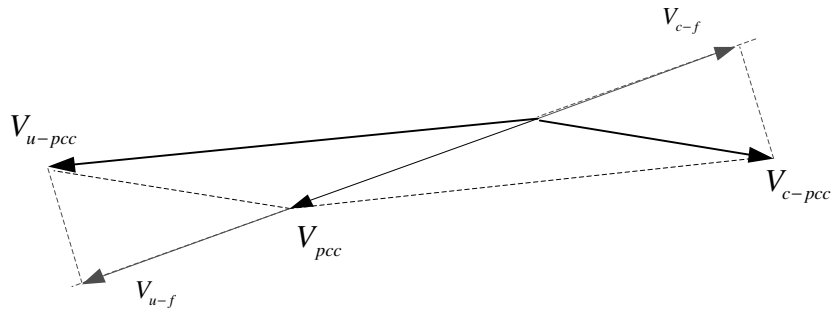

Figure 3-9: Phasor diagram of superposition voltage components for region A

For point B (the local minima), a slight variation of I_c does not impact on V_{pcc} (the slope is zero at this point). In this region, $V_{c\text{-}pcc}$ is perpendicular to V_{pcc}, and the customer harmonic contribution is zero. Figure 3-10 shows the variation of the customer HC index by changing I_c. As this figure reveals, the HC index is always negative in region A. In this region, the harmonic voltage is decreased by an increase of I_c, and the slope of the V_{pcc}-I_c graph is negative in this region (see Figure 3-8). At point B, the slope of the V_{pcc}-I_c graph is zero, and the harmonic contribution is also zero. The harmonic contribution is also positive in region C in accordance with the slope of the V_{pcc}-I_c graph.

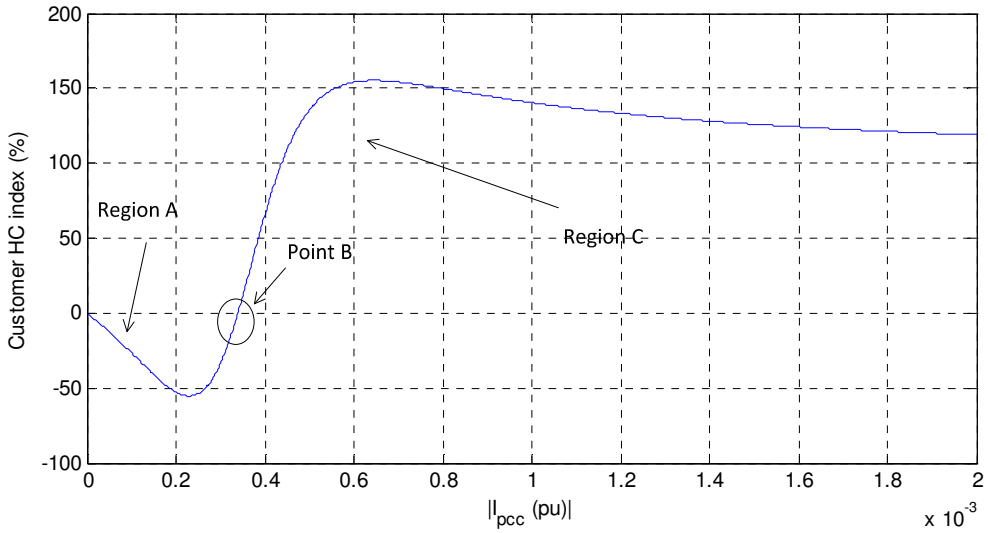

Figure 3-10: Variation of customer HC index by changing I_c

The harmonic contribution index shows the incremental impact of the harmonic load (the slope of the V_{pcc}-I_c graph). The incremental index can be defined as follows:

$$Incremental\ index(\%) = \frac{\frac{dV_{pcc}}{dI_{pcc}}}{\frac{V_{pcc}}{I_{pcc}}} \times 100\% \qquad (3\text{-}3)$$

The numerator is the slope of the V_{pcc}-I_c graph, and the denominator is the V_{pcc} over I_c to normalize the slope. The variation in the incremental index by changing I_c is calculated and shown in Figure 3-11, which shows that for the harmonic load, the incremental and HC indices are exactly the same.

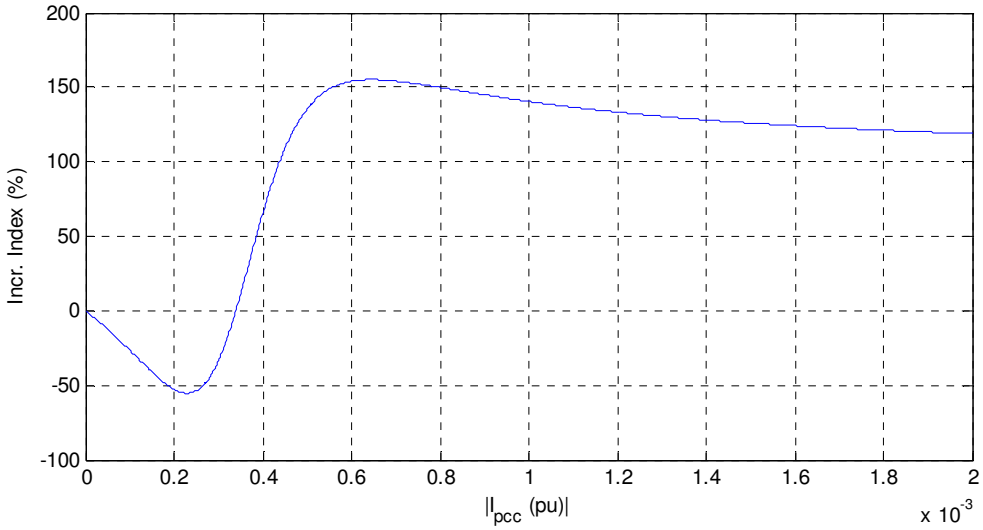

Figure 3-11: Variation of Incremental Index by changing I_c

3.3 Proposed Index and verification

It was shown that the HC index presents the incremental harmonic impact of the harmonic loads. However, the HC index does not present the impact of linear loads. To reflect this impact on the HC index, [18] suggested using Z_c as a reference and converting the impedance changes into the equivalent current source change. In this case, equivalent I_c can be calculated as follows:

$$I_{c-new} = \frac{V_{pcc}}{Z_{c-reference}} - I_{pcc}. \quad (3\text{-}4)$$

It will be shown that $Z_{reference}$ can slightly improve the HC index, but that improvement is not enough to completely present the harmonic impact of linear loads. To overcome this problem, this thesis proposes a new index named the harmonic impact index (HI index). The idea of harmonic impact is to model a customer by its PCC current. In this case, the equivalent I_c can be calculated as follows:

$$I_c = -I_{pcc}. \quad (3\text{-}5)$$

It is similar to say that the harmonic impact index uses infinity $Z_{c\text{-}reference}$. By this definition, $V_{u\text{-}pcc}$ and $V_{c\text{-}pcc}$ can be calculated as follows:

$$\begin{cases} V_{u-pcc} = Z_u I_u \\ V_{c-pcc} = -Z_u I_{pcc} \end{cases} \tag{3-6}$$

$V_{u\text{-}f}$ and $V_{c\text{-}f}$ are the projections of the $V_{u\text{-}pcc}$ and $V_{c\text{-}pcc}$ in the direction of the PCC voltage. The harmonic impact index (HI index) can be defined as follows:

$$\begin{cases} HI^{\,u}_{\,pcc} = \dfrac{\left|V_{u-pcc}\right|}{\left|V_{pcc}\right|} \cos\left(\angle V_{u-pcc} - \angle V_{pcc}\right) \times 100\% \\ HI^{\,c}_{\,pcc} = \dfrac{\left|V_{c-pcc}\right|}{\left|V_{pcc}\right|} \cos\left(\angle V_{c-pcc} - \angle V_{pcc}\right) \times 100\% \end{cases} \tag{3-7}$$

3.3.1 Case of linear load in customer side

Section 3.1 studied the HC index for linear loads. In this present section, the HC and HI indices are compared by using a case study. The following parameters are assumed:

$$\begin{cases} Z_u = 0.5829 + 11.36\text{j} \\ I_u = \left(-0.183 + 0.339\text{j}\right) \times 10^{-3} \\ Z_c = 50 + 100\,j \end{cases}$$

Table 3-1 presents the results of varying the customer impedance from 50% to 200%. The incremental index is selected as the reference to determine the impact of the customer load as this index shows the visible impact of the load variation on the harmonic voltage. As Table 3-1 shows, the HC index does not reflect the impact of the customer and is always zero. The HC index with $Z_{reference}$ shows a better performance than the original HC index while Z_c decreases. However, when Z_c increases by more than 100%, the HC-$Z_{reference}$ index shows positive values that do not coincide with the negative values of the incremental index. The harmonic impact index shows a very good performance and fully coincides with the incremental index.

Table 3-1: Results of varying customer impedance

Z_c (pu)	$V_{pcc}(pu)$	$I_{pcc}(pu)\times10^{-3}$	HC index (%)	HC-Z reference index (%)	Harmonic Impact index(%)	Incremental index (%)
50%	0.0087	0.1559	0	-25.17	-66.86	-67.26
70%	0.0098	0.1258	0	-10.78	-47.76	-48.04
80%	0.0103	0.1148	0	-6.29	-41.79	-42.03
90%	0.0106	0.1055	0	-2.79	-37.14	-37.36
Base	**0.0109**	**0.0976**	**0**	**0**	**-33.43**	**-33.43**
110%	0.0112	0.0908	0	2.28	-30.40	-30.57
120%	0.0114	0.0849	0	4.19	-27.86	-28.02
150%	0.0119	0.071	0	8.389	-22.28	-22.42
200%	0.0125	0.0558	0	12.58	-16.71	-16.81

3.3.2 Case of harmonic load in customer side

In this section, the HC and HI indices are compared by using a case study for a harmonic load on the customer side. The following parameters are assumed:

$$\begin{cases} Z_u = 0.5829 + 11.36\text{j} \\ I_u = \left(-0.183 + 0.339\text{j}\right)\times10^{-3} \\ I_c = 0.4\angle270^\circ \times10^{-3} \end{cases}$$

Table 3-2 shows the results from varying the customer harmonic load. The harmonic impact index equals the harmonic contribution index when customer is a harmonic load.

Table 3-2: Results of varying customer harmonic load

I_{pcc} (pu)	$V_{pcc}(pu)$	HC index (%)	HC-Z reference index (%)	Harmonic Impact index(%)	Incremental index (%)
50%	**0.0087**	-52.8	-52.8	-52.8	-52.8
70%	0.0073	-44.7	-44.7	-44.7	-44.03
80%	0.007	-17.96	-17.96	-17.96	-16.55
90%	0.007	22.2	22.2	22.2	24.25
Base	**0.0073**	**67.57**	**67.57**	**67.57**	**67.60**
110%	0.0079	101.7	101.7	101.7	103.38
120%	0.0087	126.81	126.81	126.81	127.97
150%	0.0121	154.11	154.11	154.11	154.27
200%	0.0188	149.91	149.91	149.91	149.71

3.4 Summary

In this chapter, the superposition method and its corresponding HC index were discussed in detail. It was observed that this index did not reflect the impact of the linear loads on the harmonic voltage. The incremental change in the voltage by variation of a customer current was chosen as the visible impact of the customer. While varying the linear loads can cause voltage changes, the HC index did not show this impact. The harmonic impact index was introduced and was found to reflect the impact of both the harmonic and the linear loads.

Chapter 4

Method for Single-Point Harmonic Impact Estimation

The single-point harmonic source identification problem is a classic scheme for harmonic source detection study. In this scheme, the system is divided into the utility- and customer-sides. In the previous chapter, the HI index was proposed for quantifying the harmonic impact of the customer loads. In this chapter, a data-based method will be proposed to estimate this HI index by using the measured harmonic voltage and current. This method will be verified and characterized by simulation and field measurement studies.

4.1 Formulization of the problem

Figure 4-1(a) shows the circuit diagram of the single-point problem. The HI index suggests that the customer load can be modeled by an equivalent harmonic source. Figure 4-1(b) shows the circuit diagram of the single-point problem by presenting the utility side by its Thevenin equivalent and the customer by its equivalent current source.

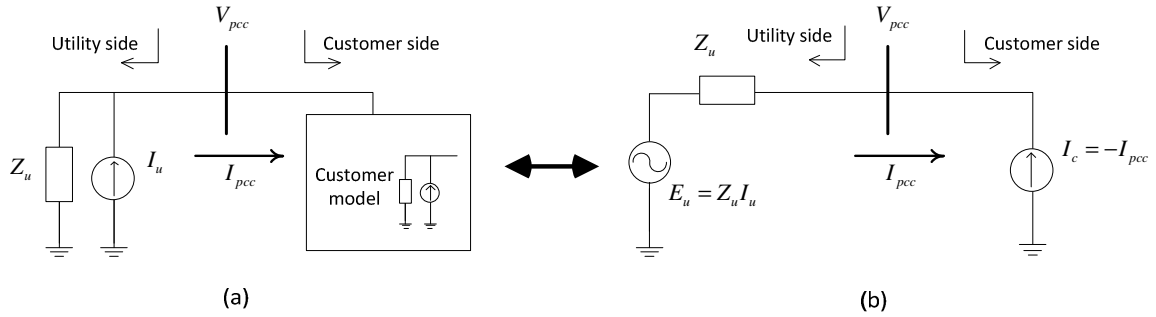

Figure 4-1: Harmonic equivalent circuit for single-point problem

(a) Norton equivalent circuit of utility (b) Thevenin equivalent circuit of utility

Two sources can cause the harmonic voltage distortion at PCC (V_{pcc}). The first source is the background harmonic of the utility. This source is presented by the E_u voltage source. The second source is the harmonic distortion generated by drawing the harmonic current from the network by the customer ($V_{c\text{-}pcc}$). As was shown by equation **(3-6)**, $V_{u\text{-}pcc}$ and $V_{c\text{-}pcc}$ can be calculated as follows:

$$\begin{cases} V_{u-pcc} = E_u = Z_u I_u \\ V_{c-pcc} = -Z_u I_{pcc} \end{cases} \tag{4-1}$$

The phasor diagram of components of the harmonic voltage is shown in Figure 4-2.

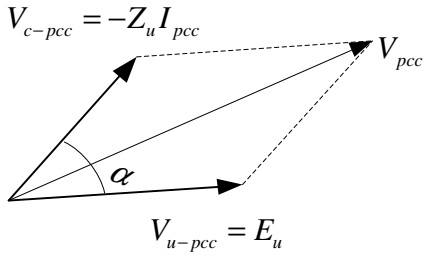

Figure 4-2: Phasor diagram of components of harmonic voltage at PCC

By using equation **(3-7)**, the HI index of the load can be calculated as follows:

$$HI_{pcc}^{c} = \frac{|V_{c-pcc}|}{|V_{pcc}|} \cos\left(\angle V_{c-pcc} - \angle V_{pcc}\right) \times 100\% \tag{4-2}$$

4.2 Impedance estimation vs. data-based estimation

The HI index can be estimated by using both impedance estimation and data-based estimation methods. However, there are some key differences between these methods. In the impedance estimation method, the utility impedance (Z_u) is firstly estimated. Then, harmonic impact can be calculated by using equations (4-1) and (4-2). In the data-based method, the harmonic impact is calculated directly by using the measurement data.

The impedance of the system can be estimated when a load disturbance happens. The disturbance can be caused by man-made or natural fluctuation of the load. The impedance can be estimated by measuring pre-disturbance harmonic voltage and current at PCC

($I_{pcc\text{-}pre}$ and $V_{pcc\text{-}pre}$) as well as post-disturbance harmonic voltage and current ($I_{pcc\text{-}post}$ and $V_{pcc\text{-}post}$). The utility harmonic impedance (Z_u) can be obtained by following equation:

$$Z_u = \frac{V_{pcc-pre} - V_{pcc-post}}{I_{pcc-pre} - I_{pcc-post}}. \quad (4\text{-}3)$$

The pre- and post-measurements should share a common time reference, so that the measured quantities are synchronized with a common time reference. In power systems, nominal frequency is 50 or 60 Hz. However, the operating frequency can vary ±0.1% of the nominal frequency. The variation will cause a phase shift between the pre-disturbance and the post-disturbance samples, leading to incorrect impedance estimate. A small phase shift at the fundamental frequency can cause significant errors at harmonic frequencies [32]. In the data-based method, such synchronization is not required. The magnitudes (not the pahsors) of the harmonic voltage and current are measured and used in the data-based method. Table 4-1 summarizes the comparison of the impedance estimation method with the data-based single-point problem.

Table 4-1: Comparison of impedance estimation method with data-based single-point problem

	Impedance estimation method	**Data-based single-point method**
Utility impedance	Be estimated by the method	Not required
Synchronized Measurement	Yes	No
Measurement type	Phasor (magnitude+phase angle)	Magnitude

4.3 Proposed method

In the previous chapter, it was shown by using case studies that the HI index equals the incremental harmonic impact of the load. This equality will theoretically be proven in this section. Thereafter, the proposed data-based method will be presented for measuring the incremental harmonic impact of the load to estimate the HI index. By using the dot product symbol, $\cos\left(\angle V_{c-pcc} - \angle V_{pcc}\right)$ can be obtained by the following equation:

$$\cos\left(\angle V_{c-pcc} - \angle V_{pcc}\right) = \frac{V_{c-pcc} \circ V_{pcc}}{\left|V_{c-pcc}\right|\left|V_{pcc}\right|}. \tag{4-4}$$

By substituting $\vec{V}_{pcc}$ by the summation of $\vec{V}_{c-pcc}$ and $\vec{E}_u$, the following equation is derived:

$$\cos\left(\angle V_{c-pcc} - \angle V_{pcc}\right) = \frac{V_{c-pcc} \circ V_{c-pcc} + V_{c-pcc} \circ E_u}{\left|V_{c-pcc}\right|\left|V_{pcc}\right|}. \tag{4-5}$$

By replacing **(4-5)** into (**4-2**), the HI index can be derived.

$$HI^{\ c}_{pcc} = \frac{\left|V_{c-pcc}\right|^2 + \left|V_{c-pcc}\right|\left|E_u\right|\cos\alpha}{\left|V_{pcc}\right|^2} \times 100\%. \tag{4-6}$$

By using the cosine low for the phasor diagram shown in Figure 4-2, the following equation can be obtained:

$$\left|V_{c-pcc}\right|^2 + \left|E_u\right|^2 + 2\left|V_{c-pcc}\right|\left|E_u\right|\cos\alpha = \left|V_{pcc}\right|^2. \tag{4-7}$$

Assume that the customer load changes causing a disturbance. After it occurs, the customer current is changed to $I_{pcc} + \Delta I_{pcc}$. Similarly, V_{pcc} and $V_{c\text{-}pcc}$ will change. If the utility does not vary during this disturbance, E_u and Z_u will be constant. After the disturbance, the following equation can be derived:

$$\left(\left|V_{c-pcc}\right| + \Delta\left|V_{c-pcc}\right|\right)^2 + \left|E_u\right|^2 + 2\left(\left|V_{c-pcc}\right| + \Delta\left|V_{c-pcc}\right|\right)\left|E_u\right|\cos\alpha = \left(\left|V_{pcc}\right| + \Delta\left|V_{pcc}\right|\right)^2. \tag{4-8}$$

By neglecting $\left(\Delta\left|V_{pcc}\right|\right)^2$ and $\left(\Delta\left|V_{c-pcc}\right|\right)^2$, one can get

$$\frac{\Delta\left|V_{pcc}\right|}{\Delta\left|V_{c-pcc}\right|} = \frac{\left|V_{c-pcc}\right| + \left|E_u\right|\cos\alpha}{\left|V_{pcc}\right|}. \tag{4-9}$$

By combining **(4-9)** and **(4-6)**, the harmonic impact of the customer can be derived by the following formula:

$$HI_C = \frac{|V_{c-pcc}|}{|V_{pcc}|} \cdot \frac{\Delta|V_{pcc}|}{\Delta|V_{c-pcc}|} \times 100\%. \tag{4-10}$$

By replacing V_{c-pcc} by $-Z_u I_{pcc}$ and assuming Z_u is constant during the analysis, $|V_{c-pcc}|$ and $\Delta|V_{c-pcc}|$ can be calculated as follows:

$$|V_{c-pcc}| = |Z_u I_{c-pcc}| = |Z_u||\Delta I_{c-pcc}| \tag{4-11}$$

$$\Delta|V_{c-pcc}| = \Delta|Z_u I_{c-pcc}| = |Z_u (I_{c-pcc} + \Delta I_{c-pcc}) - Z_u I_{c-pcc}| = |Z_u \Delta I_{c-pcc}| = |Z_u||\Delta I_{c-pcc}| \tag{4-12}$$

Finally, the HI index can be obtained by using the following incremental formula:

$$HI_C = \frac{\frac{\Delta|V_{pcc}|}{|V_{pcc}|}}{\frac{\Delta|I_{pcc}|}{|I_{pcc}|}} \times 100\%. \tag{4-13}$$

To use this formula, the disturbances caused by the customer should be identified. The key idea is use the variation of the 60 Hz load current as an identification signature. Figure 4-3 shows the variation of the fundamental current measured at the panel of a house. As this figure reveals, some rapid variation in the fundamental current can be located (shown by the dotted ovals). Variation of the 60Hz load current shows a variation of the customer. When a rapid customer variation occurs it is reasonable to assume that the utility is fairly constant (or has less variation) during this time interval.

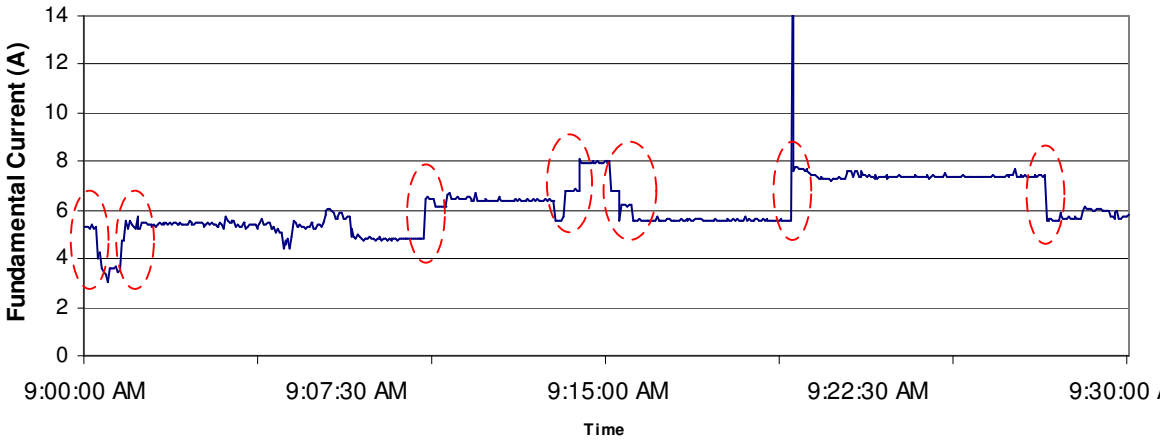

Figure 4-3: Variation of fundamental current measured at the panel of a house

In this regard, a simple two-point approach is proposed. In this approach, every two points in a sequence are investigated to calculate the variation of the fundamental current for these two points. The harmonic impact for these points is estimated by using the mentioned formula. Next, those points with the most variation in the fundamental currents are selected, and other points are filtered. By using the remaining points, the harmonic impact is calculated. The algorithm is explained below.

1. For each point k, calculate the fundamental current variation dIf(k) by using following equation:

$$\mathrm{dIf(k)} = \frac{\left|I_f(k) - I_f(k-1)\right|}{\frac{1}{2}\left|I_f(k) + I_f(k-1)\right|}.$$

2. For each point k, calculate the harmonic impact HI(k) by using the following equation:

$$\mathrm{HI(k)} = \frac{\left|V_h(k) - V_h(k-1)\right|}{\left|I_h(k) - I_h(k-1)\right|} \frac{\left|I_h(k) + I_h(k-1)\right|}{\left|V_h(k) + V_h(k-1)\right|} \times 100\% .$$

3. Filter data with ΔIf of less than the specified threshold.
4. Calculate average of the remaining (after filtering) HI's as the average of the harmonic impact of the dataset.

This algorithm is explained by the following example. The variation of the fundamental current and the 5th order harmonic current and voltage of a feeder from 10AM to 10:30AM are shown in the following figures.

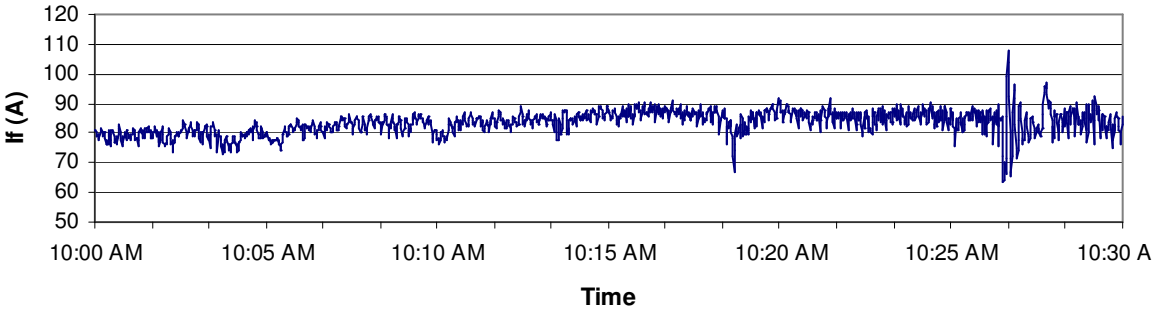

Figure 4-4: Variation of fundamental current of a feeder from 10AM to 10:30AM

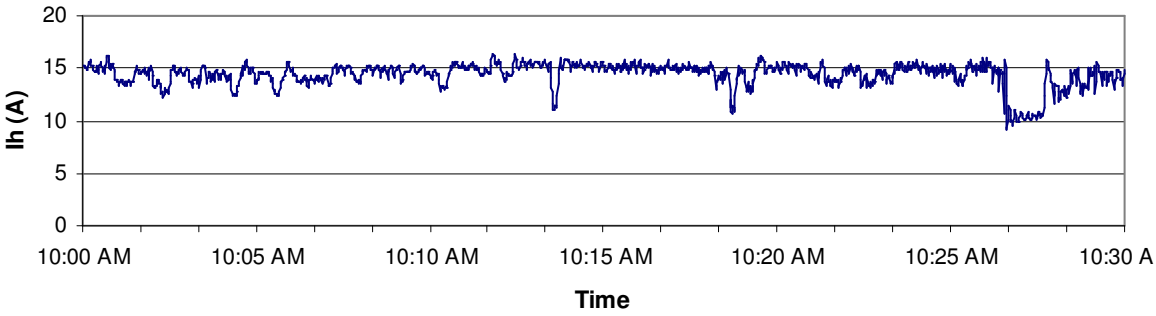

Figure 4-5: Variation of harmonic current of a feeder from 10AM to 10:30AM

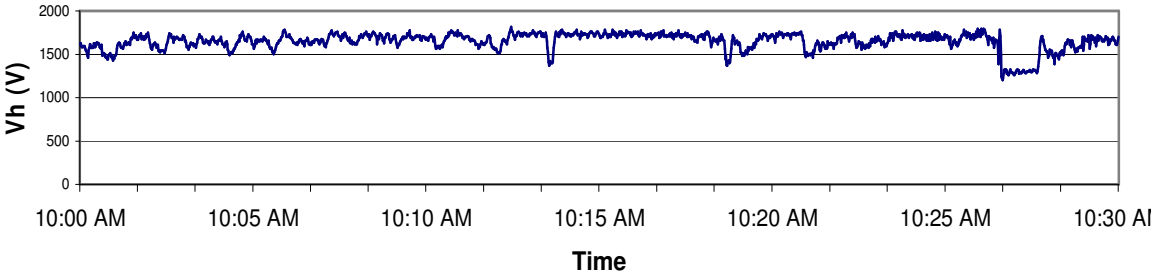

Figure 4-6: Variation of harmonic voltage of a feeder from 10AM to 10:30AM

The dIf and HI (harmonic impact) are calculated and presented in the figure below. Harmonic impact indices converge for the dIf's above the 6%. This percentage is a threshold to filter data. Average harmonic impact of the load can be estimated by getting the average of the filtered data (the data inside the red oval).

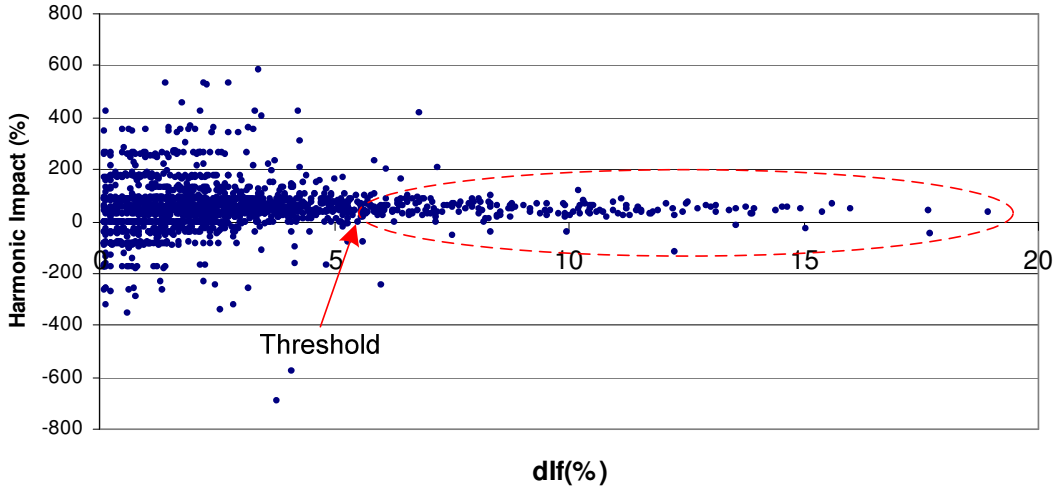

Figure 4-7: dIf (variation of fundamental current) versus Harmonic impact

One important question is how data-filtering threshold should be set. In the following sections, the proposed algorithm will be verified and characterized by simulation and field measurement studies. By using sensitivity studies, practical thresholds are achieved.

4.4 Simulation Studies

In this section, the proposed method is verfied by simulation case studies. The IEEE 118-Bus test case is studied in this case study. In our study, fifteen harmonic loads inject harmonic currents into the system. Harmonic loads are attached to the following buses: [3 7 17 23 28 33 41 47 67 75 84 94 101 109 115]. The harmonic spectra of the harmonic loads are presented in Table 4-2. The magnitudes are scaled based on the fundamental component of the load current, and the phase angles are adjusted based on the phase angle of the voltage across the load obtained from the fundamental frequency solution. This process is simulated by using the recorded field measurements of the distribution transformers in the city of Edmonton. In our simulation studies, 28800 samples (24 hours, 20 samples per minute) are generated by our process simulation algorithm.

Table 4-2: Spectrum table of Harmonic Loads

Harmonic Order	Magnitude (percent)	Relative Angle (degree)
1	100	0.00
3	25.00	-10.21

5	18.24	-55.68
7	11.90	-84.11

Figures 4-8 to 4-10 show the general profile of the harmonic voltages in the system. In the single point study, the harmonic impact of each harmonic-generating load on its PCC bus is desired. The harmonic voltages at the PCC of the harmonic loads are shown in Figure 4-11. The harmonic impact of each load is estimated and compared with its exact harmonic impact (achieved by theoretical calculation). Each load is studied individaully.

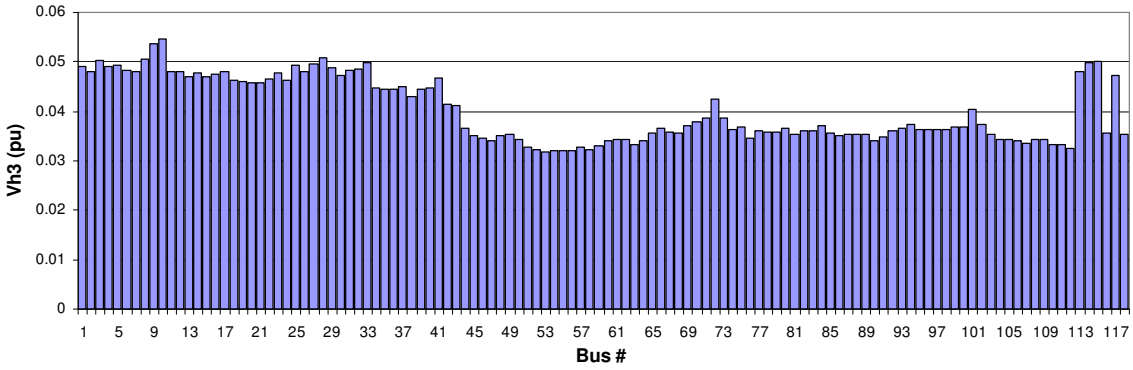

Figure 4-8: The profile of 3rd order harmonic voltage in the system

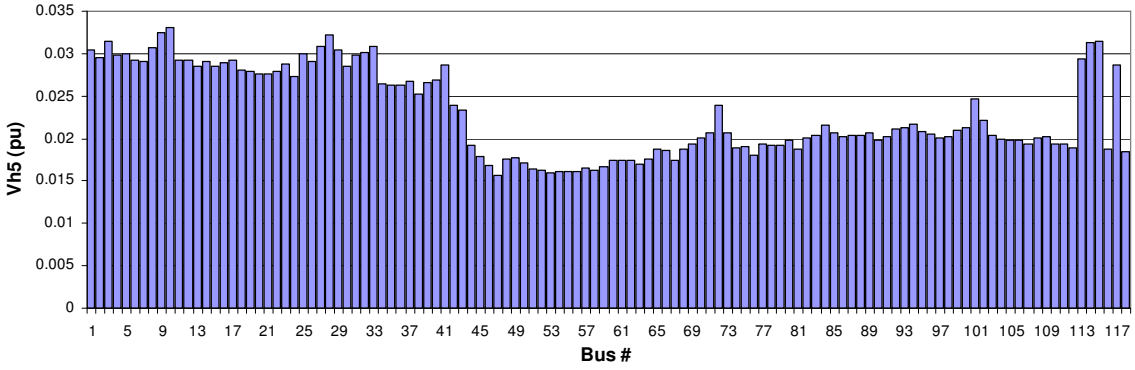

Figure 4-9: The profile of 5th order harmonic voltage in the system

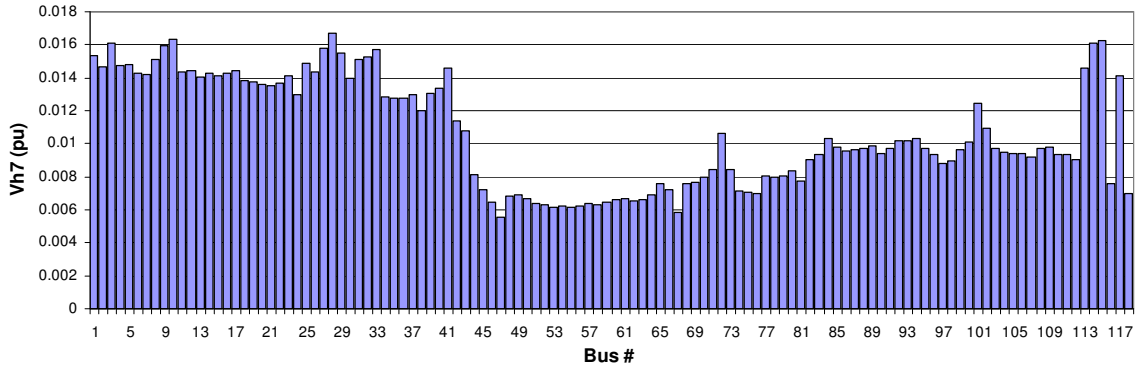

Figure 4-10: The profile of 7th order harmonic voltage in the system

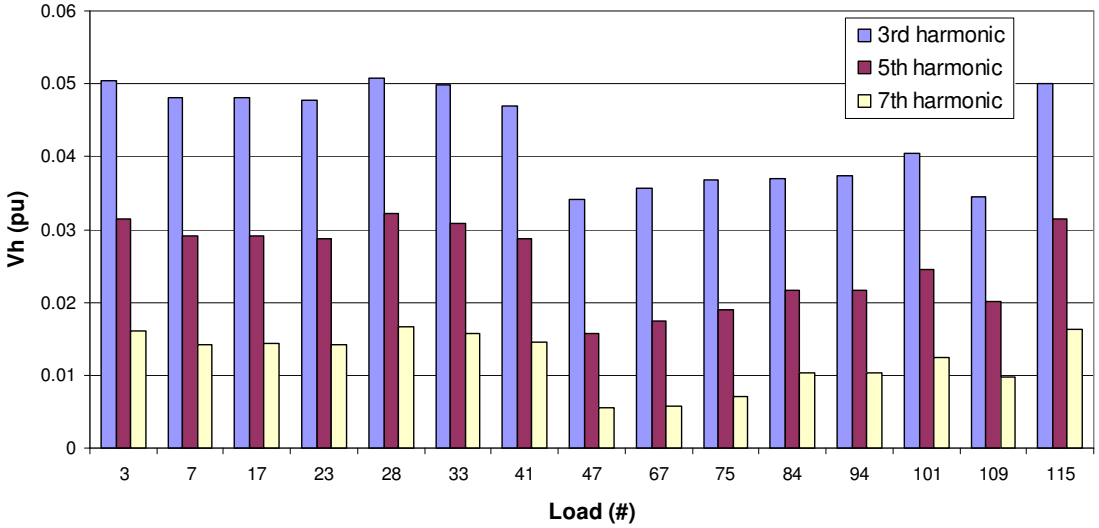

Figure 4-11: Harmonic voltages at PCC of harmonic-generating loads

4.4.1 Study of a load with high harmonic impact

Figure 4-12 shows the variation of the harmonic voltage on bus 3 during the 24 hours (the simulation period). The harmonic voltage of the bus is almost constant during the night and does not fluctutate noticeably during the day. It increases slightly in the morning and does not fluctuate significantly during the working hours. However, it drastically increases in the evening. Because the harmonic-generating loads are simulated by using the recorded data from a residential transoformer, this harmonic behaviour is expectable. The impact of load 3 on this harmonic voltage is shown in Figure 4-13.

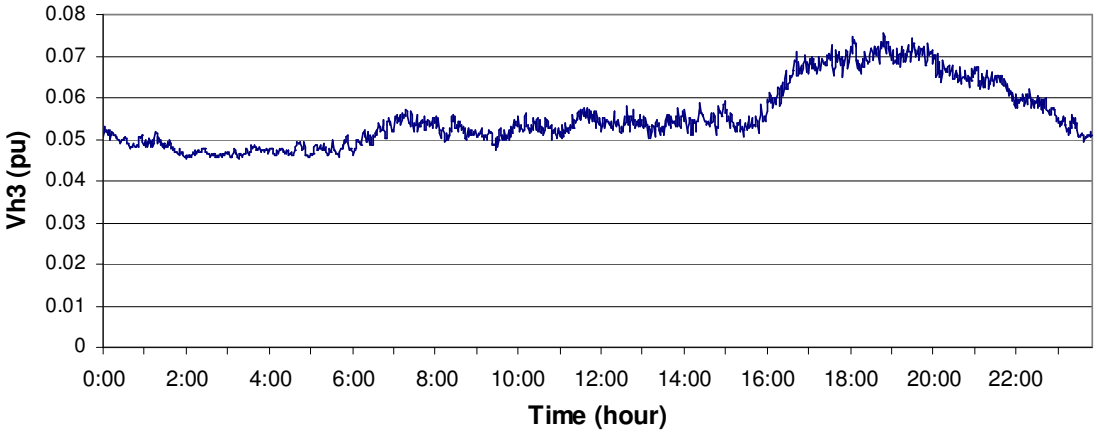

Figure 4-12: Fluctuation of harmonic voltage of bus 3 during the simulated day

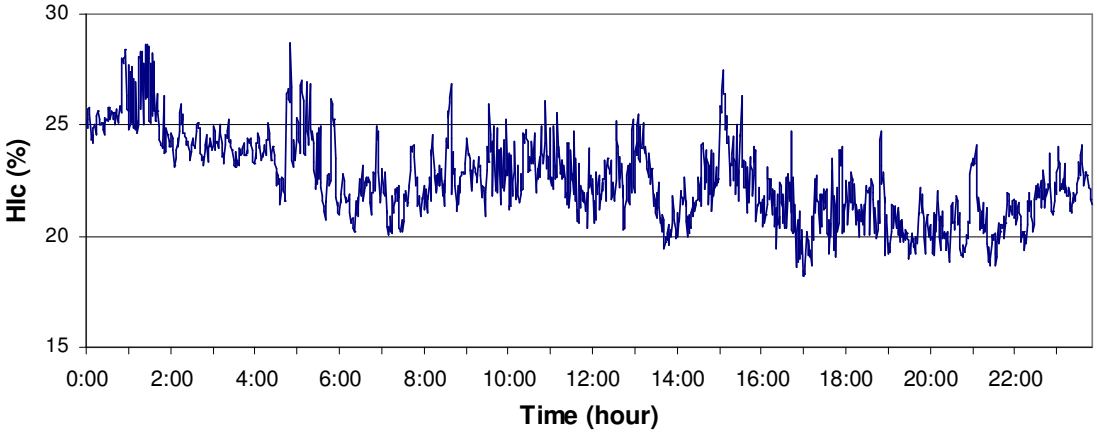

Figure 4-13: Fluctuation of harmonic impact of load 3 during the simulated day

The study window of 1 hour is selected. For every hour of data, the average of the theortical (exact) harmonic impact is calculated. Next, the harmonic impact of the load is estimated by using the proposed algorithm. Figure 4-14 compares the estimated values with the exact values.

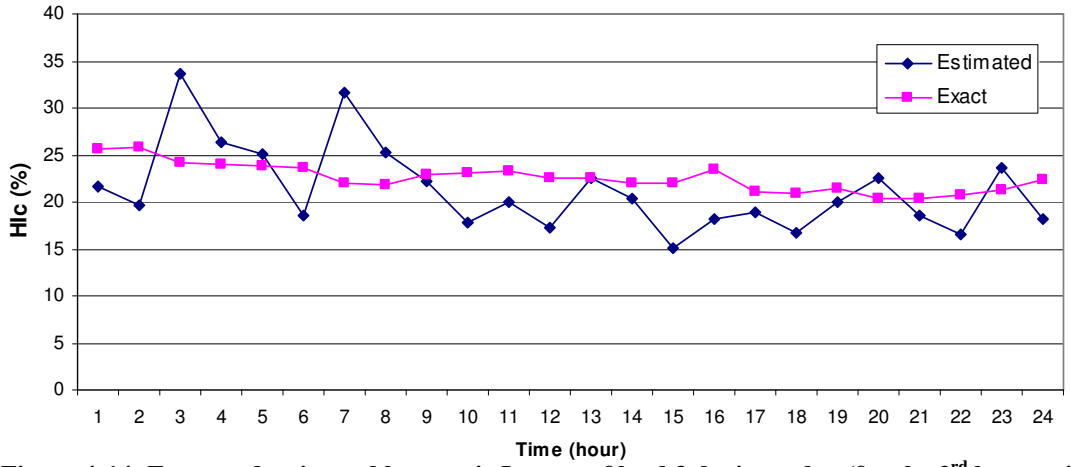

Figure 4-14: Exact and estimated harmonic Impact of load 3 during a day (for the 3rd harmonic)

As an example, the procedure for estimating the harmonic impact for the first hour of the data is explained. Figure 4-15 shows the variation of the fundamental current of this load during the first hour (from 12 AM to 1AM). For those points for which the load variation is more than 3%, the harmonic impact is calcuated and shown in Figure 4-16. The histograms of the estimated values are presented in Figure 4-17. The average of these calcuated harmonic impacts is 21.66%. The exact harmonic impact of this load is 25.56%. The estimated harmonic impacts are correlated to the variations of the dIf. Figure 4-18 shows that by increasing the dIf, the estimated values are concentrated around the exact harmonic impact of the load.

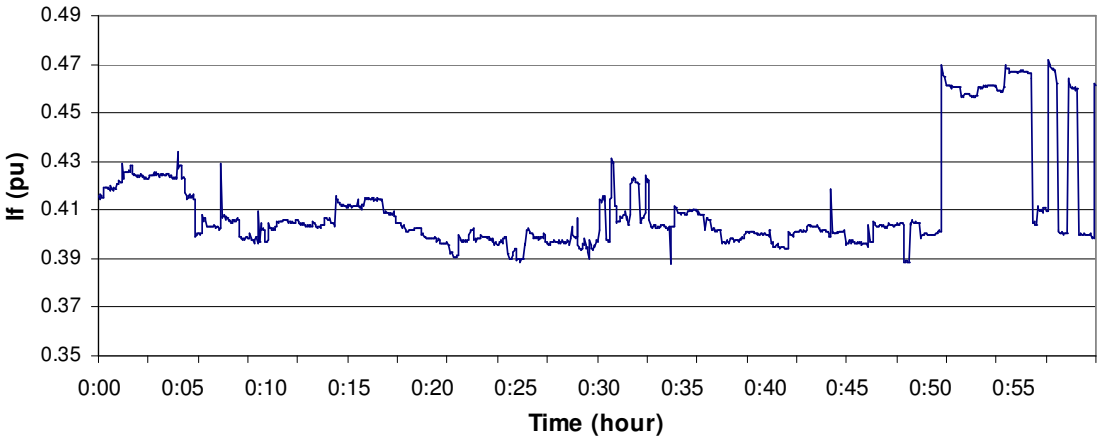

Figure 4-15: Variation of fundamental current of load 3 from 12AM to 1AM

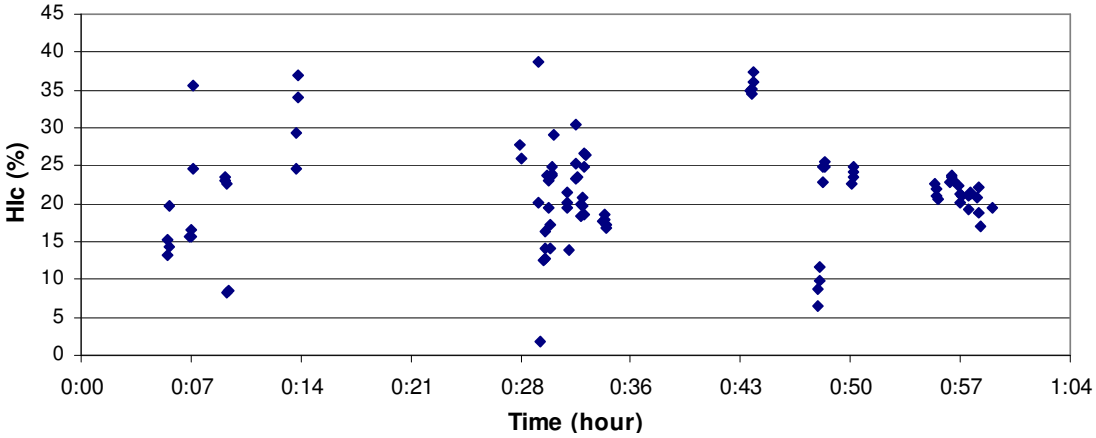

Figure 4-16: Estimated harmonic impact of load 3 for samples with dI_f > 3%

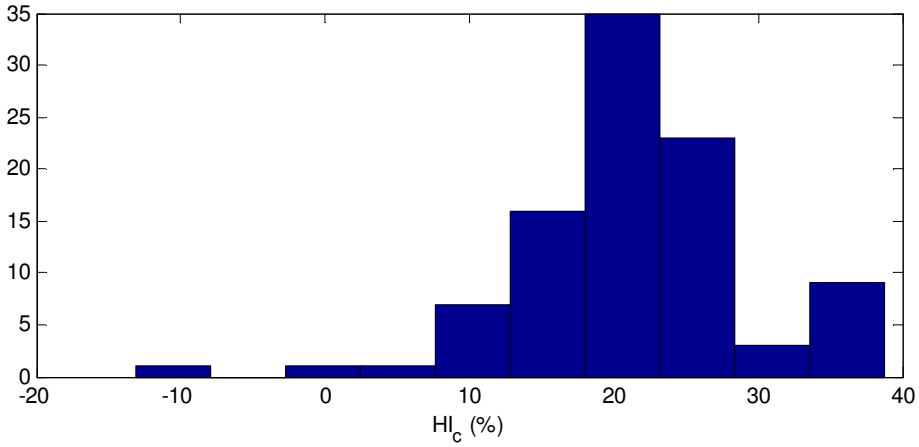

Figure 4-17: Histogram of the estimated harmonic impact of load 3

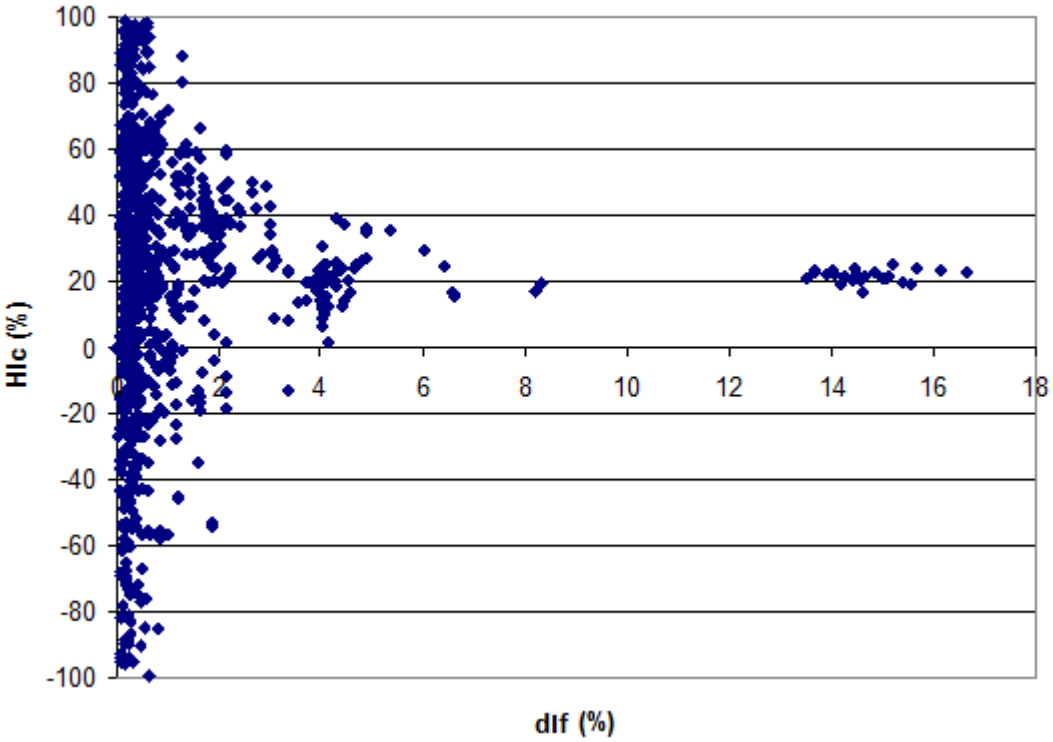

Figure 4-18: Impact of dIf on the estimated HIc

For the 5th and 7th harmonic orders, the harmonic impact of load 3 are estimated and compared with the exact values. Figure 4-19 and Figure 4-20 show the results.

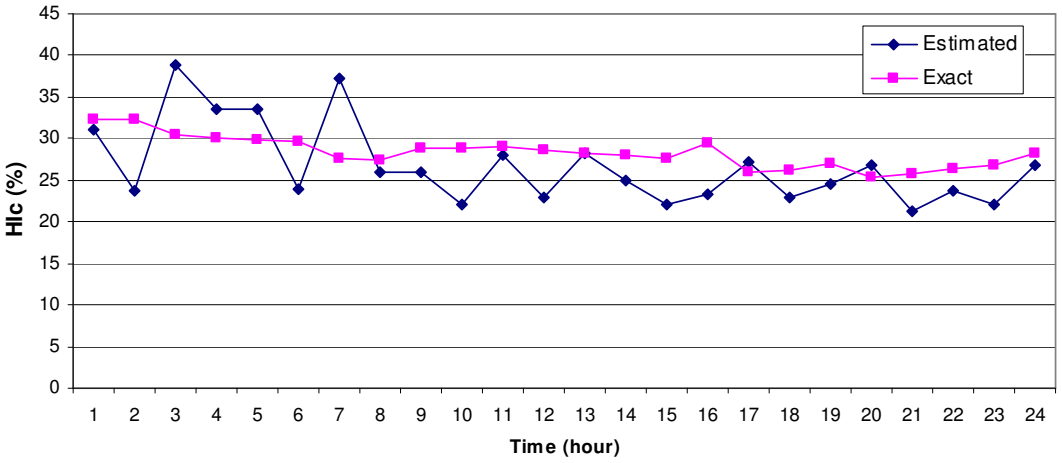

Figure 4-19: Exact and estimated harmonic Impact of load 3 during a day (for the 5th harmonic)

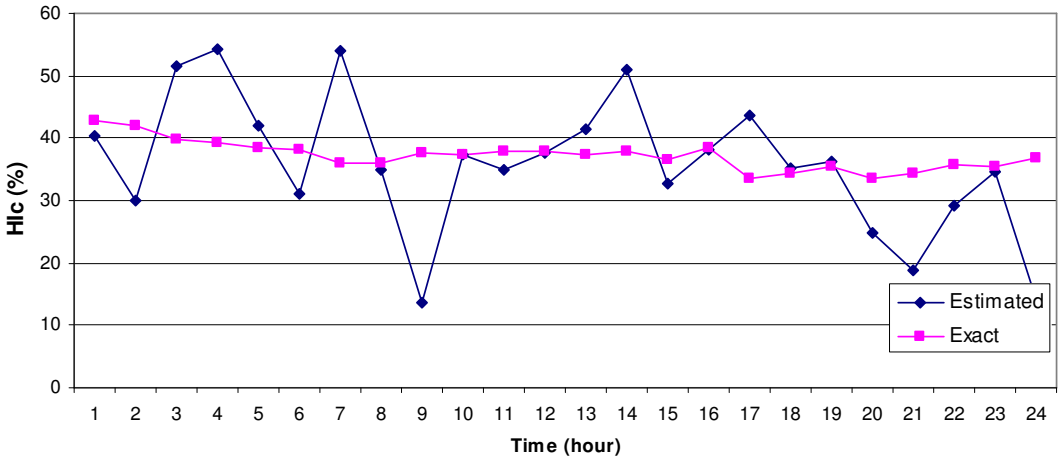

Figure 4-20: Exact and estimated harmonic Impact of load 3 during a day (for the 7th harmonic)

4.4.2 Study of a load with low harmonic impact

The harmonic impact of the previous studied load (load 3) was fairly noticable and was around 25 to 40 percent. The results showed that the proposed method estimated the harmonic impact of this load fairly well. However, load 7 is a smaller load, and its harmonic impact is always less than 10%. In this example, the performance of the method for this type of load is investigated. The results are shown in the following figures.

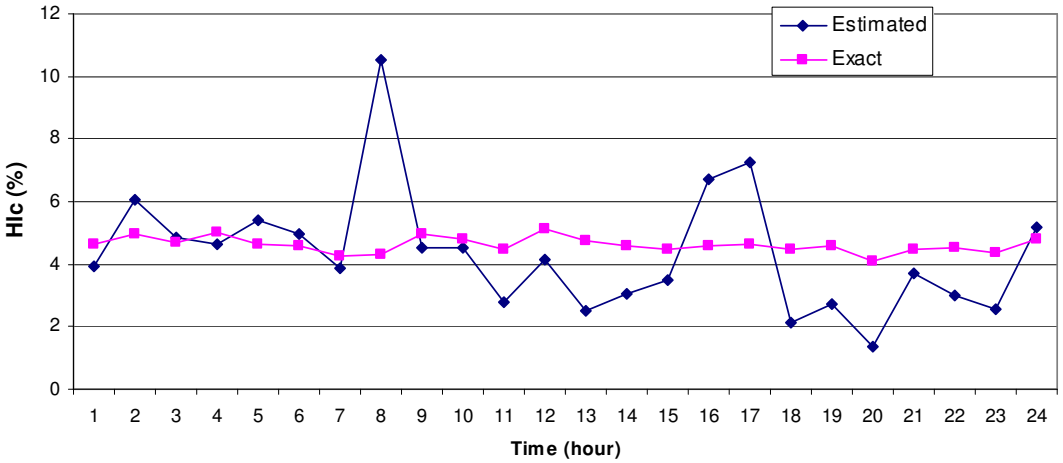

Figure 4-21: Exact and estimated harmonic Impact of load 7 during a day (for the 3rd harmonic)

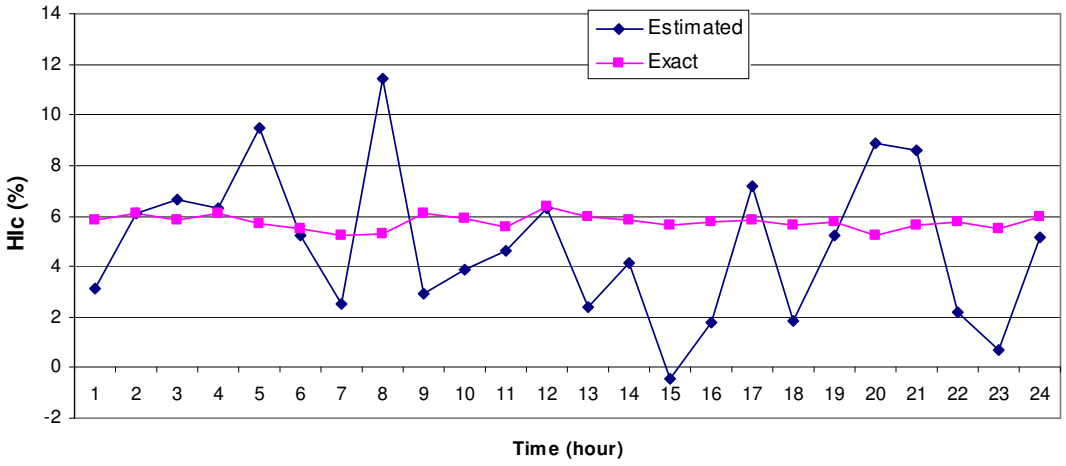

Figure 4-22: Exact and estimated harmonic Impact of load 7 during a day (for the 5th harmonic)

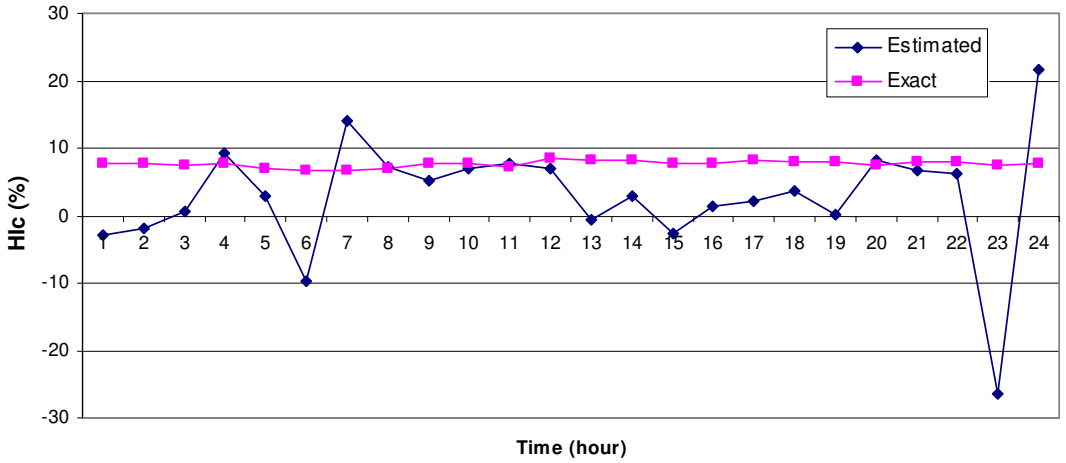

Figure 4-23: Exact and estimated harmonic Impact of load 7 during a day (for the 7th harmonic)

As these figures reveal, the method can estimate the harmonic impact of this type of load. For example, the exact harmonic impact of 3rd harmonic order is almost 5%. The estimated values are between 2 to 8%, and the average of the estimated value matches with the exact value. However, the accuracy of the method decreases with increase in the harmonic order.

4.4.3 Study of a load with high harmonic impact

Load 47 has some unique characteristics. For example in the 3rd harmonic, the harmonic impact of this load is very small and varies from negative to positive values during the day. The proposed method is able to follow this variation. Figure 4-24 shows

the results for the 3rd harmonic. As this figure reveals, the pattern of the estimated values follows that of the exact values. Thus, the method works for this type of load.

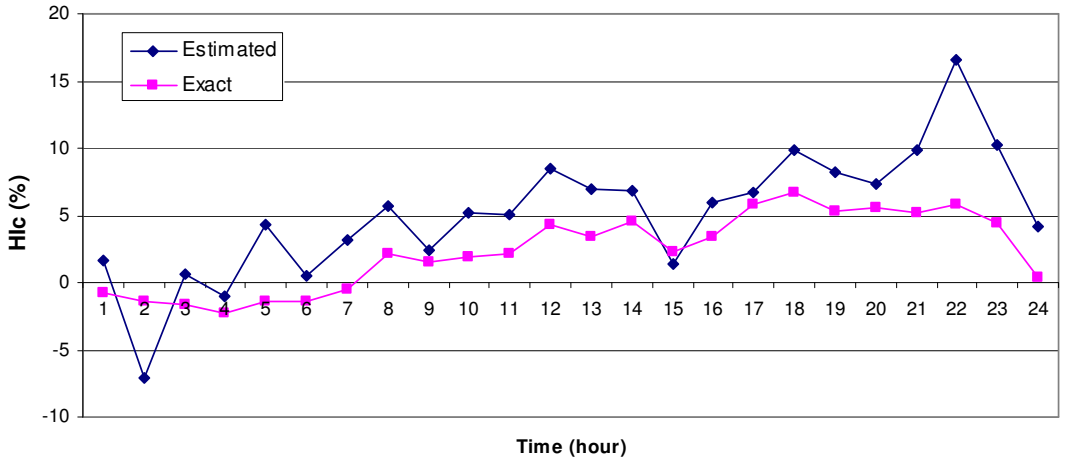

Figure 4-24: Exact and estimated harmonic impact of load 47 during a day (for the 3rd harmonic)

For the 5th and 7th harmonic orders, the harmonic impact of the load is negative. The results show that the method can estimate both the positive and negative harmonic impacts of loads.

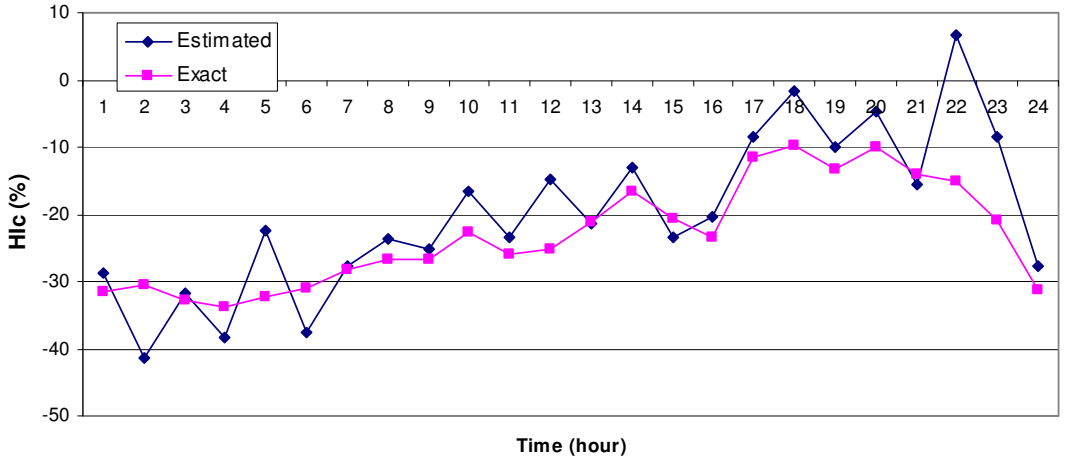

Figure 4-25: Exact and estimated harmonic impact of load 47 during a day (for the 5th harmonic)

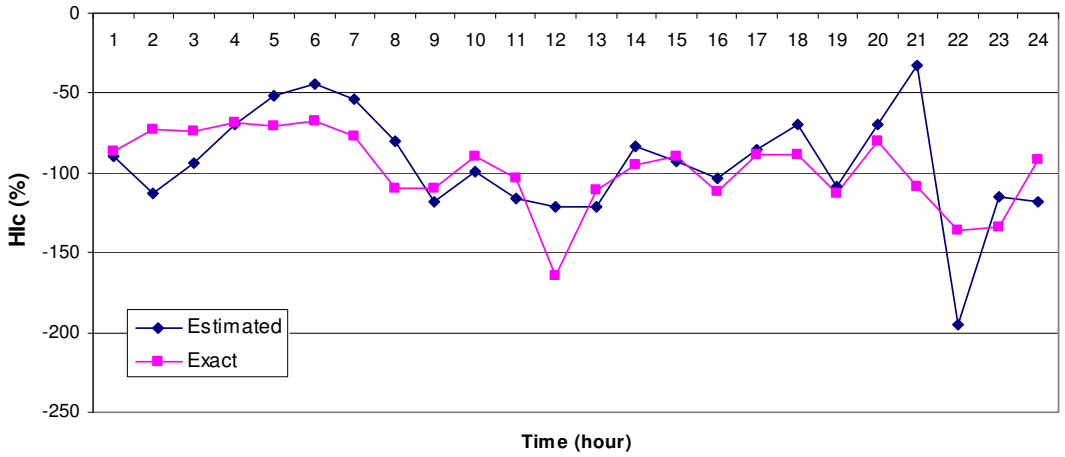

Figure 4-26: Exact and estimated harmonic impact of load 47 during a day (for the 7th harmonic)

4.4.4 Study of other loads

As the characteristics of the other remaining loads are similar to those of the previously studied loads, the detailed results are not shown here. The complete results are shown in Table 4-3. The estimated and exact harmonic impact of each load during the studied day are averaged and presented in this table.

Table 4-3: The average of exact and estimated harmonic impact of harmonic loads

harmonic	H=3		H=5		H=7	
Load	Estimated	Exact	Estimated	Exact	Estimated	Exact
3	21.3	22.6	26.7	28.4	35.9	37.2
7	6.7	7.4	6.3	7.1	5.8	5.4
17	4.3	4.6	4.8	5.7	5.9	7.6
23	3.7	4.2	4.5	5.5	5.7	7.7
28	11.4	12.8	14.8	15.9	15.3	20.1
33	15.5	17.0	20.3	20.9	27.8	26.6
41	28.8	30.9	40.5	37.5	55.9	48.0
47	5.1	2.3	-20.0	-23.1	-93.6	-97.4
67	9.5	10.8	10.5	8.5	-5.0	-0.2
75	20.5	23.6	22.1	29.2	42.6	46.2
84	14.4	13.9	17.3	18.8	19.9	27.9
94	19.4	20.2	20.7	25.5	25.0	36.7
101	21.1	22.0	29.6	28.9	40.7	38.2
109	7.9	9.5	13.0	13.1	19.4	18.4
115	10.2	13.1	15.5	16.8	24.1	22.6

4.5 Sensitivity Study

To charactrize the proposed method, the impact of the following two parameters, the level of the dIf threshold and the size of the data window should be studied.

4.5.1 dIf Threshold

In this study, the impact of the dIf threshold parameter on the performance of the proposed method is studied. For load 3 for different dIf thresholds, the harmonic impact of the load is estimated. Figure 4-27 shows the estimated values for different dIf thresholds.

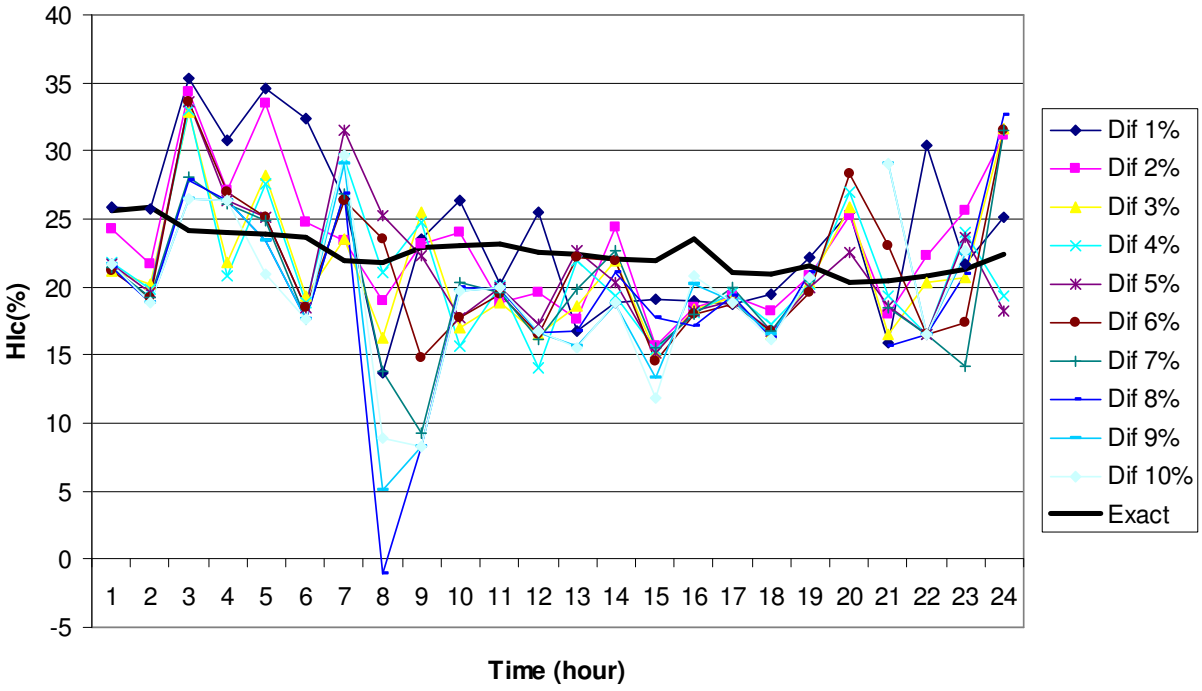

Figure 4-27: The estimated harmonic impact of load 3 for different dIf thresholds

The graph clearly does not show which dIf threshold is the best. To obtain this information, each curve should be condensed to a number, and the numbers should be compared. The MSE[1] index is proposed to quantify error in estimating the harmonic impacts of a load during a day. The index is calculated as follows:

[1] Mean Square Error

$$MSE_{Load\ X}(\%) = \sqrt{\frac{\sum_{i=1}^{N_{t-div}} \left(HI_{Loadi} - \tilde{HI}_{Loadi} \right)^2}{N_{t-div}}}, \tag{4-14}$$

where N_{t-div} is the number of time divisions during a day (For example, this number is 24 if the data window is 1 hour). HI_{Loadi} and $\tilde{HI}_{Load\,i}$ are the exact and the estimated harmonic impact of load i, respectively. The MSE indices of all loads for different dIf thresholds are presented in Figure 4-28.

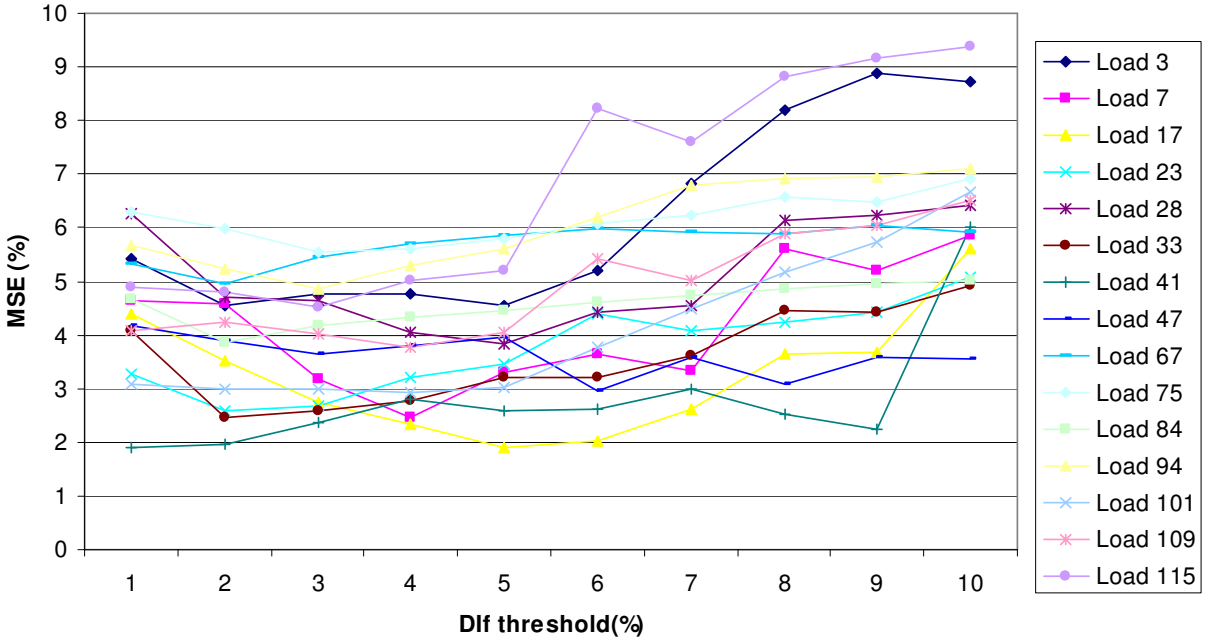

Figure 4-28: MSE indices of loads for different dIf thresholds

The MSE indices should be normalized to be comparable. The MSE indices of the loads are normalized by dividing the MSE index of a load by the minimum MSE index of that load. Figure 4-29 shows the normalized MSE index of the loads. Now, it can clearly be seen that the best range for the dIf threshold is between 3 to 5%.

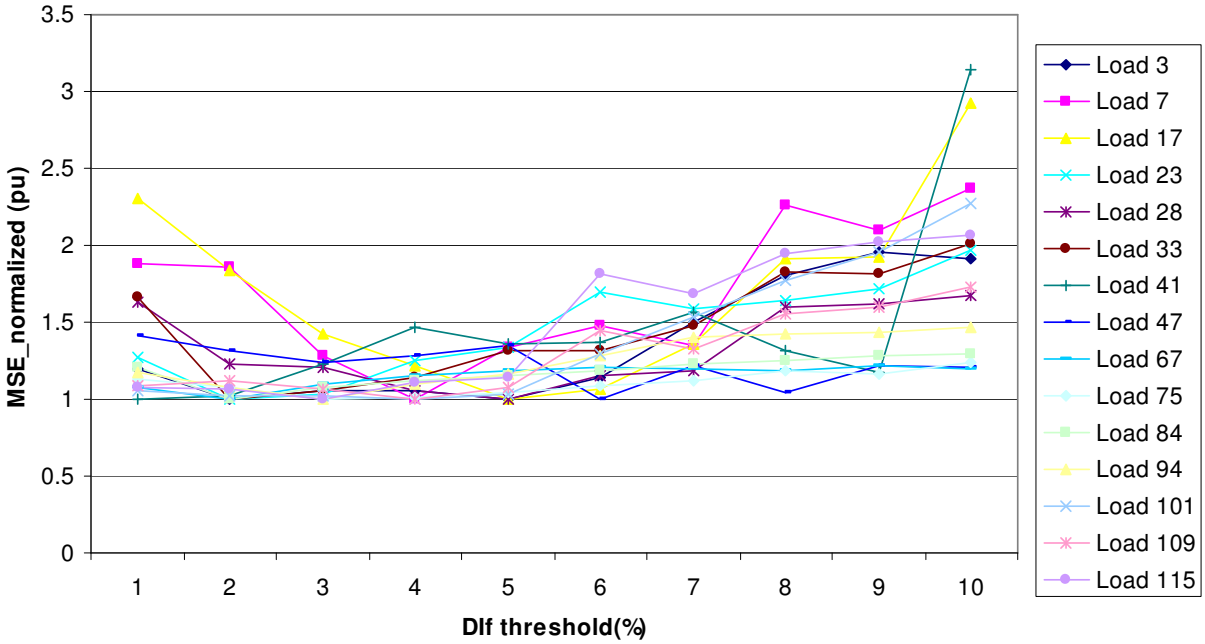

Figure 4-29 : Normalized MSE indices of loads for different dIf thresholds

4.5.2 Size of data window

Another important sensitivity study involves the size of the data window. In the previous case studies, a data window of 1 hour was used. For every one-hour period, one representative harmonic impact is estimated that is considered to be average of the harmonic impacts of that load during that hour. In this study, this data window is varied and its impact on the accuracy of the estimated parameters is studied. For example, Figure 4-30 shows the estimated values of load 3 for different data window lengths.

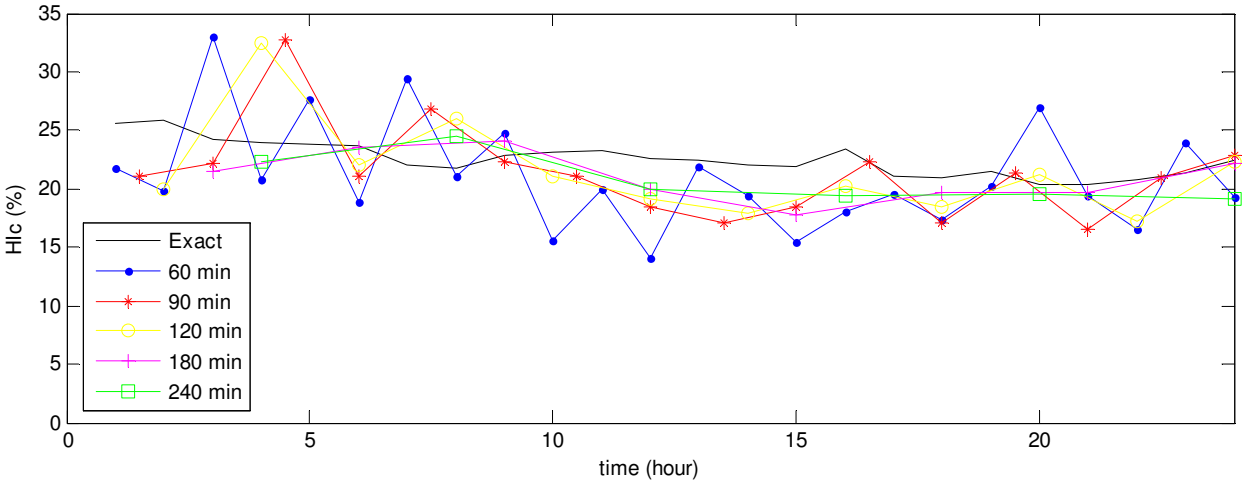

Figure 4-30: The estimated harmonic impact of load 3 for different data window lengths

Figure 4-31 shows how the MSE index decreases when the data window length increases. However, increasing the data window length decreases the number of estimated points. For example, for a data length of 360 min, the harmonic impact of the load during a day can be represented by 4 values, one for every 6 hours. Figure 4-31 shows the MSE indices do not alter noticably after 240 min. The maximum data length window can be considered as 240 min.

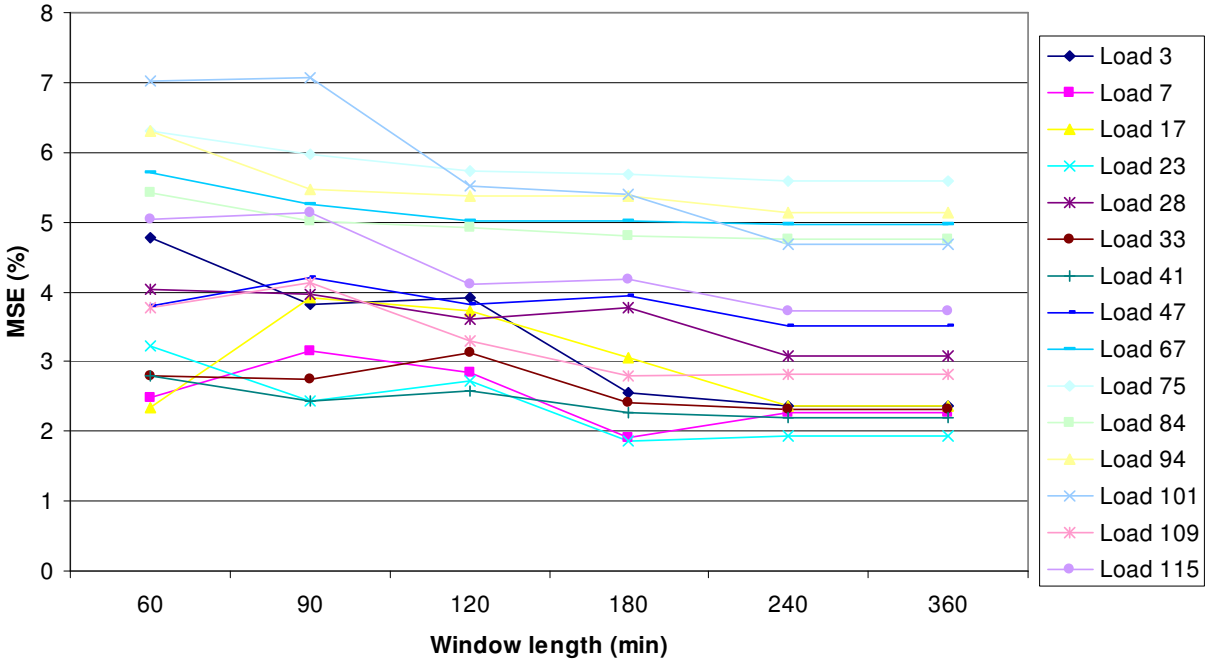

Figure 4-31: MSE indices of loads for different data window lengths

4.6 Field Measurement Case Studies

In this section, the proposed technique is applied to two sets of field measurement data: distribution transformer data and house-panel data.

4.6.1 Transformer Data

This case study applies the proposed single-point algorithms to the data measurements collected at the distribution transformers measured in a residential area in winter 2009. The measurements were recorded by using a sampling rate of 6 cycles per every 3 seconds. The harmonic impedance of the utility system was not available for this data, but the impedance of the transformer is available. By ignoring the impedance behind the transformer, this impedance is utilized as the harmonic impedance of the

system. By using this impedance, the real harmonic impact is calculated and compared with the estimated results. Table 4-4 shows the list of the available transformer datasets used in this case study. The rated power of the transformers is 37.5 kVA, and their rated fundamental impedance and resistance are 2 and 1.293 percent, respectively. The transformers are studied individually.

Table 4-4: List of studied transformer data

No	Transformer ID	Recorded days	Number of recorded days
1	37MN5	2008/11/13 to 2008/11/16	4 days
2	37MN15	2008/11/13 to 2008/11/17	5 days
3	37MNB400	2008/11/23 to 2008/11/24	2 days
4	37MNB427	2008/11/20 to 2008/11/25	6 days
5	37MNB434	2008/11/20 to 2008/11/22	3 days

4.6.1.1 Transformer 37MN5

Figure 4-32 shows the daily load pattern of this transformer. As this figure reveals, the load increases in the morning and keeps increasing until midnight. Figure 4-33 and Figure 4-34 show the daily average of the harmonic current and the voltage spectrum of this transformer, respectively.

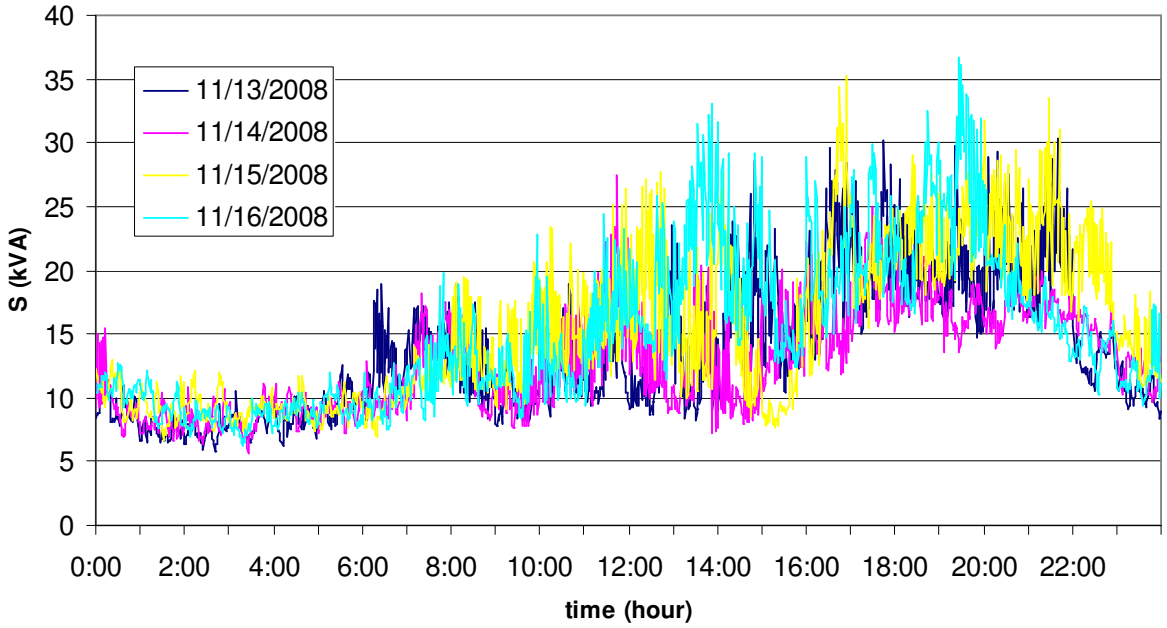

Figure 4-32: Daily load patterns of transformer 37MN5

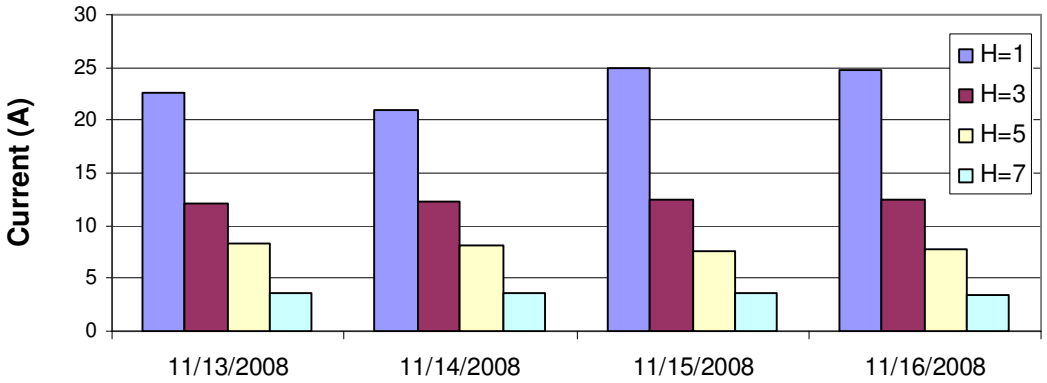

Figure 4-33: Daily average of harmonic current spectrum of transformer 37MN5 (fundamental is divided by 5)

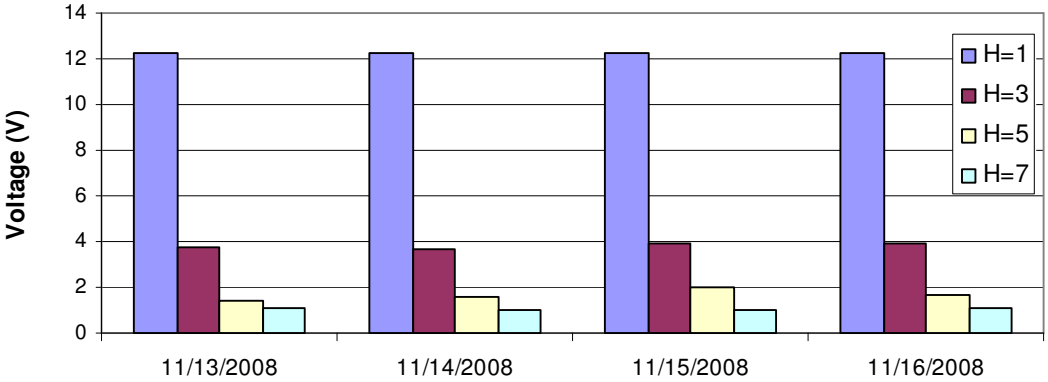

Figure 4-34: Daily average of harmonic voltage spectrum of transformer 37MN5 (fundamental is divided by 10)

Figure 4-35 shows the exact and estimated 3rd-order harmonic impact of Transformer 37MN5 based on the data recorded on the date 13/11/2008. Because the impedance of the network behind the transformer is neglected, the calculated exact harmonic impact is not accurate, and the real harmonic impact should be a bit higher.

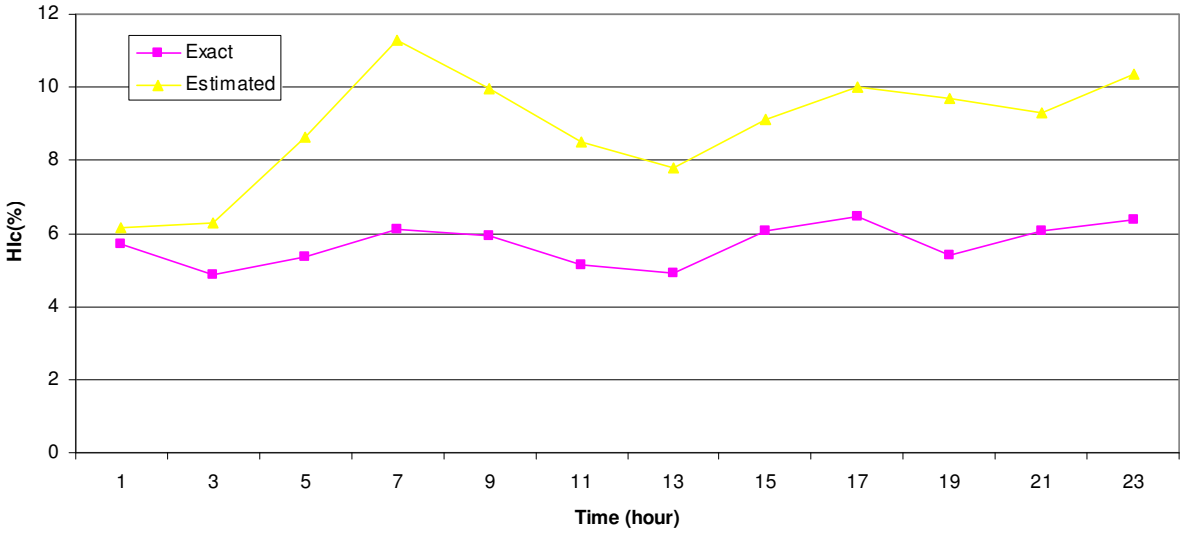

Figure 4-35: Exact and estimated harmonic impact of Transformer 37MN5 during a day on 13/11/2008

The harmonic impact of this transformer is estimated for four days in a row. The results are shown in Figure 4-36, which reveals consistent results.

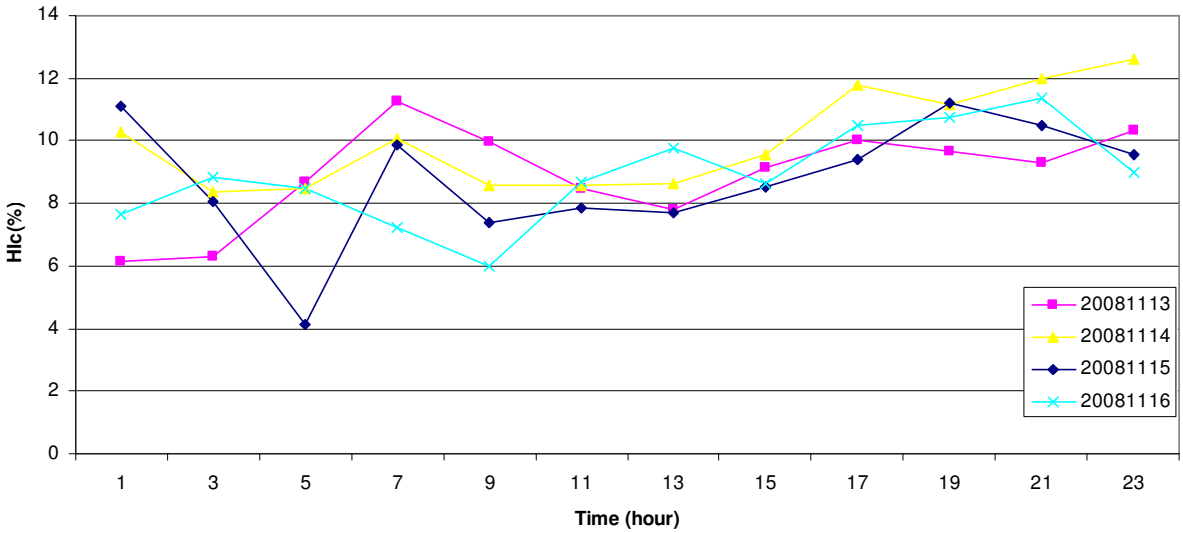

Figure 4-36: The estimated 3rd harmonic impact of Transformer 37MN5 in four days

Figure 4-37 and Figure 4-38 show the exact and estimated 5th-order harmonic impact of Transformer 37MN5 based on the data recorded on the dates 13/11/2008 and 14/11/2008, respectively. For the 3rd and 5th harmonic orders, the estimated harmonic impacts are in good agreement with the theoretically calculated harmonic impacts (the

exact impacts). However, the results for the 7th harmonic are not promising. Figure 4-39 shows the exact and estimated 7th-order harmonic impact of Transformer 37MN5 based on the data recorded on the date 13/11/2008. One possible explanation for this problem in the 7th harmonic is that ignoring the utility impedance before the transformer is not reasonable for this harmonic order. For this reason, the theoretical calculated harmonic impact is inaccurate and should not be referenced.

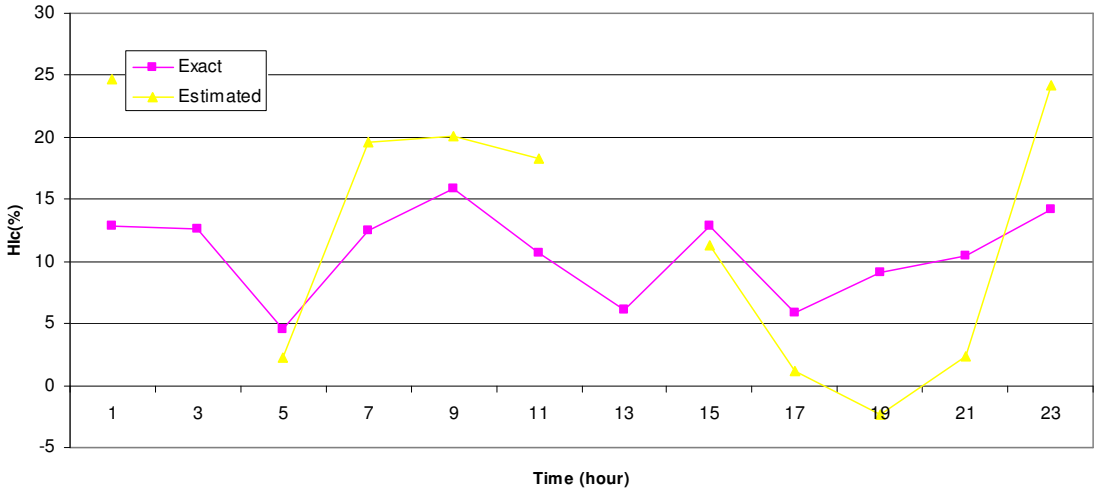

Figure 4-37: The estimated 5th harmonic impact of Transformer 37MN5 during a day on 13/11/2008

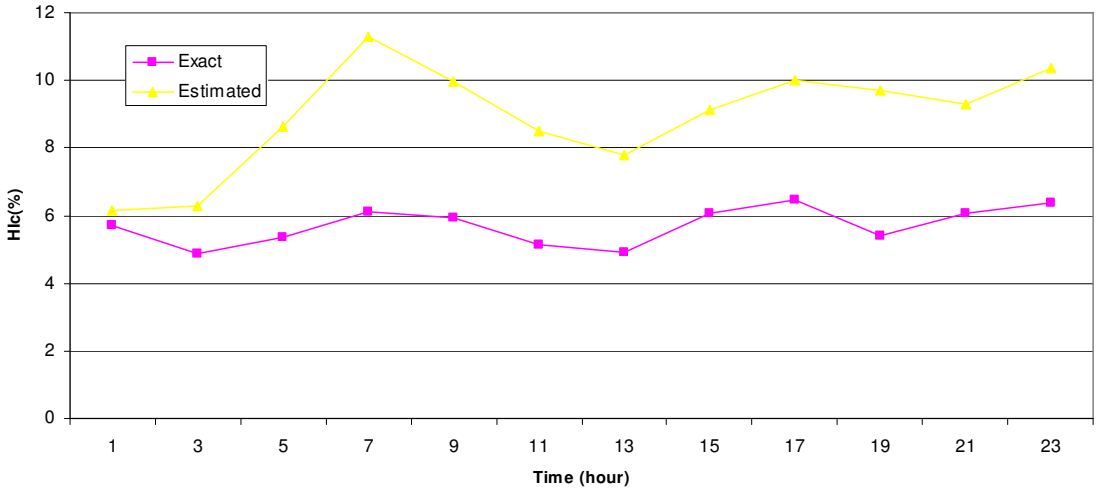

Figure 4-38: The estimated 5th harmonic impact of Transformer 37MN5 during a day on 14/11/2008

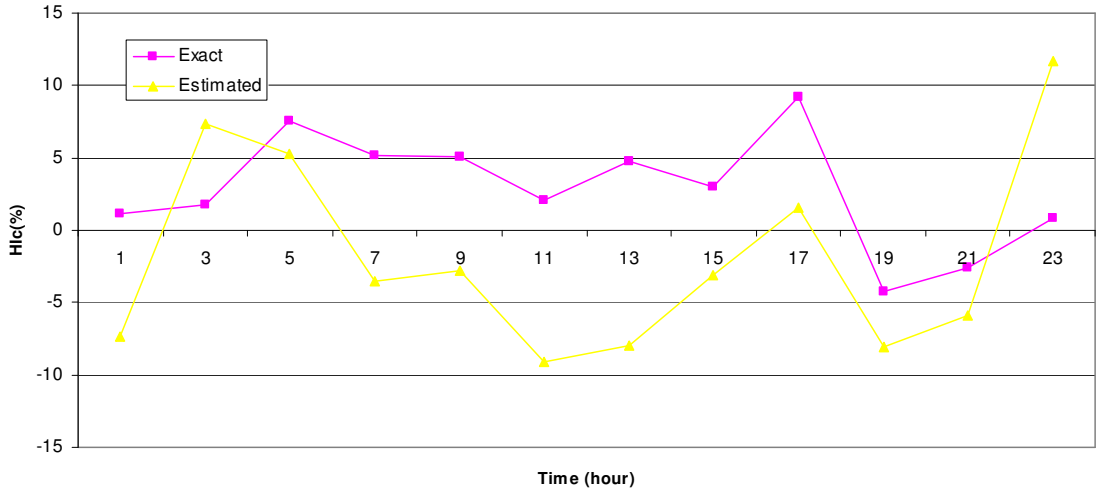

Figure 4-39: The estimated 7th harmonic impact of Transformer 37MN5 during a day on 13/11/2008

The full results for this transformer are presented in Table 4-5 . The harmonic impact of each day is averaged. The estimated parameters are compared with the theoretical harmonic impact.

Table 4-5: Estimated and Exact harmonic impact of Transformer 37MN5

Harmonic Order		Date			
		11/13/2008	11/14/2008	11/15/2008	11/16/2008
H=3	Exact	5.7	5.8	5.6	5.6
	Estimated	9.4	10.0	8.8	8.9
H=5	Exact	10.6	9.7	4.2	6.9
	Estimated	12.2	11.3	3.6	4.8
H=7	Exact	2.8	4.8	7.6	6.9
	Estimated	-1.8	0.4	5.9	5.0

4.6.1.2 Transformer 37MN15

Figure 4-40 shows the exact and estimated 3rd-order harmonic impact of Transformer 37MN15 based on the data recorded on the date 13/11/2008. Because the impedance of the network behind the transformer is ignored, the calculated exact harmonic impact is not accurate and the real harmonic impact is higher.

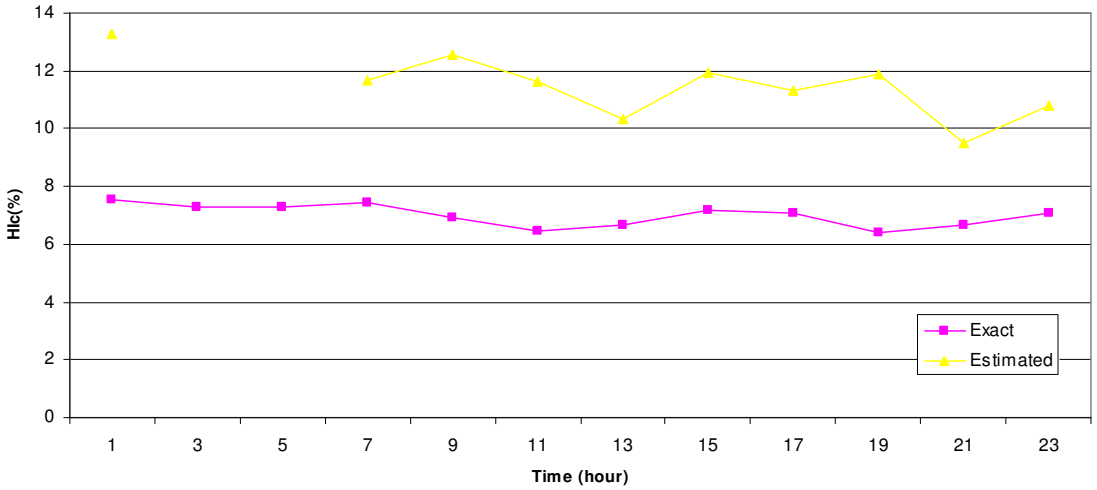

Figure 4-40: Exact and estimated harmonic impact of Transformer 37MN15 during a day on 13/11/2008

The harmonic impact of this transformer is estimated for five days in a row and compared with the average theoretical harmonic impact of transformer. The results are shown in Figure 4-41. As it can be seen, the results show consistency.

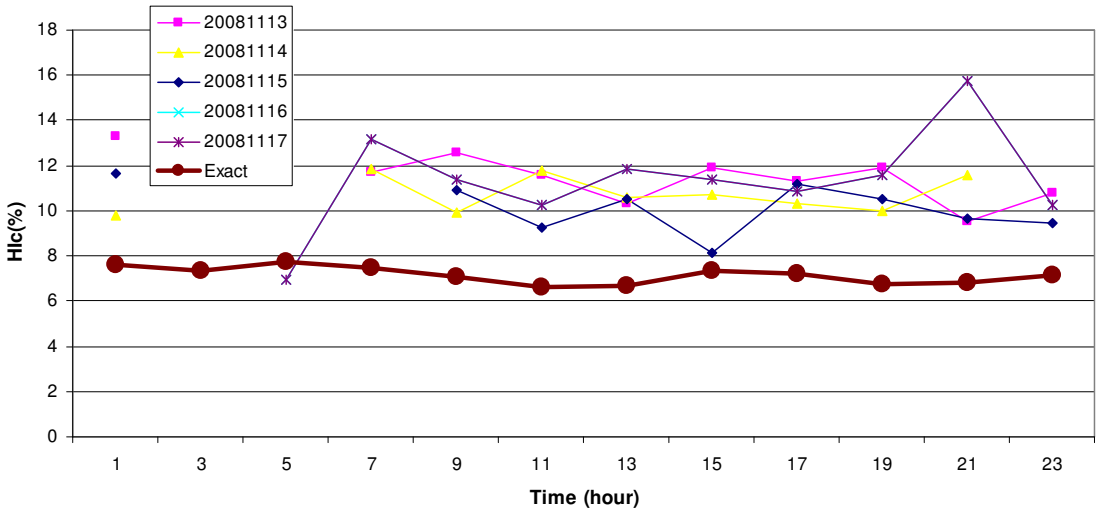

Figure 4-41: The estimated 3rd harmonic impact of Transformer 37MN15 in five days

The full results for this transformer are presented in Table 4-6. The harmonic impact of each day is averaged. Estimated parameters are compared with the theoretical harmonic impact.

Table 4-6: Estimated and Exact harmonic impact of Transformer 37MN15

Harmonic Order		Date				
		11/13/2008	11/14/2008	11/15/2008	11/16/2008	11/17/2008
H=3	Exact	7.0	7.2	6.7	7.4	7.4
	Estimated	11.5	10.7	10.2	11.3	11.3
H=5	Exact	12.4	12.0	5.0	7.3	14.4
	Estimated	15.6	12.4	5.1	3.7	8.6
H=7	Exact	5.4	6.4	7.3	7.3	5.3
	Estimated	1.7	3.1	5.3	6.9	2.7

4.6.1.3 Transformer 37MNB400

Figure 4-42 and Figure 4-43 show the exact and estimated 3rd order harmonic impact of Transformer 37MNB400 based on the data recording on the date 23/11/2008 and 24/11/2008. For the 3rd harmonic, the estimated values are in good agreement with theoretical calculated values.

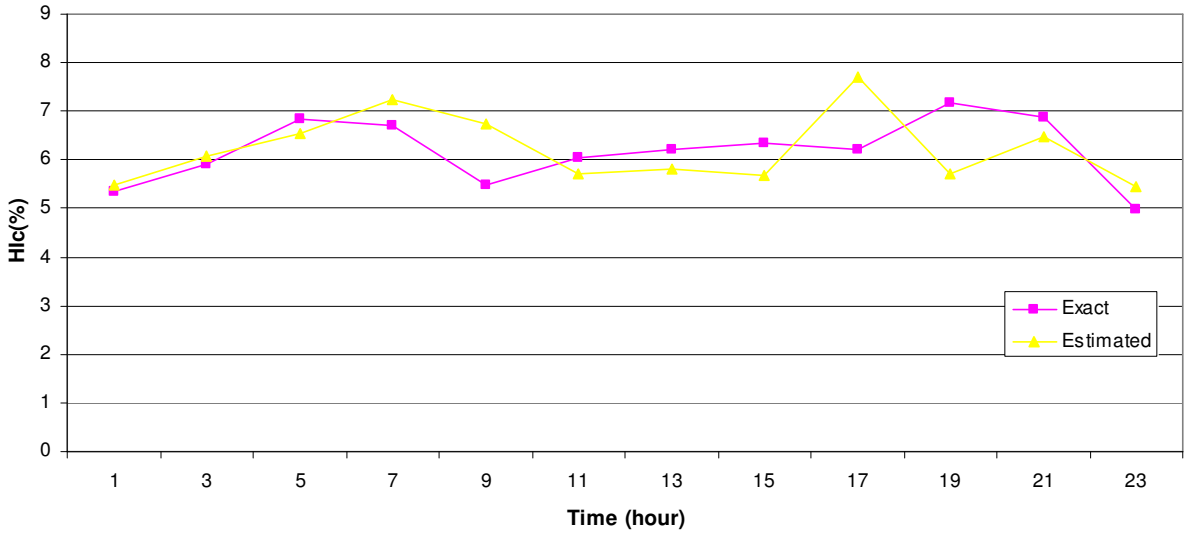

Figure 4-42: The estimated 3rd harmonic impact of Transformer 37MNB400 during a day on 23/11/2008

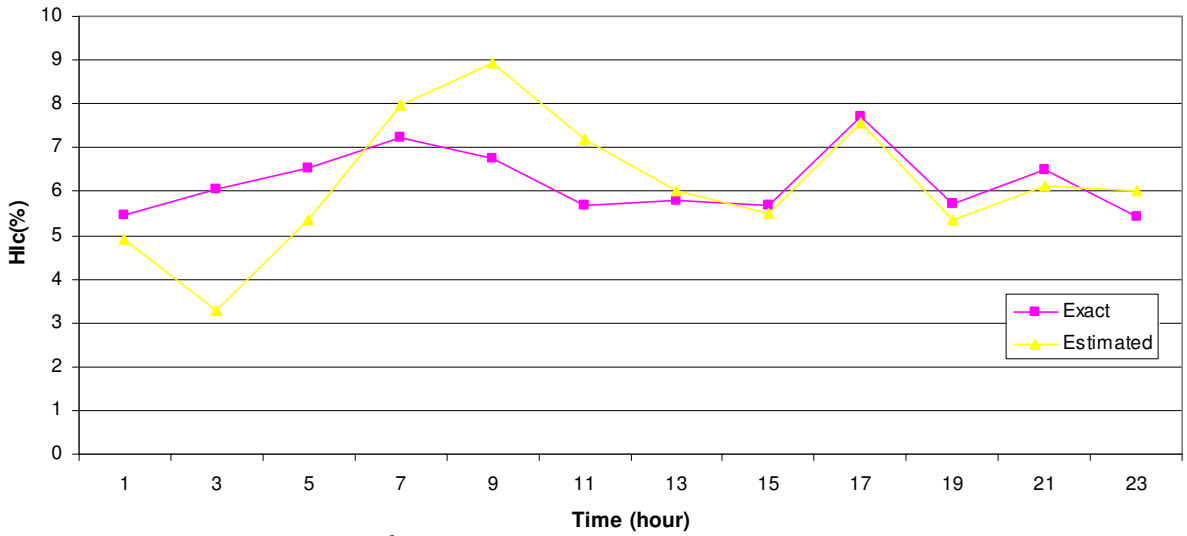

Figure 4-43: The estimated 3rd harmonic impact of Transformer 37MNB400 during a day on 24/11/2008

4.6.1.4 Transformer 37MNB427

The harmonic impact of this transformer is estimated for six days in a row and compared with the average theoretical harmonic impact of transformer. The results for the 3rd harmonic are shown in Figure 4-44 . As it can be seen, the estimated values are in good agreement with theoretical calculated values.

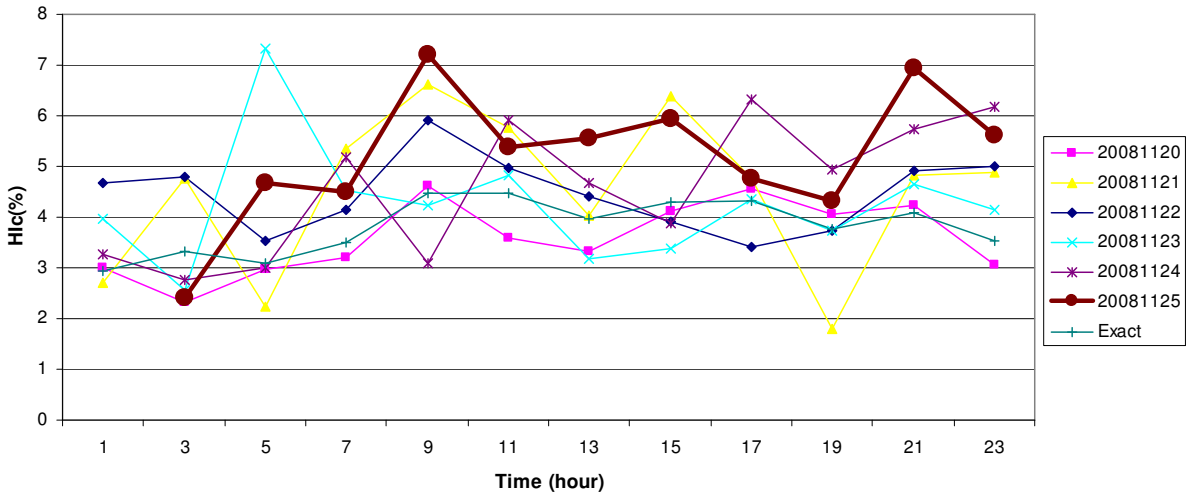

Figure 4-44: The estimated 3rd harmonic impact of Transformer 37MNB427 in six days

The full results for this transformer are presented in Table 4-7. The harmonic impact of each day is averaged. Estimated parameters are compared with the theoretical harmonic impact.

Table 4-7: Estimated and Exact harmonic impact of Transformer 37MNB427

Harmonic Order				Date			
		11/20/2008	11/21/2008	11/22/2008	11/23/2008	11/24/2008	11/25/2008
H=3	Exact	4.3	3.6	3.8	3.4	3.8	3.9
	Estimated	3.6	4.5	4.5	4.2	4.6	5.2
H=5	Exact	3.3	2.3	2.2	2.0	2.5	1.3
	Estimated	-4.5	-5.3	-7.6	-4.7	-7.1	-7.3
H=7	Exact	1.7	2.7	2.1	1.7	2.5	3.5
	Estimated	-3.3	-1.2	-0.2	0.1	-0.9	-2.5

4.6.1.5 Transformer 37MNB434

The harmonic impact of this transformer is estimated for three days in a row and compared with the average theoretical harmonic impact of transformer. The results for the 3rd, and 5th harmonic are shown in Figure 4-45 and Figure 4-47. As it can be seen, the estimated values are in good agreement with theoretical calculated values.

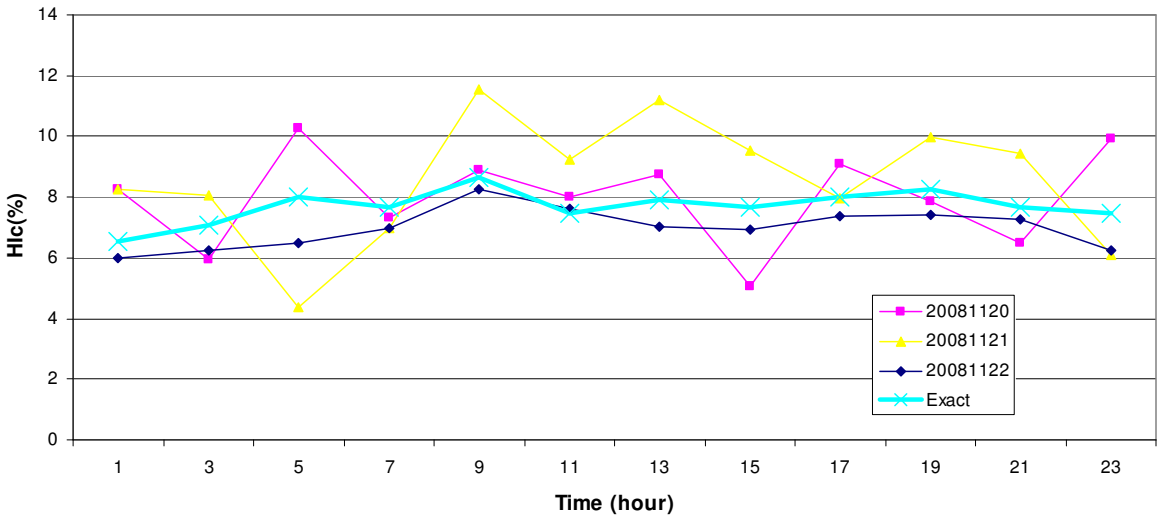

Figure 4-45: The estimated 3rd harmonic impact of Transformer 37MNB433 in three days

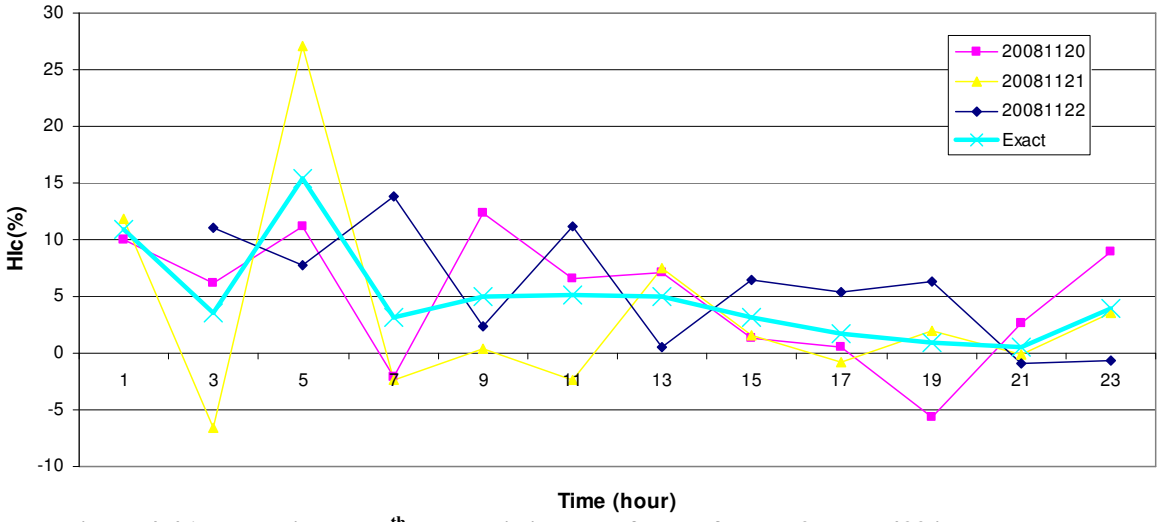

Figure 4-46: The estimated 5th harmonic impact of Transformer 37MNB433 in three days

For the 7th harmonic, the results are shown in Figure 4-45. For this harmonic order, the estimated results are not in good agreement with the theoretical results, similar to the previous cases. This shows that for this harmonic order the real harmonic impedance of the utility is necessary.

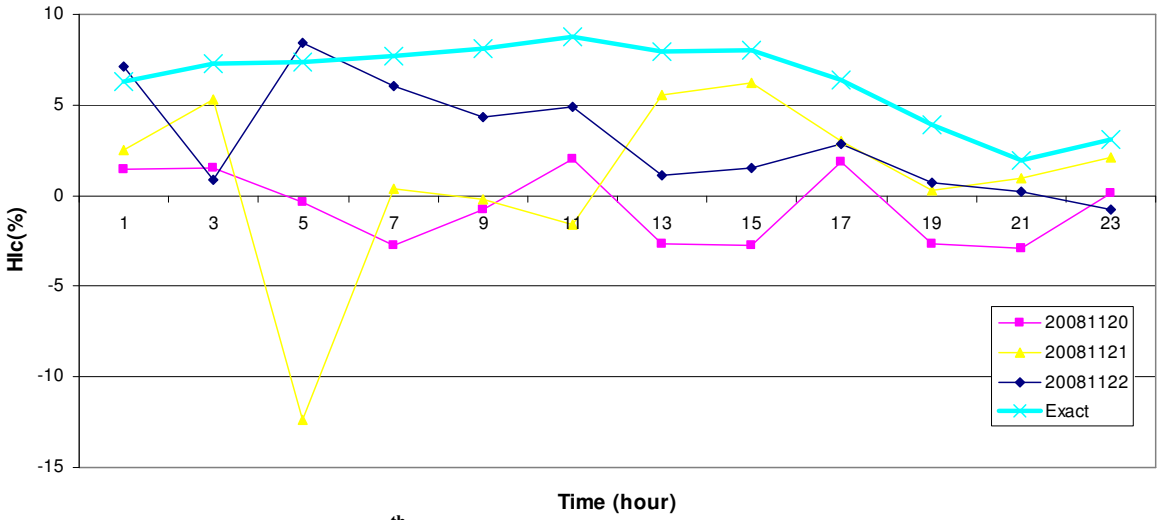

Figure 4-47: The estimated 7th harmonic impact of Transformer 37MNB433 in three days

4.6.2 House-panel Measurement

In this case, the proposed single-point method is applied to the measured data which is recorded at the panel of a house. Prior to the measurement, the utility impedance seen from the panel of the house was calculated by using the capacitor switching technique

[27]. Next, the voltage and current at the panel of the house was monitored for 24 hours with the sampling rate of 6-cycle per every 3 seconds. By using the utility impedance, the exact harmonic impact of the house is calculated and compared with the estimated results obtained by our proposed method. Figure 4-48 and Figure 4-49 shows the exact and estimated harmonic impact of the house for the 3rd and 5th harmonics. As it can be seen, the estimated and exact harmonic impacts are in good agreement

.

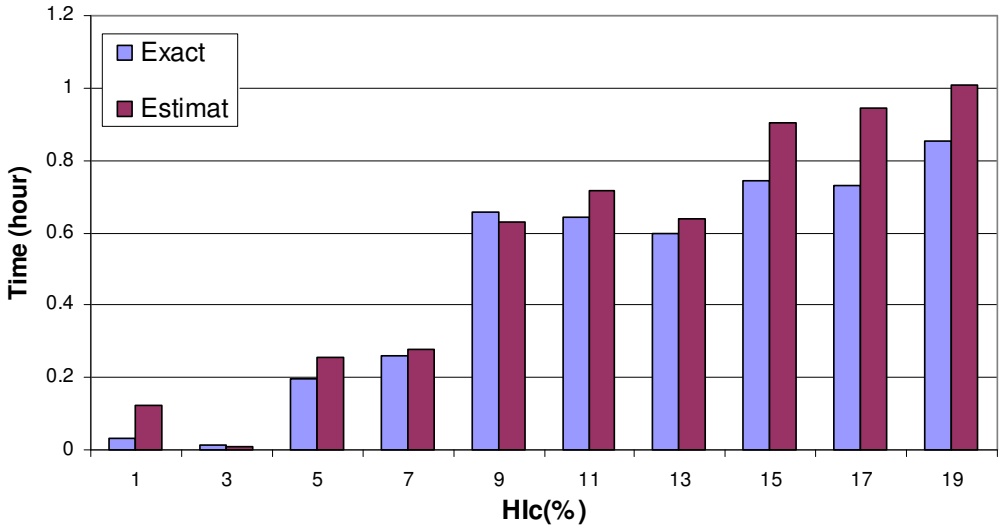

Figure 4-48: Exact and estimated harmonic impact of the house for the 3rd harmonic

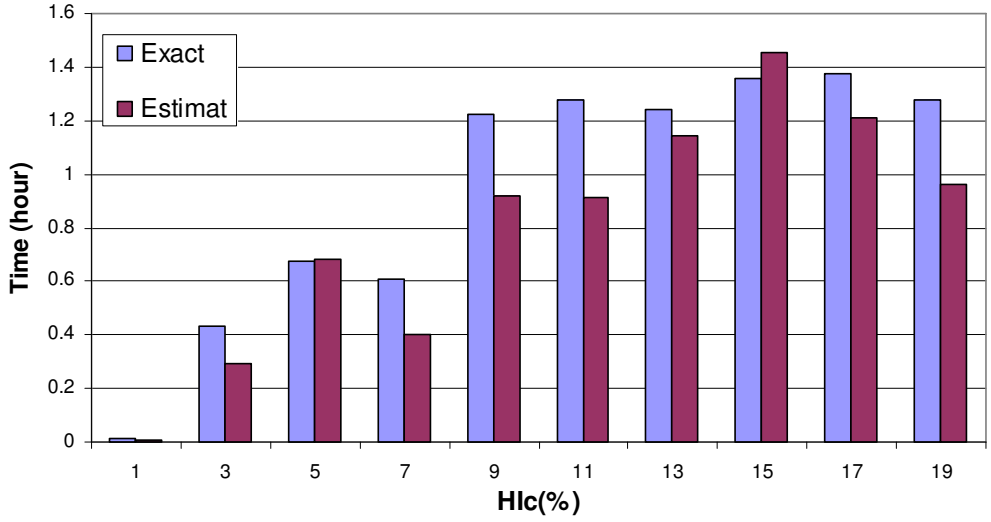

Figure 4-49: Exact and estimated harmonic impact of the house for the 5th harmonic

Chapter 5

Methods for Multi-Point Harmonic Impact Estimation

In the previous chapters, a harmonic impact index was proposed to quantify the harmonic impact of the loads and identify the harmonic polluters. In this chapter, the multi-point problem will be formulated for the harmonic impact index. Next, two data-based methods will be proposed to estimate this index for the multi-point harmonic source identification problem. The first method is the Least Square method. In this method, the measured data are searched to find the appropriate time intervals for applying the method. The second method is the Partial Least Square method, which uses data directly. Both methods are presented in this chapter. These methods will be verified and characterized by using simulation studies and real field test results in the next chapter.

5.1 Formulization of the problem

The proposed harmonic impact index can be applied to the multi-point harmonic source identification problem. This concept can be understood by referring to Figure 5-1. As [19]-[20] show, the components of the power system network can be modeled by a set of impedances and harmonic current sources. By replacing the components with harmonic current sources, the *h-th* harmonic voltage at bus *X* can be calculated by using the harmonic impedance matrix of the network ($[\mathbf{Z_h}]$) as follows:

$$\vec{V}_{hX} = \underbrace{Z_{hXA}\vec{I}_{hA}}_{\vec{V}_{hXA}} + \underbrace{Z_{hXB}\vec{I}_{hB}}_{\vec{V}_{hXB}} + \underbrace{Z_{hXC}\vec{I}_{hC}}_{\vec{V}_{hXC}} + \vec{V}_{hX0}, \tag{5-1}$$

where Z_{hXi} is the element of row X and column i of the harmonic impedance matrix of the network. In the previous chapter, it was shown that the customer should be converted to current sources in order to measure their impacts. The harmonic currents I_{hA}, I_{hB} and I_{hC} are the harmonic currents of the customers at the customer-utility interface point.

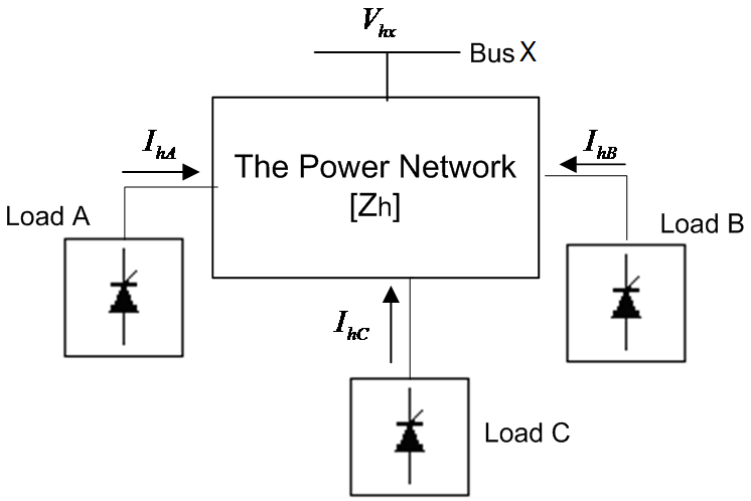

Figure 5-1: Schematic diagram of the power system

The phasor diagram of the harmonic voltage at bus X and its constructive components are shown in Figure 5-2. To quantify the harmonic impact of each load on the harmonic voltage, the projection of each voltage component on the $\vec{V}_{hX}$ is used. As Figure 5-2 shows, the harmonic voltage at bus X can be written as follows:

$$|V_{hX}| = |V_{hXA-f}| + |V_{hXB-f}| + |V_{hXC-f}| + |V_{hX0-f}|. \tag{5-2}$$

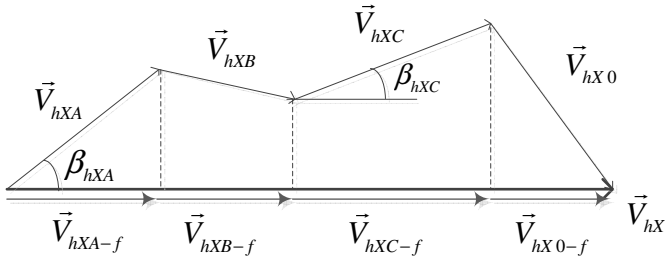

Figure 5-2: Phasor diagram of harmonic voltage at bus X caused by harmonic loads A, B and C

The harmonic impact of *Load A* on *Bus X* can be quantified by using the projection of $\vec{V}_{hXA}$ on $\vec{V}_{hX}$. The harmonic impact index (*HI*) of *Load A* on *Bus X* is defined as follows:

$$HI_{Load\ A}^{BusX} = \frac{|V_{hXA-f}|}{|V_{hX}|} \times 100\% = \frac{|V_{hXA}|}{|V_{hX}|} \cos\beta_{hXA} \times 100\%. \tag{5-3}$$

The same procedure can be applied to quantify the harmonic impacts of the other loads (*B*, *C*, etc.).

5.2 Proposed measurement scheme

Utility companies are currently able to routinely perform continuous harmonic monitoring. The most common power-quality-monitoring systems have multiple monitors placed at various points in a system. The monitors can collect data continuously. Two recording strategies are commonly used to record the waveforms: recording the data stream fully or recording snapshots of the data. In the first strategy, the waveforms are recorded completely with attached time tags. The time tag is the clock time of the measurement device. In snapshot recording, the measurement device takes some snapshots of the waveform. For example, one can record only five seconds of the waveform in the beginning of every minute. The process of snapshot recording is illustrated in Figure 5-3.

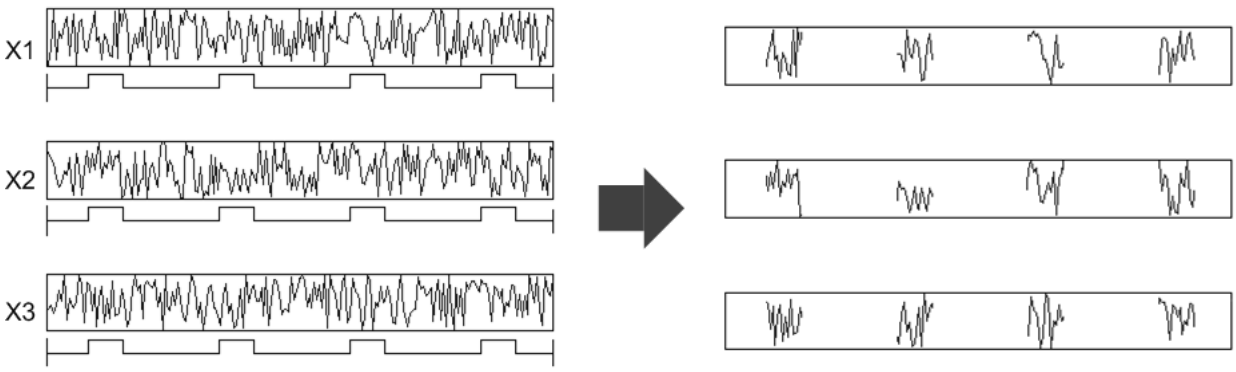

Figure 5-3: Taking snapshots of the waveforms

The waveforms of the currents and voltages are recorded by the measurement devices. The clock time of the measurement devices in the network should be synchronized. In view of the current condition of PQ monitoring systems, the multi-point recorded data can be synchronized to the accuracy of 1 second. This synchronization level can be achieved by using the Internet. The measurement device is connected to the Internet in order to synchronize the clock time of the device prior to the measurement. The synchronization should be re-established every day to avoid the time-drift problem. This level of synchronization does not provide adequate accuracy to determine the phase differences among the measured quantities. In this regard, the magnitudes of harmonic voltages and currents are accessible for harmonic-impact determination.

Figure 5-4 shows the proposed measurement scheme for the multi-point system. Measurement devices are installed at each site, and measurements are performed simultaneously. Continuous harmonic measurement at sites X, A, B and C is performed. The data recorded include the harmonic currents of the suspicious loads (loads A, B and C) and the harmonic voltage for the indicator point (bus X). They are not normalized with respect to the fundamental frequency component. The measurements should have the following specifications:

- Data recording resolutions of one sample per 1 to 5 seconds are suggested (to be acceptable for adequate correlation analysis).
- The sampling period should be at least 6 cycles (IEEE Standard).
- The sampling rate of 256/cycle is suggested
- The measurement sets should be synchronized to capture data simultaneously. A synchronization level of 1 second is acceptable.

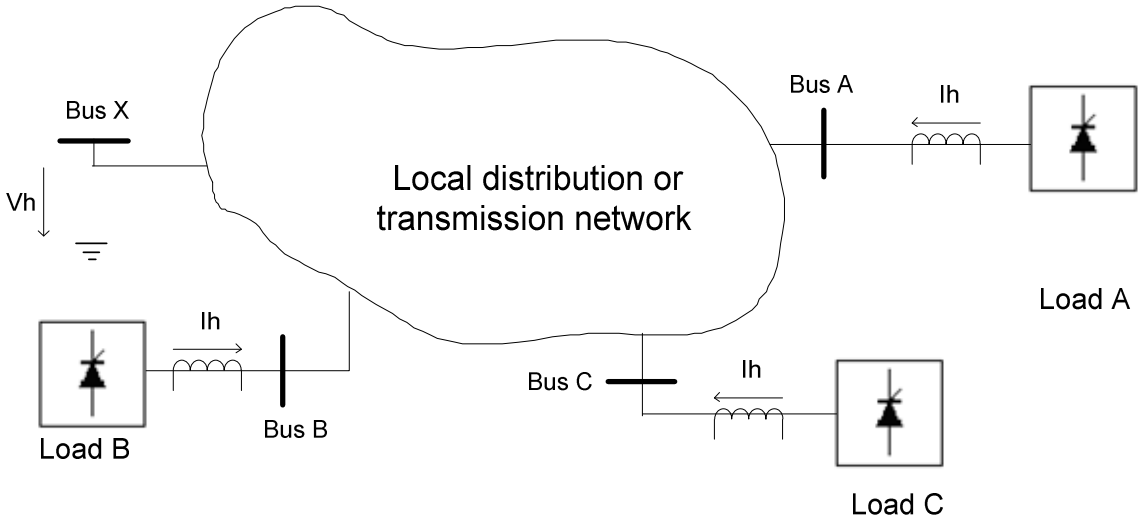

Figure 5-4: Proposed multi-point measurement scheme

For example, the field measurement data for the 5th harmonic voltages in bus *X* and the 5th harmonic currents of load *A* taken from 10:00AM to 10:30AM are shown in Figure 5-5.

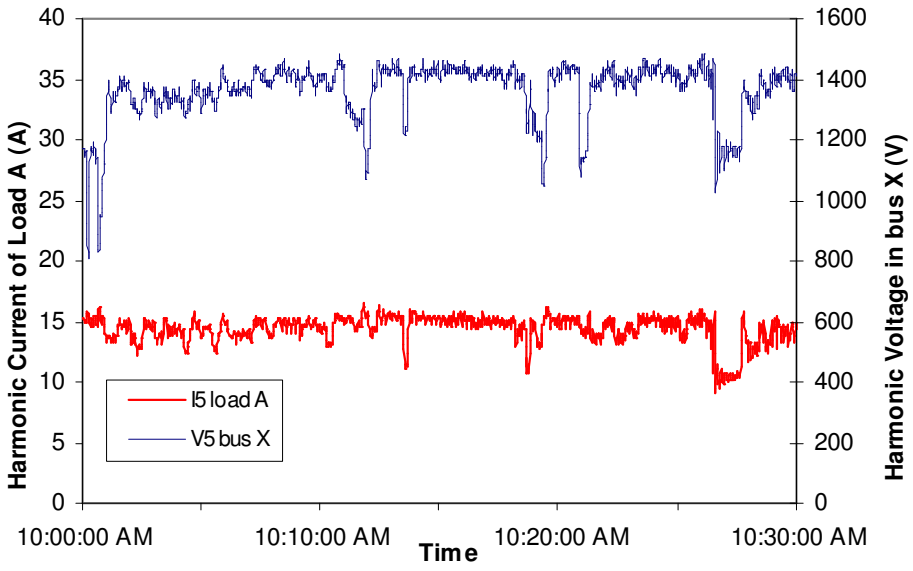

Figure 5-5: Example of the field measurement harmonic voltage and current.

The main problem is to utilize these continuous measurements (for the harmonic voltage and currents) to identify the harmonic polluters and estimate their harmonic impacts. To solve this problem, two methods are proposed in the following sections.

5.3 Multi-point problem and HSE problem

Before presenting the proposed multi-point methods, some clarifications are useful. The harmonic state estimation (HSE) problem should not be confused with the multi-point harmonic source identification problem. Apparently, these two problems are similar, but there are some key differences between them.

By referring to Figure 5-1, the power system can be partitioned into two parts: an AC backbone ([Zh]) and a set of suspicious harmonic sources (I_{hA}, I_{hB} and I_{hC}). AC backbone consists of interconnected linear network parts of the system such as generators, transformers, and transmission lines. In the HSE problem [33]-[35], it is assumed that the parameters of the components within the backbone, and information on the network topology can be obtained from the utilities that own and/or operate them. A bus admittance (or impedance) matrix of the backbone for any particular harmonic can be formed. For any harmonic order, following equation can be derived.

$$[I_h] = [Z_h]^{-1}[V_h]. \tag{5-4}$$

Several measurement instruments are then placed at the selected buses and lines within the backbone to perform synchronized measurement of the node harmonic voltages and injection harmonic currents. The equation can be portioned into following three subsets [35]- [37]:

1. Instrumented buses and lines, at which measurement instrument measures the harmonic voltage and/or current. These known parameters are presented by V_{hk} and I_{hk}.
2. Uninstrumented buses and lines, for which injection harmonic currents should be estimated. These unknown parameters are presented by V_{hu} and I_{hu}.
3. Uninstrumented buses and lines, for which no information is sought. These not-studied parameters are presented by V_{hn} and I_{hn}.

By portioning the parameters, following equation can be derived.

$$\begin{bmatrix} I_{hk} \\ I_{hu} \\ I_{hn} \end{bmatrix} = \begin{bmatrix} Y_{hkk} & Y_{hku} & Y_{hkn} \\ Y_{huk} & Y_{huu} & Y_{hun} \\ Y_{hnk} & Y_{hnu} & Y_{hnn} \end{bmatrix} \begin{bmatrix} V_{hk} \\ V_{hu} \\ V_{hn} \end{bmatrix}. \tag{5-5}$$

In the HSE problem, the estimated voltages and currents (V_{hu} and I_{hu}) are achieved by using the measured voltage and current (V_{hk} and I_{hk}) and admittance matrix of the system ([Yh]). This is one of the key differences of the HSE problem with the multi-point harmonic source identification problem. In the multi-point problem, the admittance matrix of the system is unknown. In the multi-point problem, the parameters are estimated just by using the measurements (V, I) without any information of the system impedance.

The implementation of the HSE problem requires that the measurement instruments share a common time reference, so that the measured quantities are synchronized between each other. This can be obtained, for instance, by using Global-Positioning-System-synchronized phasor measurement units (PMUs), i.e., instruments that are capable of measuring voltages or current phasors synchronized to an absolute time (synchrophasors) with a synchronization accuracy on the order of 1 μs [38]. Similarly, the multi-point problem also needs synchronized measurement. However, phasor synchronized measurement are not required. In the multi-point problem, the magnitude (not the phasor) of the harmonic voltages and currents are measured. In this regard, the synchronization accuracy on the order of 1s is sufficient. Table 5-1 summarizes the comparison of the HSE problem with the multi-point problem.

Table 5-1: Comparison of HSE problem with Multi-point harmonic source problem

	HSE problem	**Multi-point problem**
Admittance matrix of the system ([Yh])	Known	Unknown
Synchronized Measurement	Yes	Yes
Measurement type	Phasor (magnitude+phase angle)	Magnitude
Synchronization Accuracy	1 μs	1 s

5.4 Method 1: Least Square method

This proposed method uses field measurement data to determine the harmonic-impact index. By using measurements data with the specifications mentioned in the previous section, the following data-processing algorithm is developed. By referring to equation **(5-1)** , $\vec{V}_{hX}$ is decomposed into two components:

$$\vec{V}_{hX} = \underbrace{Z_{hXA}\vec{I}_{hA}}_{\vec{V}_{hXA}} + \underbrace{Z_{hXB}\vec{I}_{hB} + Z_{hXC}\vec{I}_{hC} + \vec{V}_{hX,0}}_{E_h} . \tag{5-6}$$

$\vec{V}_{hX,A}$ is caused by load A, and E_h is caused by the other loads. Figure 5-6 shows the phasor diagram of this decomposition.

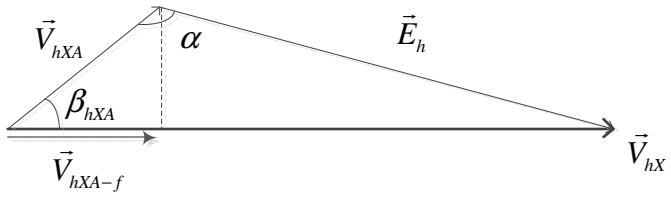

Figure 5-6: Phasor diagram of the harmonic voltage on bus X caused by load A

By applying the cosine law to Figure 5-6 for the i[th] sample of the measured data, the following equation can be derived.

$$\left|V_{hX}(t_i)\right|^2 = \left|V_{hXA}(t_i)\right|^2 + \left|E_h(t_i)\right|^2 - 2\left|V_{hXA}(t_i)\right|\left|E_h(t_i)\right| Cos\left(\alpha(t_i)\right) \tag{5-7}$$

Since $\left|V_{hXA}(t_i)\right| = \left|Z_{hXA}\right|\left|I_{hA}(t_i)\right|$, the following equation can be obtained.

$$\left|V_{hX}(t_i)\right|^2 = \left|Z_{hXA}\right|^2\left|I_{hA}(t_i)\right|^2 + \left|E_h(t_i)\right|^2 - 2\left|Z_{hXA}\right|\left|I_{hA}(t_i)\right|\left|E_h(t_i)\right| Cos\left(\alpha(t_i)\right) \tag{5-8}$$

As the system/load always varies, all quantities of the above equation will change. A group of data selected for analysis (i=1,….n) has an average value of α. This value is labeled as α_{eq}. If α_{eq}, instead of the true α, is used in the above equation, an error will appear. Equation **(5-8)** can be rewritten as shown in **(5-9)**.

$$\left|V_{hX}(t_i)\right|^2 = \left|Z_{hXA}\right|^2 \left|I_{hA}(t_i)\right|^2 + \left|E_h\right|^2 - 2\left|Z_{hXA}\right|\left|I_{hA}(t_i)\right|\left|E_h\right| Cos\left(\alpha_{eq}\right) + \varepsilon_i \tag{5-9}$$

$$\text{By defining} \quad \begin{cases} \theta_0 = \left|E_h\right|^2 \\ \theta_1 = -2\left|Z_{hXA}\right|\left|E_h\right| Cos\left(\alpha_{eq}\right) \\ \theta_2 = \left|Z_{hXA}\right|^2 \end{cases},$$

the following set of equations are derived:

$$\mathbf{Y} = \mathbf{X\theta} + \boldsymbol{\varepsilon}, \tag{5-10}$$

where

$$\mathbf{Y} = \left[\left|V_{hX}(t_1)\right|^2 \quad \left|V_{hX}(t_2)\right|^2 \quad \cdots \quad \left|V_{hX}(t_n)\right|^2\right]^T;$$

$$\boldsymbol{\theta} = [\theta_0 \quad \theta_1 \quad \theta_2]^T;$$

$$X = \begin{bmatrix} 1 & \left|I_{hA}(t_1)\right| & \left|I_{hA}(t_1)\right|^2 \\ 1 & \left|I_{hA}(t_2)\right| & \left|I_{hA}(t_2)\right|^2 \\ \vdots & \ddots & \vdots \\ 1 & \left|I_{hA}(t_n)\right| & \left|I_{hA}(t_n)\right|^2 \end{bmatrix}.$$

In the above equation, E_h and Z_{hXA} are assumed to be constant for the instants i=1….n when the correlation analysis is to be performed. This assumption is critical for the proposed method. The physical meaning is that when one conducts correlation analysis between two variables X and Y, no other variables will change. Since other variables do change, the simplest approach is to select data that can guarantee this condition. This approach is adopted in the proposed method. The method of data selection is described later. The unknown parameters $\boldsymbol{\theta}$ can be estimated by using the following linear regression:

$$\hat{\boldsymbol{\theta}} = \left(\mathbf{X^T X}\right)^{-1} \mathbf{X^T Y}. \tag{5-11}$$

The last step is to find the harmonic impact by using the estimated parameters. By applying the cosine law to Figure 5-6, the following equation can be derived for each sample.

$$\left|E_h(t_i)\right|^2 = \left|V_{hX}(i)\right|^2 + \left|V_{hXA}(t_i)\right|^2 - 2\left|V_{hXA}(t_i)\right|\left|V_{hX}(i)\right| Cos\left(\beta_{hXA}(t_i)\right). \tag{5-12}$$

The following equation can be derived by reordering the above equation.

$$\left|V_{hXA}(t_i)\right| Cos\left(\beta_{hXA}(t_i)\right) = \frac{\left|V_{hX}(i)\right|^2 + \left|V_{hXA}(t_i)\right|^2 - \left|E_h(t_i)\right|^2}{2\left|V_{hX}(i)\right|} \tag{5-13}$$

By replacing the above value in the harmonic impact equation **(5-3)**, the harmonic impact index can be estimated as follows:

$$HI_{load\,A}^{Bus\,X}(t_i) = \frac{\left|V_{hX}(t_i)\right|^2 + \left|V_{hXA}(t_i)\right|^2 - \left|E_h\right|^2}{2\left|V_{hX}(t_i)\right|^2} \times 100\%. \tag{5-14}$$

By using the estimated parameters (θ), the harmonic impact can be estimated.

$$HI_{load\,A}^{Bus\,X}(t_i) = \frac{\left|V_{hX}(t_i)\right|^2 + \theta_2\left|I_{hA}(t_i)\right|^2 - \theta_0}{2\left|V_{hX}(t_i)\right|^2} \times 100\% = \left(\frac{1}{2} + \frac{\theta_2\left|I_{hA}(t_i)\right|^2 - \theta_0}{2\left|V_{hX}(t_i)\right|^2}\right) \times 100\%. \tag{5-15}$$

The above equation shows that the harmonic impact varies with time. Since it is more useful to know the average harmonic impact over a specified period, the following simple average is proposed for this purpose:

$$HI_{load\,A}^{Bus\,X} = \left(\frac{1}{2} + \frac{1}{n}\sum_{i=1}^{n}\frac{\theta_2\left|I_{hA}(t_i)\right|^2 - \theta_0}{2\left|V_{hX}(t_i)\right|^2}\right) \times 100\%. \tag{5-16}$$

Based on the analytical (i.e., least square) solution of $\boldsymbol{\theta}$, the equation to determine the harmonic impact can be concisely written as

$$HI_{load\,A}^{Bus\,X} = \left(\frac{1}{2} + \boldsymbol{\beta}\hat{\boldsymbol{\theta}}\right) \times 100\%, \tag{5-17}$$

where $\boldsymbol{\beta} = \left[-\frac{1}{2n}\sum_{i=1}^{n}\frac{1}{\left|V_{hX}(t_i)\right|^2} \quad 0 \quad \frac{1}{2n}\sum_{i=1}^{n}\frac{\left|I_{hA}(t_i)\right|^2}{\left|V_{hX}(t_i)\right|^2}\right]$.

In other words, if one has the measured data series I_{hA} and V_{hX}. (i=1,…,n), the above equation will be able to calculate the harmonic impact of the load current I_{hA}. After estimating the harmonic impact of a load, the confidence interval of the estimated parameter can be calculated as an indication of the reliability of the estimated parameter. For example, if the estimated harmonic impact of a suspicious load is 32%, and the confidence interval is ±7% for a 90-percent confidence level, then the harmonic impact of the suspicious load is between 25% and 39% (with the probability of more than 90%). The confidence interval of the estimated harmonic impact can be calculated as follows [29]:

$$CI_{load\ A}^{Bus\ X} = \pm t_{n-3,1-\alpha/2}\sqrt{Var(\hat{HI}_{load\ A}^{Bus\ X})}\ , \tag{5-18}$$

where $t_{n-3,1-\alpha/2}$ stands for t-distribution with n-3 degree of freedom, n presents number of analyzed samples, and α is the confidence level that usually sets at 90%. The variance of the estimated harmonic impact of load A on bus X ($\hat{HI}_{load\ A}^{Bus\ X}$) can be achieved by the following equation.

$$Var(\hat{HI}_{load\ A}^{Bus\ X}) = \frac{\sum_{i=1}^{n}(y_i - \hat{y}_i)^2}{n-3} \times \mathbf{\beta}(\mathbf{X}^{\mathbf{T}}\mathbf{X})^{-1}\mathbf{\beta}^{\mathbf{T}} \tag{5-19}$$

As discussed earlier, E_h must be constant in order to use the proposed method. This prerequisite transforms the problem of harmonic-impact determination into the problem of selecting the proper data set for the least square estimation. The basic idea adopted in this work is to find the time intervals in which only one of the harmonic loads changes. For example, the harmonic load A varies in Figure 5-7 in time interval T_1, and the other harmonic loads are roughly unchanged (the variation is less than 5%). This time interval can be used by our proposed method to estimate the harmonic impact of load *A*. Similarly, the time interval T_2 can be used to estimate the harmonic impact of load *B*. It is assumed that finding a proper dataset with sufficient length among the measurement data

is possible. If the proper set of data is not available, the estimation is not possible. However, our analysis of the real field-measurement data showed that such a set of data is usually available when less than six major harmonic loads are present within the local power network. In multiple harmonic source identification, only major harmonic loads should be investigated. In this analysis, the minor harmonic loads are considered as background harmonic.

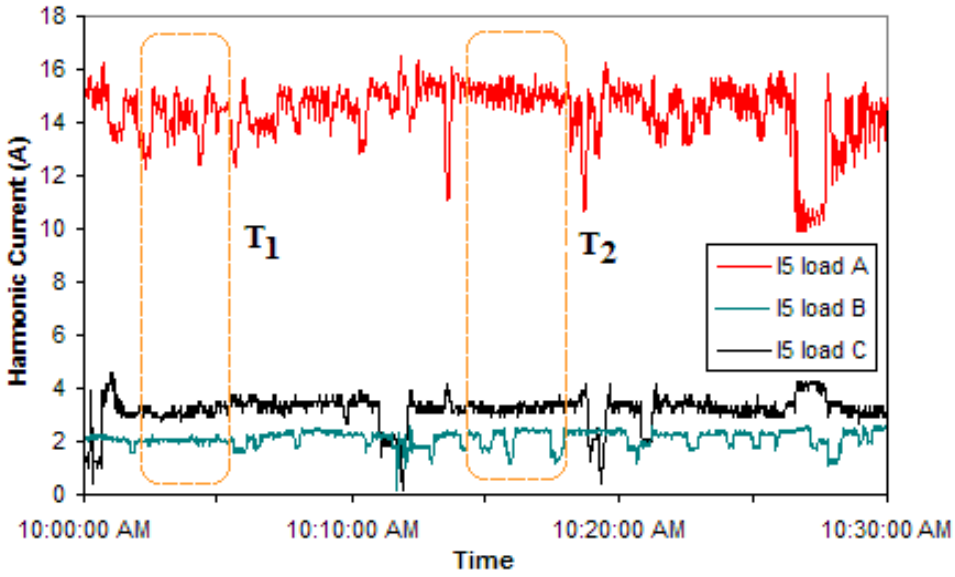

Figure 5-7: Selecting appropriate time intervals for estimation analysis

5.4.1 Sample case

In this section, a sample case is solved by applying the least square method. Figure 5-8 shows the effect of applying the data selection algorithm to the measurement data. The correlation of the 5th harmonic current of load A and the 5th harmonic voltage of bus X (presented in Figure 5-5) is shown in Figure 5-8(a). When applying the data-selection algorithm, only those data within the time interval T_1 are selected. The correlation of the harmonic voltage and current of these selected data is shown in Figure 5-8(b), which reveals that the selected data are less spread and more strongly correlated than the data shown in Figure 5-8(a). By applying **(5-11)** to the selected data, the parameters can be estimated. For this case, $|E_h|$ is 883.12V, Z_{hXA} is 42.4 Ohm, and α_{eq} is 130.1 degrees. By

using equation 10, the harmonic impact of load A on bus X is estimated to be 36.7%. The confidence interval of this estimation is ±5.2%. The p-value of the estimated parameter is almost 0.0001, which shows a strong correlation between the analyzed data. The coefficient correlation parameter (r^2) is almost 0.82, which shows a good explanation of the data by the estimators.

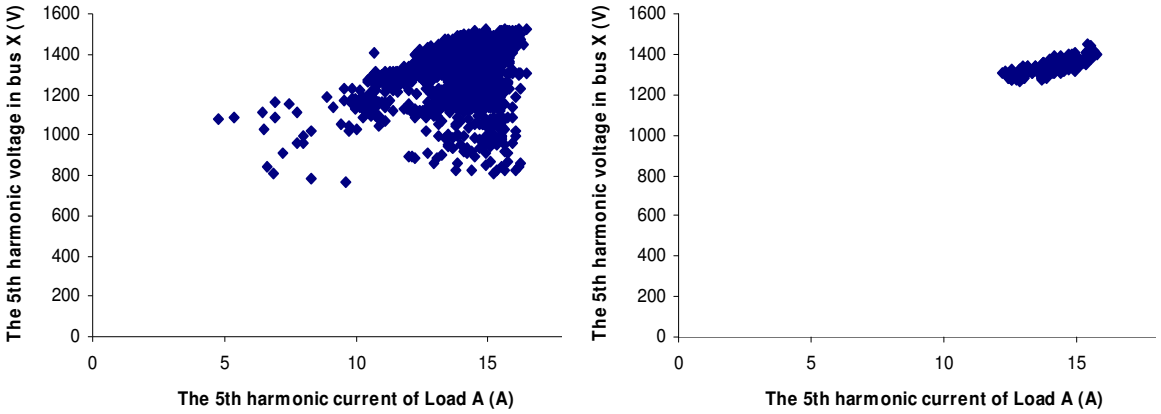

(a) before data selection (b) after data selection

Figure 5-8: Correlation of harmonic current of load A and harmonic voltage of bus X

5.4.2 Sensitivity study of LS Method

The characteristics of the propose LS method can be better understood by using the sensitivity studies. Firstly, the impact of the phase angle variations on the LS estimation method is studied. In this case, I_h varies from 1pu to 1.4 pu and Z_{hAX}= 1pu. Three cases are analyzed. In the first case, the load has the dominant impact on the harmonic voltage. The additive impacts of the other loads are weak (E_h=0.3pu). Table 5-2 presents the impacts of the phase angle variations of the estimated result. For example, the harmonic impact of the load is 85.6% when phase angle is 60 degrees. A 5 degrees phase angle variation causes 1.57% variations of the estimated harmonic impact. As Table 5-2 reveals, the estimation error of the LS method is confined to 5% with a 10 degrees phase angle variation when load is dominant.

Table 5-2: Impact of the phase angle variations on the estimated results, when load is dominant

Phase Angle (deg)	Harmonic impact (%)	Phase angle variation, $\Delta\alpha$ (deg)				
		±0	±5	±10	±20	±30
$\alpha = 0^\circ$	79.9	±0.00	±0.03	±0.13	±0.53	±1.21
$\alpha = 60^\circ$	85.6	±0.00	±1.57	±3.06	±6.17	±9.48
$\alpha = 120^\circ$	107.6	±0.00	±2.54	±5.20	±10.50	±14.6
$\alpha = 180^\circ$	133.9	±0.00	±0.10	±0.41	±1.56	±3.42

In the second case, the additive impacts of the other loads (background harmonic) are comparable (E_h=1pu). Table 5-3 presents the impacts of the phase angle variations of the on the estimated result.

Table 5-3: Impact of phase angle variations on the estimated results, when load is comparable

Phase Angle (deg)	Harmonic impact (%)	Phase angle variation, $\Delta\alpha$ (deg)				
		±0	±5	±10	±20	±30
$\alpha = 0^\circ$	54.4	±0.00	±0.05	±0.20	±0.84	±1.98
$\alpha = 60^\circ$	55.9	±0.00	±2.57	±5.31	±10.62	±16.81
$\alpha = 120^\circ$	66.9	±0.00	±7.66	±15.18	±33.74	±56.15

In the last case, the load has a weak impact on the harmonic voltage. Additive impacts of other loads is strong (E_h=3pu). Table 5-4Table 5-3 presents the impacts of the phase angle variations on the estimated result.

Table 5-4: Impact of the phase angle variations on the estimated results, when load is weak

Phase Angle (deg)	Harmonic impact (%)	Phase angle variation, $\Delta\alpha$ (deg)				
		±0	±5	±10	±20	±30
$\alpha = 0^\circ$	28.5	±0.00	±0.04	±0.17	±0.69	±1.56
$\alpha = 60^\circ$	23.0	±0.00	±2.01	±4.23	±8.58	±12.99
$\alpha = 120^\circ$	-5.04	±0.00	±4.44	±9.32	±19.08	±27.27
$\alpha = 180^\circ$	-67.37	±0.00	±0.30	±1.15	±4.36	±9.18

In the second sensitivity study, the impact of unknown harmonic sources on the estimated results is studied. During the time interval in which the studied load changes, E_h also changes due to the variation of an unknown harmonic source. To cancel out this impact, the idea is to find multiple proper time intervals for the estimation. Then, the average value of the estimated harmonic impact in the time intervals will be used. This analysis shows that when the number of time intervals increases the absolute error of the estimation method decreases. In our analysis, variation of load is 40% and variation of E_h is ±20%. Again, three cases are studied. The results are presented in the following tables. The minimum required samples are two. As the number of samples (time interval) increases, the estimation error of the LS method decreases.

Table 5-5: Impact of the unknown harmonic source on the estimation error, when load is dominant

Phase-angle (deg)	Harmonic Impact	Time interval (samples)					
		2	3	5	10	100	1000
$\alpha = 0^\circ$	79.88	10.43	8.97	4.84	2.85	0.35	0.04
$\alpha = 60^\circ$	85.57	15.56	15.57	15.54	10.51	4.99	0.03
$\alpha = 120^\circ$	107.62	21.97	21.95	21.89	21.77	19.72	0.12
$\alpha = 180^\circ$	133.91	26.20	26.18	26.11	25.98	23.67	0.23

Table 5-6: Impact of unknown harmonic source on the estimation method, when load is comparable

Phase-angle (deg)	Harmonic Impact	Time intervals (samples)					
		2	3	5	10	100	1000
$\alpha = 0^\circ$	54.42	24.19	16.99	10.06	6.57	0.78	0.09
$\alpha = 60^\circ$	55.86	2.67	2.68	2.63	2.69	2.47	0.13
$\alpha = 120^\circ$	66.93	11.55	11.56	11.55	11.47	10.33	1.24

Table 5-7: Impact of unknown harmonic source on the estimation method, when load is weak

Phase-angle (deg)	Harmonic Impact	Time intervals (samples)					
		1	2	5	10	100	1000
$\alpha = 0^{\circ}$	28.52	2.59	0.84	1.57	1.09	0.98	1.02
$\alpha = 60^{\circ}$	23.05	5.03	5.02	5.04	4.98	4.54	1.32
$\alpha = 120^{\circ}$	-5.04	26.42	26.35	26.28	26.08	23.62	1.97
$\alpha = 180^{\circ}$	-67.37	60.75	60.61	60.41	59.97	53.76	6.81

5.4.3 Data selection

As previously discussed, the Least Square method transforms the problem of harmonic impact determination into a problem of selecting a proper dataset. The data selection algorithm seeks the time intervals where only the harmonic current of one suspicious load varies while that of the others remains roughly unchanged. Three data-mining algorithms are proposed for this problem: 1) fast sliding window, 2) complete sliding window, and 3) top-down method. The methods are introduced in this chapter. The performances of the methods are compared in the next chapter.

5.4.3.1 Algorithm 1: Fast sliding window [30]

The sliding window algorithm works by anchoring the left point of a potential segment at the first data point of the time series t_i, then attempting to approximate the data to the right with an increasing longer segment L_i. At some point t_j ($j=i+L_i$), the error for the potential segment is greater than the user-specified threshold, so the subsequence from the anchor to one point before that t_{j-1} is chosen as an appropriate time interval for analysis. Next, the anchor is moved to location t_j, and the process is repeated until the entire time series has been scanned.

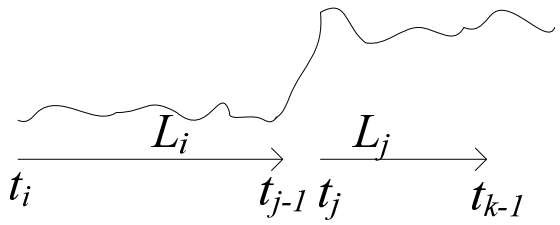

Figure 5-9: Classic Sliding window

The pseudo-code for the algorithm is shown below:

```
anchor =1;
While not finished segmenting time series
    I=2;
    While calculate_error(T[anchor: anchor + i] ) < max_error
            i=i+1;
    end;
    seg_TS=concat (Seg_TS, create_segment(T[anchor:anchor+(i-1)]);
    anchor = anchor + i;
end
```

5.4.3.2 Algorithm 2: Complete sliding window

This algorithm is similar to the previous one, but is more complete. As we did with the previous algorithm, we first start to find the longest segment after t_i that remains within the specific error (L_i). Next, the anchor is moved to t_{i+1}, and the longest segment after t_{i+1} are determined, (see Figure 5-10).

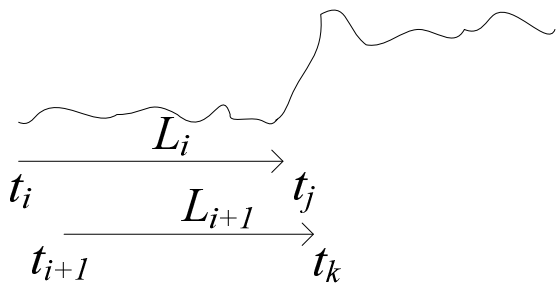

Figure 5-10: First step of complete sliding window Algorithm

Once a maximum length segment is assigned to each point, the longest time segment can be obtained. This algorithm is guaranteed to catch the longest time interval of the appropriate data. The pseudo-code for the algorithm is shown below:

```
anchor =1;
While not finished segmenting time series
    i=2;
    While calculate_error(T[anchor: anchor + i] ) < max_error
            i=i+1;
    end;
    L(anchor)=i-1;
    anchor = anchor + 1;
end
 [Index maxs]=local_max_finder(L);
[a b]=sort(maxs,'descend');
for k=1:length(a)
   if a(k)>Min_L
    seg_TS=concat (Seg_TS, create_segment(T[Index(b(k)):
Index(b(k))+a(k)-1]);
end
```

The only problem with this algorithm is the possibility of time-interval collisions. For example, if time interval [t_1,t_2] and [t_3, t_4] are selected by this algorithm, t_2 might be greater than t_3, so the data in the time interval [t_2, t_3] will be used two times.

5.4.3.3 Algorithm 3: Bottom- Up [30]

The bottom-up algorithm begins by creating the finest possible approximation of the time series, so that n/2 segments are used to approximate the n-length time series. Next, the cost of merging each pair of adjacent segments is calculated, and the algorithm begins to interactively merge the lowest cost pair until the stopping criteria is met.

The pseudo-code for the algorithm is shown below

```
for i=1:2:length(T)  // Create initial fine approximation
    seg_TS = concat (Seg_TS, create_segment(T[i : i+1]));
end;
for i=1 : length (Seg_Ts) -1 // find the cost of merging each pair of segment
    merge_cost (i) = calculate_error ( [merge (Seg_TS(i) , Seg_TS (i+1)) ] );
end
while min (merge_cost) < max_error
    i= min (merge_cost);          // Find cheapest pair to merge
    Seg_TS (i) =merge (Seg_TS(i), Seg_TS(i+1))); // Merge Them
    Delete (Seg_TS (i+1));   // Update Records
    merge_cost (i) = calculate_error (merge (Seg_TS (i), Seg_TS( i+1)));
    merge_cost(i-1)= calculate_error(merge(Seg_TS(i-1), Seg_TS(i)));
end
```

5.4.3.4 Comparison of data selection algorithms

In this section, empirical comparisons of the three data-selection algorithms are presented. The field data measurements from 6AM to 12PM are used for this study. The

data are divided into 1-hour datasets. Algorithms are compared from three aspects: longest time segment, the percentage of used data, and the processing time of algorithms.

Firstly, the algorithms are applied to the datasets, and the longest time intervals are obtained for each algorithm. Figure 5-11 shows the longest time segment obtained by the algorithms when the acceptable load variation is 3%. As Figure 5-11 shows, the second algorithm (the complete sliding window algorithm) always finds the longest time interval. This fact can be verified by applying the algorithms to the datasets with different acceptable load variations as shown in the following figures.

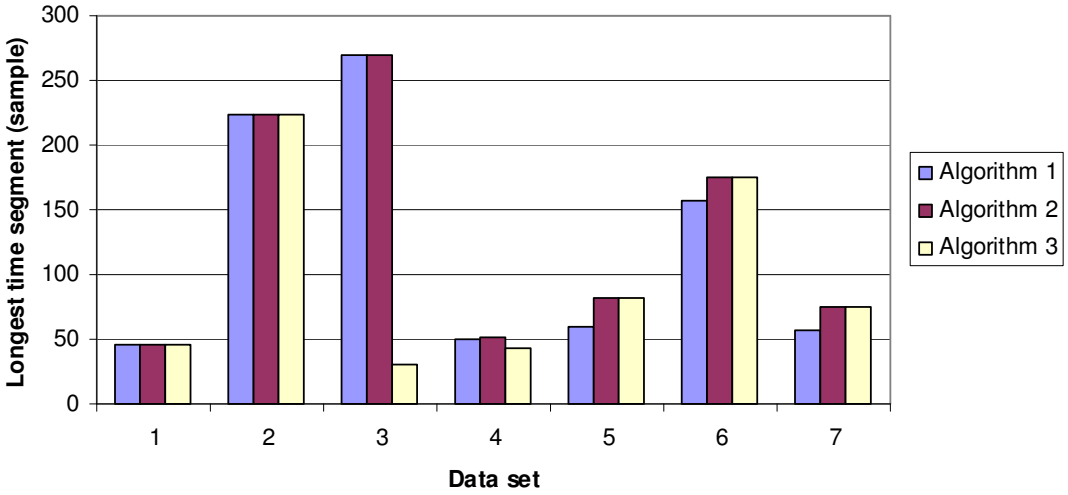

Figure 5-11: Longest time segment obtained by algorithms with 3% acceptable load variation

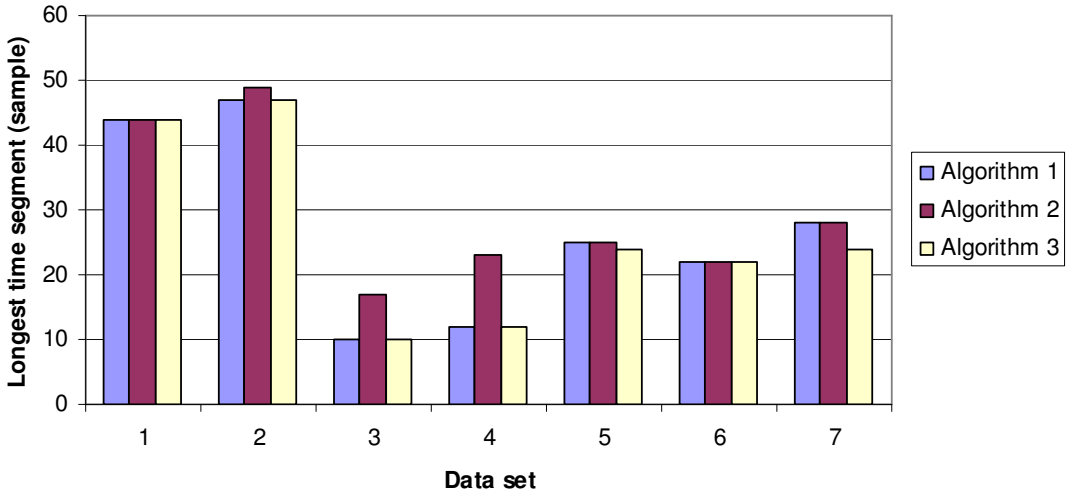

Figure 5-12: Longest time segment obtained by algorithms with 2% acceptable load variation

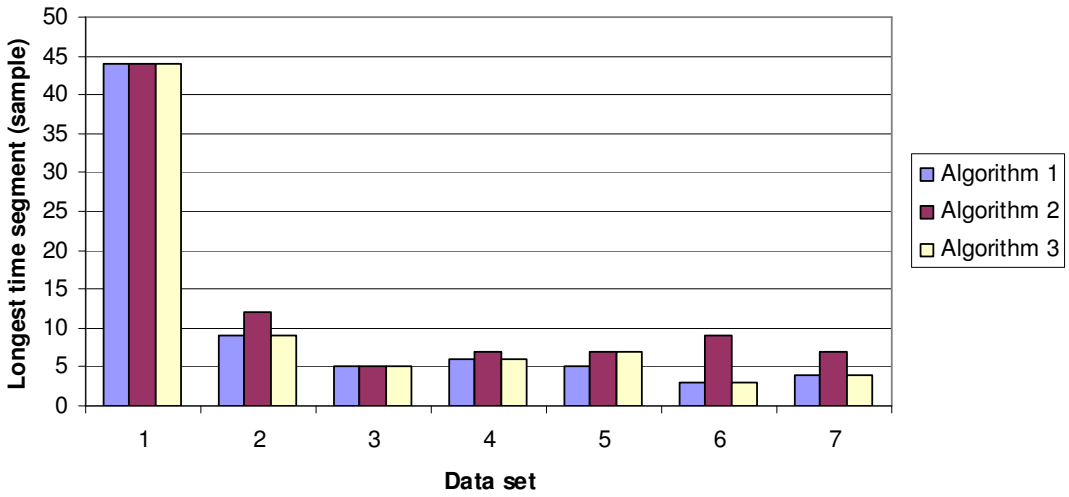

Figure 5-13: Longest time segment obtained by algorithms with 1% acceptable load variation

The complete sliding window algorithm finds the longest time segment, but does not guarantee that this algorithm uses data more efficiently than the other algorithms. Not only the longest time segment, but also the other time segments (such as the second-longest and the third-longest) are important. The percentage of used data is a good indicator of which algorithm uses data most efficiently. In the second study, we want to analyze the percentage of data that each algorithm utilizes. Figure 5-14 shows the percentage of data used by the algorithms. As Figure 5-14 shows, none of the algorithms performs significantly better than the others.

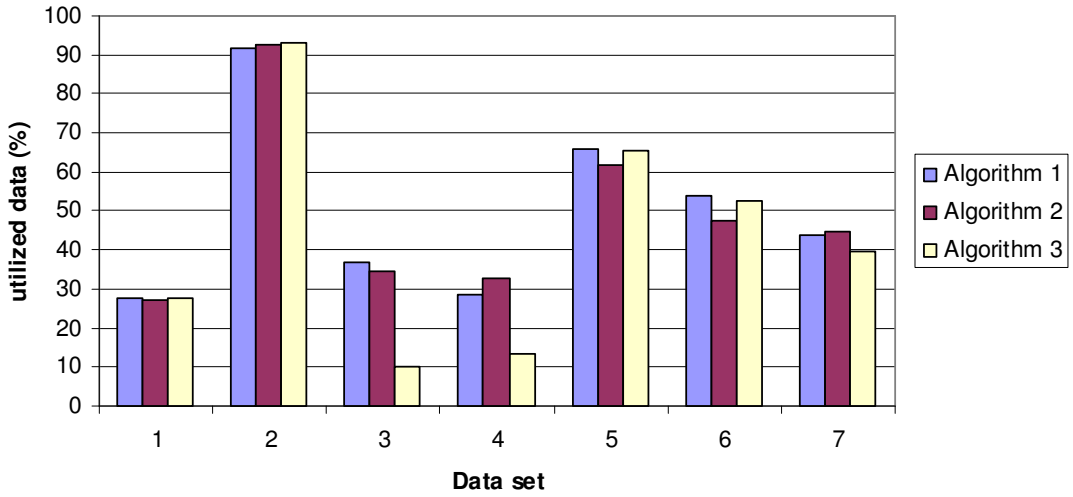

Figure 5-14: Percentage of data utilized by algorithms

In the last study, we compare the processing time of each algorithm to find the fastest algorithm. Figure 5-15 shows the average processing time of the algorithms. As Figure 5-15 reveals, the bottom-up algorithm is the slowest, and the classic sliding window is the fastest.

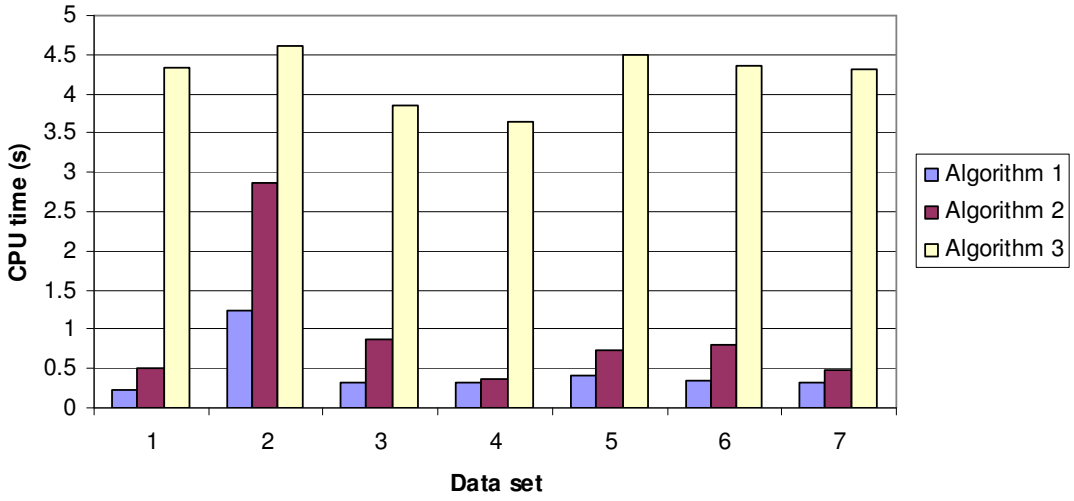

Figure 5-15: The average process time of the algorithms

5.5 Method 2: Partial Least Square method

The Least Square method searches the measurement data to the find appropriate time segment so that only one load changes, and the other loads are roughly unchanged. Finding the appropriate time segments becomes more difficult as the number of loads increases. The length of the found appropriate time segment will also decrease. For a studied field test measurement, Figure 5-16 shows the average length of the proper selected data when the number of major harmonic loads is increased. Increasing the number of harmonic loads makes finding longer data sets for analysis more difficult. If 100 samples are assumed to be the minimum acceptable data length, then finding the proper data set becomes highly difficult (sometimes impossible) when the harmonic loads are higher than six. This limitation confines the application of Lease Square method to local power networks. In multi-point harmonic source identification, only major harmonic loads should be investigated, and minor loads should be treated as background unknown random harmonic loads. In this regard, the Least Square method can be applied to most local networks. To expand the application of the multi-point harmonic source

identification methods to larger power networks, a new method that can use all the measurement data must be developed.

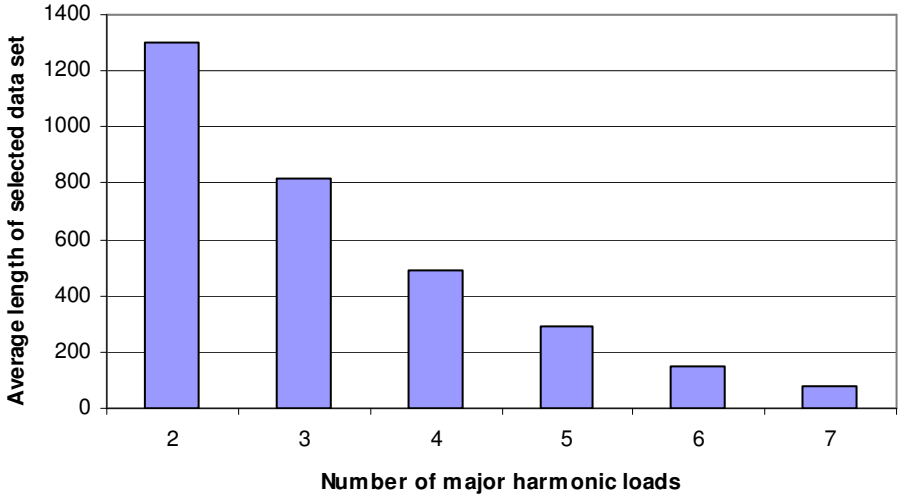

Figure 5-16: Average length of selected data set by Lease Square method for a studied field measurement

5.5.1 Linearization of the multi-point problem

The multi-point harmonic impact estimation is not a linear problem. In Section 5.4, the equation **(5-2)** was relaxed and linearlized by considering some assumptions and solved by using least square method. In this section, the equation will be further linearlized by some relaxation assumptions. Referring to **(5-2)**, V_{hX} can be stated as follows:

$$|V_{hX}| = |I_{hA}||Z_{hXA}|\cos\beta_{hAX} + |I_{hB}||Z_{hXB}|\cos\beta_{hBX} + |I_{hC}||Z_{hXC}|\cos\beta_{hCX} + |V_{hX0}|\cos\beta_{hX0} \quad (5\text{-}20)$$

For the i[th] sample of the measured data, the following equation can be derived:

$$\begin{aligned}|V_{hX}(t_i)| = {} & |I_{hA}(t_i)||Z_{hXA}|\cos(\beta_{hAX}(t_i)) + |I_{hB}(t_i)||Z_{hXB}|\cos(\beta_{hBX}(t_i)) + \cdots \\ & + |I_{hC}(t_i)||Z_{hXC}|\cos(\beta_{hCX}(t_i)) + |V_{hX0}(t_i)|\cos\beta_{hX0}(t_i)\end{aligned} \quad (5\text{-}21)$$

As the system/load always varies, all quantities of the above equation will change. However, the equation can be simplified by some assumptions:

1. A group of data selected for analysis (i=1,..,n) has an average value of β_{hAX}. This value is labeled as β_{hAX-eq}. If β_{hAX-eq} is used in the above equation

instead of $\beta_{hAX}(t_i)$, an error will appear in the equation. A similar average value can be used for $\beta_{hBX}(t_i)$ and $\beta_{hCX}(t_i)$.

2. The impact of the background harmonic is assumed to be constant. $|V_{hX0}(t_i)|$ will be replaced with a constant parameter and will cause an error to appear in the equation.

By considering these assumptions, the equation **(5-21)** can be rewritten in the form of a linear algebraic equation as shown in **(5-22)**, when M harmonic loads are in the system.

$$|V_{hX}(t_i)| = |V_{hX0}|\cos\beta_{hX0-eq} + |I_{hA}(t_i)||Z_{hXA}|\cos\beta_{hAX-eq} + |I_{hB}(t_i)||Z_{hXB}|\cos\beta_{hBX-eq} + \cdots + |I_{hM}(t_i)||Z_{hXM}|\cos\beta_{hMX-eq} + \varepsilon_i \quad (5\text{-}22)$$

By defining

$$\begin{cases} B_0 = |V_{hX0}|\cos\beta_{hX0-eq} \\ B_1 = |Z_{hXA}|\cos\beta_{hAX-eq} \\ B_2 = |Z_{hXB}|\cos\beta_{hBX-eq} \\ \vdots \\ B_M = |Z_{hXM}|\cos\beta_{hCM-eq} \end{cases} \quad (5\text{-}23)$$

the following set of equations is derived:

$$Y = XB, \quad (5\text{-}24)$$

where

$$Y = \begin{bmatrix} |V_{hX}(t_1)| & |V_{hX}(t_2)| & \cdots & |V_{hX}(t_n)| \end{bmatrix}^T \quad (5\text{-}25)$$

$$B = \begin{bmatrix} B_0 & B_1 & \cdots & B_M \end{bmatrix}^T$$

$$X = \begin{bmatrix} 1 & |I_{hA}(t_1)| & |I_{hB}(t_1)| & \cdots & |I_{hM}(t_1)| \\ 1 & |I_{hA}(t_2)| & & & |I_{hM}(t_2)| \\ \vdots & & & \ddots & \vdots \\ 1 & |I_{hA}(t_n)| & |I_{hB}(t_2)| & & |I_{hM}(t_N)| \end{bmatrix}$$

By this linearization, the problem can be treated as a multiple linear regression (MLR) problem by using the harmonic current as an explanatory variable (X) and the harmonic voltage as a response variable (Y).

5.5.2 Multiple Linear Regression (MLR)

The linearization transformed the multi-point harmonic impact estimation into a multiple linear regression. Theoretically, ordinary least square method can be used to solve this problem. By using ordinary least square method, matrix *B* can be achieved as follows:

$$B_{MLR} = \left(X^T X\right)^{-1} X^T Y . \tag{5-26}$$

However, this solution causes some practical issues. When suspicious loads (Y) are few in number, are not significantly redundant (collinear), then multiple linear regression works fine. However, if any of these conditions breaks down, MLR can be inefficient and inappropriate. Multicollinearity among loads is a major problem when number of loads increases. Multicollinearity refers to a situation in which two or more explanatory variables (*X*) in a multiple regression model are highly linearly related. Perfect multicollinearity exists if the correlation between two independent variables is equal to 1 or -1. In practice, perfect multicollinearity rarely exists in a data set. More commonly, the issue of multicollinearity arises when there is a strong linear relationship among two or more independent variables. Mathematically, a set of variables is perfectly multicollinear if one or more exact linear relationships among some of the variables exist. For example, we may have

$$\lambda_0 + \lambda_1 X_{1i} + \lambda_2 X_{2i} + \cdots + \lambda_k X_{ki} = 0 . \tag{5-27}$$

holding for all observations *i*, where λ_j are constants and X_{ji} is the i^{th} observation on the j^{th} explanatory variable. The ordinary least square estimates involve inverting the matrix $X^T X$. If there is an exact linear relationship (perfect multicollinearity) among the independent variables, the rank of *X* (and therefore of $X^T X$) is less than *k+1*, and the matrix $X^T X$ will not be invertible. In most applications, perfect multicollinearity is unlikely. An analyst is more likely to face a high degree of multicollinearity. For example, suppose that instead of the above equation holding, we have that equation in modified form with an error term ε_i:

$$\lambda_0 + \lambda_1 X_{1i} + \lambda_2 X_{2i} + \cdots + \lambda_k X_{ki} + \varepsilon_i = 0 . \tag{5-28}$$

In this case, there is no exact linear relationship among the variables, but the X_j variables are nearly perfectly multicollinear if the variance of ε_i is small for some set of

values for the λ's. In this case, the matrix X^TX has an inverse, but is ill-conditioned so that a given computer algorithm may or may not be able to compute an approximate inverse, and if it does so the resulting computed inverse may be highly sensitive to slight variations in the data (due to magnified effects of rounding error) and so may be very inaccurate.

The standard measure of ill-conditioning in a matrix is the condition index [39]. It will indicate that the inversion of the matrix is numerically unstable with finite-precision numbers (standard computer floats and doubles). This indicates the potential sensitivity of the computed inverse to small changes in the original matrix. The condition index is computed by finding the square root of the maximum eigenvalue divided by the minimum eigenvalue. If the Condition Number is above 30, the regression is said to have significant multicollinearity. Figure 5-17 shows condition index of matrix X^TX for field measurement data. When there is only one suspicious harmonic load in the system, matrix X^TX is 1×1 matrix with one eigenvalue and its condition index is 1. As the number of suspicious loads increases, the condition index of the matrix X^TX rapidly increase. For the 3rd harmonic, the condition index reaches above 30 for seven suspicious harmonic loads. For the 5th and 7th harmonics, up to nine and fifteen harmonic loads may be tolerated, respectively. However, high condition indices show poor performance of the ordinary linear regression.

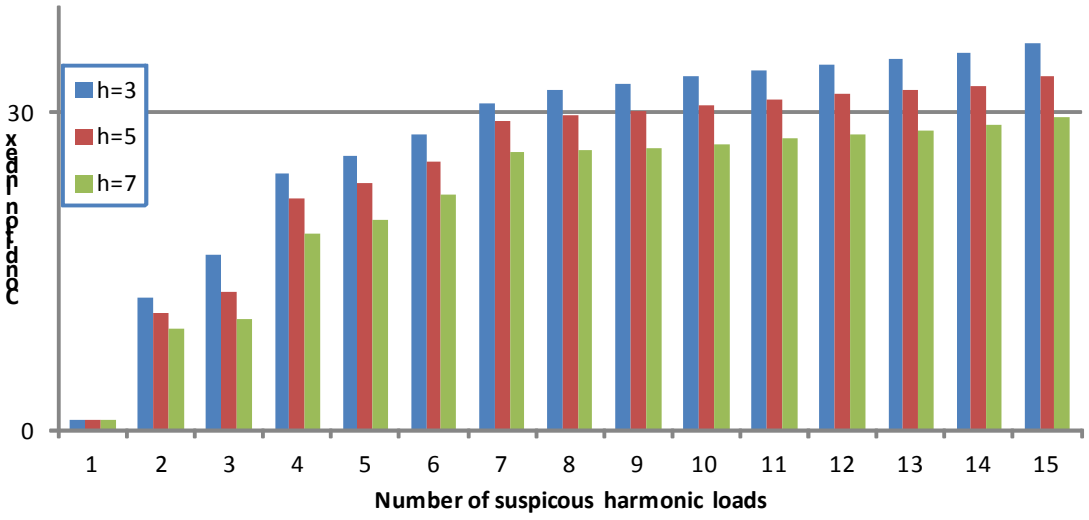

Figure 5-17: Condition index of matrix X^TX for field measurement data

Traditionally, MLR has been used for explaining response variable (Y) by the explanatory variables (X) and it works well as long as the X-variables are fairly few and fairly uncorrelated. The multicollinearity study of the field measurement harmonic loads showed that MLR is not suitable for the multi-point harmonic impact estimation when suspicious loads are more than seven. In principle, MLR still can be used with more loads. However, MLR is likely to give a model that fits the sampled data perfectly but that will fail to predict new data well. The model will be very sensitive to the samples and removing some samples and adding new samples will cause huge change on the model. This phenomenon is called over-fitting. In handling numerous and collinear X-variables, and response profiles Y. Partial Least Square Regression allows us to investigate more complex problems than before, and analyze available data in a more realistic way.

5.5.3 Partial Least Square Regression

PLS regression was developed in the 1960's by Herman Wold as an econometric technique. In the multicollinearity cases, although there are many explanatory factors, there may be only a few underlying or latent factors that account for most of the variation in the response. The general idea of PLS is to try to extract these latent factors, accounting for as much of the explanatory factor variation as possible while modeling the responses well. Figure 5-18 gives a schematic outline of the method. The overall goal is to use the factors to predict the responses in the population. This is achieved indirectly by extracting latent variables T and U from sampled factors and responses, respectively. The extracted factors T (also referred to as X-scores) are used to predict the Y-scores U, and then the predicted Y-scores are used to construct predictions for the responses. The X- and Y-scores are chosen so that the relationship between successive pairs of scores is as strong as possible. PLS seeks directions in the factor space that are associated with high variation in the responses but biases them toward directions that are accurately predicted. PLS is based on the singular value decomposition of $X'Y$ matrix.

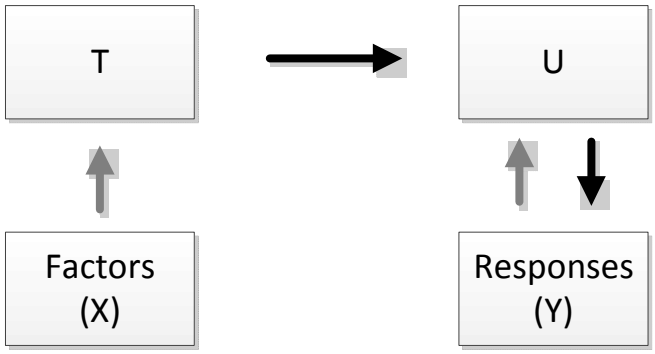

Figure 5-18: PLS modeling

PLS finds latent variables stored in a matrix T that model X and simultaneously predict Y. Formally, this is expressed as a double decomposition of X and the predicted Y:

$$X = TP', \tag{5-29}$$

and

$$Y = TBC', \tag{5-30}$$

where P and C are loadings (or weights). Matrix B is a diagonal matrix and should not be confused with the not-diagonal matrix B in equation (5-24). The latent variables are ordered according to the amount of variance of Y that they explain. Rewriting equation (5-30), Y can also be expressed as a regression model as:

$$Y = TBC' = XB_{PLS}, \tag{5-31}$$

with

$$B_{PLS} = \left(P'\right)^{+} BC', \tag{5-32}$$

where $\left(P'\right)^{+}$ is the pseudo-inverse of P' [40]. In the multi-point harmonic impact estimation problem described in Section 5.5.1, the matrix B_{PLS} has M rows and 1 column and is equivalent to the multiple linear regression B_{MLR}. Each latent variable of X describes a unique aspect of the overall variance of the suspicious harmonic sources that best predicts the harmonic voltage of the observation point.

5.5.3.1 Geometric representation of PLS regression

PLS regression is a projection method and thus has a simple geometric interpretation as a projection of the *X*-matrix (a swarm of *N* points in a *K*-dimensional space) down on an *A*-dimensional hyper-plane in such a way that the coordinates of the projection (t_i) are good predictors of *Y*. This is indicated in Figure 5-19.

As an example, the *X* matrix is represented as *N* points in the *3*-dimensional space where each column of *X* defines one coordinate axis. As the PLS model defines a *2*-dimensional hyper-plane can be constructed by using the two first components. Therefore, the third component is ignored. Thus, PLS regression develops a *2*-dimensional hyper plane in *X*-space such that this plane well approximates *X,* and at the same time, the positions of the projected data points on this plane.

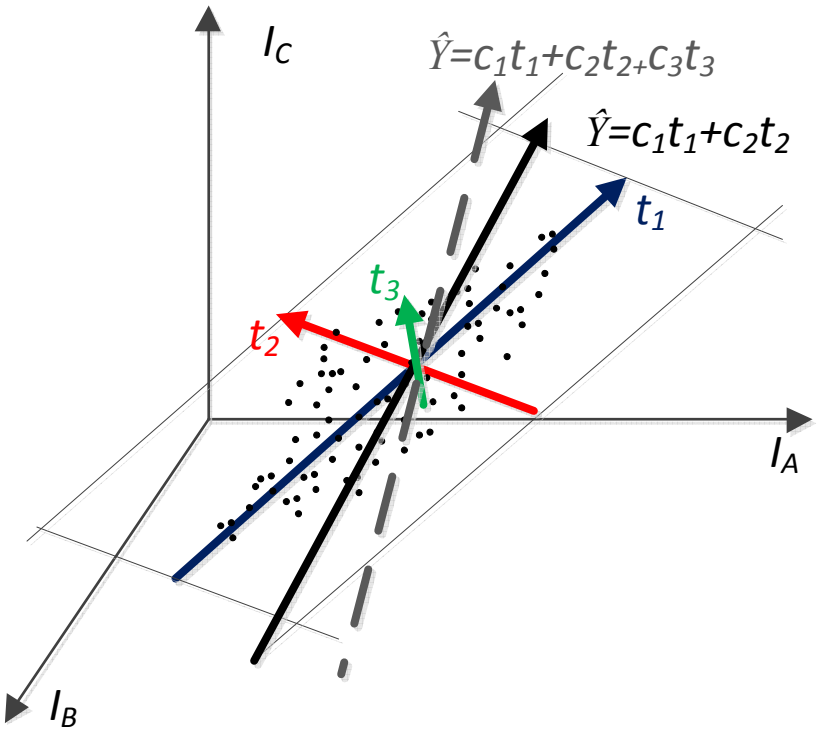

Figure 5-19: Geometric presentation of PLS regression

By addition of the third component, the PLS model can be further developed and has less estimation error. . If this component is considered, the PLS regression will be similar to MLR. Because PLS is based on the singular value decomposition of *X'Y* matrix, the

third component corresponds to the lowest eigenvalue that will be affected by noise more than other components. For example, when most of points are confined in the 2-dimensional plane constructed by two first components and only a few points are out of the plane, then third component will be very sensitive to those points and a small change in the observation can lead to a huge change in the results. In this case, third component will be ignored by PLS regression.

5.5.3.2 PLS regression algorithm

The PLS algorithm is explained by using an example. Figure 5-20 presents harmonic currents of 15 suspicious loads during a day. The harmonic voltage of the studied bus (observation point) is shown in Figure 5-21.

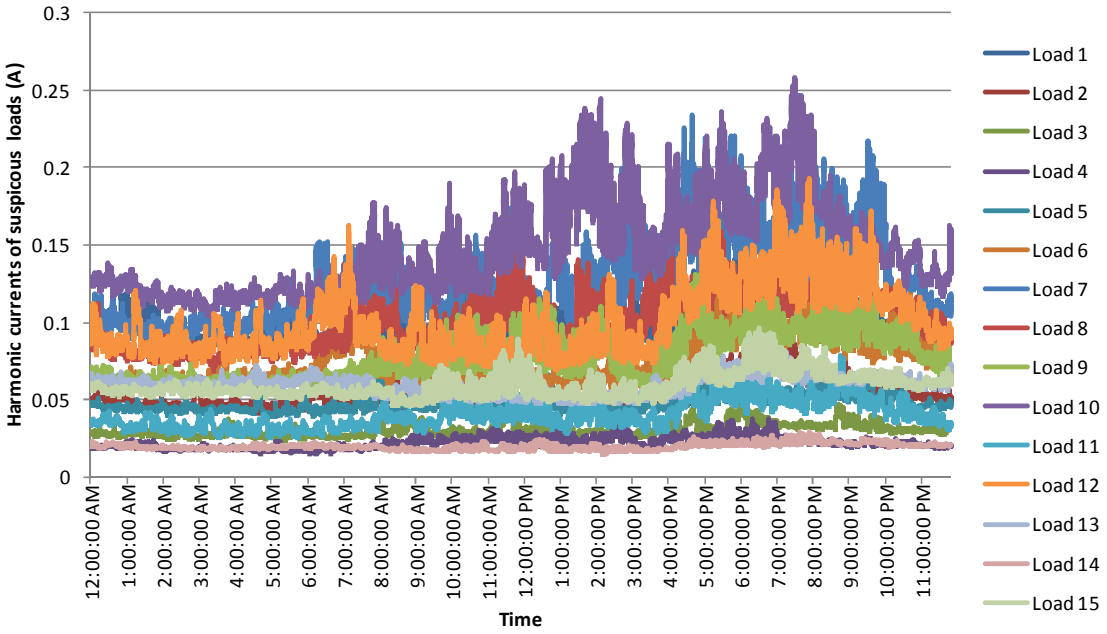

Figure 5-20: Harmonic current of suspicious loads (X)

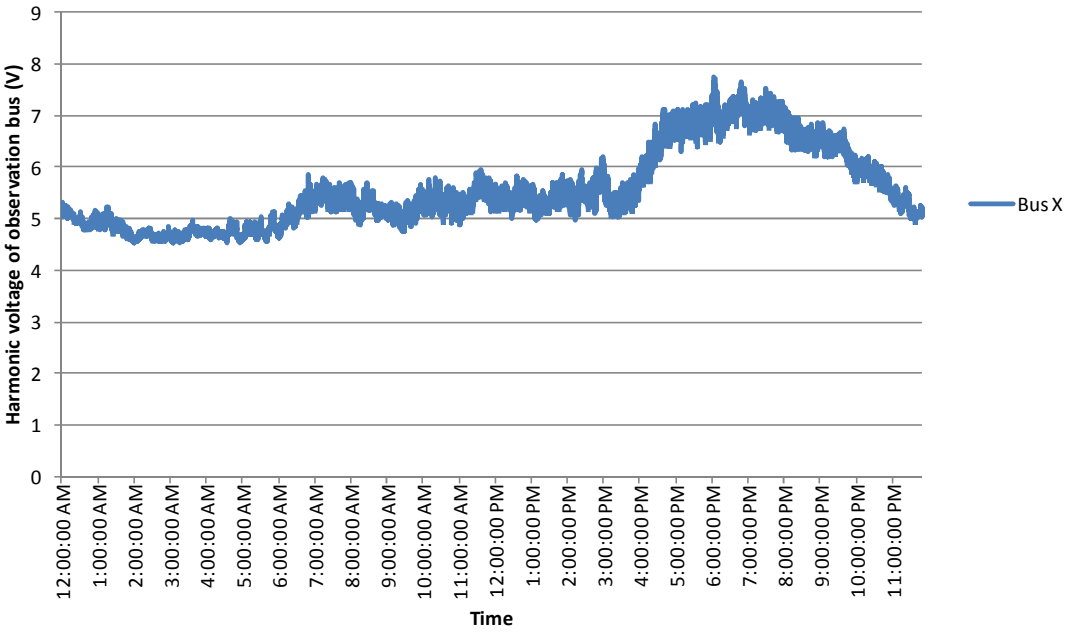

Figure 5-21: Harmonic voltage of observation bus (Y)

1. Step one

X and Y are mean-centered and normalized and stored in matrices X_0 and Y_0. The matrix of correlations between X_0 and Y_0 is computed as:

$$R_1 = X_0^{'} Y_0 . \tag{5-33}$$

In PLS, the latent variables are computed by iterative applications of the SVD. Each run of the SVD produces orthogonal latent variables for X and Y and corresponding regression weights. The SVD is then performed on R_1 and produces two sets of orthogonal singular vectors W_1 and C_1, and the corresponding singular values Δ_1.

$$R_1 = W_1 \Delta_1 C_1^{'} . \tag{5-34}$$

The first pair of singular vectors (i.e., the first columns of W_1 and C_1) are denoted w_1 and c_1 and the first singular value (i.e., the first diagonal entry of Δ_1) is denoted δ_1. The singular value represents the maximum covariance between the singular vectors. The first latent variable of X is given by:

$$t_1 = X_0 w_1 \tag{5-35}$$

where, t_1 is normalized such that $t_1^{'} t_1 = 1$. Figure 5-22 shows the first latent variable of X. This variable is the main common component in the harmonic currents of suspicious

loads and harmonic voltage of observation bus. This component explains more than 50.7% of harmonic currents and 95% of harmonic voltage.

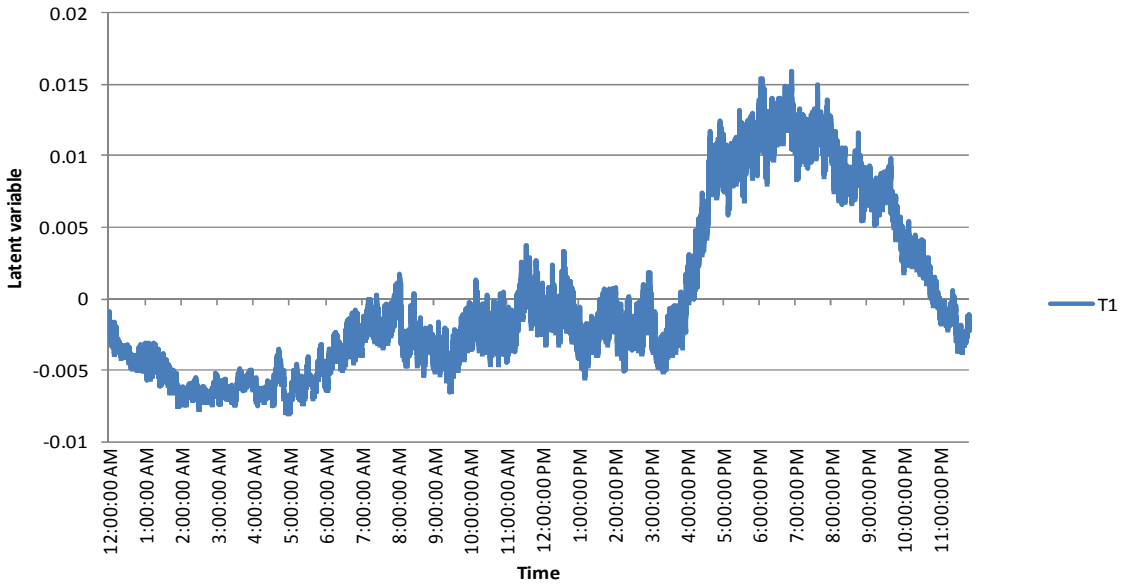

Figure 5-22: Firs latent variable of *X*

The loadings of X_0 on t_1 (i.e., the projection of X_0 onto the space of t_1) are given by:

$$p_1 = X_0' t_1 . \tag{5-36}$$

The least square estimate of X from the first latent variable is given by:

$$\hat{X}_1 = t_1' p_1 . \tag{5-37}$$

The latent variable of Y is obtained as

$$u_1 = Y_0 c_1 . \tag{5-38}$$

Figure 5-23 shows the first latent variable of Y.

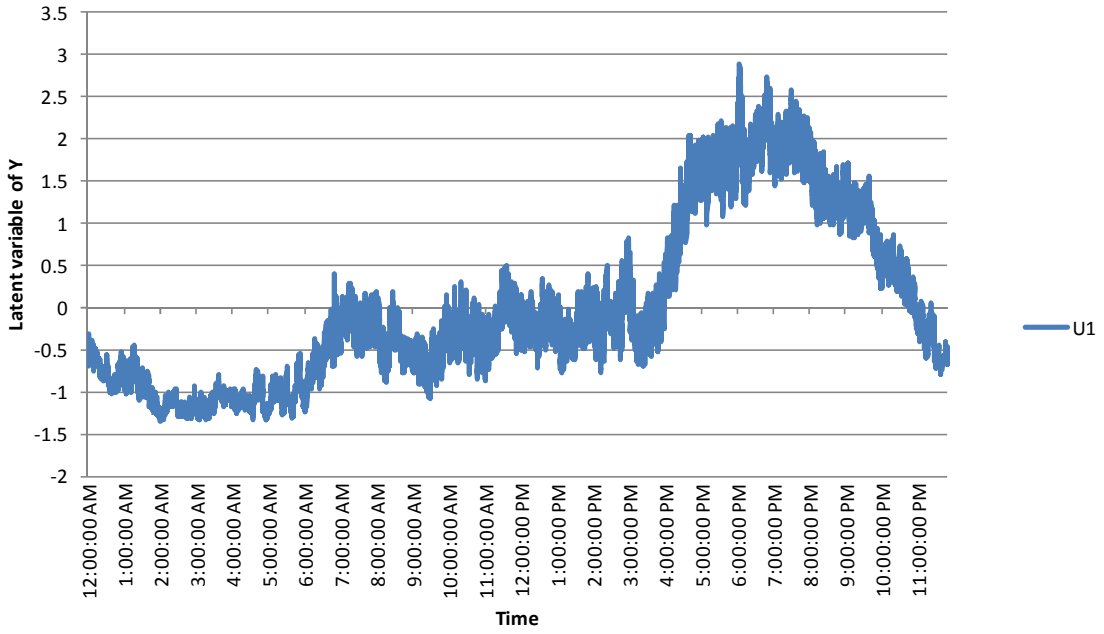

Figure 5-23: Firs latent variable of *Y*

The next step specifies Y from the X-latent variable t_1. This is obtained by first reconstituting Y from its latent variable as:

$$\hat{Y}_1 = u_1 c_1'. \tag{5-39}$$

and then rewriting the equation as:

$$\hat{Y}_1 = t_1 b_1 c_1'. \tag{5-40}$$

with

$$b_1 = t_1' u_1. \tag{5-41}$$

The scalar b_1 is the slope of the regression of $\hat{Y}_1$ on t_1. Because Y and X are centered the regression equation requires only the slope and so there is no intercept in the equation. $\hat{Y}_1$ is obtained as a linear regression from the latent variable extracted from X_0. The regression weight for the example is b_1=167.25. Matrices $\hat{X}_1$ and $\hat{Y}_1$ are then subtracted from the original X_0 and original Y_0 respectively to give deflated X_1 and Y_1:

$$X_1 = X_0 - \hat{X}_1, \tag{5-42}$$

and

$$Y_1 = Y_0 - \hat{Y}_1 . \tag{5-43}$$

2. Step two

The first set of latent variables has now been extracted. Matrices X_1 and Y_1 now become the input matrices for the next iteration and play the roles of X_0 and Y_0, respectively. From the SVD of matrix $R_2 = X_1^{'} Y_1$, we get w_2, c_2, t_2 and b_2 and the new deflated matrices X_2 and Y_2. Figure 5-24 and Figure 5-25 show second latent variables of X and Y, respectively.

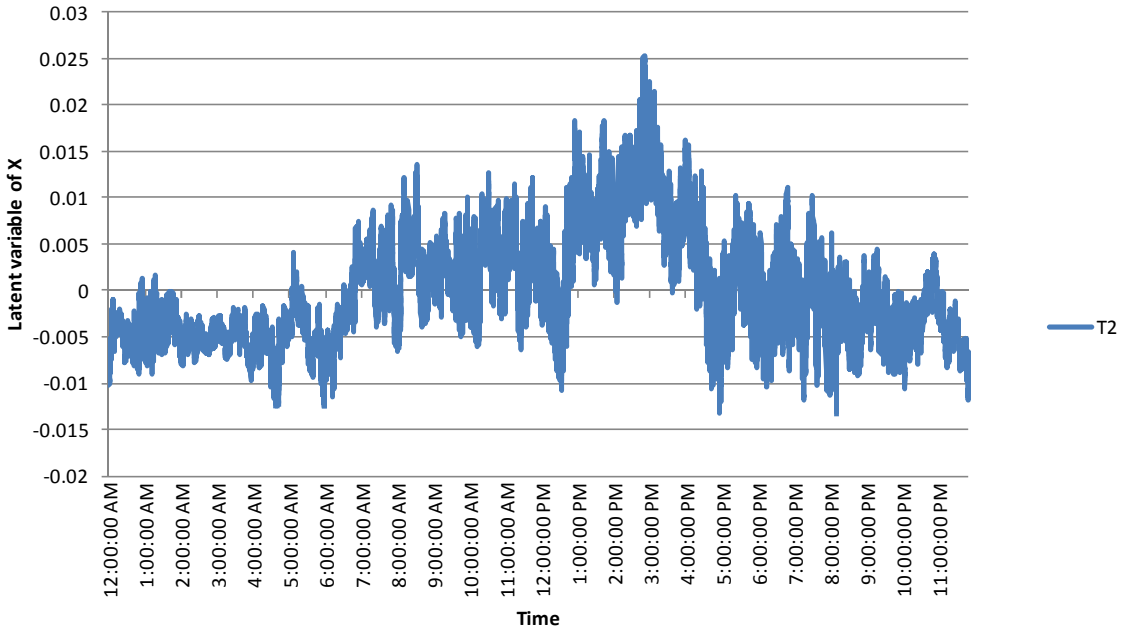

Figure 5-24: Second latent variable of *X*

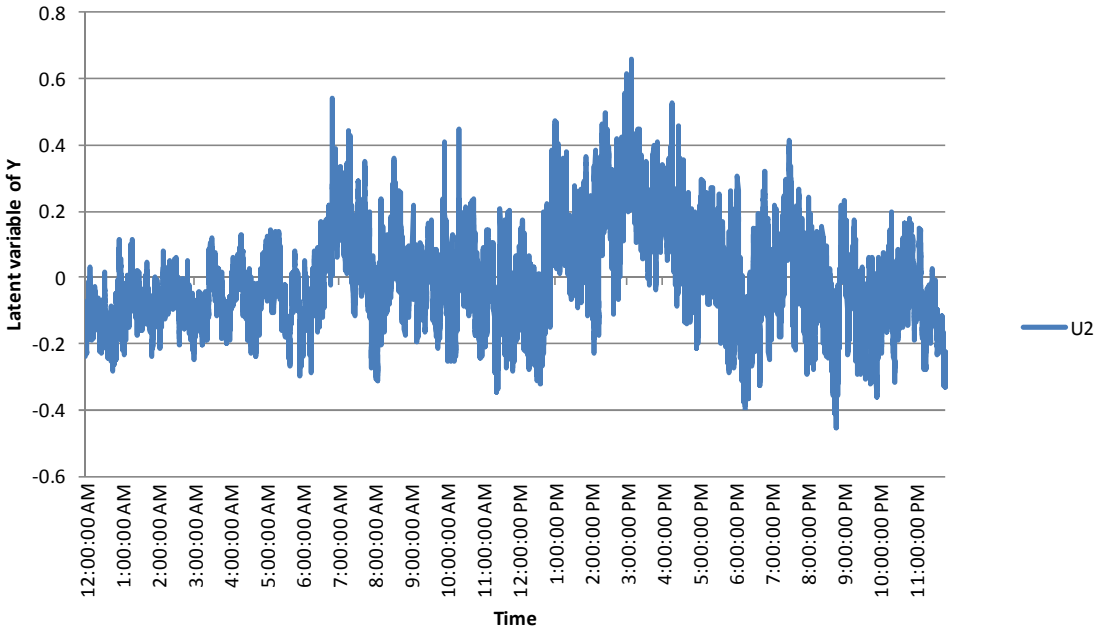

Figure 5-25: Second latent variable of *Y*

3. Step three

Return to step two and continue iterative process until X is completely decomposed into L components (where L in this example can be any integer value equal or less than 15). L is the number of components that construct PLS model. An obvious problem with PLS regression is to find the optimum number of latent variables. A common measure of the quality of fitness of a model is the Residual Estimated Sum of Squares (*RESS*), which is given by:

$$RESS = \left\| Y - \hat{Y} \right\|^2. \tag{5-44}$$

where $\| \|^2$ is the square of the norm of a vector. Lower value of *RESS* indicates better fitted model. However, the lower fitness error does not guarantee the lower prediction error. In multi-point harmonic source estimation problem, if some of the suspicious loads are not relevant to the observation bus, PLSR will over-fit the data. In this case, the model will have very low estimation error but will do very poorly with new observations. The performance of PLS with respect to prediction is done through cross-validation techniques such as the leave-one-out procedure. In this procedure, each observation is

removed in turn from both *X* and *Y*, and a PLS model is recomputed for each of the remaining observations. Then B_{PLS} is used to predict the left-out observation of *Y* from its *X* values. The predicted observations are stored in $\tilde{Y}$. The quality of prediction is measured in a way similar to *RESS*, and is called the Predicted Residual Estimated Sum of Squares (*PRESS*). PRESS is obtained as:

$$PRESS = \left\| Y - \tilde{Y} \right\|^2 . \tag{5-45}$$

The smaller *PRESS* is, the better the prediction. For example, Table 5-8 presents the fit and prediction error analysis for a case study. . If there is over-fitting, the quality of prediction will first decrease and then increase as more latent variables are used for the prediction of new observations. The number of latent variables at which PRESS increases gives an indication of the optimum number of latent variables to be retained. In this case, five latent variables yield the best results.

Table 5-8: PLS fit and prediction error analysis

Number of PLS Factors	Percent Variation Accounted for				RESS	PRESS
	Factors (X)		Responses (Y)			
	Individual (%)	Total(%)	Individual (%)	Total(%)		
1	50.7	50.7	93.2	93.2	0.114	0.116
2	24.4	75.1	4.2	97.4	0.113	0.117
3	13.3	88.4	2.5	99.9	0.112	0.115
4	5.4	93.8	0.1	100	0.110	0.110
5	**3.3**	**97.1**	**0**	**100**	**0.105**	**0.108**
6	1.3	98.4	0	100	0.104	0.110
7	0.8	99.2	0	100	0.103	0.112
8	0.4	99.6	0	100	0.101	0.111
9	0.2	99.8	0	100	0.99	0.111
10	0.1	100	0	100	0.97	0.112
11	0	100	0	100	0.96	0.114
12	0	100	0	100	0.95	0.115
13	0	100	0	100	0.093	0.120
14	0	100	0	100	0.091	0.125
15	0	100	0	100	0.090	0.133

4. Step four

The predicted Y is given by

$$\hat{Y} = TBC^{'} = XB_{PLS}\,, \tag{5-46}$$

where, $B_{PLS} = \left(P'\right)^{+} BC^{'}$. By referring to the definition of the harmonic impact index in equation **(5-3)**, the harmonic impact index of load A, B ,.. , and M can be calculated by using the estimated parameters as follows:

$$\begin{cases} HI_{load\ A}^{Bus\ X}(t_i) = \dfrac{\left|I_{hA}(t_i)\right|}{\left|V_{hX}(t_i)\right|} B_{PLS}(2)\times 100\% \\ HI_{load\ B}^{Bus\ X}(t_i) = \dfrac{\left|I_{hB}(t_i)\right|}{\left|V_{hX}(t_i)\right|} B_{PLS}(3)\times 100\% \\ \vdots \\ HI_{load\ M}^{Bus\ X}(t_i) = \dfrac{\left|I_{hM}(t_i)\right|}{\left|V_{hX}(t_i)\right|} B_{PLS}(M+1)\times 100\% \end{cases} \tag{5-47}$$

The harmonic impact of the other loads can be calculated similarly. The above equation shows that the harmonic impact varies with time. Since knowing average harmonic impacts over a specified period is more useful, the following averaging is proposed for this purpose:

$$\begin{cases} HI_{load\ A}^{Bus\ X} = \dfrac{B_{PLS}(2)}{n} \displaystyle\sum_{i=1}^{n} \frac{\left|I_{hA}(t_i)\right|}{\left|V_{hX}(t_i)\right|} \times 100\% \\ HI_{load\ B}^{Bus\ X} = \dfrac{B_{PLS}(3)}{n} \displaystyle\sum_{i=1}^{n} \frac{\left|I_{hB}(t_i)\right|}{\left|V_{hX}(t_i)\right|} \times 100\% \\ \\ HI_{load\ M}^{Bus\ X} = \dfrac{B_{PLS}(M+1)}{n} \displaystyle\sum_{i=1}^{n} \frac{\left|I_{hM}(t_i)\right|}{\left|V_{hX}(t_i)\right|} \times 100\% \end{cases} \tag{5-48}$$

After applying the algorithm A_{PLS} can be estimated as follows:

$$B_{PLS} = \left(P'\right)^{+} BC^{'}, \tag{5-49}$$

where $\left(P'\right)^{+}$ is the pseudo-inverse of P', and $Y = XA_{PLS}$.

The proposed methods will be studied and characterized in the following chapter. The methods will be verified by using simulation studies and real field test results.

5.6 Summary

In this chapter, the multi-point harmonic source identification problem was formulated. Two data-based methods were proposed to solve the multi-point problem. The first method was the Least Square method that searches the measured data to find the appropriate time intervals for analysis. The second method was the Partial Least Square method that uses data directly. Both methods were presented in this chapter. These methods will be verified and characterized by using simulation studies and real field test results in the next chapter.

Chapter 6

Verification Studies of Multi-point Methods

This chapter presents the verification studies. In the first case, the proposed algorithms (LS and PLS) are verified by using the computer simulations. In the second case, the PLS method is applied to a large-scale system. Finally, the field test results are presented in Section 6.3.

6.1 Case Study #1: IEEE 13-bus test system

The IEEE test system No. 3 for harmonic modeling and simulation is used in this case study (see Figure 6-1). This test system consists of 13 buses and represents a medium-sized industrial plant. The plant is fed from a utility supply at 69 kV (bus 1, slack bus) and the local plant distribution system that operates at 13.8 kV (bus 4, PV bus). Seven PQ loads are attached to the system. These harmonic-producing loads are modeled as current sources with the specified harmonic spectrum presented in Table 6-1. The magnitudes are scaled based on the fundamental component of the load current, and the phase angles are adjusted based on the phase angle of the voltage across the load obtained from the fundamental frequency solution. The aim of this study is to verify the proposed methods (the LS and PLS methods). Three scenarios are studied for this system. In the first scenario, three harmonic-producing loads are attached to the system. Four and five harmonic loads are attached to the system in the second and third scenarios, respectively.

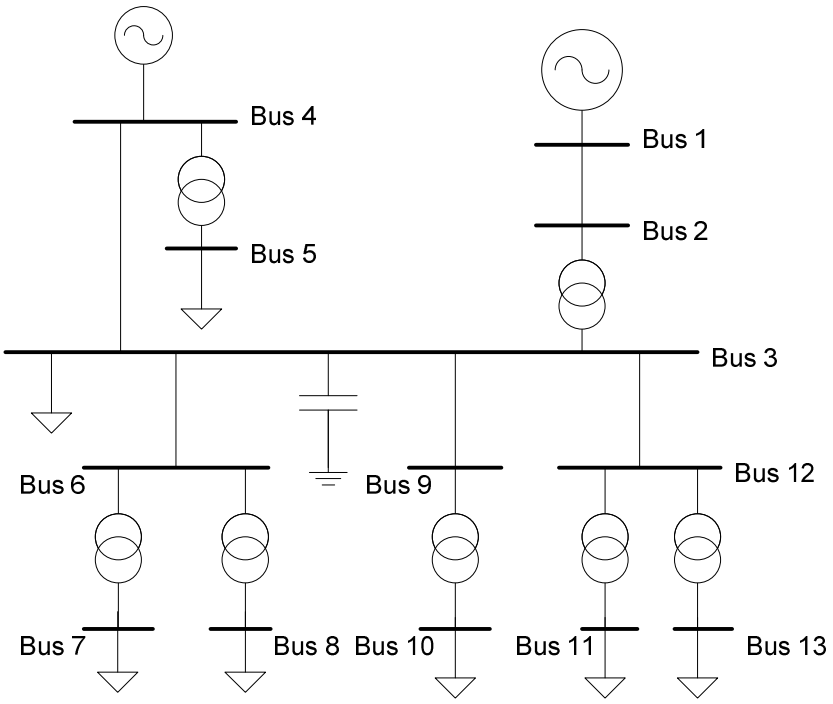

Figure 6-1: A 13-bus power system

Table 6-1: Harmonic spectrum table of harmonic-producing loads

Harmonic Order	Magnitude (percent)	Relative Angle (degree)
1	100	0.00
5	18.24	-55.68
7	11.90	-84.11
11	5.73	-143.56
13	4.01	-175.58

Before applying the proposed method, the simulation procedure should be done to provide the measurement data. In our study, 5000 sample points are generated by the algorithm. The algorithm of the procedure is as follows:

1. Start
2. Until end of the simulation, do
    2.1.Randomly change PQ loads
    2.2.Perform load flow
    2.3.Assign harmonic-injected current sources by using a spectrum table
    2.4.Perform harmonic load flow

2.5. Save harmonic currents of suspicious loads and harmonic voltages of observation points

2.6. Calculate the harmonic impact of each harmonic load

2.7. Save exact harmonic impact for later comparison

2.8. Go back to 2

3. End

After the simulation, the measurement data are ready to be used by our proposed method. The harmonic currents of the suspicious loads and the harmonic voltage of the studied buses (observation points) are used by our proposed method as input data.

6.1.1 Scenario A: Three harmonic loads

Three harmonic loads exist in the system in this scenario and are attached to the buses 7, 10 and 13. To calculate the actual harmonic impact for the simulation studies, the current source method is used. The procedure is explained below.

- Solve the fundamental frequency power flow of the network.
- Determine the fundamental current of loads.
- For harmonic loads, calculate the harmonic source injected currents (I_{hS}).
- Construct the network ***Y*** matrix for harmonic *h*. Calculate Z matrix, $[\mathbf{Z_h}]=[\mathbf{Y_h}]^{-1}$.
- Calculate the network harmonic voltages, $[\mathbf{V_h}]=[\mathbf{Z_h}][\mathbf{I_{hS}}]$.
- Decompose the harmonic voltage of each bus into the components caused by each harmonic load. For example, for bus 1, we have $V_{h1}=\underbrace{Z_{h1,7}I_{hS7}}_{V_{h1,7}}+\underbrace{Z_{h1,10}I_{hS10}}_{V_{h1,10}}+\underbrace{Z_{h1,13}I_{hS13}}_{V_{h1,13}}$.
- Calculate the harmonic impact of each harmonic load. For example, the harmonic impact of load 7 to bus 1 can be calculated by the following formula (Figure 6-2):

  $HI_{load1}^{Bus7}=\dfrac{V_{h1,7-p}}{|V_{h1}|}\times 100\%$,

  where $V_{h1,7-p}$ is the projection of $V_{h1,7}$ into V_{h1}.

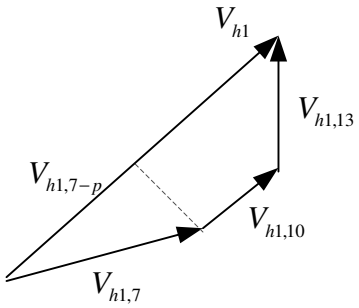

Figure 6-2: Decomposing harmonic voltage at bus 1 into its components

The profile of the harmonic voltage and the fundamental current of the system are shown in Figure 6-3. The figure reveals that the 5th harmonic order is the main harmonic component in the system except for bus 7. For this bus, the 7th harmonic is the main harmonic component. The harmonic impacts of the loads on the system for the 5th, 7th, 11th and 13th harmonic orders are studied. The harmonic impact of the loads on each bus for the 5th harmonic order is presented in Figure 6-4, which shows that load 13 is the main harmonic contributor. Load 7 has a negative harmonic impact on the buses. Therefore, the harmonic voltage caused by load 7 partially cancels out the harmonic voltage generated by the other loads and results in a reduction of the harmonic voltage in the system.

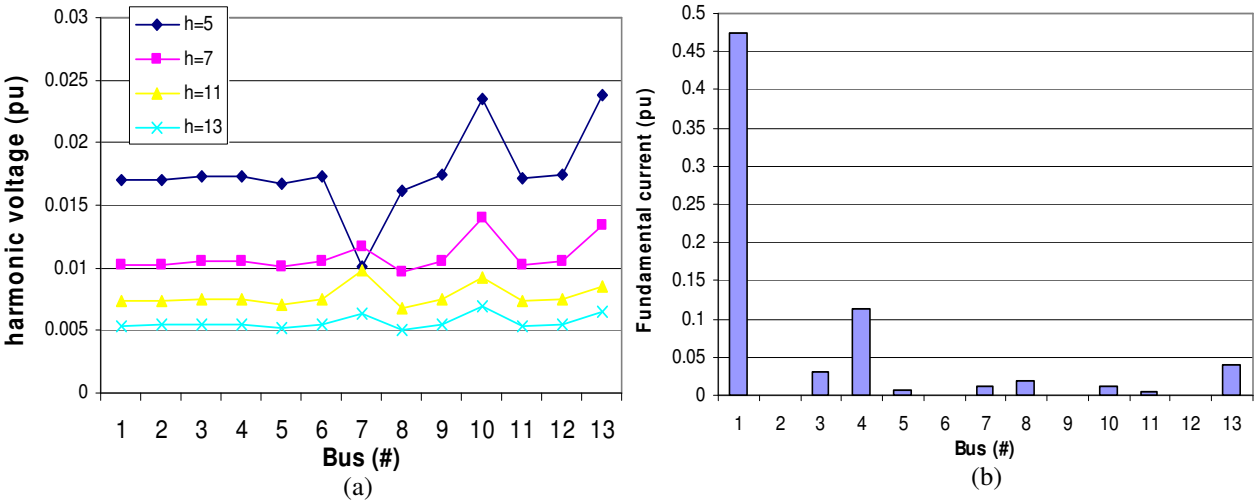

Figure 6-3: Profile of the harmonic voltage (a) and the fundamental current (b) in system

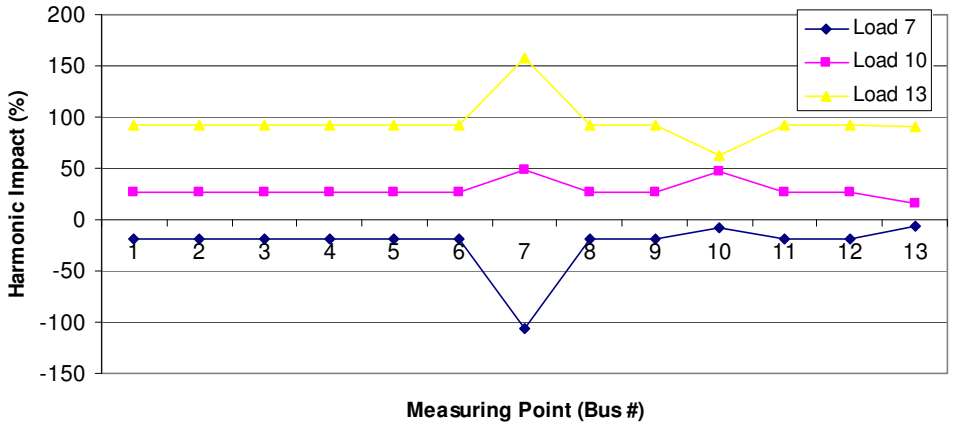

Figure 6-4: Harmonic Impact of loads on the system for the 5th harmonic order in Scenario A

The estimated harmonic impacts of the loads for the 5th harmonic order are presented in Table 6-2. All the methods are successful in distinguishing the negative and positive harmonic impacts of the loads.

Table 6-2: Exact and estimated harmonic impact of loads for the 5th harmonic order in Scenario A

Load	Method	Measuring Point (#Bus)												
		1	2	3	4	5	6	7	8	9	10	11	12	13
Load 7	Exact	-18.3	-18.3	-18.3	-18.3	-18.3	-18.5	-106.3	-18.5	-18.3	-8.6	-18.2	-18.2	-5.7
	LS	-15.1	-15.1	-15.1	-15.1	-15.1	-15.3	-114	-15.1	-15.1	-4.8	-15	-15	-3.3
	PLS	-13.9	-13.9	-13.9	-13.9	-13.8	-14	-107.9	-14	-13.8	-4.7	-13.8	-13.8	-1.7
Load 10	Exact	26.5	26.5	26.5	26.5	26.5	26.5	47.9	26.5	26.7	46.1	26.3	26.3	14.9
	LS	27.5	27.5	27.5	27.5	27.4	27.5	46.1	27.7	27.7	49.4	27.2	27.3	15.1
	PLS	25.7	25.7	25.7	25.7	25.8	25.8	46.7	25.9	25.9	47.7	25.5	25.6	13.5
Load 13	Exact	91.9	91.9	91.9	91.9	91.9	92	158.3	92	91.6	62.4	91.9	91.9	90.8
	LS	89.1	89.1	89.1	89.1	89.2	89.2	161.6	89.2	88.8	56.1	89	89.1	89.6
	PLS	89.4	89.4	89.4	89.4	89.4	89.5	160.8	89.5	89.1	56.9	89.3	89.4	89.7

As Table 6-2 shows, the estimated results of the three methods are quite close to each other, and no significant difference can be observed. To compare the methods, the total estimation error of each method should be quantified. To quantify the error in

estimating the harmonic impacts of loads for each bus, two indices are proposed: MSE and AE. The MSE index is the mean square error and is calculated as follows:

$$MSE_{BusX}(\%) = \sqrt{\frac{\sum_{i=1}^{N_{sus}} \left(HI_{loadi}^{BuxX} - \tilde{HI}_{loadi}^{BuxX} \right)^2}{N_{sus}}}, \tag{6-1}$$

where N_{sus} is the number of suspicious harmonic loads, and HI_{loadi}^{BuxX} and $\tilde{HI}_{loadi}^{BuxX}$ are the exact and the estimated harmonic impact of load i on bus X, respectively. The AE index is the absolute error index and is defined as follows:

$$AE_{BusX}(\%) = Max\left\{ \left| HI_{loadi}^{BuxX} - \tilde{HI}_{loadi}^{BuxX} \right| \right\} \text{ where } i = 1 \text{ to } N_{sus}, \tag{6-2}$$

The MSE and AE errors in estimating the harmonic impacts of loads for the buses are shown in Figure 6-5, which reveals that the PLS method has an overall greater estimation error in comparison to the LS method. However, the PLS method has less estimation errors for buses 7 and 10.

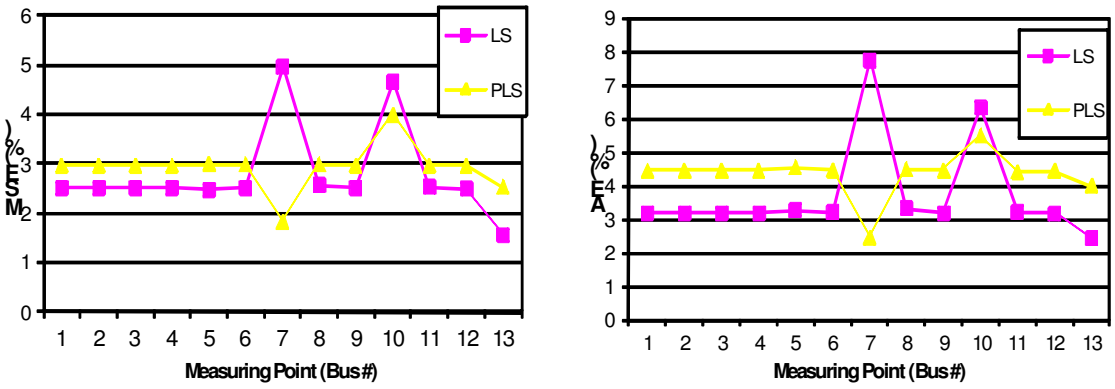

(a) (b)

Figure 6-5: Estimation error of the proposed methods for the 5th harmonic order in Scenario A (a) MSE index (b) AE index

The harmonic impact of the loads on each bus for the 7th harmonic order is presented in Figure 6-6. This figure shows that load 13 is still the main harmonic contributor and the load 7 has a negative harmonic impact on the buses (except for bus 7).

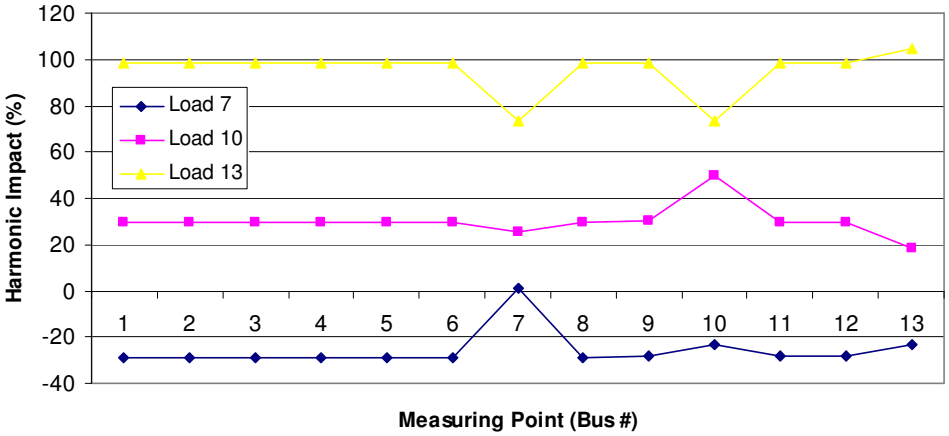

Figure 6-6: Harmonic Impact of loads on the system for the 7th harmonic order in Scenario A

The estimated harmonic impacts of the loads for the 7th harmonic order are presented in Table 6-3. The harmonic impact of these loads on the buses can be estimated fairly well except for bus 7. For this bus, all the proposed methods fail to successfully estimate the harmonic impact of load 7. The estimation error indices for this harmonic order are shown in Figure 6-7.

Table 6-3: Exact and estimated harmonic impact of loads for the 7th harmonic order in Scenario A

Load	Method	Measuring Point (#Bus)												
		1	2	3	4	5	6	7	8	9	10	11	12	13
Load 7	Exact	-28.6	-28.6	-28.6	-28.6	-28.6	-28.7	1.3	-28.7	-28.5	-23.1	-28.5	-28.5	-23.6
	LS	-34.3	-34.3	-34.3	-34.3	-34.3	-34.5	-20.3	-34.4	-34.2	-24.1	-34.1	-34.2	-25
	PLS	-31.5	-31.5	-31.5	-31.5	-31.4	-31.6	-15.7	-31.6	-31.4	-23.1	-31.3	-31.3	-22.4
Load 10	Exact	29.9	29.9	29.9	29.9	29.9	29.9	25.4	29.9	30	49.5	29.7	29.7	18.6
	LS	28.6	28.6	28.6	28.6	28.5	28.6	21.8	28.7	28.8	53.2	28.3	28.4	16.6
	PLS	28.8	28.8	28.8	28.8	28.8	28.8	25.2	28.9	29	52.5	28.6	28.6	16
Load 13	Exact	98.7	98.7	98.7	98.7	98.7	98.8	73.3	98.8	98.4	73.6	98.7	98.7	105
	LS	102.3	102.3	102.3	102.3	102.4	102.4	86.7	102.4	102	68.2	102.2	102.3	107.8
	PLS	102.5	102.5	102.5	102.5	102.6	102.6	87.1	102.6	102.3	69.1	102.5	102.6	107.8

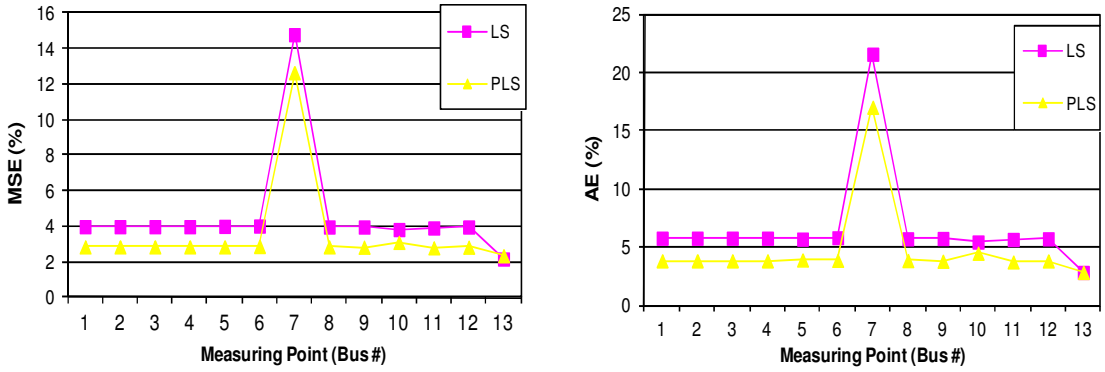

(a) (b)

Figure 6-7: Estimation error of the proposed methods for the 7th harmonic order in Scenario A (a) MSE index (b) AE index

The harmonic impacts of the loads on each bus for the 11th harmonic order are presented in Figure 6-8. In this harmonic, all the harmonic-producing loads have a positive harmonic impact. Load 13 has the major harmonic impact, and loads 7 and 10 are minor harmonic contributors. The estimated harmonic impacts of the loads are presented in Table 6-4. The proposed methods can estimate fairly well the harmonic impact of loads 10 and 13. However, the performance of the methods in estimating the harmonic impact of load 7 is not satisfactory. The proposed methods usually have difficulty in estimating the minor harmonic contributors. The estimation error indices are shown in Figure 6-9.

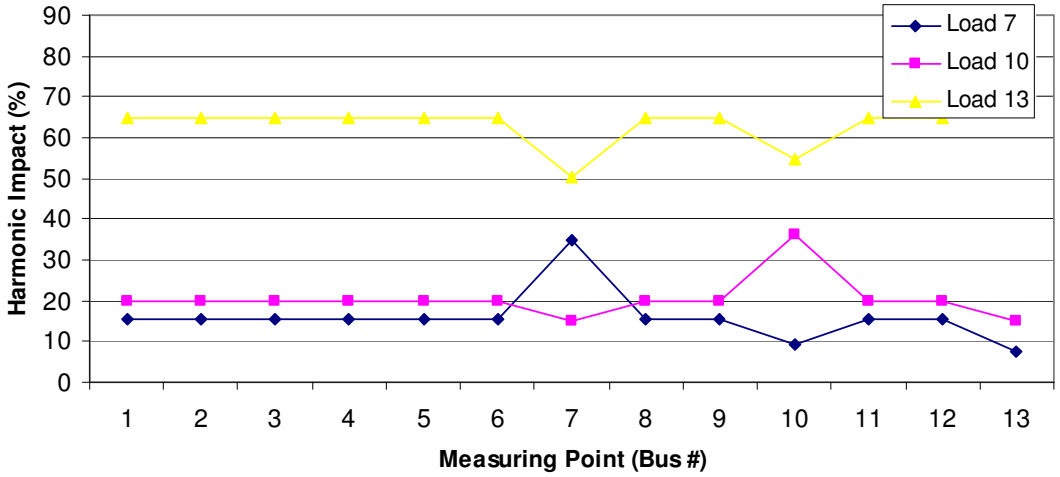

Figure 6-8: Harmonic impact of loads on the system for the 11th harmonic order in Scenario A

Table 6-4: Exact and estimated harmonic impact of loads for the 11th harmonic order in Scenario A

Load	Method	Measuring Point (#Bus)												
		1	2	3	4	5	6	7	8	9	10	11	12	13
Load 7	Exact	15.3	15.3	15.3	15.3	15.3	15.4	34.9	15.4	15.3	9.4	15.2	15.2	7.7
	LS	7	7	7	7	7.1	7.1	32	7.2	7	1.8	7	6.9	-2.8
	PLS	9.2	9.2	9.2	9.2	9.3	9.3	33.1	9.3	9.2	3.3	9.1	9.1	0.3
Load 10	Exact	19.9	19.9	19.9	19.9	19.9	19.9	14.8	19.9	20.1	36	19.8	19.8	15.1
	LS	17.9	17.9	17.9	17.9	17.7	17.9	14.3	18	18	39	17.7	17.8	10.2
	PLS	18.3	18.3	18.3	18.3	18.4	18.3	13.5	18.5	18.5	39.4	18.2	18.2	11.4
Load 13	Exact	64.7	64.7	64.7	64.7	64.7	64.7	50.3	64.7	64.6	54.6	64.9	64.9	77.3
	LS	71.7	71.7	71.7	71.7	71.8	71.6	53.4	71.7	71.5	53.5	71.7	71.8	88.5
	PLS	72.2	72.2	72.2	72.2	72.3	72.1	53.8	72.1	72	54.7	72.2	72.4	88.7

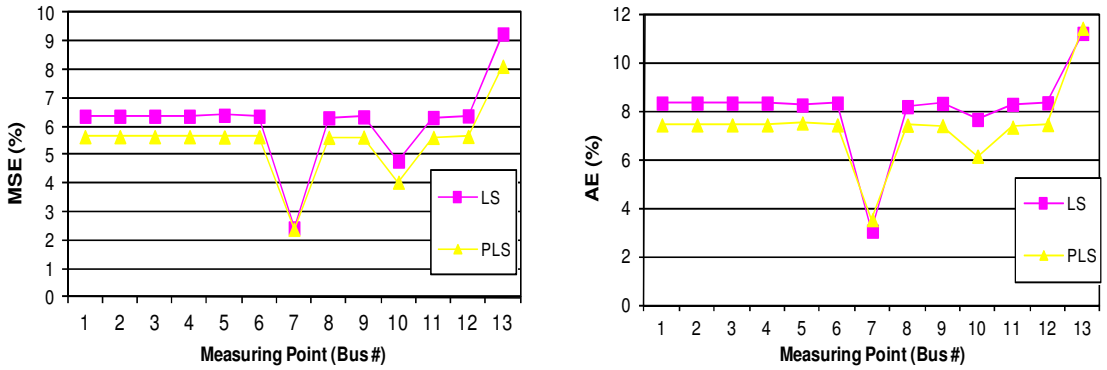

(a) (b)

Figure 6-9: Estimation error of the proposed methods for the 11th harmonic order in Scenario A (a) MSE index (b) AE index

The harmonic impacts of the loads on each bus for the 13th harmonic order are presented in Figure 6-10. Similarly to harmonic 11, all the harmonic-producing loads have a positive harmonic impact for this harmonic order. Load 13 is the major harmonic contributor, and loads 7 and 10 are minor harmonic contributors. The estimated harmonic impacts of the loads are presented in Table 6-5. The proposed methods estimate fairly

well the harmonic impact of the loads. The estimation error indices are shown in Figure 6-11.

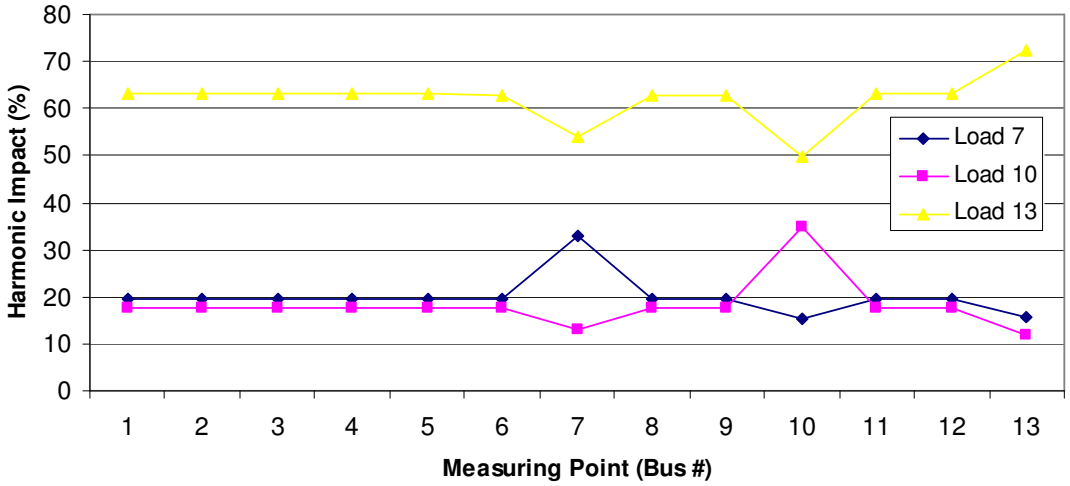

Figure 6-10: Harmonic impact of loads on the system for the 13th harmonic order in Scenario A

Table 6-5: Exact and estimated harmonic impact of loads for the 13th harmonic order in Scenario A

Load	Method	Measuring Point (#Bus)												
		1	2	3	4	5	6	7	8	9	10	11	12	13
Load 7	Exact	19.4	19.4	19.4	19.4	19.4	19.5	32.9	19.5	19.4	15.3	19.4	19.4	15.8
	LS	18.8	18.8	18.8	18.8	18.9	18.9	42.9	19.1	18.8	13.8	18.8	18.7	11.1
	PLS	20	20	20	20	20.1	20	42.7	20.1	19.9	14.3	19.8	19.9	13.2
Load 10	Exact	17.6	17.6	17.6	17.6	17.6	17.6	13.1	17.6	17.7	34.9	17.5	17.5	11.8
	LS	16.4	16.4	16.4	16.4	16.2	16.3	14.1	16.6	16.5	38	16.1	16.3	7.8
	PLS	15.2	15.2	15.2	15.2	15.2	15.1	10.8	15.3	15.3	37	15	15.1	7.7
Load 13	Exact	63	63	63	63	63	62.9	54	62.9	62.9	49.8	63.1	63.1	72.4
	LS	66	66	66	66	66.2	65.9	49.8	66	65.9	46.6	66	66.2	80.5
	PLS	66.4	66.4	66.4	66.4	66.5	66.3	49.9	66.3	66.3	47.6	66.4	66.5	80.7

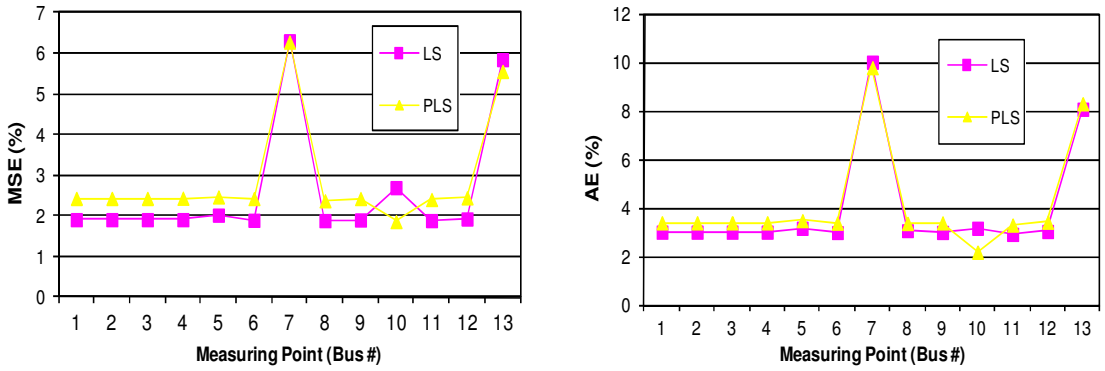

(a) (b)

Figure 6-11: Estimation error of the proposed methods for the 13th harmonic order in Scenario A (a) MSE index (b) AE index

To finalize this scenario, the total estimation errors of the proposed methods are compared by using two indices. The MSE and AE indices, which were previously defined for each bus, are modified to give indices for the total system. The MSE index for the method X is defined as follows:

$$MSE_{Method\ X}(\%) = \sqrt{\frac{\sum_{i=1}^{N_{Bus}} MSE_{Bus\ X}^2}{N_{Bus}}}, \tag{6-3}$$

where N_{Bus} is the number of buses in the system, and $MSE_{Bus\ X}$ is the MSE index for each bus. Similarly, the AE index for method X is defined as follows:

$$AE_{Method\ X}(\%) = Max\left\{AE_{Bus\ X}\right\} \text{ where } i = 1 \text{ to } N_{Bus}, \tag{6-4}$$

The MSE and AE indices for the LS and PLS methods for scenario A are presented in Figure 6-12. This figure shows that for both indices, the PLS method is more accurate for the 7th and 11th harmonic orders, whereas LS method has more accuracy for the 5th and 13th harmonic orders.

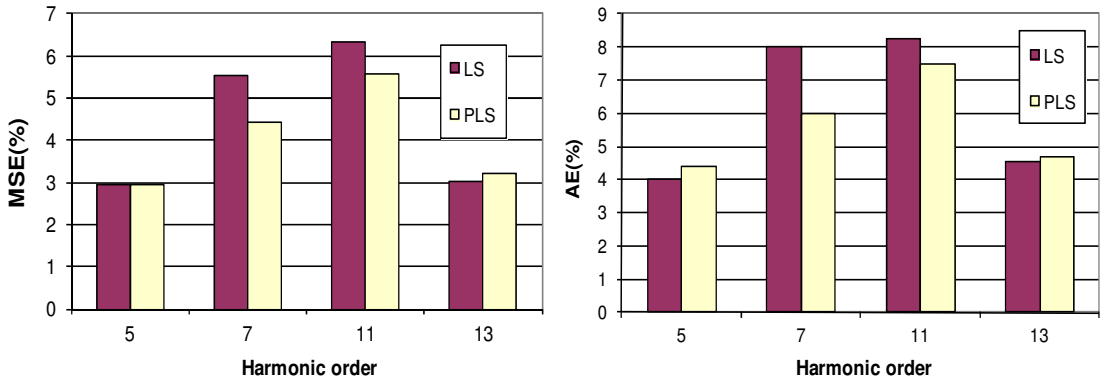

(a) (b)

Figure 6-12: The total estimation error indices of methods in Scenario A

(a) MSE index (b) AE index

6.1.2 Scenario B: Four harmonic loads

In this scenario, the system has four harmonic loads, which are attached to the buses 5, 7, 10 and 13. The profile of the harmonic voltage and the fundamental current of the system is shown in Figure 6-13. As in the previous scenario, the 5th harmonic order is the main harmonic component in the system. The harmonic impacts of the loads on the system for the 5th, 7th, 11th and 13th harmonic orders are studied. The harmonic impacts of the loads on each bus for the 5th harmonic order are presented in Figure 6-14. Load 13 is the main harmonic contributor, and load 5 and 10 are minor contributors. Load 7 has a negative harmonic impact on the buses.

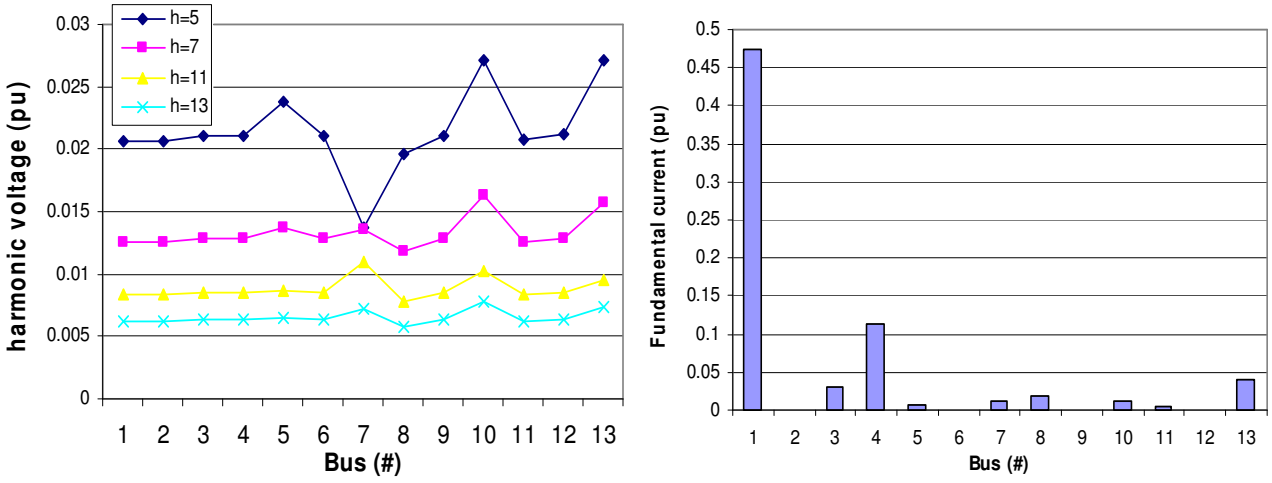

(a) (b)

Figure 6-13: Profile of the system in Scenario B

(a)Harmonic voltage (b) Fundamental current

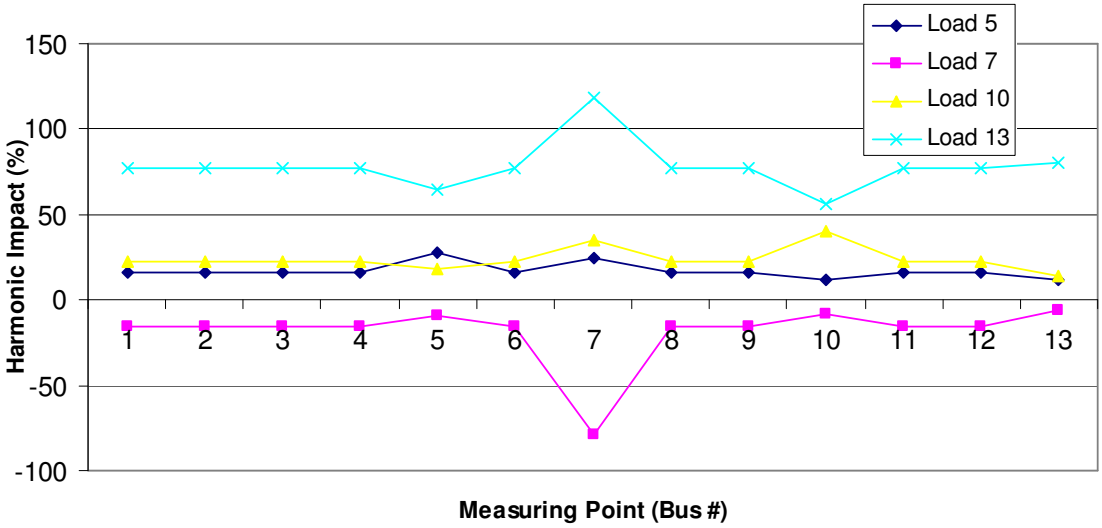

Figure 6-14: Harmonic Impact of loads on the system for the 5th harmonic order in Scenario B

Table 6-6: Exact and estimated harmonic impact of loads for the 5th harmonic order in Scenario B

Load	Method	Measuring Point (#Bus)												
		1	2	3	4	5	6	7	8	9	10	11	12	13
Load 5	Exact	16.2	16.2	16.2	16.3	27.7	16.2	24.4	16.2	16.2	12.2	16.1	16.1	11.7
	LS	16.5	16.5	16.5	16.6	28.8	16.5	27.9	16.8	16.4	11.2	16.6	16.4	11.4
	PLS	16.5	16.5	16.5	16.6	29.7	16.5	24.6	16.6	16.5	12.2	16.4	16.4	11.5
Load 7	Exact	-15.4	-15.4	-15.4	-15.4	-9.6	-15.5	-78.4	-15.5	-15.4	-8.2	-15.3	-15.3	-6.1
	LS	-11.8	-11.8	-11.8	-11.7	-6.4	-11.9	-82.9	-11.6	-11.7	-3.9	-11.7	-11.7	-2.8
	PLS	-11.7	-11.7	-11.7	-11.7	-5.9	-11.8	-79.2	-11.8	-11.7	-4.8	-11.7	-11.6	-2.5
Load 10	Exact	22.2	22.2	22.2	22.2	17.6	22.2	35.5	22.2	22.4	39.9	22.1	22.1	14
	LS	23.1	23.1	23.1	23	18.1	23.1	33.6	23	23.2	42.8	22.9	23	14.4
	PLS	21.6	21.6	21.6	21.5	16.6	21.6	34.5	21.7	21.8	41.5	21.4	21.5	12.8
Load 13	Exact	77	77	77	76.9	64.2	77.1	118.6	77.1	76.8	56.1	77.1	77.1	80.4
	LS	76	76	76	75.9	60.5	76.1	119.4	76.8	75.8	52.3	76	76.1	81.1
	PLS	75	75	75	74.8	59.4	75	119.4	75	74.8	51.7	75	75.1	80.3

The estimated harmonic impacts of the loads for the 5th harmonic order are presented in Table 6-6. All the methods successfully distinguish the negative and positive harmonic impacts of the loads. The estimation error is always less than 5%. The estimation error indices are presented in Figure 6-15. The estimation error is usually higher in the buses with harmonic-producing loads to them (buses 5, 7 and 10). Because

load 13 is the main harmonic contributor, the performance of the methods in its bus is higher, and the estimation error is lower.

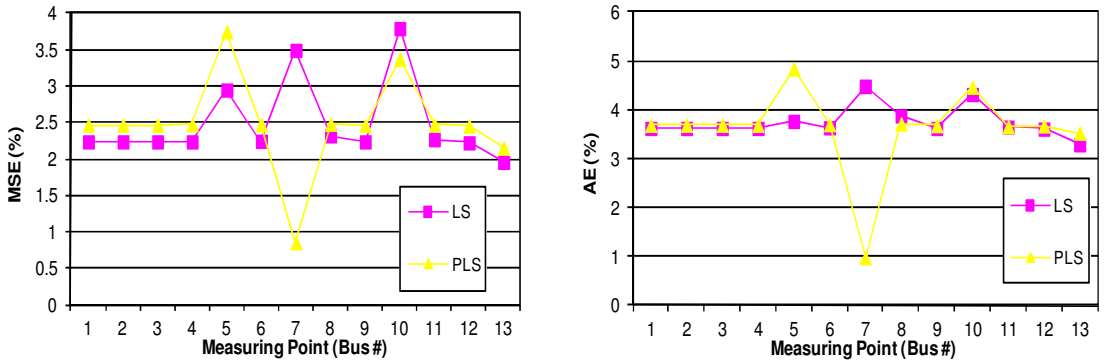

(a) (b)

Figure 6-15: Estimation error of the proposed methods for the 5th harmonic order in Scenario B (a) MSE index (b) AE index

The harmonic impacts of the loads on each bus for the 7th harmonic order are presented in Figure 6-16. In this harmonic, all the harmonic-producing loads have a positive harmonic impact. Load 13 is the main harmonic contributor, and loads 5 and 10 are minor contributors. Load 7 has a negative harmonic impact on the buses. The estimated harmonic impacts of the loads are presented in Table 6-7. The PLS method clearly has the best estimation among the proposed methods. The estimation error indices presented in Figure 6-17 supports this conclusion.

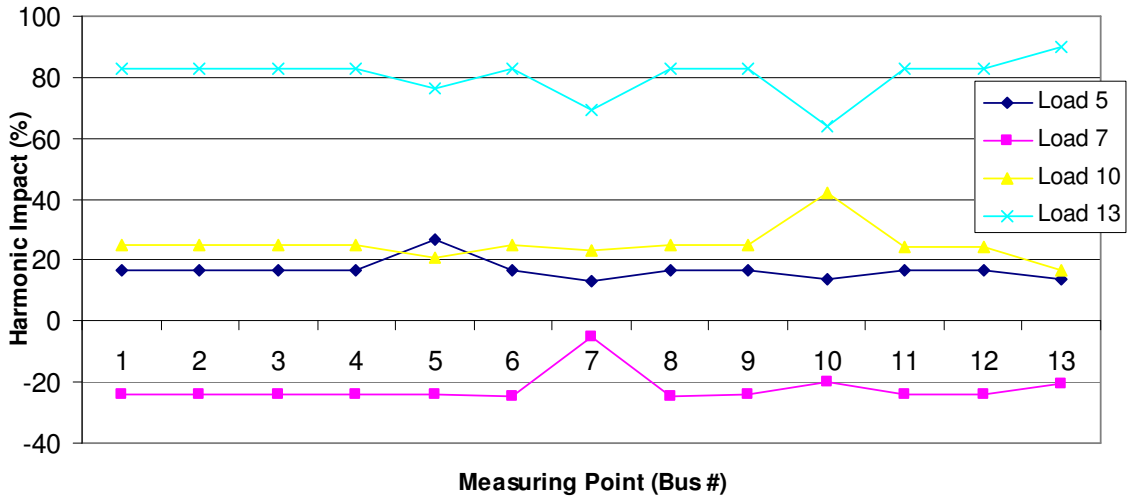

Figure 6-16: Harmonic impacts of loads on the system for the 7th harmonic order in Scenario B

Table 6-7: Exact and estimated harmonic impacts of loads for the 7th harmonic order in Scenario B

Load	Method	Measuring Point (#Bus)												
		1	2	3	4	5	6	7	8	9	10	11	12	13
Load 5	Exact	16.7	16.7	16.7	16.8	26.5	16.8	12.9	16.8	16.7	13.7	16.7	16.7	13.9
	LS	19.6	19.6	19.6	19.7	30.6	19.7	19.8	20.0	19.6	13.6	19.7	19.6	15.1
	PLS	17.2	17.2	17.2	17.3	30.1	17.2	13.0	17.2	17.1	13.7	17.1	17.1	13.5
Load 7	Exact	-24.3	-24.3	-24.3	-24.3	-23.8	-24.4	-5.1	-24.4	-24.2	-20.2	-24.2	-24.2	-20.7
	LS	-28.7	-28.7	-28.7	-28.7	-26.4	-28.9	-25.8	-28.6	-28.7	-20.7	-28.6	-28.6	-21.4
	PLS	-26.4	-26.4	-26.4	-26.4	-24.2	-26.6	-19.8	-26.5	-26.4	-20.2	-26.4	-26.3	-19.8
Load 10	Exact	24.7	24.7	24.7	24.7	21.1	24.7	23.0	24.7	24.9	42.3	24.6	24.6	16.6
	LS	23.4	23.4	23.4	23.3	19.1	23.4	19.0	23.3	23.5	45.0	23.2	23.2	15.1
	PLS	23.6	23.6	23.6	23.6	19.1	23.6	22.3	23.7	23.8	44.9	23.4	23.5	14.4
Load 13	Exact	82.8	82.8	82.8	82.8	76.2	82.9	69.2	82.9	82.7	64.2	82.9	82.9	90.2
	LS	84.3	84.3	84.3	84.2	72.2	84.4	75.5	85.2	84.1	60.1	84.3	84.4	93.4
	PLS	84.8	84.8	84.8	84.7	72.1	84.9	78.9	84.9	84.6	60.4	84.8	84.9	93.4

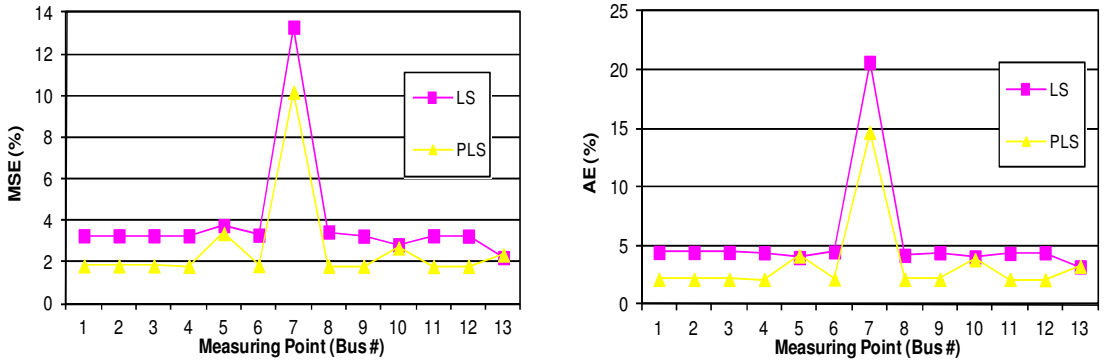

(a) (b)

Figure 6-17: Estimation error of the proposed methods for the 7th harmonic order in Scenario B (a) MSE index (b) AE index

The harmonic impacts of the loads on each bus for the 11th and 13th harmonic orders are presented in Figure 6-18 and Figure 6-19, respectively. In this harmonic order, all the harmonic-producing loads have a positive harmonic impact. Load 13 is the main harmonic contributor, and the other loads are minor contributors. The estimated harmonic

impacts of the loads are presented in Table 6-8 and Table 6-9. Again, the PLS method clearly has less estimation error.

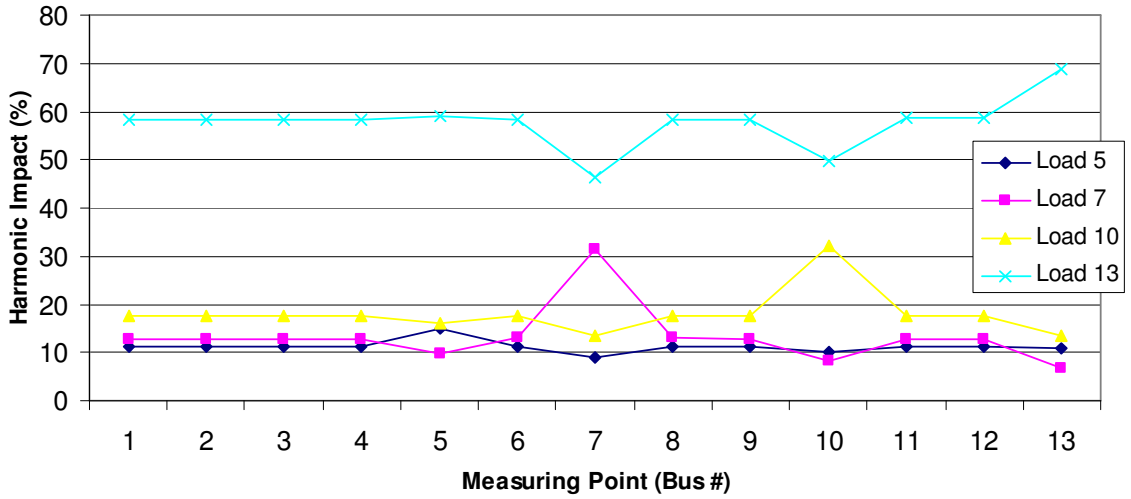

Figure 6-18: Harmonic impacts of loads on the system for the 11th harmonic order in Scenario B

Table 6-8: Exact and estimated harmonic impacts of loads for the 11th harmonic order in Scenario B

Load	Method	Measuring Point (#Bus)												
		1	2	3	4	5	6	7	8	9	10	11	12	13
Load 5	Exact	11.1	11.1	11.1	11.2	15.1	11.1	9	11.1	11.1	10	11.1	11.1	11
	LS	15.6	15.6	15.6	15.7	22.6	15.6	11.5	16	15.6	11.9	15.8	15.6	15.4
	PLS	11.8	11.8	11.8	11.9	19.9	11.8	9.6	11.9	11.8	10.2	11.8	11.8	10.6
Load 7	Exact	12.9	12.9	12.9	12.8	9.7	12.9	31.2	12.9	12.8	8.2	12.8	12.8	6.7
	LS	4.5	4.5	4.5	4.4	-0.8	4.5	28.2	4.8	4.4	0.6	4.4	4.4	-3.1
	PLS	6.9	6.9	6.9	6.9	2.5	7	29.1	7	6.9	2.4	6.8	6.8	0
Load 10	Exact	17.5	17.5	17.5	17.5	16.1	17.5	13.4	17.5	17.7	32.3	17.5	17.5	13.5
	LS	15.2	15.2	15.2	15.2	11.9	15.2	12.8	15.1	15.4	34.1	15	15.1	9.4
	PLS	15.7	15.7	15.7	15.7	13.2	15.7	12	15.9	15.9	35.1	15.6	15.7	10.1
Load 13	Exact	58.5	58.5	58.5	58.5	59	58.4	46.3	58.4	58.4	49.5	58.6	58.6	68.8
	LS	61.9	61.9	61.9	61.9	56.7	61.9	47.9	62.8	61.8	47.3	61.9	62.1	76.6
	PLS	63.4	63.4	63.4	63.4	58.3	63.4	48.7	63.4	63.3	48.9	63.5	63.6	78.6

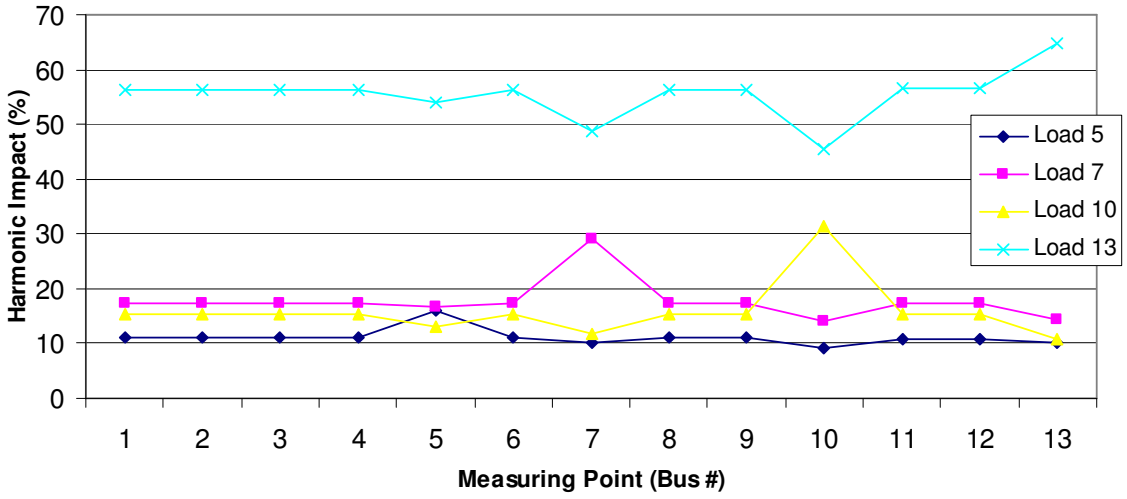

Figure 6-19: Harmonic Impact of loads on the system for the 13th harmonic order in Scenario B

Table 6-9: Exact and estimated harmonic impact of loads for the 13th harmonic order in Scenario B

Load	Method	Measuring Point (#Bus)												
		1	2	3	4	5	6	7	8	9	10	11	12	13
Load 5	Exact	11	11	11	11	16.1	11	10.2	11	11	9.3	10.9	10.9	10.1
	LS	13.8	13.8	13.8	13.9	22.4	13.8	9.1	14.3	13.8	10.2	14	13.8	13.2
	PLS	12.1	12.1	12.1	12.1	21.5	12	11.3	12.1	12	9.8	12	12	9.9
Load 7	Exact	17.3	17.3	17.3	17.3	16.6	17.4	29.3	17.4	17.3	13.9	17.3	17.3	14.3
	LS	16.8	16.8	16.8	16.8	12.9	16.9	40	17.2	16.8	12.7	16.8	16.8	10.4
	PLS	17.3	17.3	17.3	17.3	14.5	17.4	37.8	17.4	17.3	12.8	17.2	17.2	11.9
Load 10	Exact	15.4	15.4	15.4	15.3	13.2	15.3	11.7	15.3	15.5	31.3	15.3	15.3	10.7
	LS	14	14	14	14	9.9	14	13	13.9	14.2	33.5	13.9	14	7.5
	PLS	12.9	12.9	12.9	12.9	9.7	12.9	9.5	13	13	33.1	12.8	12.8	6.9
Load 13	Exact	56.3	56.3	56.3	56.3	54.1	56.3	48.8	56.3	56.2	45.4	56.5	56.5	64.9
	LS	57.8	57.8	57.8	57.8	49.5	57.8	46.5	58.8	57.7	42.2	57.8	58	71.2
	PLS	57.9	57.9	57.9	57.8	49.9	57.9	44.6	57.8	57.8	42.8	58	58.1	72.2

To finalize this scenario, we compare the total estimation error of the proposed methods by using the MSE and AE indices methods. As Figure 6-19 shows, PLS method is more accurate and has less estimation error.

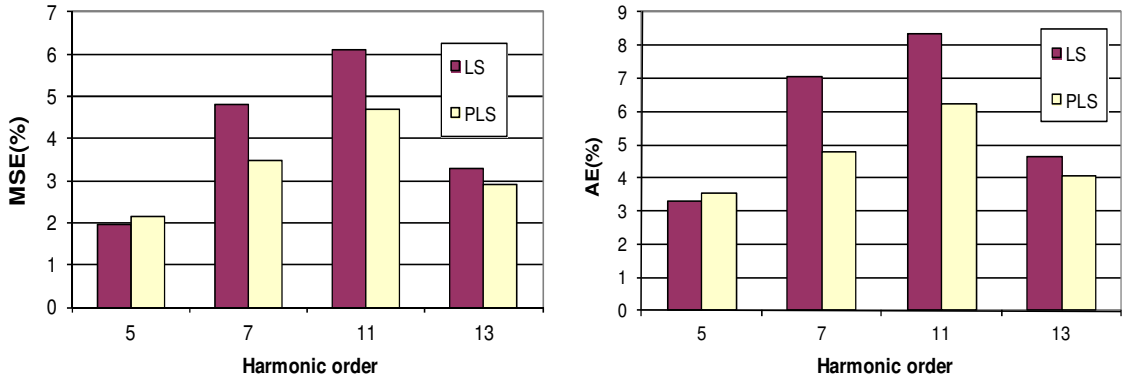

(a) (b)

Figure 6-20: The total estimation error indices of methods in Scenario B

(a) MSE index (b) AE index

6.1.3 Scenario C: Five harmonic loads

In this scenario, the system has five harmonic producing-loads attached to the buses 3, 5, 7, 10 and 13. The profiles of the harmonic voltage and the fundamental current of the system are shown in Figure 6-21. The 5th harmonic order is the main harmonic component in the system. The harmonic impacts of the loads on each bus for the 5th harmonic order are presented in Figure 6-22. The estimated harmonic impacts of the loads are presented in Table 6-10.

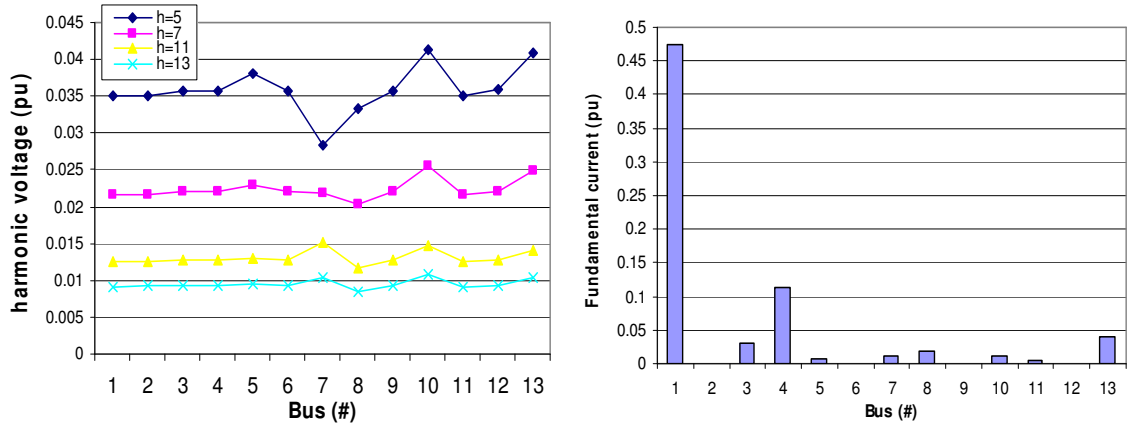

(a) (b)

Figure 6-21: Profile of the system in Scenario C

(a)Harmonic voltage (b) Fundamental current

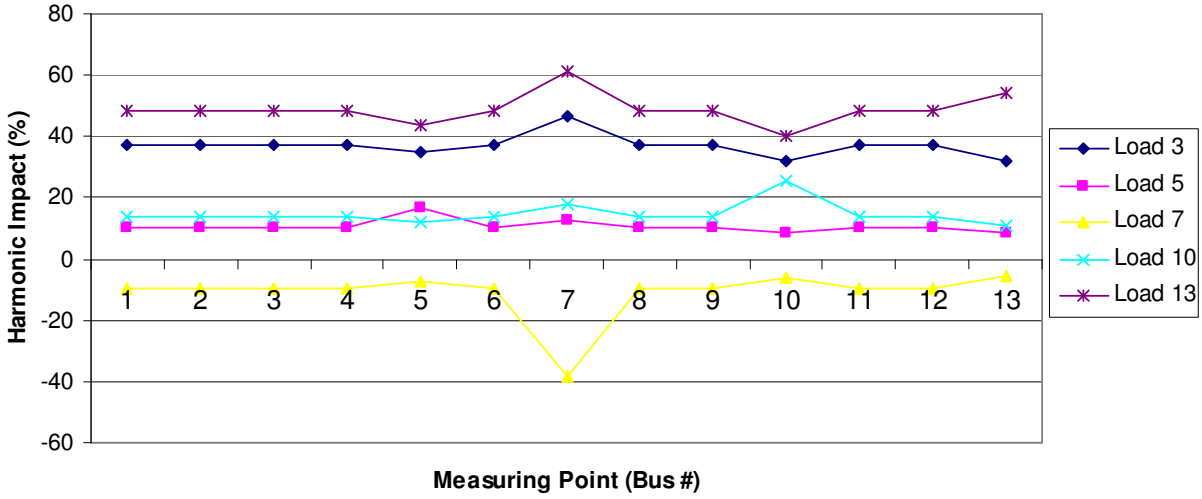

Figure 6-22: Harmonic Impact of loads on the system for the 5th harmonic order in Scenario C

Table 6-10: Exact and estimated harmonic impact of loads for the 5th harmonic order in Scenario C

Load	Method	Measuring Point (#Bus)												
		1	2	3	4	5	6	7	8	9	10	11	12	13
Load 3	Exact	37.3	37.3	37.3	37.3	34.8	37.3	46.4	37.3	37.2	32.1	37.2	37.2	31.9
	LS	36.3	36.3	36.3	36.3	34.4	36.3	42.6	36.3	36.3	32.3	36.2	36.2	30.8
	PLS	37.4	37.4	37.4	37.4	35	37.4	46.3	37.5	37.3	32.1	37.3	37.3	32.1
Load 5	Exact	10.2	10.2	10.2	10.2	16.5	10.2	12.8	10.2	10.2	8.6	10.1	10.1	8.5
	LS	5.3	5.3	5.3	5.3	12	5.3	9.2	6.8	5.3	2.7	5.9	5.3	4.2
	PLS	10.3	10.3	10.3	10.4	17.9	10.3	12.8	10.4	10.3	8.7	10.3	10.3	8.5
Load 7	Exact	-9.4	-9.4	-9.4	-9.4	-7.1	-9.5	-38.2	-9.5	-9.4	-6.4	-9.4	-9.4	-5.5
	LS	-6.9	-6.9	-6.9	-6.9	-5.5	-7	-38.1	-6.9	-6.9	-2.9	-6.8	-6.9	-3.5
	PLS	-7	-7	-7	-7	-4.8	-7.1	-38	-7.1	-7	-4.1	-7	-7	-3.1
Load 10	Exact	13.8	13.8	13.8	13.8	12.2	13.8	17.9	13.8	13.9	25.6	13.8	13.8	10.6
	LS	12.9	12.9	12.9	12.8	10.9	12.9	13.5	11.9	13	26.6	12.6	12.8	9.8
	PLS	13.4	13.4	13.4	13.4	11.6	13.4	17.3	13.5	13.5	27	13.3	13.4	9.9
Load 13	Exact	48.1	48.1	48.1	48.1	43.7	48.2	61.2	48.2	48.1	40	48.3	48.3	54.4
	LS	46.4	46.4	46.4	46.3	41.1	46.4	58.1	48	46.3	37.8	46.6	46.5	55.2
	PLS	46.6	46.6	46.6	46.6	41	46.6	60.4	46.6	46.6	37.3	46.7	46.8	55.3

The harmonic impacts of the loads for the 7th, 11th and 13th harmonic orders are presented in Figure 6-23, Figure 6-24 and Figure 6-25, respectively. The estimated harmonic impacts of the loads are presented in Table 6-11, Table 6-12 and Table 6-13.

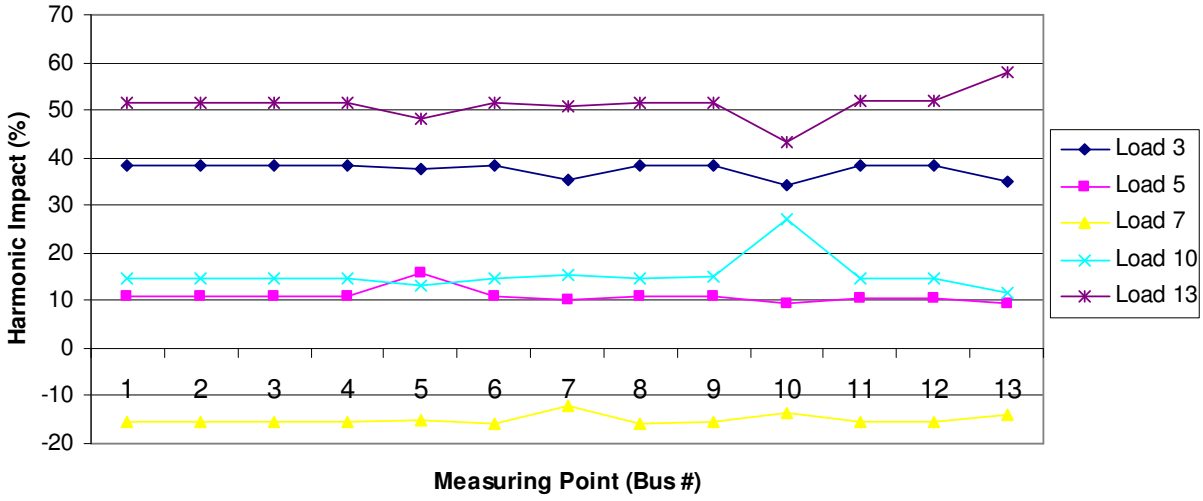

Figure 6-23: Harmonic impacts of loads on the system for the 7th harmonic order in Scenario C

Table 6-11: Exact and estimated harmonic impact of loads for the 7th harmonic order in Scenario C

Load	Method	Measuring Point (#Bus)												
		1	2	3	4	5	6	7	8	9	10	11	12	13
Load 3	Exact	38.5	38.5	38.5	38.5	37.7	38.5	35.4	38.5	38.5	34	38.4	38.4	35
	LS	35.9	35.9	35.9	35.9	35.8	35.9	30.3	35.8	35.8	33.2	35.8	35.8	32.4
	PLS	38.3	38.3	38.3	38.3	37.7	38.4	34.7	38.4	38.3	33.9	38.2	38.3	35
Load 5	Exact	10.7	10.7	10.7	10.8	15.9	10.7	10.1	10.7	10.7	9.3	10.7	10.7	9.4
	LS	8	8	8	8	13.2	8	13.5	9.6	8	4.4	8.6	8	6.7
	PLS	10.8	10.8	10.8	10.9	18.1	10.8	9.9	10.9	10.8	9.3	10.7	10.8	9.2
Load 7	Exact	-15.7	-15.7	-15.7	-15.7	-15.2	-15.7	-11.9	-15.7	-15.6	-13.7	-15.6	-15.6	-14
	LS	-16.5	-16.5	-16.5	-16.5	-16.4	-16.5	-21.3	-16.5	-16.4	-12.6	-16.3	-16.4	-14.2
	PLS	-16.3	-16.3	-16.3	-16.3	-15.3	-16.4	-20.3	-16.4	-16.3	-13.6	-16.3	-16.3	-13.6
Load 10	Exact	14.8	14.8	14.8	14.8	13.2	14.8	15.6	14.8	14.9	27	14.8	14.8	11.5
	LS	11.2	11.2	11.2	11.2	8.8	11.2	7.4	10.2	11.3	26.5	11	11.2	8.5
	PLS	13.8	13.8	13.8	13.8	11.9	13.8	14.4	13.9	13.9	28.7	13.7	13.8	10
Load 13	Exact	51.6	51.6	51.6	51.6	48.3	51.7	50.9	51.7	51.6	43.4	51.8	51.8	58.1
	LS	48.2	48.2	48.2	48.2	43.7	48.3	46.4	50	48.2	39.4	48.4	48.4	58.8
	PLS	50.8	50.8	50.8	50.8	45.3	50.9	53.3	50.8	50.7	40.5	50.9	51	60.7

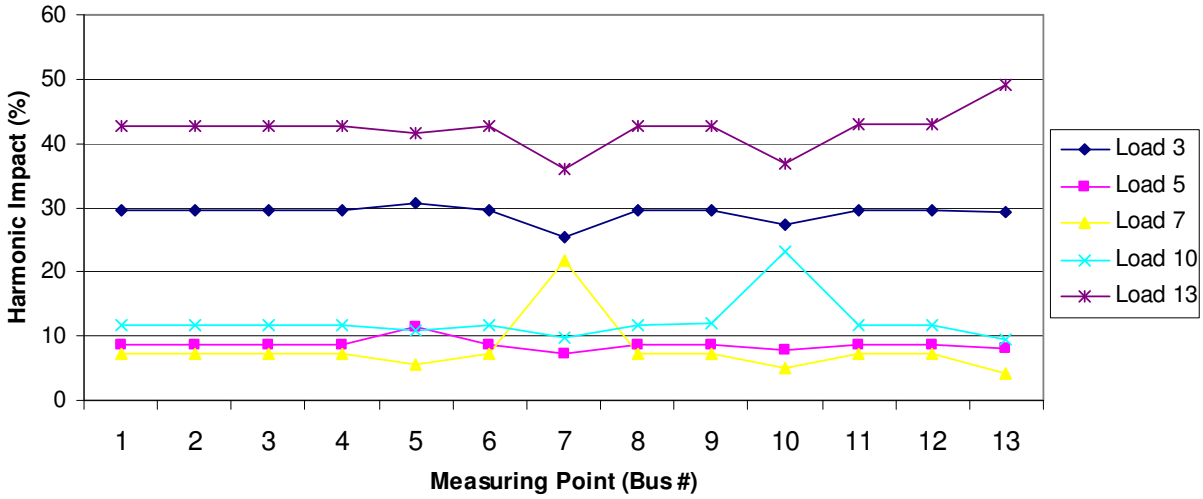

Figure 6-24: Harmonic Impact of loads on the system for the 11th harmonic order in Scenario C

Table 6-12: Exact and estimated harmonic impact of loads for the 11th harmonic order in Scenario C

Load	Method	Measuring Point (#Bus)												
		1	2	3	4	5	6	7	8	9	10	11	12	13
Load 3	Exact	29.6	29.6	29.6	29.6	30.7	29.6	25.3	29.6	29.6	27.2	29.6	29.6	29.3
	LS	26.9	26.9	26.9	26.9	28.3	26.9	24.5	26.8	26.9	26	26.8	26.9	25.8
	PLS	29.2	29.2	29.2	29.2	30.4	29.1	25.1	29.2	29.1	26.8	29.1	29.1	29
Load 5	Exact	8.6	8.6	8.6	8.6	11.4	8.6	7.3	8.6	8.6	7.7	8.6	8.6	8.2
	LS	9.6	9.6	9.6	9.7	13.3	9.6	6.9	11.5	9.6	6.6	10.4	9.6	10.4
	PLS	8.7	8.7	8.7	8.7	14.3	8.7	7.4	8.7	8.6	7.6	8.6	8.6	7.7
Load 7	Exact	7.2	7.2	7.2	7.2	5.5	7.3	21.8	7.3	7.2	5	7.2	7.2	4.1
	LS	2.2	2.2	2.2	2.2	-1.1	2.3	19.2	2.3	2.2	1.2	2.3	2.2	-2
	PLS	2.4	2.4	2.4	2.4	0.2	2.4	19.1	2.4	2.4	0.4	2.3	2.4	-0.9
Load 10	Exact	11.8	11.8	11.8	11.8	10.8	11.8	9.7	11.8	11.9	23.2	11.8	11.8	9.4
	LS	6.2	6.2	6.2	6.2	2.6	6.2	6.6	4.9	6.3	20.6	5.9	6.2	3.3
	PLS	9.7	9.7	9.7	9.7	8.2	9.7	8	9.8	9.8	24.5	9.6	9.7	6.7
Load 13	Exact	42.8	42.8	42.8	42.8	41.6	42.7	35.9	42.7	42.7	37	42.9	42.9	49.1
	LS	37.5	37.5	37.5	37.5	34.4	37.5	31.8	39.6	37.5	30.8	37.7	37.7	48.9
	PLS	42.7	42.7	42.7	42.6	38.8	42.7	35.2	42.6	42.6	34.5	42.7	42.8	54.3

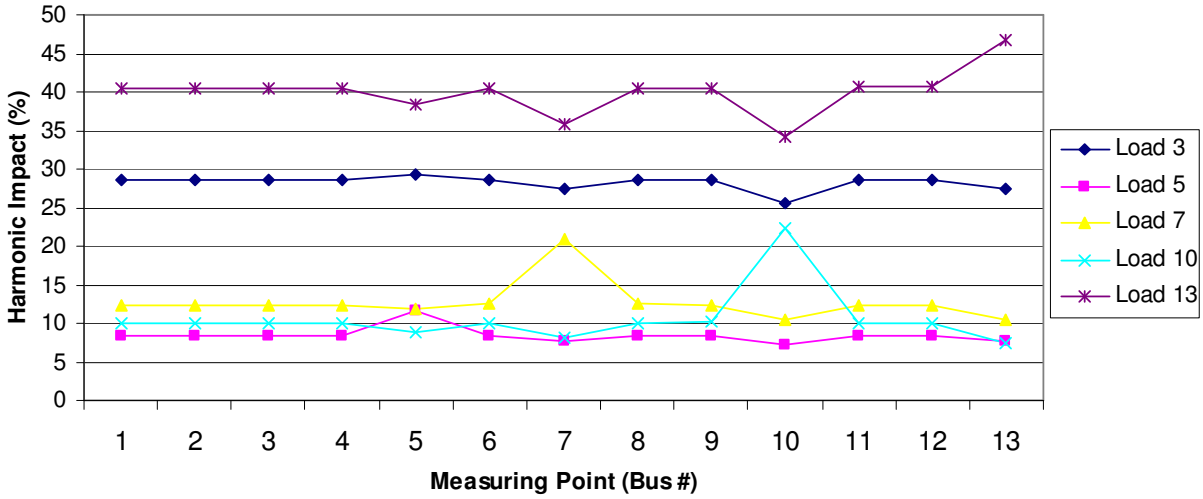

Figure 6-25: Harmonic Impact of loads on the system for the 13th harmonic order in Scenario C

Table 6-13: Exact and estimated harmonic impact of loads for the 13th harmonic order in Scenario C

Load	Method	Measuring Point (#Bus)												
		1	2	3	4	5	6	7	8	9	10	11	12	13
Load 3	Exact	28.7	28.7	28.7	28.7	29.3	28.7	27.5	28.7	28.7	25.6	28.7	28.7	27.5
	LS	27.5	27.5	27.5	27.5	28.4	27.5	29.2	27.4	27.5	25.6	27.4	27.5	25.2
	PLS	28.5	28.5	28.5	28.5	29.2	28.5	27.7	28.6	28.4	25.4	28.4	28.4	27.4
Load 5	Exact	8.3	8.3	8.3	8.4	11.7	8.3	7.7	8.3	8.3	7.3	8.3	8.3	7.6
	LS	6.5	6.5	6.5	6.6	11.3	6.5	0.7	8.6	6.5	4	7.4	6.5	7.9
	PLS	8.6	8.6	8.6	8.7	15.1	8.6	8.2	8.7	8.6	7.4	8.6	8.6	7.3
Load 7	Exact	12.4	12.4	12.4	12.4	11.8	12.5	20.9	12.5	12.4	10.5	12.4	12.4	10.5
	LS	11.7	11.7	11.7	11.7	8.8	11.8	26.8	11.9	11.7	10.3	11.8	11.7	7.8
	PLS	11.4	11.4	11.4	11.4	9.7	11.5	26.3	11.5	11.4	9.1	11.3	11.4	8.4
Load 10	Exact	10.1	10.1	10.1	10.1	8.8	10.1	8.1	10.1	10.2	22.4	10	10	7.5
	LS	6.5	6.5	6.5	6.5	2.3	6.5	9.3	5.2	6.6	21.4	6.2	6.5	3.2
	PLS	7.5	7.5	7.5	7.5	5.8	7.5	6	7.7	7.6	23	7.4	7.5	4.4
Load 13	Exact	40.5	40.5	40.5	40.4	38.4	40.4	35.7	40.4	40.4	34.2	40.6	40.6	46.8
	LS	34.9	34.9	34.9	34.8	30.7	34.9	31.8	37.1	34.8	28	35.1	35	46.6
	PLS	38	38	38	38	33.3	38	30.8	38	38	30.2	38.1	38.2	50.5

To finalize this scenario, we compare the total estimation error of the proposed methods by using the MSE and AE indices methods. As Figure 6-26 reveals, the PLS method is clearly more accurate and has less estimation error.

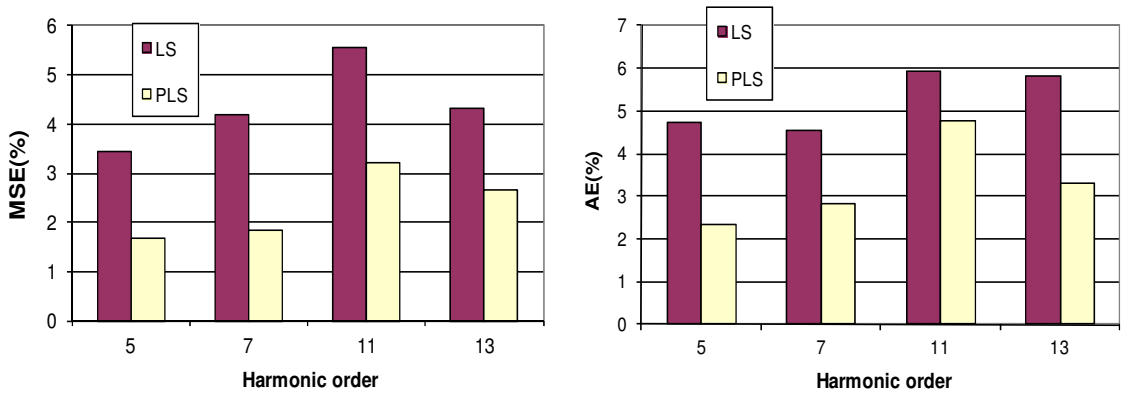

(a) (b)

Figure 6-26: The total estimation error indices of methods in Scenario C
(a) MSE index (b) AE index

6.2 Case study #2: IEEE 118 Bus System

The IEEE 118 Bus test case is studied in this case study. In our study, nine harmonic loads inject a harmonic current into the system. Harmonic loads are attached to buses *7*, *17*, *23*, *28*, *47*, *67*, *84*, *94* and *115*. The goal of this case study is to characterize the PLS method. The harmonic spectra of the harmonic loads are presented in Table 6-14. The magnitudes are scaled based on the fundamental component of load current, and the phase angles are adjusted based on the phase angle of the voltage across the load obtained from the fundamental frequency solution. The 5th order harmonic of the voltages and currents is studied. In the study, the harmonic impacts of the loads are estimated by using the PLS method. These estimated impacts are compared with their exact theoretical counterparts.

Table 6-14: Spectrum table of Harmonic Loads

Harmonic Order	Magnitude (percent)	Relative Angle (degree)
1	100	0.00
5	18.24	-55.68

The profile of the harmonic voltage of the system is presented in Figure 6-27. The 5th order harmonic voltage varies from 0.0059 pu to 0.0184 pu. The profile of the fundamental current drawn by the loads is presented in Figure 6-28.

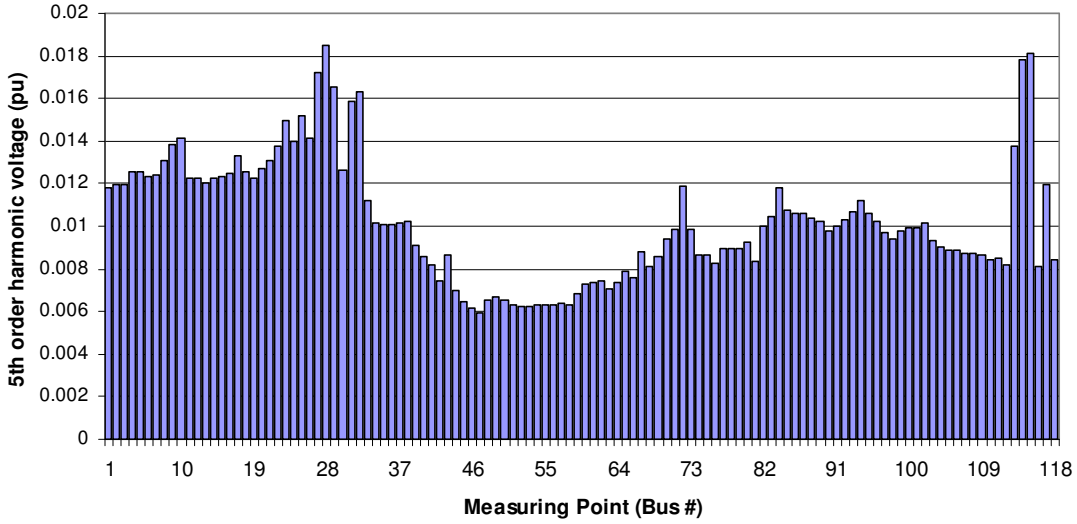

Figure 6-27: 5th order harmonic voltage (pu) in buses in the system

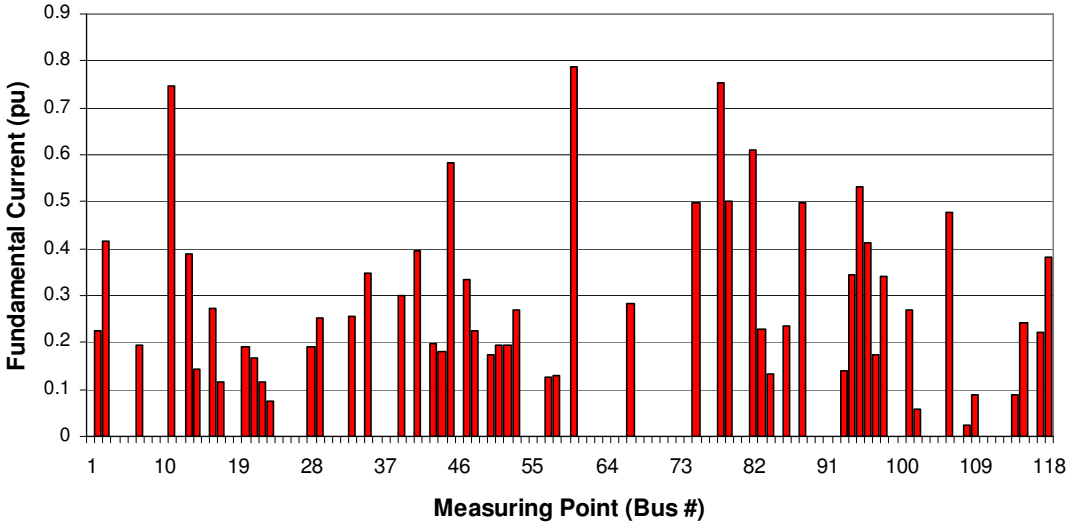

Figure 6-28: Fundamental current drawn by PQ loads attached to the buses in the system

The profiles of the harmonic impacts of the loads on the buses in the systems for the 5th order harmonic are shown in Figure 6-29 to Figure 6-37 .

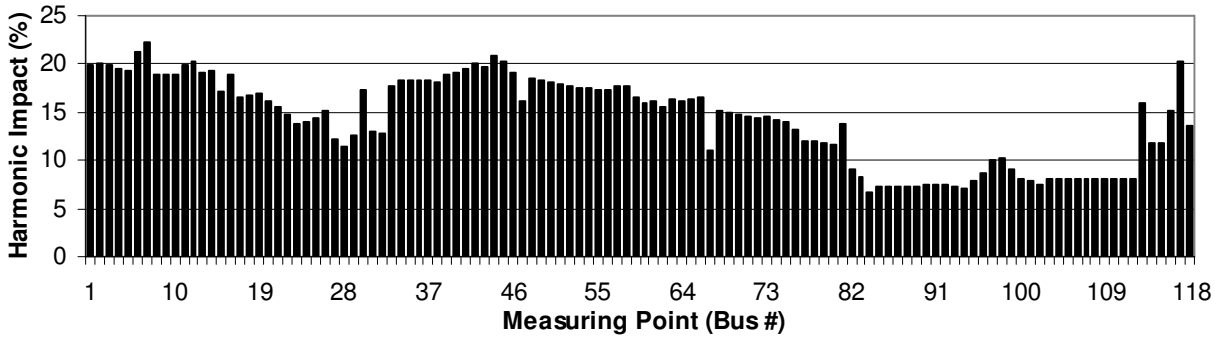

Figure 6-29: Harmonic impact of load 7 on buses in the system for the 5th order harmonic

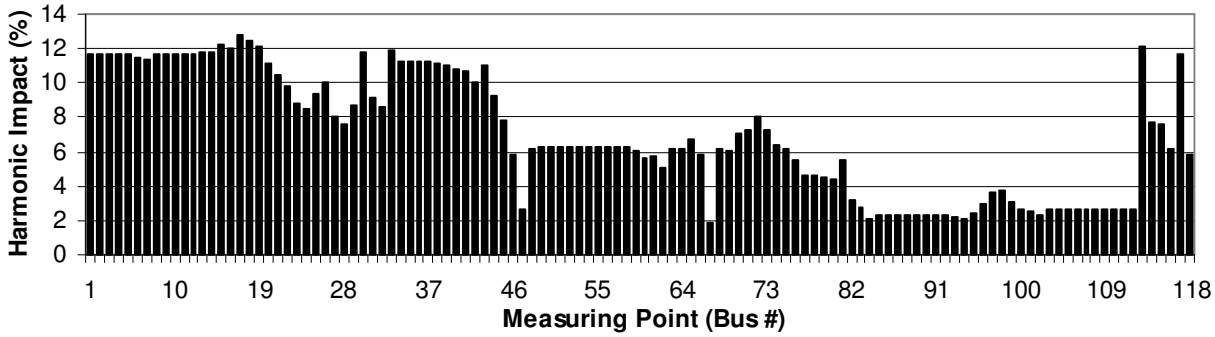

Figure 6-30: Harmonic impact of load 17 on buses in the system for the 5th order harmonic

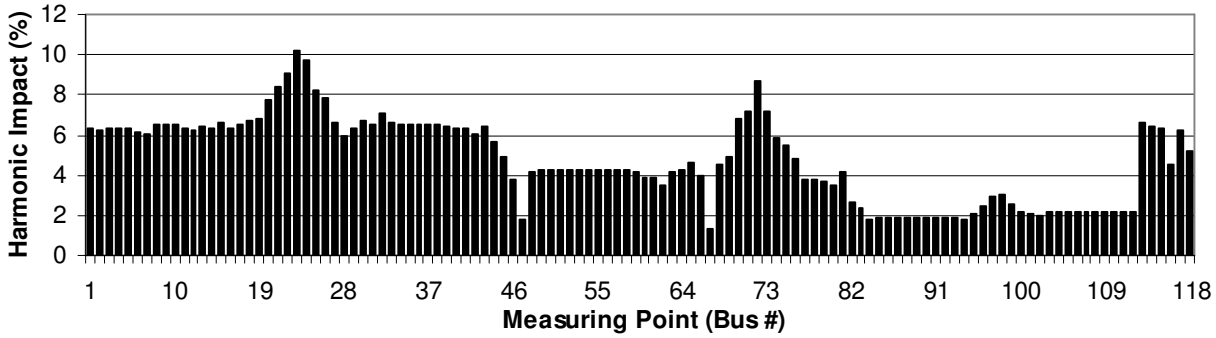

Figure 6-31: Harmonic impact of load 23 on buses in the system for the 5th order harmonic

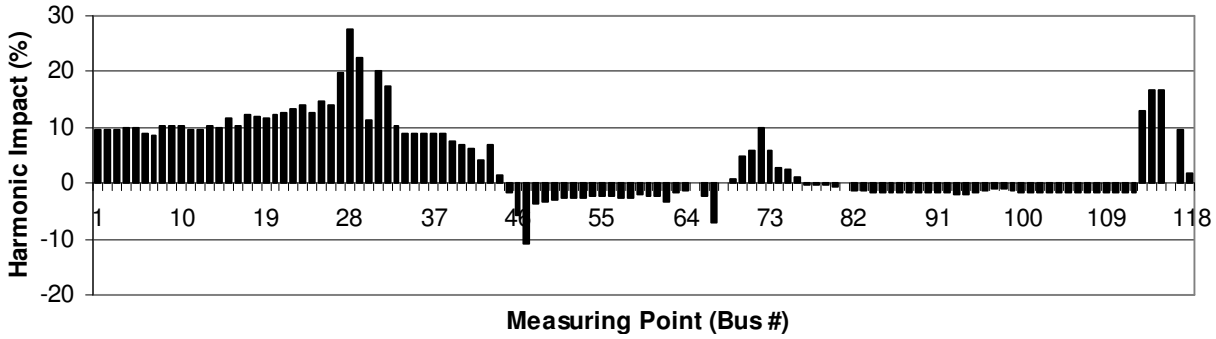

Figure 6-32: Harmonic impact of load 28 on buses in the system for the 5th order harmonic

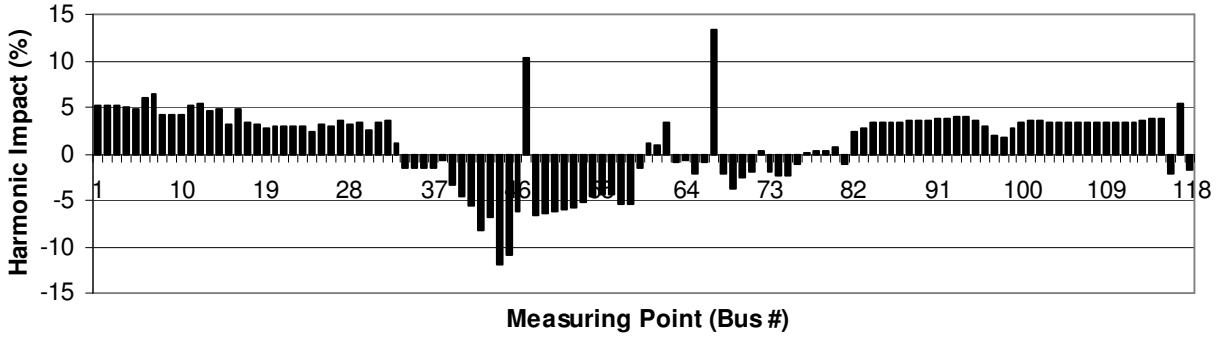

Figure 6-33: Harmonic impact of load 47 on buses in the system for the 5th order harmonic

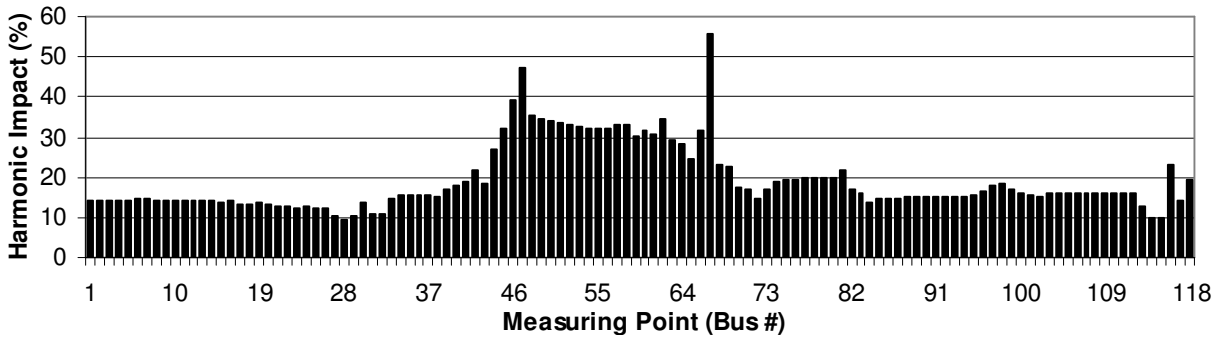

Figure 6-34: Harmonic impact of load 67 on buses in the system for the 5th order harmonic

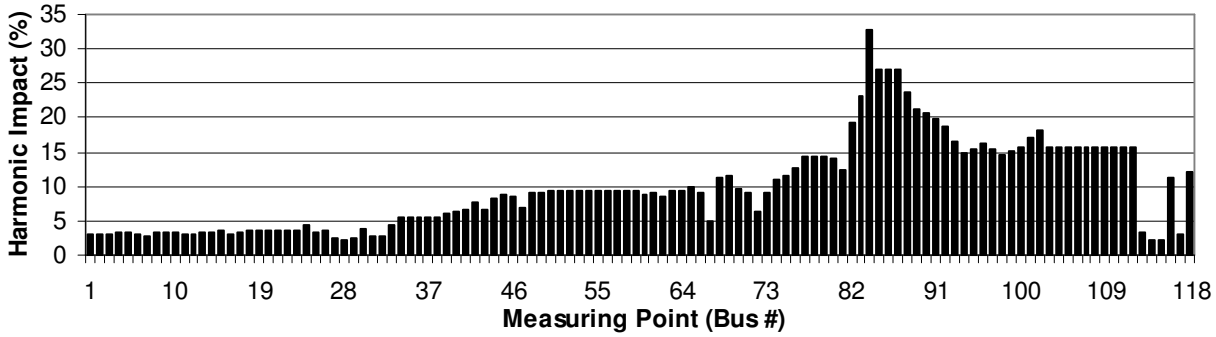

Figure 6-35: Harmonic impact of load 84 on buses in the system for the 5th order harmonic

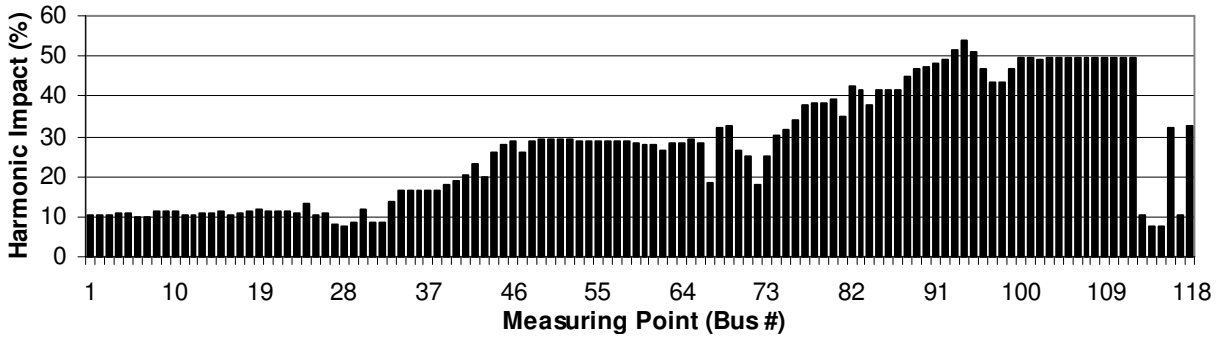

Figure 6-36: Harmonic impact of load 94 on buses in the system for the 5th order harmonic

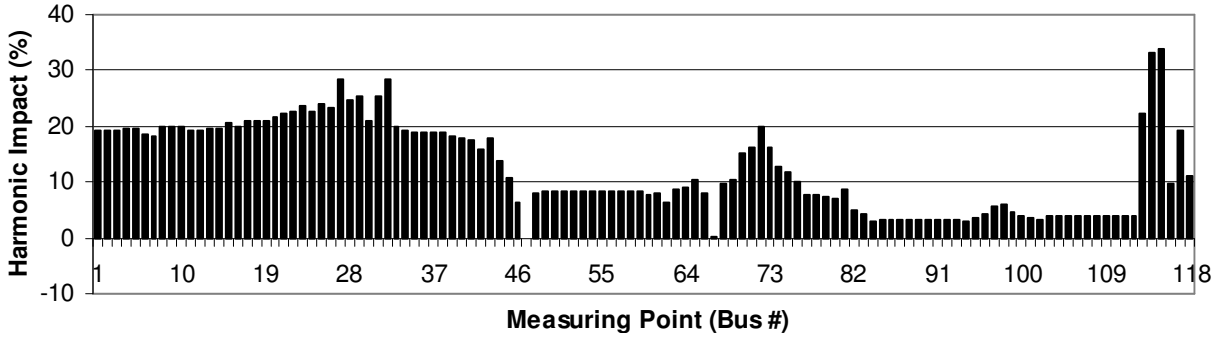

Figure 6-37: Harmonic impact of load 115 on buses in the system for the 5th order harmonic

The harmonic impacts of the loads on some selected buses are estimated by the PLS method, and the results are compared with their exact harmonic contribution. The results are presented in Table 6-15. The results show that the method is promising and is able to estimate the harmonic impact of loads, even when these loads are distributed and no harmonic load is dominant.

Table 6-15: Exact and estimated harmonic impacts of the loads on the selected buses

Loads	Bus	7	17	23	28	47	67	84	94	115
2	Exact	20.07	11.66	6.26	9.56	5.30	14.39	3.08	10.42	19.26
	PLS	19.54	14.31	3.72	3.10	8.52	17.13	1.17	11.02	21.49
7	Exact	22.16	11.34	6.01	8.50	6.38	14.68	2.80	9.78	18.35
	PLS	21.65	14.48	3.07	0.49	9.91	17.50	0.29	10.91	21.69
12	Exact	20.20	11.66	6.24	9.51	5.36	14.39	3.06	10.36	19.21
	PLS	19.68	14.33	3.68	2.99	8.59	17.13	1.12	10.99	21.50
17	Exact	16.55	12.78	6.53	12.20	3.47	13.20	3.35	10.82	21.11
	PLS	16.46	14.33	4.82	8.89	6.15	15.48	2.56	10.25	21.07
23	Exact	13.82	8.77	10.19	13.90	2.98	12.06	3.55	10.97	23.76
	PLS	14.25	9.77	9.35	11.75	5.00	14.12	2.90	9.74	23.12
28	Exact	11.36	7.63	5.95	27.75	3.24	9.55	2.31	7.53	24.67
	PLS	11.47	8.43	5.23	26.76	4.51	10.90	1.73	6.62	24.35
32	Exact	12.79	8.57	7.05	17.46	3.50	10.80	2.70	8.72	28.40
	PLS	13.08	9.59	6.30	15.71	4.93	12.41	2.03	7.73	28.23
39	Exact	18.84	11.00	6.43	7.67	-3.37	17.07	5.97	18.04	18.35
	PLS	19.34	12.10	4.26	4.19	0.21	22.05	5.92	16.68	15.23
47	Exact	16.20	2.60	1.82	-10.96	10.34	47.48	6.90	25.78	-0.16
	PLS	17.25	0.14	0.60	-14.02	27.26	59.94	5.26	16.75	-13.19
55	Exact	17.38	6.24	4.21	-2.41	-4.33	32.15	9.32	28.91	8.54
	PLS	18.40	6.14	1.83	-3.90	2.42	40.82	10.25	23.47	0.58
67	Exact	11.04	1.92	1.30	-7.07	13.47	55.82	4.97	18.33	0.22
	PLS	12.43	2.73	-0.81	-4.51	16.30	60.77	7.39	10.81	-5.11
74	Exact	14.21	6.36	5.84	2.96	-2.38	18.94	11.14	30.29	12.64
	PLS	14.83	6.30	4.16	0.73	1.34	24.50	11.80	29.07	7.26
84	Exact	6.79	2.11	1.79	-1.55	3.35	13.84	32.89	37.72	3.06
	PLS	7.01	1.46	0.77	-3.08	5.76	17.15	34.19	37.93	-1.20
94	Exact	7.15	2.15	1.82	-1.86	4.03	15.00	14.86	53.86	3.00
	PLS	7.13	1.19	1.11	-3.05	6.56	18.55	15.28	55.03	-1.81
103	Exact	8.11	2.62	2.17	-1.62	3.40	16.06	15.59	49.81	3.85
	PLS	8.20	1.75	1.31	-2.93	6.18	20.02	16.12	50.54	-1.19
115	Exact	11.74	7.60	6.30	16.68	3.87	10.02	2.27	7.54	33.97
	PLS	12.18	8.59	5.86	15.21	4.76	11.37	1.60	6.54	33.89

To characterize the PLS method sensitivity analysis are performed. In the first analysis, the impact of window size on the PLS method is studied. The impact of background harmonic studied in the second analysis.

6.2.1 Impact of window size

The impact of the window size on the PLS method is studied in this section. For the case study #3 (IEEE 118 bus), the harmonic impact of loads are estimated when window size are varied. For example, Table 6-16 shows the estimated harmonic impact of loads on the bus 7 for different window size. As the results shows, increasing the window size increases the accuracy of the method.

Table 6-16: The impact of window size on PLS method in estimation for bus 7

Window Size (samples)	Load 7	Load 17	Load 23	Load 28	Load 47	Load 67	Load 84	Load 94	Load 115
Exact	22.16	11.34	6.01	8.50	6.38	14.68	2.80	9.78	18.35
100	37.12	0.71	19.78	-2.85	8.44	11.15	-0.30	-6.75	32.70
200	31.00	-0.112	-2.86	8.65	5.32	18.65	3.27	20.06	16.02
300	35.79	6.78	-3.472	-6.23	8.67	23.21	-4.14	21.58	17.81
400	26.80	7.69	7.39	16.297	2.00	35.13	1.02	-10.16	13.85
500	37.05	20.14	6.20	-4.48	5.8844	22.95	0.61	8.78	2.86
600	16.07	5.79	7.15	7.51	12.45	16.323	10.25	10.50	13.97
700	25.73	9.20	12.10	5.87	12.02	13.65	7.3168	1.69	12.42
800	35.79	7.74	-4.17	15.37	5.42	19.35	-7.98	12.788	15.69
900	22.71	-0.78	1.72	-0.73	17.31	16.16	14.69	13.51	15.41
1000	39.91	16.29	4.43	0.23	8.50	15.26	-9.38	4.88	19.87
1250	17.97	10.14	5.2476	6.95	9.68	20.23	3.14	10.41	16.23
1500	26.38	12.85	3.38	12.13	4.26	15.76	4.54	3.94	16.75
2000	21.26	13.53	6.29	5.89	9.91	16.26	4.87	8.84	13.14
3000	24.99	13.95	3.73	3.10	7.09	19.16	3.24	9.78	14.96
5000	26.41	12.91	4.24	3.71	8.45	16.89	4.21	7.79	15.39

The MSE and AE errors in estimating the harmonic impacts of the loads on the studied buses are shown in Figure 6-38 and Figure 6-39. As the results shows, increasing the size of the window decreases the error. A window size greater than 600 samples nearly guarantees the minimum possible error.

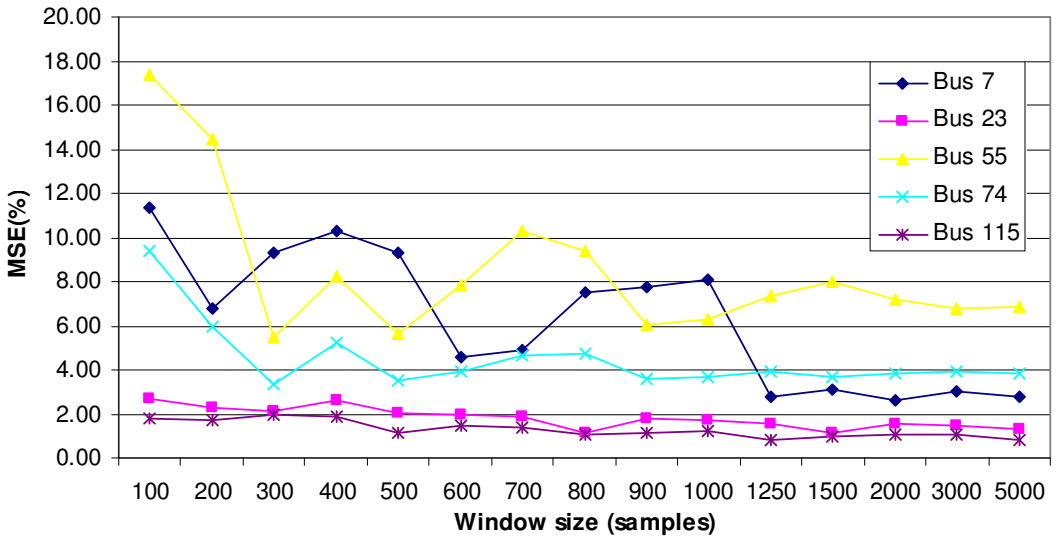

Figure 6-38: The MSE error versus window size

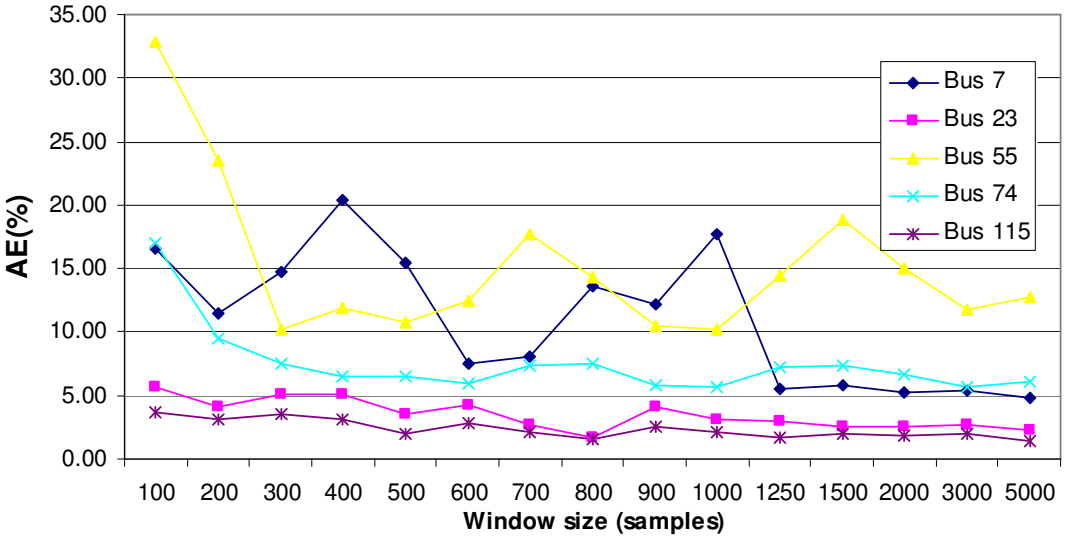

Figure 6-39: The AE error versus window size

6.2.2 Impact of Background harmonic

The impact of the background harmonic is studied in this section. In this study, the harmonic impacts of the loads for two buses (buses 23 and 67) are estimated when the

data for one of the suspicious loads are unavailable. For example, Table 6-17 shows the results for bus 67. The first row of the table presents the exact harmonic impact of each load. The second row presents the estimated harmonic impacts when no background harmonic is present. The third row presents the results when load 7 is considered as a background harmonic. As the results show, the background harmonic reduces the accuracy of the PLS method, but the results are still promising. A similar study was performed for bus 23, and the results are presented in Table 6-18.

Table 6-17: Impact of background harmonic on the PLS estimation in bus 67

	Load 7	**Load 17**	**Load 23**	**Load 28**	**Load 47**	**Load 67**	**Load 84**	**Load 94**	**Load 115**
Exact	11.04	1.92	1.30	-7.07	13.47	55.82	4.97	18.33	0.22
No-Background	12.43	2.73	-0.81	-4.51	16.30	60.77	7.39	10.81	-5.11
Load 7 missing	-	3.04	-1.32	-3.70	16.86	61.76	8.43	10.61	-4.43
Load 17 missing	12.64	-	-.080	-4.57	16.52	61.61	7.42	10.96	-5.07
Load 23 missing	13.90	9.83	-	11.79	4.93	13.88	3.00	9.53	23.08
Load 28 missing	15.10	9.78	9.39	-	5.39	14.19	2.65	9.94	23.04
Load 47 missing	14.42	9.83	9.33	11.94	-	13.95	2.76	9.94	22.94
Load 67 missing	14.57	10.28	8.97	11.82	4.45	-	2.33	9.46	22.57
Load 84 missing	14.50	9.74	9.40	11.71	4.92	14.03	-	9.70	23.14
Load 94 missing	14.02	9.88	9.13	11.92	5.36	13.94	2.69	-	23.14
Load 115 missing	15.65	10.56	9.17	11.52	3.95	13.19	2.74	9.71	-

Table 6-18: Impact of background harmonic on the PLS estimation in bus 23

	Load 7	Load 17	Load 23	Load 28	Load 47	Load 67	Load 84	Load 94	Load 115
Exact	13.82	8.77	10.19	13.90	2.98	12.06	3.55	10.97	23.76
No-Background	14.25	9.77	9.35	11.75	5.00	14.12	2.90	9.74	23.12
Load 7 missing	-	10.11	8.79	12.76	5.41	14.44	3.99	9.38	24.00
Load 17 missing	14.50	-	9.40	11.76	5.08	14.49	2.73	9.85	23.49
Load 23 missing	13.90	9.83	-	11.79	4.93	13.88	3.00	9.53	23.08
Load 28 missing	15.10	9.78	9.39	-	5.39	14.19	2.65	9.94	23.04
Load 47 missing	14.42	9.83	9.33	11.94	-	13.95	2.76	9.94	22.94
Load 67 missing	14.57	10.28	8.97	11.82	4.45	-	2.33	9.46	22.57
Load 84 missing	14.50	9.74	9.40	11.71	4.92	14.03	-	9.70	23.14
Load 94 missing	14.02	9.88	9.13	11.92	5.36	13.94	2.69	-	23.14
Load 115 missing	15.65	10.56	9.17	11.52	3.95	13.19	2.74	9.71	-

6.3 Field test results

The network of the field measurement study is shown in Figure 6-40. The harmonic voltages and currents of the buses and their corresponding loads were collected from 5AM to 5PM. The variation of the THD of the voltage is also shown in Figure 6-41. Loads increase in the morning and decrease in the evening. The harmonic impacts of the loads on the buses for the 5^{th} harmonic in the whole day are estimated by applying the PLS method.

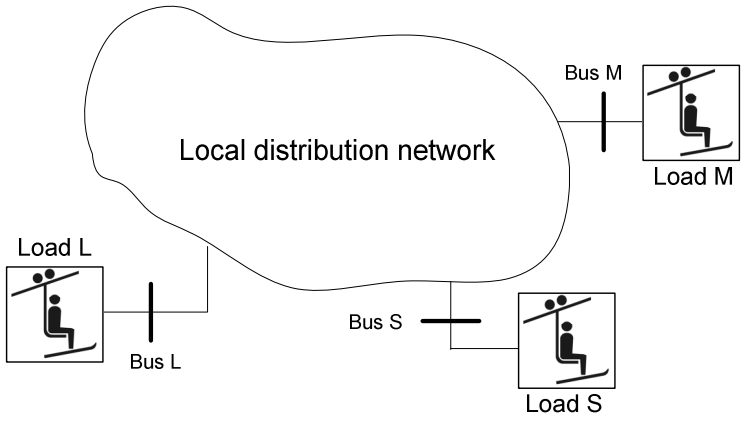

Figure 6-40: Corresponding network of field test

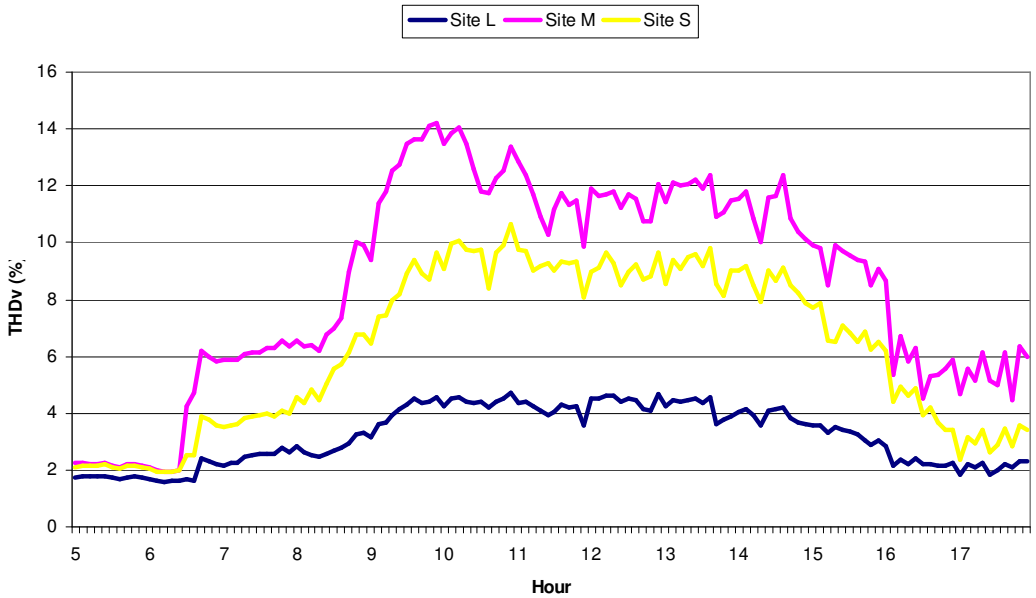

Figure 6-41: Variation of THD of voltage during one day

To better determine the importance of each harmonic, the voltage individual harmonic distortion indices for the buses are presented in Figure 6-42, the 5th harmonic is obviously the most important harmonic.

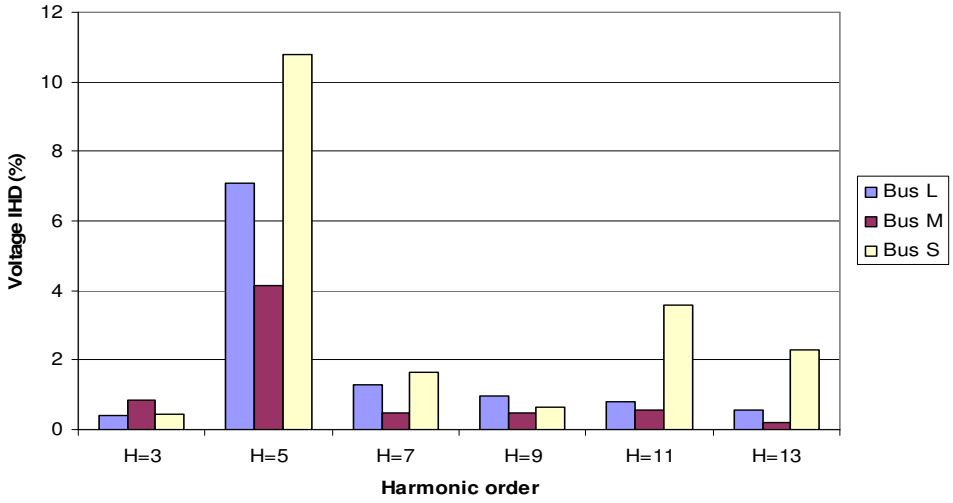

Figure 6-42: The voltage individual harmonic distortion indices for buses

Table 6-19 shows the harmonic impacts of the loads on the buses for the 5th harmonic. For example, the harmonic impact of load M on the harmonic voltage of bus L is 2.1% at 5AM.

Table 6-19: Harmonic impacts of loads on the buses for the 5th harmonic

Hour	Bus L			Bus M			Bus S		
	Load L	Load M	Load S	Load L	Load M	Load S	Load L	Load M	Load S
5	6.5	2.1	6.2	1.6	3.6	3.1	3.7	2.3	21.4
6	33.8	20.2	30.6	30.9	40.1	5.9	15.3	9.3	63.2
7	34.2	13.9	-10.64	36.4	21.6	-11.7	22.9	16.8	8.3
8	2.6	-6.9	57.4	-7.0	11.1	43.7	0.8	2.5	85.0
9	9.13	14.1	26.98	3.7	19.4	38.3	4.6	10.4	63.5
10	14.3	0.3	16.6	6.0	2.5	27.0	9.8	1.2	59.1
11	10.1	0.1	36.3	-8.7	0.7	65.73	5.0	1.3	76.8
12	-2.6	-5.5	39.4	-31.2	-2.0	86.8	-2.5	0.4	84.6
13	2.7	1.0	9.58	-20.6	7.5	44.0	-14.4	5.0	79.1
14	13.8	1.0	32.8	1.8	-0.5	57.6	4.2	2.1	75.5
15	-1.1	8.4	6.4	-20.6	7.5	44.1	-3.0	10.6	64.3
16	13.8	15.9	23.9	-9.1	32.9	20.2	2.1	15.0	62.0
17	56.9	1.0	3.7	60.18	17.8	-11.3	32.8	-1.1	41.5

The impacts of load S on the buses are shown in Figure 6-43. Load S impacts most on the bus directly connected to it (bus S). The impacts of the other loads on the buses are shown in Figure 6-44 and Figure 6-45.

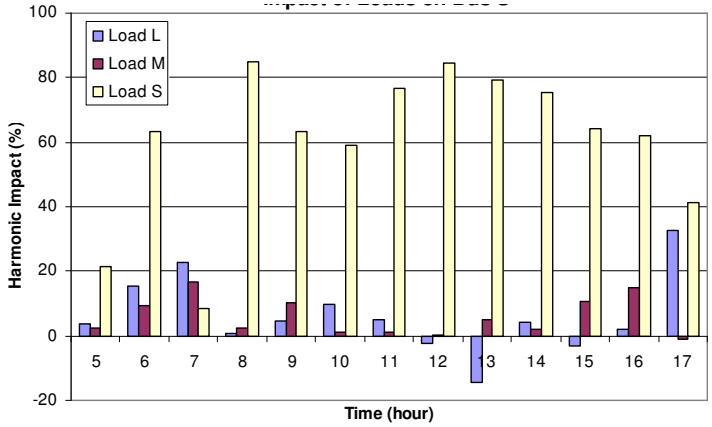

Figure 6-43: Harmonic impacts of load S on the buses

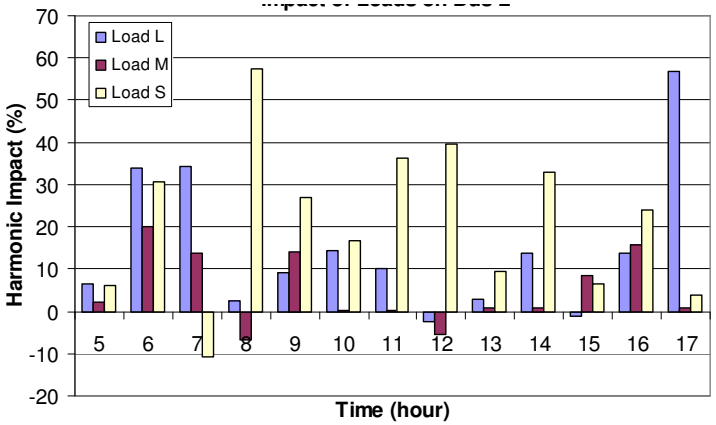

Figure 6-44: Harmonic impacts of load L on the buses

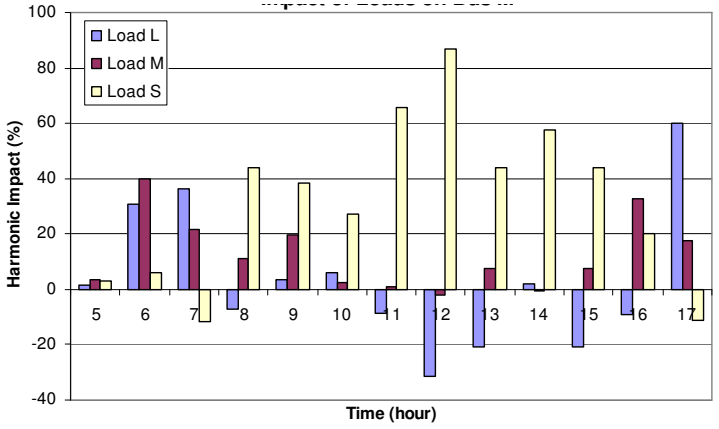

Figure 6-45: Harmonic impacts of load M on the buses

The average harmonic impacts of the loads on the buses during the day are presented in Figure 6-46. The results are consistent and agree with the results achieved with the Statistical Correlation method [28].

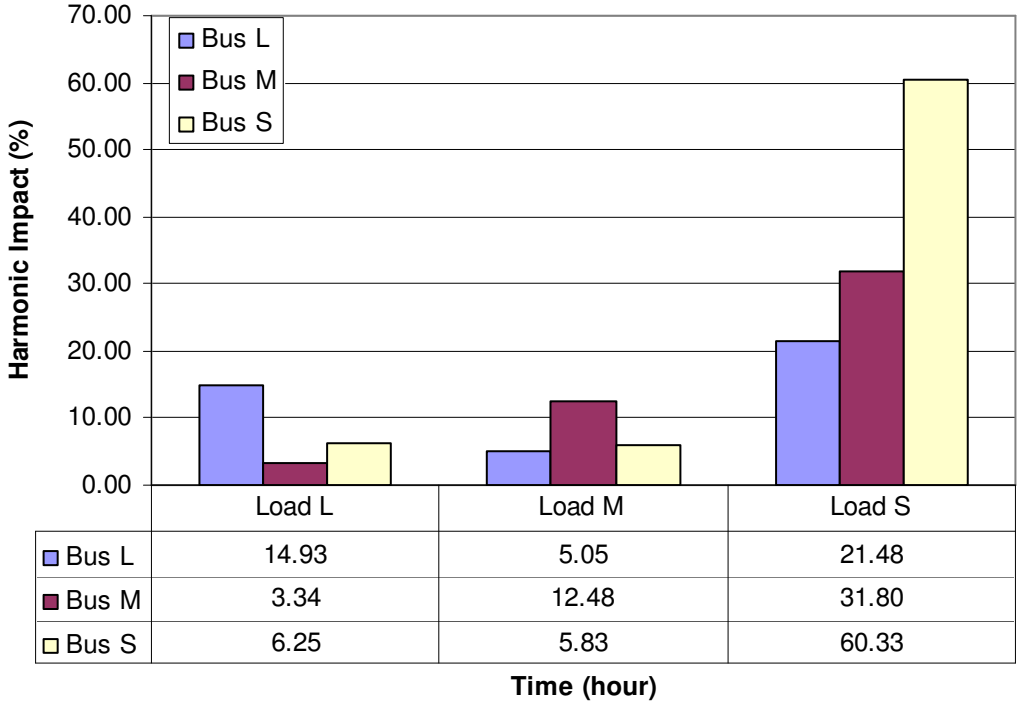

	Load L	Load M	Load S
Bus L	14.93	5.05	21.48
Bus M	3.34	12.48	31.80
Bus S	6.25	5.83	60.33

Figure 6-46: Average harmonic impacts of loads on the buses for the 5th harmonic

The similar studies are performed for the other harmonics. The results are presented below. Table 6-20 shows the harmonic impacts of the loads on the buses for the 7th harmonic. The average harmonic impacts of the loads on the buses for the 7th harmonic during the day are presented in Figure 6-47.

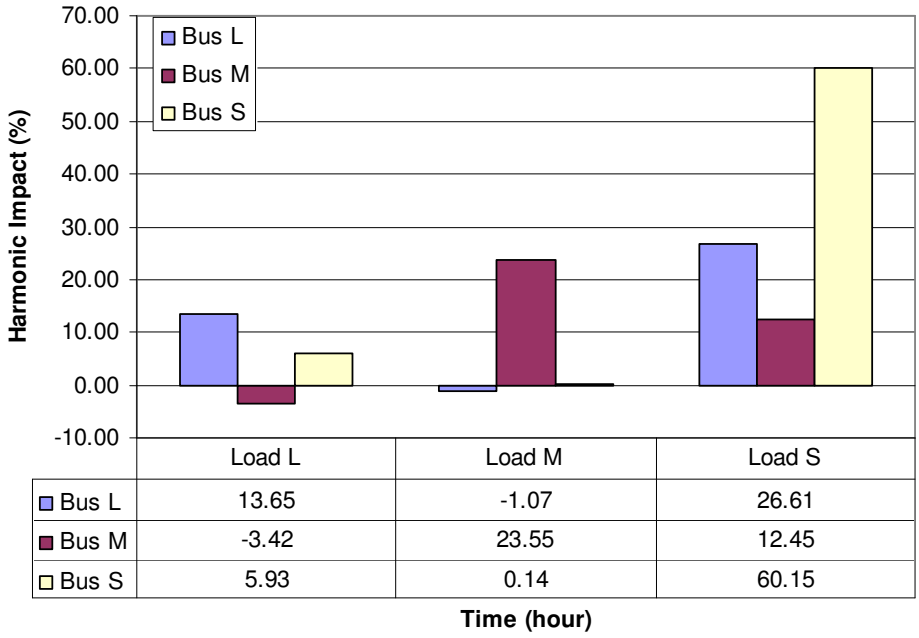

Figure 6-47: Average harmonic impacts of the loads on the buses for the 7th harmonic

Table 6-20: Harmonic impacts of loads on the buses for the 7th harmonic

Hour	Bus L			Bus M			Bus S		
	Load L	Load M	Load S	Load L	Load M	Load S	Load L	Load M	Load S
5	1.4637	1.1512	0.001102	3.0547	-2.3421	0.27457	4.4248	3.3616	-6.4128
6	6.3979	-12.576	79.46	15.25	-33.909	69.626	7.2971	-18.448	88.68
7	1.0664	1.2373	-0.68449	-1.4006	0.40614	12.088	-0.96791	0.8001	41.131
8	0.47094	3.6508	9.5918	5.622	5.0217	-2.8986	-3.6799	4.6805	61.564
9	41.178	1.3044	14.428	17.664	17.651	15.007	19.691	17.812	36.163
10	41.415	-6.8211	29.204	17.152	1.6191	24.13	24.906	-5.3211	57.517
11	10.107	0.75397	25.695	-6.4933	8.5416	48.279	4.8583	0.47838	70.415
12	16.078	-1.2073	27.12	0.79043	7.0662	20.155	6.7628	1.9556	63.691
13	35.183	0.75192	21.187	8.1671	5.9109	10.751	15.148	0.43896	49.47
14	18.178	3.2098	40.358	7.2141	6.5325	38.983	2.2336	-2.0728	74.244
15	11.276	0.19246	15.531	6.2948	0.18305	12.138	-1.7429	-3.0471	70.905
16	-14.936	-3.82	65.141	7.891	63.99	-50.241	-2.6005	-2.5123	93.374
17	9.5143	-1.7193	18.953	-125.71	225.49	-36.413	0.7156	3.6399	81.237

The average harmonic impacts for the other harmonic are shown in the following figures.

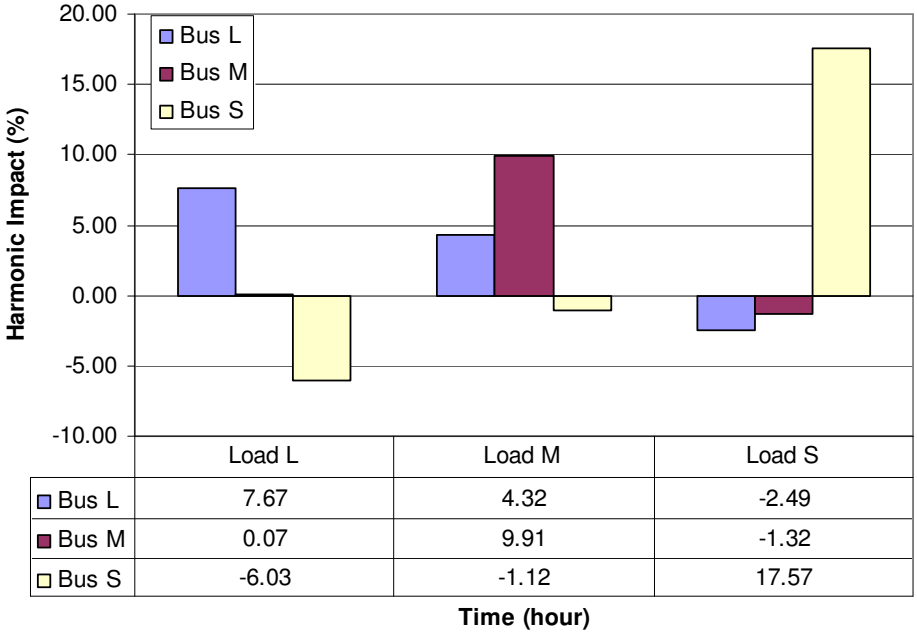

	Load L	Load M	Load S
Bus L	7.67	4.32	-2.49
Bus M	0.07	9.91	-1.32
Bus S	-6.03	-1.12	17.57

Figure 6-48: Average harmonic impacts of the loads on the buses for the 3rd harmonic

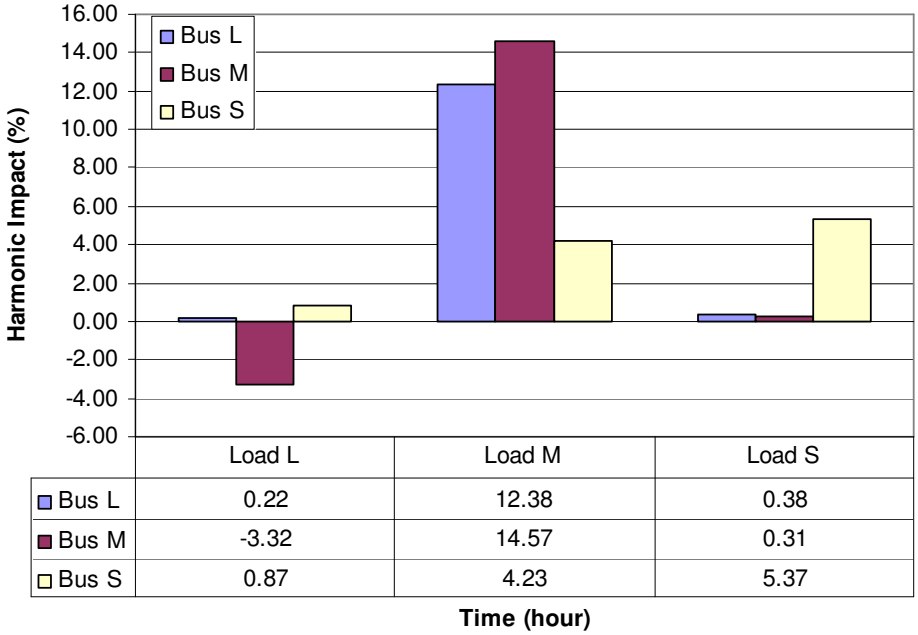

	Load L	Load M	Load S
Bus L	0.22	12.38	0.38
Bus M	-3.32	14.57	0.31
Bus S	0.87	4.23	5.37

Figure 6-49: Average harmonic impacts of the loads on the buses for the 9th harmonic

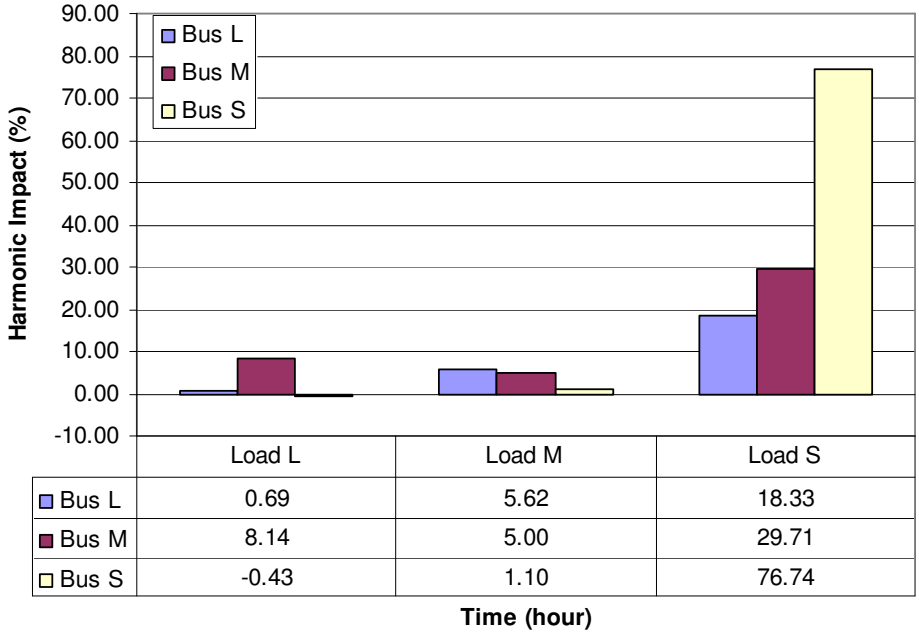

	Load L	Load M	Load S
Bus L	0.69	5.62	18.33
Bus M	8.14	5.00	29.71
Bus S	-0.43	1.10	76.74

Figure 6-50: Average harmonic impacts of the loads on the buses for the 11th harmonic

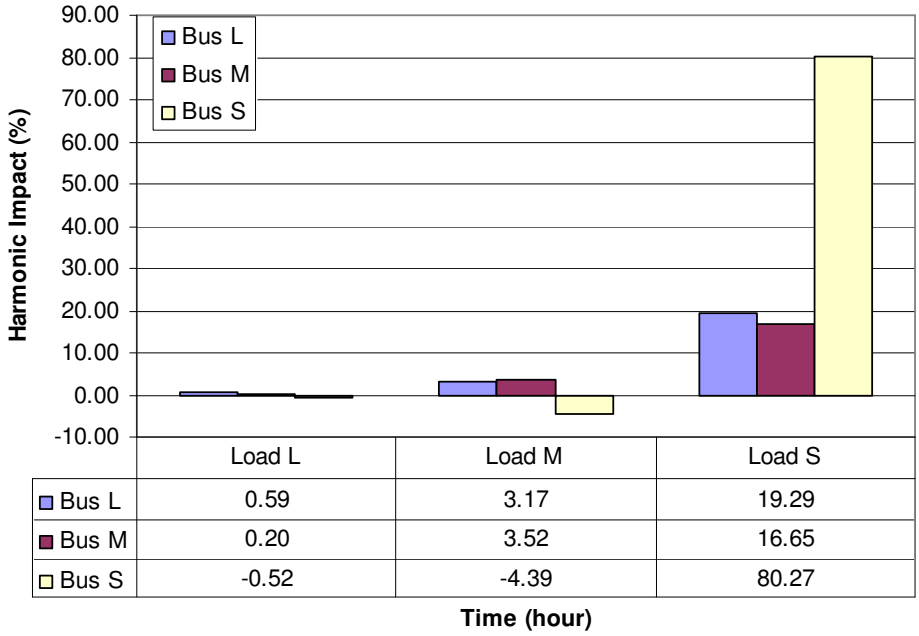

	Load L	Load M	Load S
Bus L	0.59	3.17	19.29
Bus M	0.20	3.52	16.65
Bus S	-0.52	-4.39	80.27

Figure 6-51: Average harmonic impacts of the loads on the buses for the 13th harmonic

As the results show, load S is the main harmonic contributor for the 5th, 7th, 11th and 13th harmonics. However, load M seems to have more impacts for the 3rd and 9th harmonic orders.

Chapter 7

Conclusions and Future Work

This chapter summarizes the main findings of the thesis and provides suggestions for future work.

7.1 Thesis conclusions and contributions

This thesis has approached topics related to the harmonic source identification problem. Data-based methods were proposed for the identification of the harmonic sources in the power systems. The main conclusions and contributions of this thesis are summarized as follows:

- A new harmonic-source-identification problem was introduced in this thesis. The single-point harmonic source identification problem is a classic scheme for harmonic source detection study. While this approach is still very important and worthwhile, another type of harmonic-source-identification problem was introduced primarily because an increasing number of loads in the power systems now contain harmonic sources. In this multi-point problem, the goal is to quantify the harmonic impacts of the suspicious loads in the network on a reported harmonic problem. It must be determined if these loads are causing the problem and, if so, which load is producing the most significant impact.

- The existing methods for the single-point harmonic identification problem were reviewed. Two classes of methods were identified: model-based and data-based methods. The model-based methods' use the utility and customer impedances and it

makes them impractical in most real applications. In contrast, data-based methods are very practical because they use regular measurement data and do not need any information about the system. However, it was found that the existing data-based methods do not have strong theoretical support.

- A new quantification index was proposed to quantify the harmonic impact of the loads. The well-known harmonic-contribution index was studied in detail and it was shown that this index did not reflect the impact of the linear loads on the harmonic problem. The harmonic-impact index which can reflect the impact of both the harmonic and linear loads was introduced. The important contribution of this part of the thesis to the research area is the new proposed index, which can be used for both the multi-point and single-point problems.

- A new data-based method with strong theoretical support was proposed for the single-point problem. The contributions of the research to the field are the new proposed method; the consideration of practical issues; and the verifications through computer simulations and several field tests. The algorithm proposed for this purpose does not depend on the load model and works with the natural fluctuations of the load current to estimate the harmonic impact of the load. The method was applied to two sets of the field measurement data: the distribution transformer and the house-panel measurement data. For transformer measurement, the estimated results were compared with the theoretical results calculated by using the transformer impedance. The utility impedance behind the transformer was ignored. For the 3^{rd} and 5^{th} harmonics, the results were in very good agreement. For the house-panel measurements data, the method was verified by comparing the estimated results with the theoretical results calculated by using the house impedance which was previously obtained by using the capacitor switching technique.

- Two data-based methods were proposed for the multi-point harmonic source identification problem. These proposed methods are one of the main contributions of the thesis to the research area. The first method is the Least Square method, which

searches the measurements data to find the appropriate time intervals for applying the least-square estimation method. The basic idea adopted in this method is to find the time intervals in which only one of the harmonic loads varies and the other harmonic loads are roughly unchanged. This time interval is used by the method to estimate the harmonic impact of the varying load. Three data-mining algorithms were proposed to search the measurement data for finding the appropriate time intervals. The sensitivity study showed that the application of the LS method is confined to the local power networks with few harmonic sources. The PLS method was proposed for the large-scale power systems. In order to estimate the harmonic impact of the loads on a observation point, the method decomposes the measured harmonic currents of the loads into the independent imaginary variables and construct a linear relationship between these imaginary variables and the harmonic voltage of the observation point. Both methods were verified and characterized by using the computer simulations and field measurement.

- A harmonic identification software package was developed based on the proposed methods in the thesis. The input for this software is the measurement data recorded at the suspicious loads and observation points. Using this data, the program estimates the harmonic impacts of the loads.

7.2 Suggestions for future work

As with any study, something can always be done to extend the research. Several extensions and modifications of this thesis can be explored as follows:

- The incremental index proposed in Chapter 3 for quantification of the load`s harmonic impact can be extended for quantification of the load`s unbalance impact. The unbalance impact index can be used to separate contributions of the customer and utility system on the voltage unbalance. The similar data-based method proposed in this thesis can be developed to estimate the load unbalance impact for the single-point and multi-point problems.

- Current power quality monitoring systems are unable to collect synchronized data. For harmonic measurements, the synchronization requirement is higher than that of PMU. However, with the rapid advancement of telecommunication technology, GPS sampled data will be available in the future. As a result, determining the phase differences among the data will be possible and will open up new ways to utilize the data and likely lead to more accurate harmonic-impact-estimation results.

- More and more utilities are deploying PQ monitoring systems. The current systems can report only what is observed in a power system, but not what is causing harmonic distortions or if two observations are related. The proposed technique pushes PQ monitoring to a higher level that involves identifying patterns and useful information from the observed data. Advanced applications that extract useful information from data will make the PQ monitoring system truly useful to utility companies. For example, the proposed techniques can be added as a subroutine into the existing PQ monitoring system. The data server can use these techniques to scan for the major harmonic polluters in the system.

Chapter 8

References

[1] M. F. McGranaghan, R. C. Dugan, and H. W. Beaty, "Electrical Power Systems Quality," *New York: McGraw-Hill*, 1996.

[2] E. Thunberg, L. Soder, "A Norton approach to distribution network modeling for harmonic studies," *IEEE Trans. on Power Delivery*, vol.14, no.1, pp.272-277, Jan 1999.

[3] "IEEE recommended practices and requirements for harmonic control in electrical power systems," *IEEE Std. 519-1992*, 12 Apr 1993.

[4] "Electromagnetic Compatibility (EMC) Part 3: Limits- Section 6: Assessment of Emission Limits for Distorting Loads in MV and HV Power Systems," *IEC 1000-3-6*, 1996.

[5] A. E. Emanuel, J. A. Orr, D. Cyganski, and E. M. Gulachenski, "A Survey of Harmonic Voltages and Currents at the Customer's Bus," *IEEE Trans. on Power Delivery*, vol. 8, no. 1, pp. 411-421, Jan 1993.

[6] G.T. Heydt, "Identification of harmonic sources by a state estimation technique," *IEEE Trans. on Power Delivery*, vol. 4, no. 1, pp. 569-576, Jan 1989.

[7] A. Teshome, "Harmonic source and type identification in a radial distribution system," *IEEE Industry Applications Society Annual Meeting 1991,* pp. 1605-1609, vol. 2, 28 Sep-4 Oct 1991.

[8] P. H. Swart, M. J. Case, and J. D. Van Wyk, "On techniques for localization of sources producing distortion in three-phase network," *Eur. Trans. Elect. Power Eng.*, vol. 6, no. 6, Nov-Dec 1996.

[9] L. Cristaldi, A. Ferrero, "Harmonic power flow analysis for the measurement of the electric power quality," *IEEE Trans. on Instrumentation and Measurement*, vol. 44, no. 3, pp. 683-685, Jun 1995.

[10] L. Cristaldi, A. Ferrero, "A digital method for the identification of the source of distortion in electric power systems," *IEEE Trans. on Instrumentation and Measurement*, vol. 44, no. 1, pp. 14-18, Feb 1995.

[11] W. Xu, X. Liu, and Y. Liu, "An investigation on the validity of power-direction method for harmonic source determination," *IEEE Trans. on Power Delivery*, vol. 18, no. 1, pp. 214-219, Jan 2003.

[12] P.V. Barbaro, A. Cataliotti, V. Cosentino, and S. Nuccio, "A Novel Approach Based on Nonactive Power for the Identification of Disturbing Loads in Power Systems," *IEEE Trans. on Power Delivery*, vol. 22, no. 3, pp. 1782-1789, July 2007.

[13] A. Cataliotti, V. Cosentino, and S. Nuccio, "Comparison of Nonactive Powers for the Detection of Dominant Harmonic Sources in Power Systems," *IEEE Trans. on Instrumentation and Measurement*, vol. 57, no. 8, pp. 1554-1561, Aug. 2008.

[14] P.V. Barbaro, A. Cataliotti, V. Cosentino, and S. Nuccio, "Detection of Disturbing Loads in Distorted and/or Unbalanced Power Systems: a Technique Based on a Comparison among Nonactive Powers," *Instrumentation and Measurement Technology Conference Proceedings 2007*, pp. 1-6, May 2007.

[15] A. Cataliotti, V. Cosentino, "Harmonic sources detection in power systems via nonactive power measurements according to IEEE Std. 1459–2010: Theoretical approach and experimental results," *IEEE International Workshop on Applied Measurements for Power Systems (AMPS) 2010*, pp. 53-58, Sept. 2010.

[16] W. Shepherd, P. Zakikhani, and D. Sharon, "Reactive-power definitions and power-factor improvement in nonlinear systems," *Proceedings of the Institution of Electrical Engineers*, vol. 121, no. 5, pp. 390-392, May 1974.

[17] K. Srinivasan, "On separating customer and supply side harmonic contributions," *IEEE Trans. on Power Delivery*, vol. 11, no. 2, pp. 1003-1012, Apr 1996.

[18] W. Xu; Y. Liu, "A method for determining customer and utility harmonic contributions at the point of common coupling," *IEEE Trans. on Power Delivery*, vol. 15, no. 2, pp. 804-811, Apr 2000.

[19] Task Force on Harmonics Modeling and Simulation, "The modeling and simulation of the propagation of harmonics in electric power networks---Part I:

Concepts, models and simulation techniques," *IEEE Trans. on Power Delivery*, vol. 11, no. 1, pp. 452-465, Jan.1996.

[20] Task Force on Harmonics Modeling and Simulation, "Modeling devices with nonlinear Voltage-current Characteristics for harmonic studies," *IEEE Trans. on Power Delivery*, vol.19, no.4, pp. 1802- 1811, Oct. 2004.

[21] CIGRE Working Group 36.05/CIRED 2, "Review of methods for measurement and evaluation of the harmonic emission level from an individual distorting load," *WG CC02*, Jan 1999.

[22] A.M. Dan, Z. Czira, "Identification of harmonic sources," *Proceedings of 8th International Conference on Harmonics and Quality of Power,* vol. 2, pp. 831-836, Oct. 1998.

[23] A. Oliveira, J. Oliveira, J. Resende, and M. Miskulin, "Practical approaches for AC system harmonic impedance measurements," *IEEE Trans. on Power Delivery*, vol. 6, pp. 1721–1726, Oct. 1991.

[24] M. Sumner, B. Palethorpe, and D. W. P. Thomas ,"Impedance Measurement for Improved Power Quality—Part 1: The Measurement Technique," *IEEE Trans. on Power Delivery*, vol. 19, no. 3, pp. 1442-1448, July, 2004.

[25] E.E. Nino, W. Xu, "Measurement of Harmonic Sources in Three-Wire Single-Phase Supply Systems," *IEEE Trans. on Power Delivery*, vol.22, no.4, pp. 2527-2533, Oct. 2007.

[26] A. Robert, T. Deflandre, "Guide for assessing the network harmonic impedances," *Proc. Inst. Elect. Eng.,* vol. 2, pp. 301–310, 1997.

[27] H.E. Mazin, E.E. Nino, W. Xu, and J. Yong, "A Study on the Harmonic Contributions of Residential Loads," *IEEE Trans. on Power Delivery*, vol. 26, no. 3, pp. 1592-1599, July 2011.

[28] W. Xu, R. Bahry, H.E. Mazin, and T. Tayjasanant, "A method to determine the harmonic contributions of multiple loads," *Power & Energy Society General Meeting 2009,* pp.1-6, July 2009.

[29] R. A. Johnson, D. W. Wicher, "Applied Multivariate Statistical Analysis," *Prentice–Hall, Upper Saddle River*, 1998.

[30] E. Keogh, S. Chu, D. Hart, and M. Pazzani, "An online algorithm for segmenting time series," *Proceedings IEEE International Conference on Data Mining*, pp.289-296, 2001.

[31] Task Force on Harmonic Modeling and Simulation, "Test systems for harmonics modeling and simulation," *IEEE Trans. on Power Delivery*, vol. 14, no. 2, pp. 579-587, Apr 1999.

[32] E.E. Nino, W. Xu, "Measurement of Harmonic Sources in Three-Wire Single-Phase Supply Systems," *IEEE Trans. on Power Delivery*, vol. 22, no. 4, pp. 2527-2533, Oct. 2007.

[33] G. T. Heydt, "Identification of harmonic sources by a state estimation technique," *IEEE Trans. on Power Delivery*, vol. 4, no. 1, pp. 569-576, Jan 1989.

[34] Z. P. Du, J. Arrillaga, and N. Watson, "Continuous harmonic state estimation of power systems," *IEE Pro. Generation, Transmission and Distribution,* vol. 143, no. 4, pp. 329-336, Jul 1996.

[35] Z. P. Du, J. Arrillaga, N. Watson and S. Chen, "Identification of harmonic sources of power systems using state estimation," *IEE Pro. Generation, Transmission and Distribution,* vol. 146, no. 1, pp. 7-12, Jan 1999.

[36] C. Madtharad, S. Premrudeepreechacharn, N. Watson, S.U. Ratchai, "An optimal measurement placement method for power system harmonic state estimation," *IEEE Trans. on Power Delivery*, vol. 20, no. 2, pp. 1514- 1521, April 2005.

[37] H. Liao, "Power System Harmonic State Estimation and Observability Analysis via Sparsity Maximization," *IEEE Trans. on Power Systems*, vol. 22, no. 1, pp. 15-23, Feb. 2007.

[38] *IEEE Standard for Synchrophasors for Power Systems*, IEEE Std. C37.118–2005 (Revision of IEEE Std. 1344–1995).

[39] L.N. Trefethen, D. Bau, "Numerical Linear Algebra," *Society for Industrial and Applied Mathematics, Philadelphia*, 1997.

[40] H. Abdi, "Partial Least Square Regression and Projection on Latent Structure Regression (PLS Regression)," *Wiley Interdisciplinary Reviews: Computational Statistics*, vol. 2, pp. 97-16, 2010.

Appendix A:

The Harmonic Identification Software

A harmonic identification software package is developed based on the proposed methods in the thesis. The input for this software is the measurement data recorded at the suspicious loads and observation points. Using this data, the program estimates the harmonic impacts of the suspicious loads on the observation point.

A.1 Accessing the software and requirements

The program has the following requirements:

- Windows Vista™ or Windows XP® SP2
- 512 MB RAM or higher
- Microsoft Excel 2003 or higher

The software is available for downloading from the following website:
http://www.ece.ualberta.ca/~apic/index.php?n=People.HoomanErfanianMazin

To install the software, follow the following instructions:

- Download MCRInstaller.exe
- Run the downloaded file (*MCRInstaller.exe*). This file needs to be installed only once to copy all the required *.dll* files on your PC.
- Download the "harmonic_identifier.zip" file
- Unzip the downloaded file
- From now on, the program will be accessible by clicking on the provided stand-alone exe file (*harmonic_identifier.exe*).

A.2 Brief Tutorial for the Software

In this brief tutorial, it is illustrated how to use the provided software to solve the problem represented in Figure A-1. The program uses field measurement data to estimate the impacts of the suspicious loads on the observation point. Figure A-1 shows the

measurement scheme for the problem in Figure 2-10. Continuous harmonic measurements at sites X, A, B and C are performed. The data recorded include the harmonic currents of the suspicious loads (loads A, B and C) and harmonic voltage for the observation point (bus X). The data are not normalized with respect to the fundamental frequency component. Measurement devices are installed at each site, and the measurements are performed simultaneously. In our measurement, a DAQ pad and a laptop with appropriate probes are utilized as one measurement set. The measurement should have the following specifications:

- Our experience shows that data recording resolutions of one sample per 1 to 5 seconds are acceptable for adequate correlation analysis.
- The sampling period should be at least 6 cycles (IEEE Standard).
- The sampling rate used for our measurement is 256/cycle.
- The measurement sets should be synchronized to capture data simultaneously. Our experience shows that a synchronization level of 1 to 5 seconds is acceptable for our correlation analysis. We found that synchronizing the laptops provides enough synchronization for 24 hours, so the laptops should be synchronized daily.

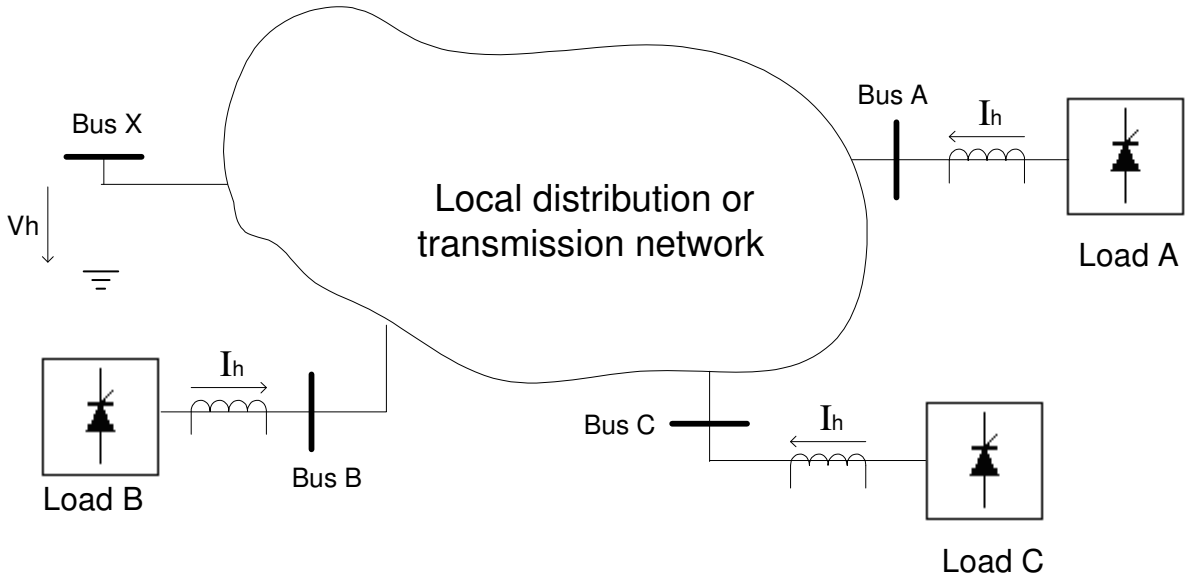

Figure A-1: Proposed measurement system

After recording the measurement data, the data should be entered into the software for analysis. Figure A-2 shows the first screen shot of the program which provides two types of analysis, namely Multi-Point Analysis and Single-Point Analysis.

A.1.1 Multi-Point Analysis

For our case, we click on the Multi-Point Analysis pushbuttons. The Single-Point Analysis is explained later.

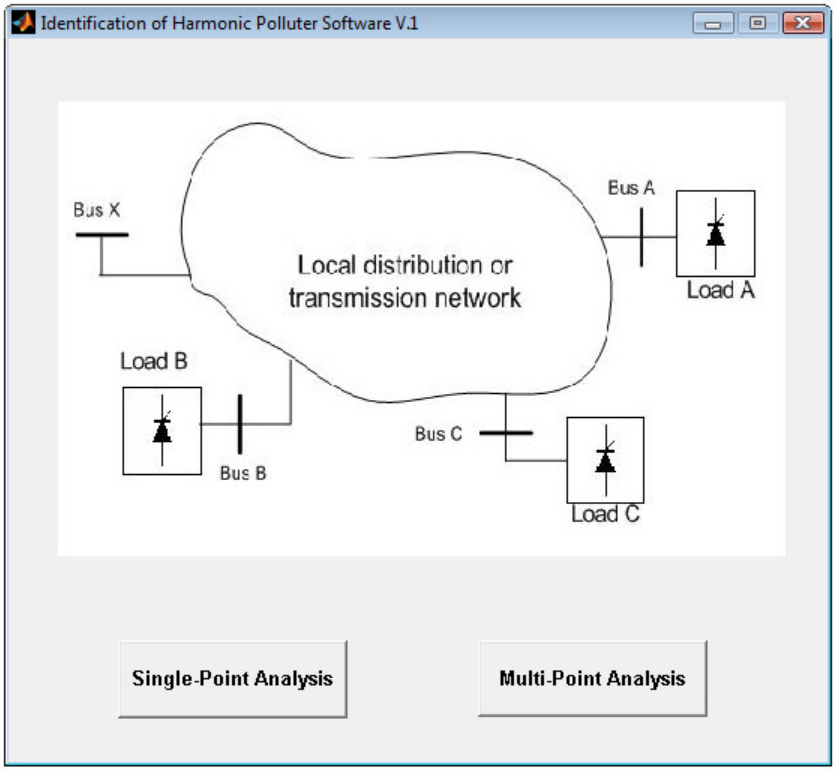

Figure A-2: First screen shot of the software package window

Figure A-3 shows the screen shot of the Multi-Point Analysis window. The four pushbuttons are *Add Load/Bus*, *Remove Load/Bus*, *Settings*, and *Analyze*. One Edit text to enter the harmonic order and one table to show the added suspicious loads and observation buses are also provided. The *Add Load/Bus* pushbutton can be used to add new suspicious loads or observation buses. In our case, three suspicious loads and one observation bus need to be added.

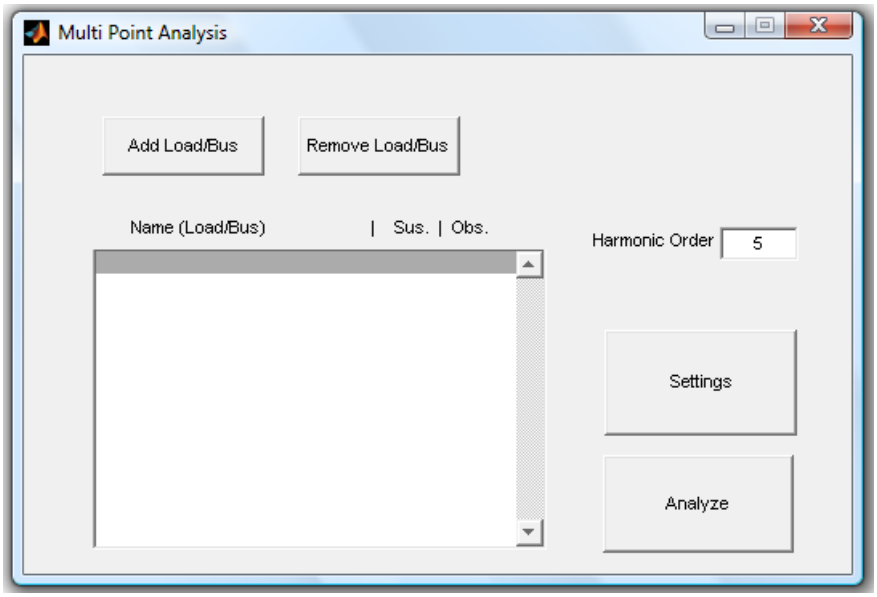

Figure A-3: Screen shot of Multi Point Analysis window

Once the *Add Load/Bus* pushbutton is pushed, the following window (shown in Figure A-4) will appear. To add a suspicious load or an observation bus, the user should provide the path file of the measurement data (input file) and the name of the Bus/Load. Also specify the type of the load/bus. Any load/bus can be either an observation point, a suspicious load, or both. For our case, loads A, B, and C are suspicious loads and bus X is an observation point. In addition to this study, if one wants also to study the impact of these loads on the bus with load B attached to it, both the observation and suspicious options should be selected for load B. In other words, if a bus and the load attached to it have the same name, they do not need to be added twice.

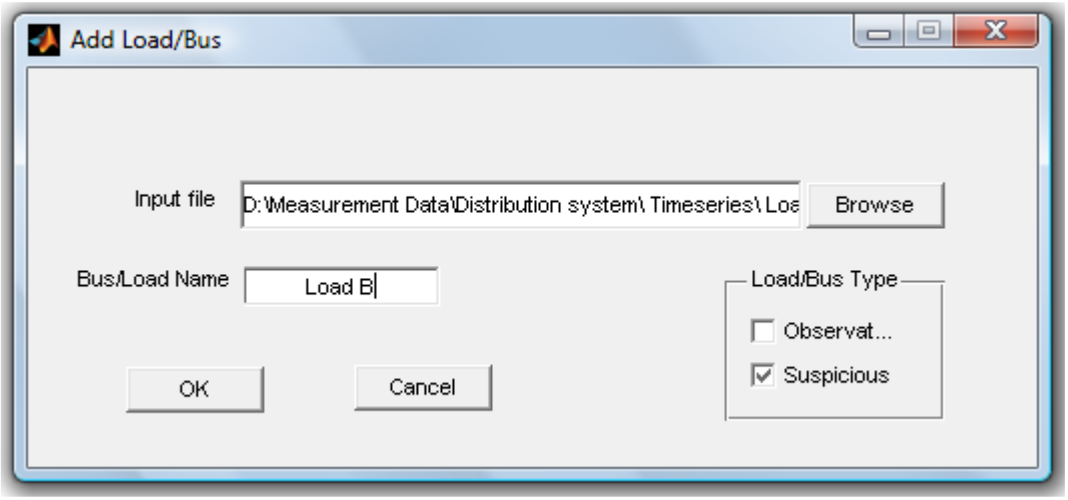

Figure A-4: Screen shot of Add Load/Bus window

For the observation point, the measurement data of the harmonic voltage is necessary, and for the suspicious loads, the measurement data of the harmonic current is necessary. Figure A-5 shows the format of the input file, which should have the following specifications:

- The sheet names containing the harmonic voltages and currents measurements should be Voltage and Current, respectively.
- The power system is considered to be symmetrical, so the input file should contain only the measurement data of one of the phases.
- The first column of each sheet is devoted to the time.
- The time interval between all the measurements should be constant.
- The second column is devoted to the fundamental harmonic, the third column to the second harmonic, and so on.

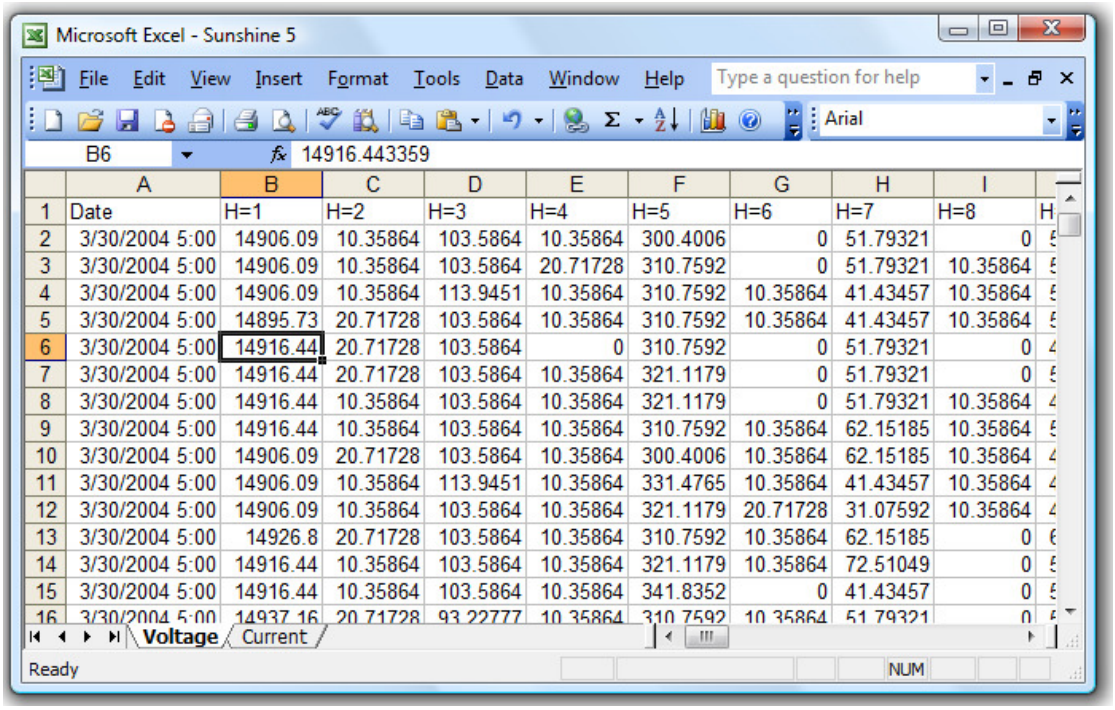

	A	B	C	D	E	F	G	H	I
1	Date	H=1	H=2	H=3	H=4	H=5	H=6	H=7	H=8
2	3/30/2004 5:00	14906.09	10.35864	103.5864	10.35864	300.4006	0	51.79321	0
3	3/30/2004 5:00	14906.09	10.35864	103.5864	20.71728	310.7592	0	51.79321	10.35864
4	3/30/2004 5:00	14906.09	10.35864	113.9451	10.35864	310.7592	10.35864	41.43457	10.35864
5	3/30/2004 5:00	14895.73	20.71728	103.5864	10.35864	310.7592	10.35864	41.43457	10.35864
6	3/30/2004 5:00	14916.44	20.71728	103.5864	0	310.7592	0	51.79321	0
7	3/30/2004 5:00	14916.44	20.71728	103.5864	10.35864	321.1179	0	51.79321	0
8	3/30/2004 5:00	14916.44	10.35864	103.5864	10.35864	321.1179	0	51.79321	10.35864
9	3/30/2004 5:00	14916.44	10.35864	103.5864	10.35864	310.7592	10.35864	62.15185	10.35864
10	3/30/2004 5:00	14906.09	20.71728	103.5864	10.35864	300.4006	10.35864	62.15185	10.35864
11	3/30/2004 5:00	14906.09	10.35864	113.9451	10.35864	331.4765	10.35864	41.43457	10.35864
12	3/30/2004 5:00	14906.09	10.35864	103.5864	10.35864	321.1179	20.71728	31.07592	10.35864
13	3/30/2004 5:00	14926.8	20.71728	103.5864	10.35864	310.7592	10.35864	62.15185	0
14	3/30/2004 5:00	14916.44	10.35864	103.5864	10.35864	321.1179	10.35864	72.51049	0
15	3/30/2004 5:00	14916.44	10.35864	103.5864	10.35864	341.8352	0	41.43457	0
16	3/30/2004 5:00	14937.16	20.71728	93.22777	10.35864	310.7592	10.35864	51.79321	0

Figure A-5: Format of the input file

Figure A-6 shows the program when three suspicious loads and one observation bus are added. The *Remove Load/Bus* pushbuttons can be used to remove an already added load/bus.

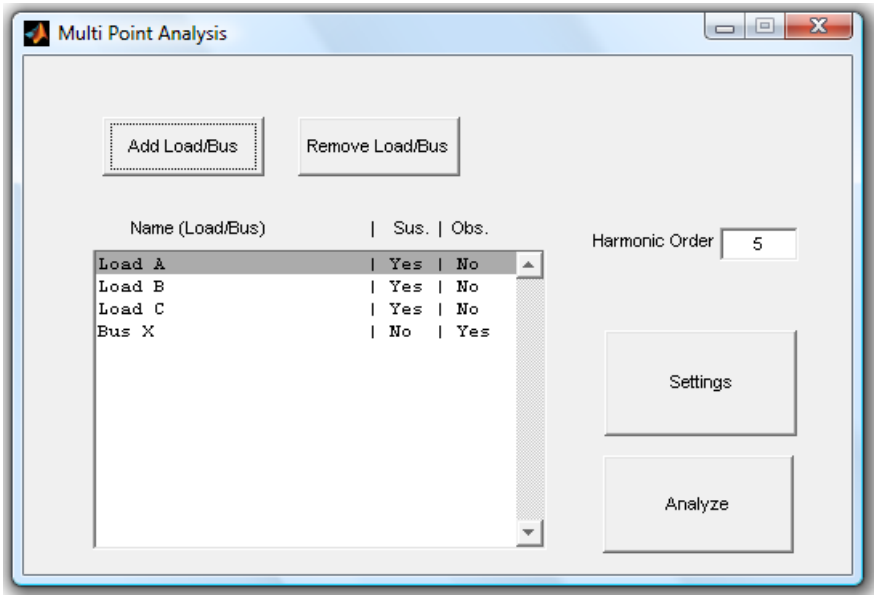

Figure A-6: Three suspicious loads and one observation bus added to the program

The preset settings of the software can be changed by pushing the *Settings* pushbutton. Figure A-7 shows the screen shot of the Settings window. The user is able to choose between the algorithms and the data selection methods. Some pre-set settings such as the load variation threshold and the minimum length of the data selected for analysis can also be modified. We use the Statistical Correlation Method and the Load Level data selection method. We also set the Load variation to 10% and the minimum length of the data to be analyzed to 20%.

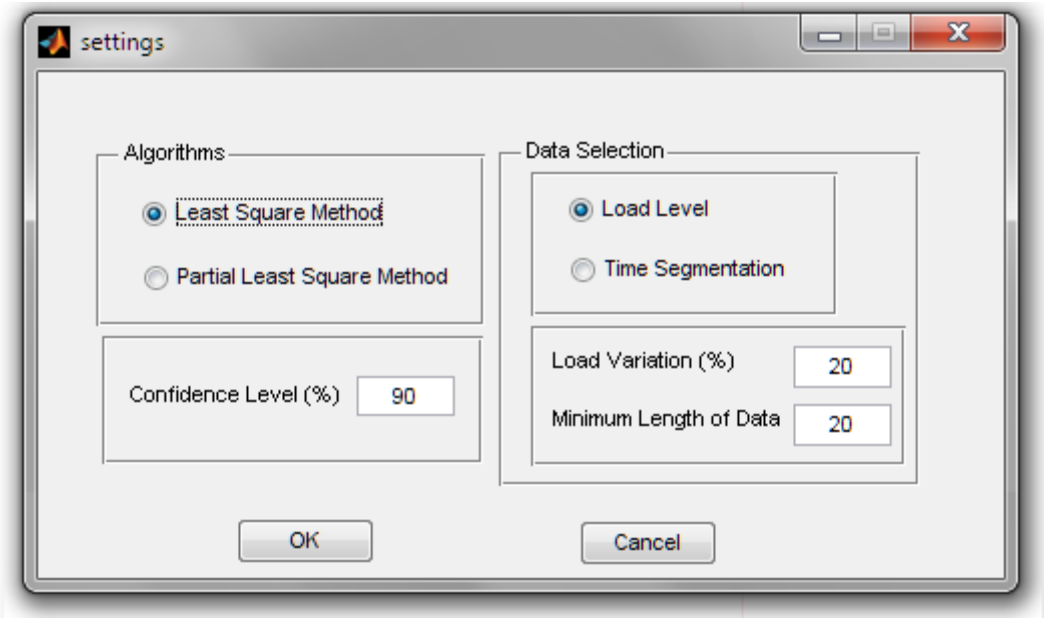

Figure A-7: Screen shot of the Settings window

Finally, to perform the analysis, the *Analyze* pushbutton should be pushed. The software evaluates the harmonic impact of all the suspicious loads on all the observation points. Figure A-8 shows the format of the output file, which will be a table of the harmonic impacts of the suspicious loads on the observation points. For example, cell A2 in Figure A-8 shows the harmonic impact of the harmonic current of Load B on the harmonic voltage of the observation point.

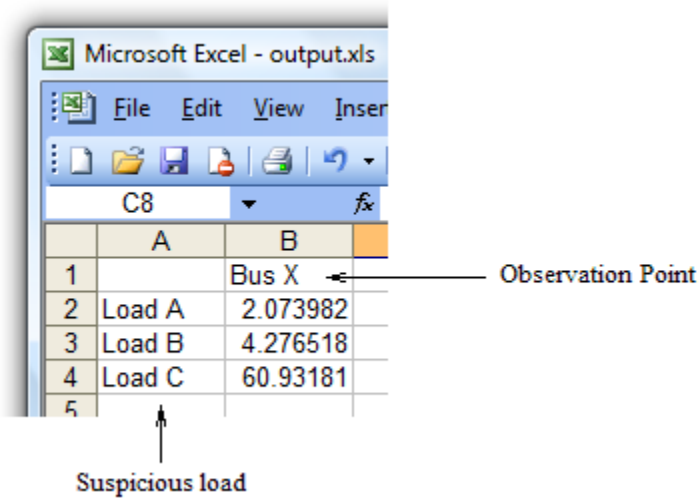

Figure A-8: Format of the output file

To study the impact of the suspicious loads on the bus with load B attached to it, both the observation and suspicious options should be selected for load B. First, load B is

removed and added again as both a suspicious load and an observation point (see Figure A-9).

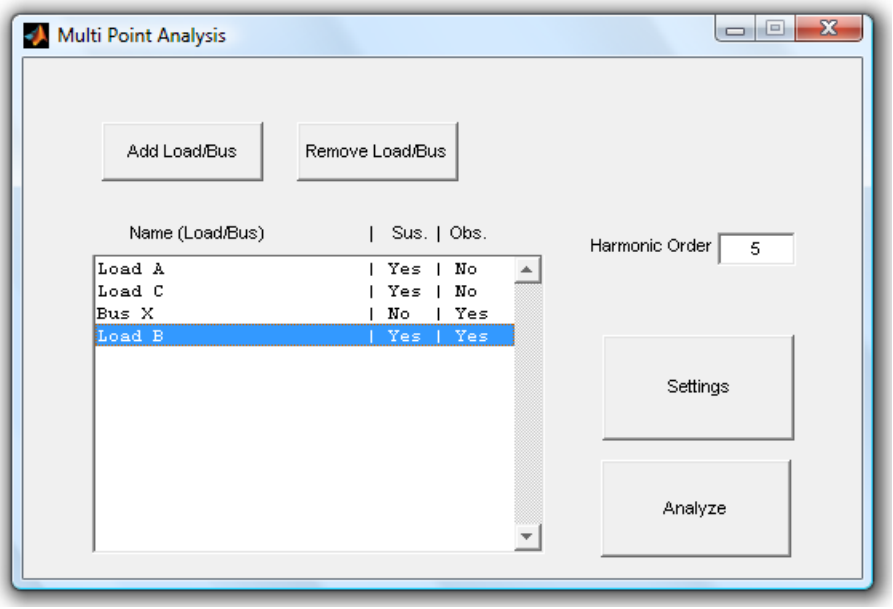

Figure A-9: Load B added to the program as both observation and suspicious type

The output file for this new case is shown in Figure A-10.

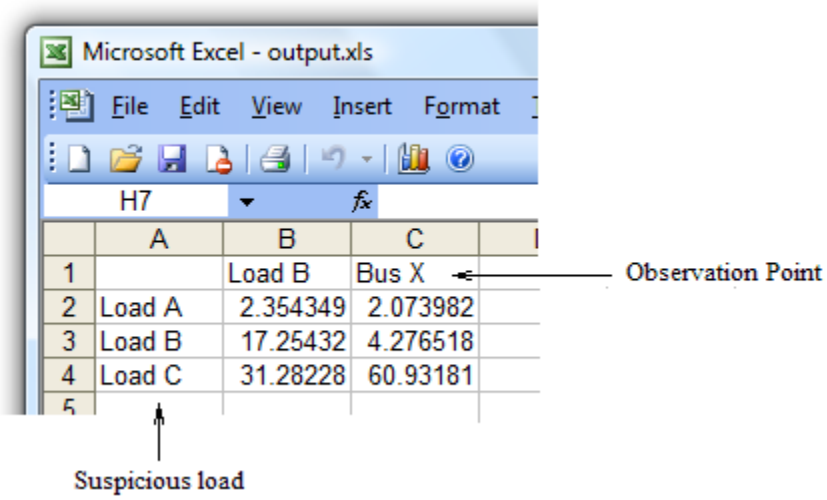

Figure A-10: Output file for the new case

A.1.2 Single-Point Analysis

Another analysis possible by the program is the single-point analysis. In the single-point case, both observation point and suspicious load are the same, so the self-impact of

a load to its PCC harmonic voltages is calculated without having any information about the other major suspicious loads. Figure A-11 shows the screen shot of Single Point Analysis.

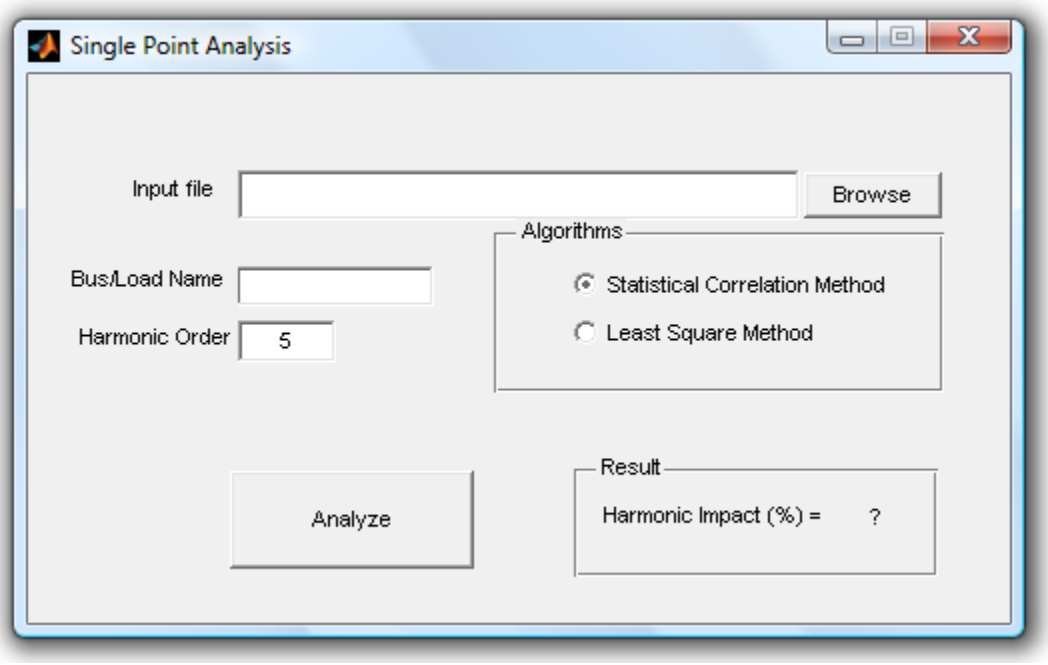

Figure A-11: The screen shot of Single Point Analysis

It is important to notice that input file should contain measurement data for both harmonic voltage and current. For single point analysis, both Statistical Correlation and Least Square methods can be applied. After entering the data, the self harmonic impact of the load is estimated and shown in Result box. As an example, this analysis is performed for the harmonic 7^{th} of load B (see Figure A-12).

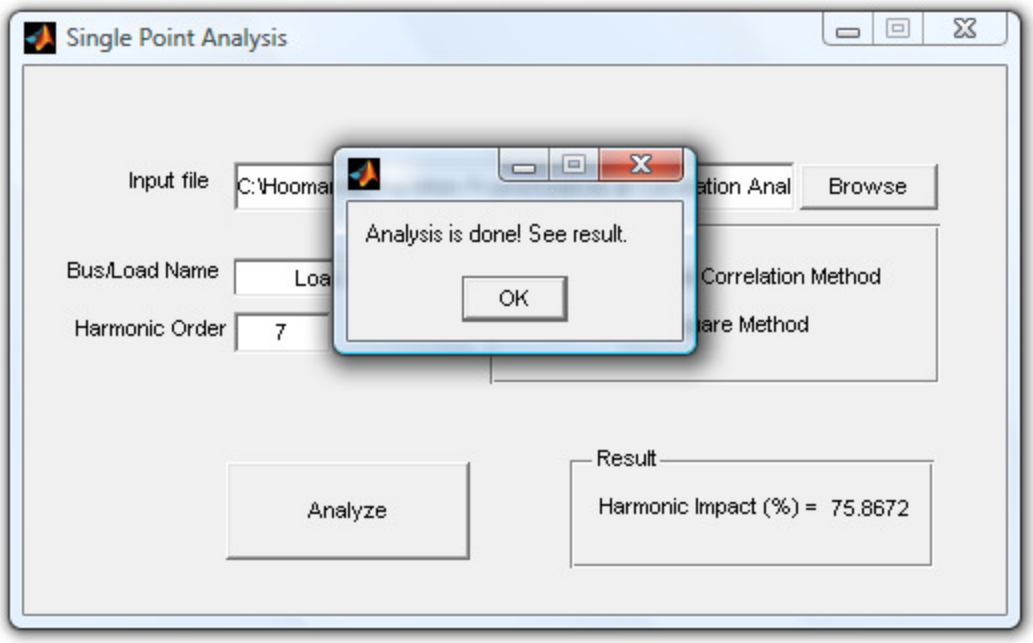

Figure A-12: Single Point Analysis for the harmonic 7th of load B

A.3 Application Examples

Two application examples are explained in this section.

A.1.3 Example 1

The network of first application example is shown in Figure A- 13. Harmonic voltages and currents of buses and their corresponding loads are collected from 5AM to 5PM. Figure A-14 shows the variation of fundamental current during this period. The variation of THD of voltage is also shown in Figure A-15. Loads pick up in the morning and they decrease in the evening. Harmonic impacts of loads to the buses for the 5th harmonic in the whole day are estimated by applying the proposed method.

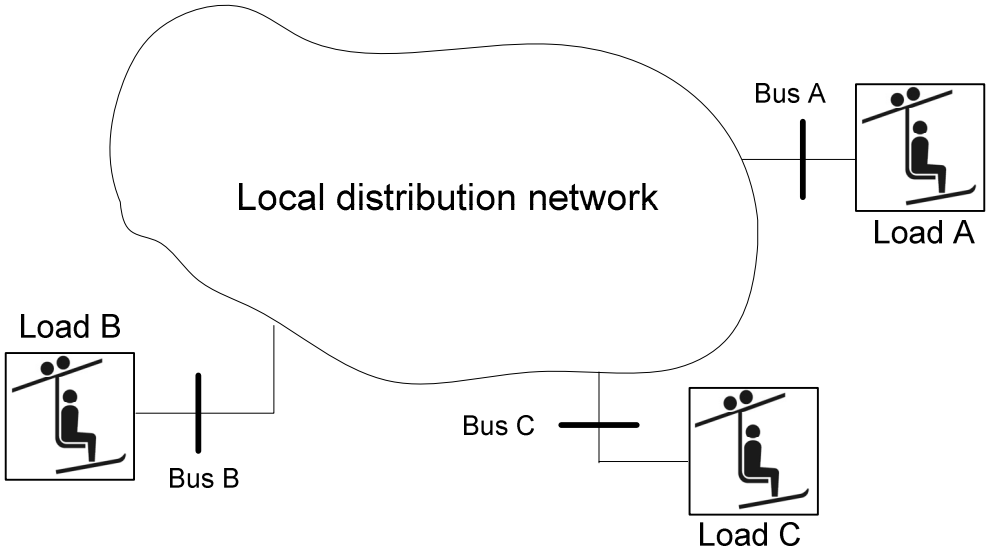

Figure A- 13: Corresponding network of benchmark 1

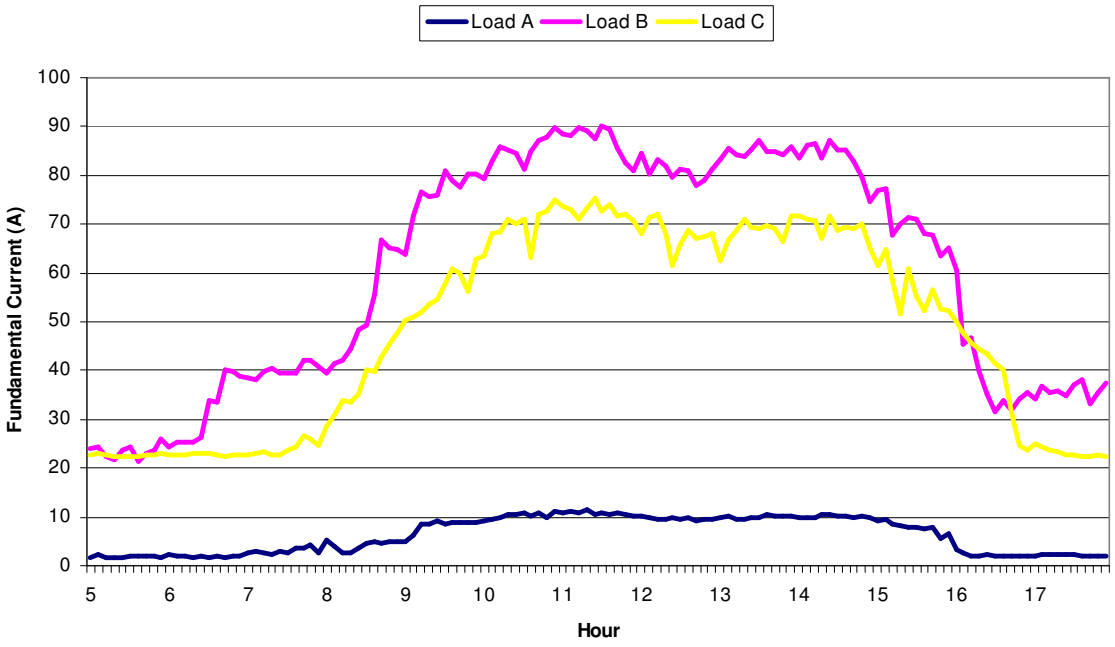

Figure A-14: Variation of fundamental current during one day

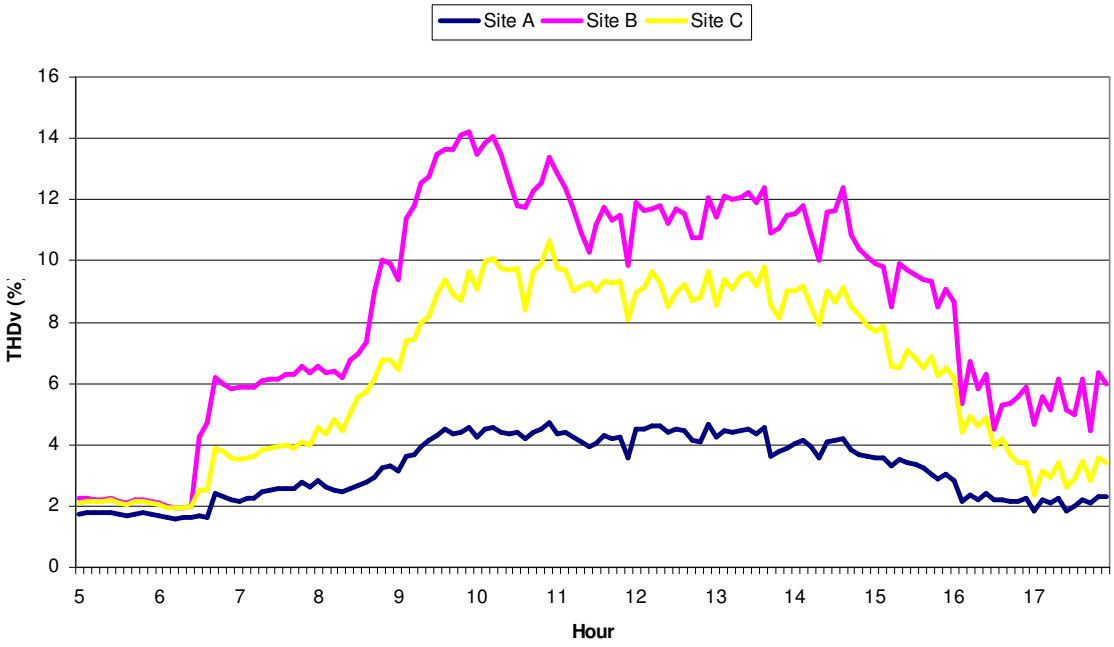

Figure A-15: Variation of THD of voltage during one day

This problem is studied using the Multi Point Analysis section of the program. Three loads should are added as suspicious bus and observation bus.

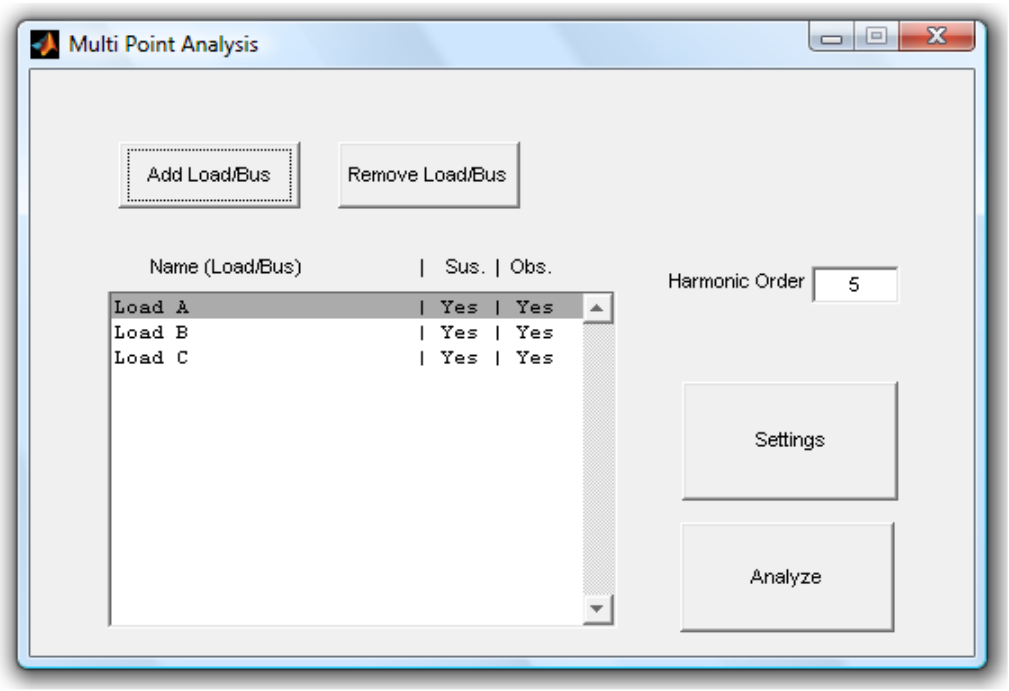

Figure A- 16: Loads A, B and C added to the program as both observation points and suspicious loads

Table A-1 shows the results using the least square method. For example, harmonic impact of load B to harmonic voltage of bus A is 47.46% at 10AM.

Table A-1: Harmonic impacts of Loads to the buses for the 5th harmonic

Hour	Bus A			Bus B			Bus C		
	Load A	Load B	Load C	Load A	Load B	Load C	Load A	Load B	Load C
5	12.58	16.33	3.80	4.23	41.62	4.38	5.58	22.03	8.86
6		20.39			56.47			31.82	
7	6.70	-11.77		4.17	44.82		3.68	-7.27	
8	1.48	36.30	-6.93	-1.67	75.65	-7.40	-2.96	43.54	4.38
9	20.35	82.07	4.69	16.51	91.85	3.61	18.72	70.74	9.12
10	2.81	47.46	1.20	0.94	69.06	0.21	1.76	42.00	13.95
11	0.21	44.19	-20.35	1.26	69.18	-21.03	-0.44	37.28	-5.14
12	-7.18	47.35	-12.26	-8.19	67.88	-9.20	-8.84	36.94	-5.67
13	3.89	55.32	-9.02	1.25	74.04	-5.06	1.67	36.89	4.05
14	-19.13	59.67	-7.53	-20.76	74.28	-7.98	-11.69	47.39	6.24
15	20.01	38.22	-7.67	15.27	76.23	-4.66	17.74	33.57	-1.90
16	5.50			6.21			6.20		
17	20.96	-7.39		9.24	54.40		16.60	9.20	

Average harmonic impacts of loads to the buses during the day are presented in Figure A- 17.

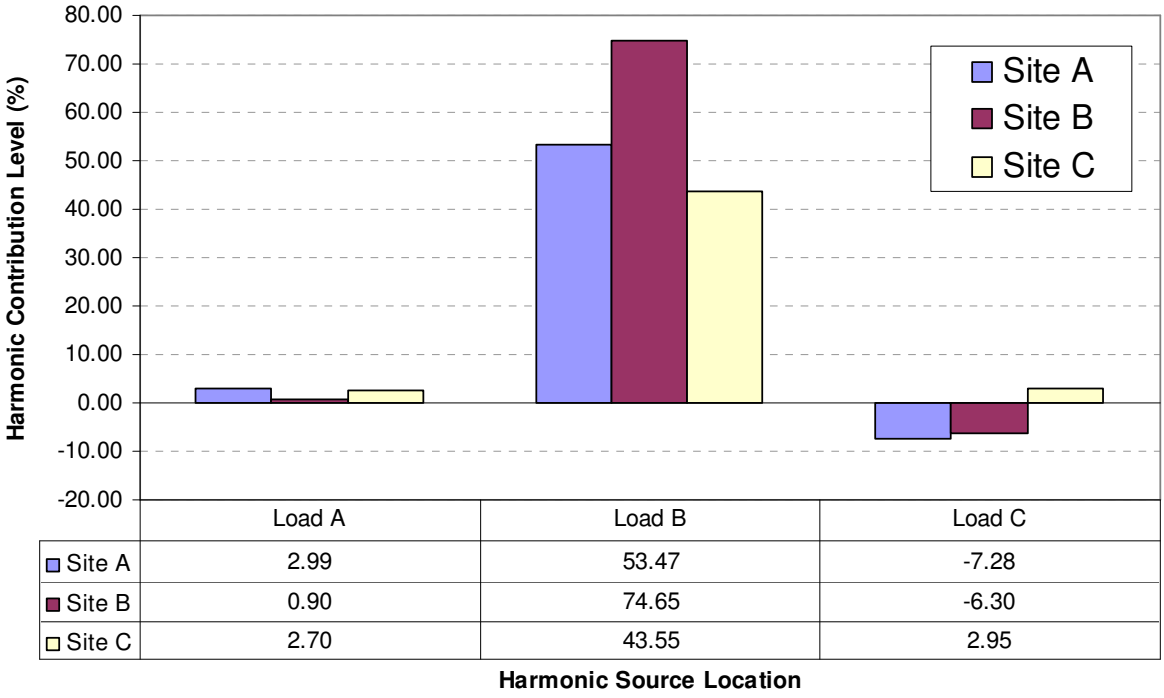

Figure A- 17: Average harmonic impacts of loads to the buses

8.1.1 Example 2

Figure A-18 shows the corresponding network for Example 2. In this case, three feeders are fed by a bus bar. The harmonic impact of each feeder on the utility side bus bar is studied.

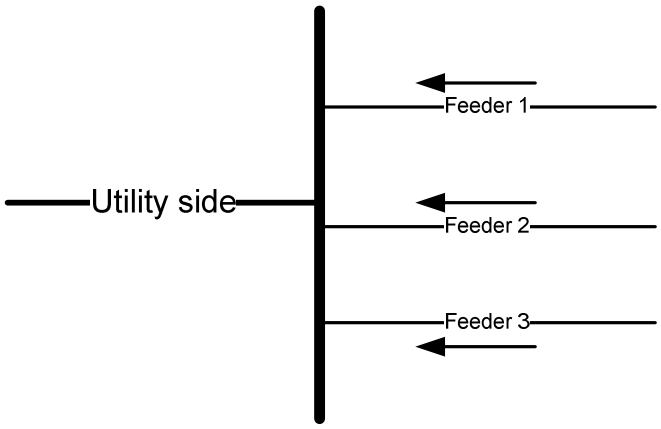

Figure A-18: The corresponding network of benchmark 2

Figure A-19 shows the variation of fundamental currents of feeders. Variation of THD voltage at the bus bar is also shown in Figure A-20.

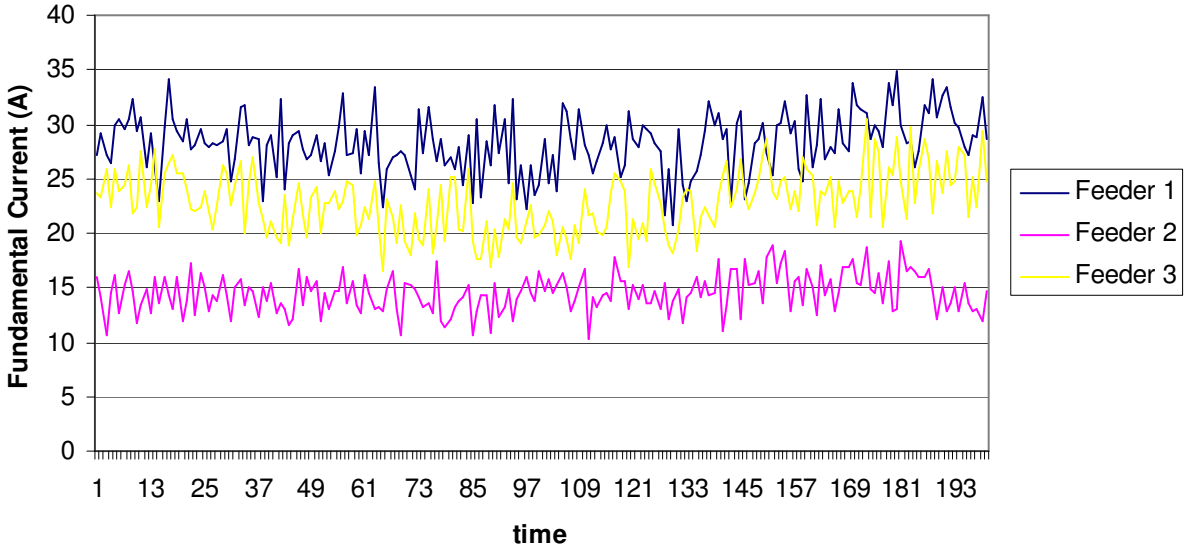

Figure A-19: Variation of fundamental currents of feeders

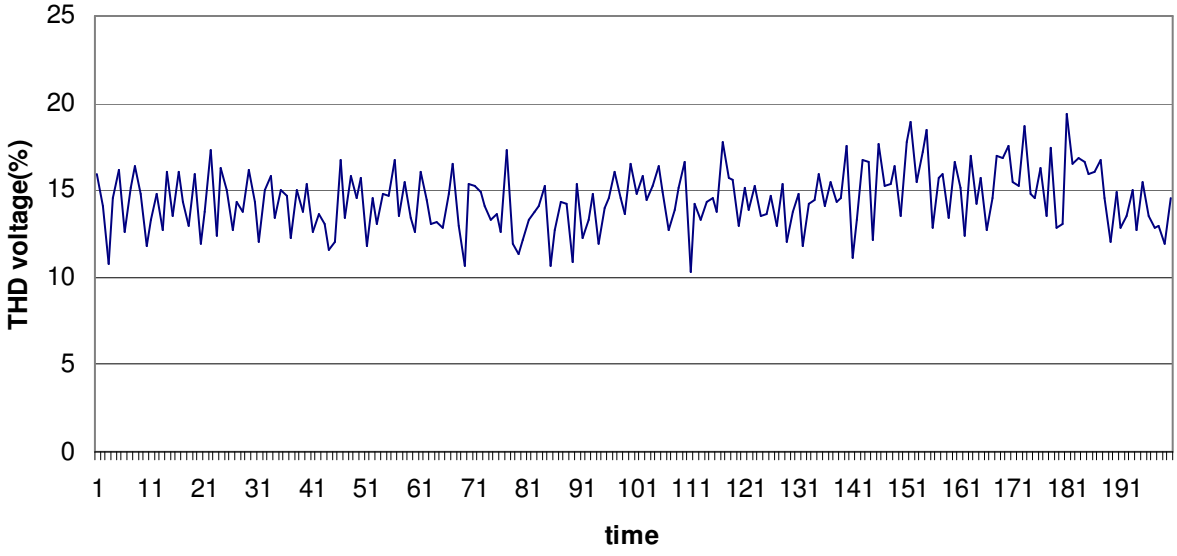

Figure A-20: Variation of THD voltage of utility bus bar

To study impact of each feeder, the software can be used. Three feeders should be added as suspicious loads. The utility side bus bar should also be added as the observation bus. Figure A-21 shows the Multi Point Analysis window after adding loads.

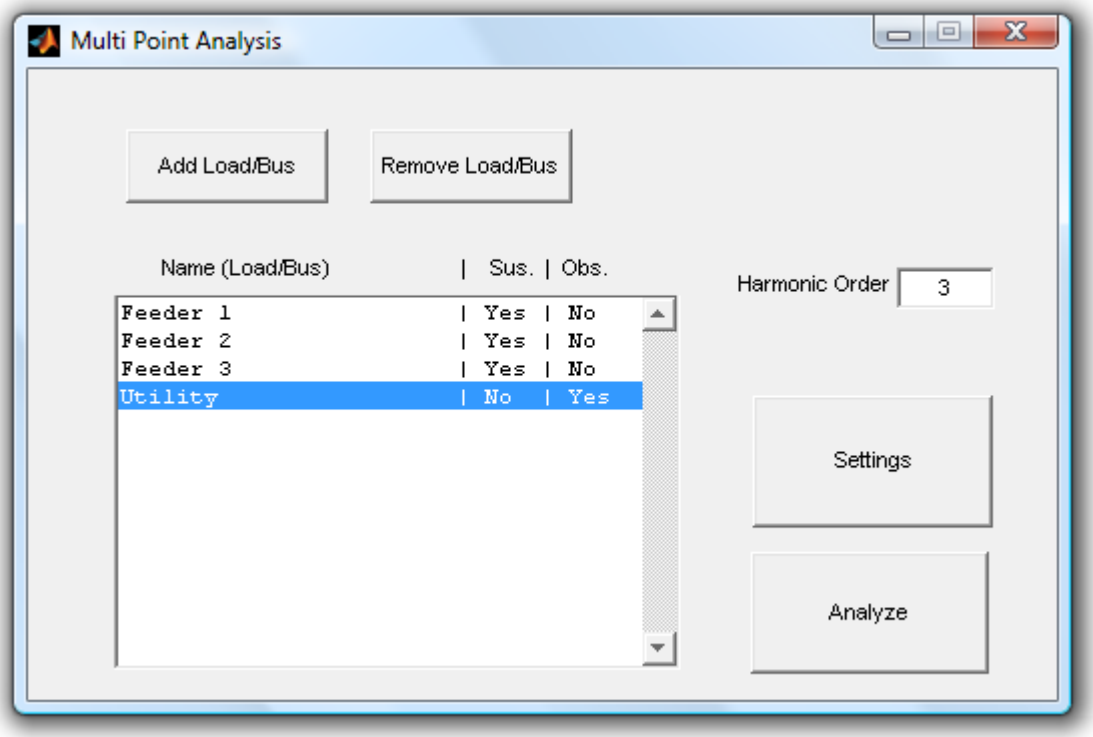

Figure A-21: Multi Point Analysis window after adding feeder for benchmark 2

The harmonic impacts of loads are achieved and presented in Table A-2 and shown in Figure A-22.

Table A-2: Harmonic impacts of feeders on the common bus

Harmonic order	H=3	H=5	H=7	H=9	H=11	H=13
Feeder 1	51.07845	46.76039	45.92523	29.03542	31.71449	32.63236
Feeder 2	40.88266	33.07066	42.92634	71.19881	59.35371	32.40536
Feeder 3	-7.24619	12.43488	15.85155	-3.85784	-2.91378	14.56789

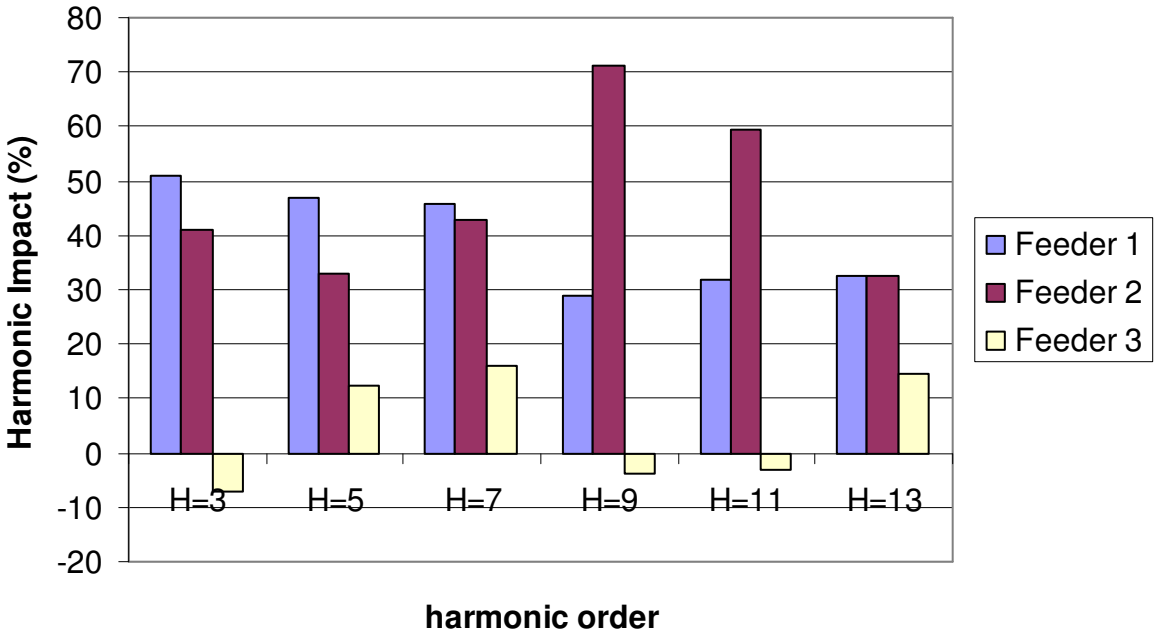

Figure A-22: Harmonic impacts of feeders on the common bus